JYU DISSERTATIONS 863

Alessandra Giangrande

# Advanced Methods and Instrumentation to Examine Sensorimotor Integration and Corticomuscular Coupling

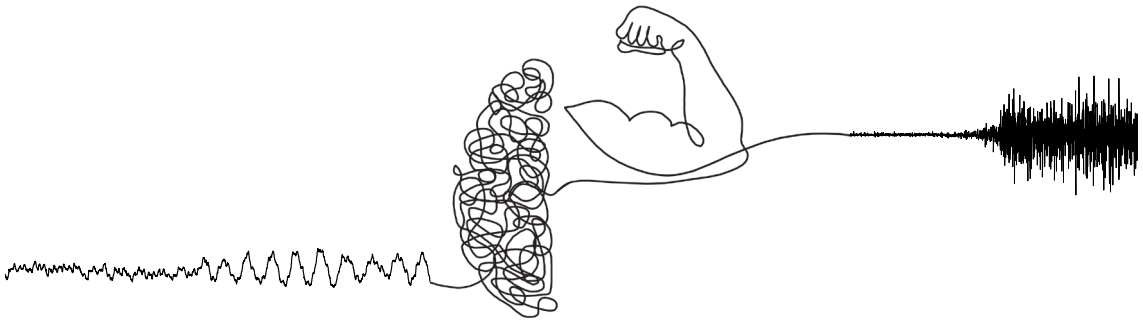

UNIVERSITY OF JYVÄSKYLÄ
FACULTY OF SPORT AND
HEALTH SCIENCES

JYU DISSERTATIONS 863

Alessandra Giangrande

# Advanced Methods and Instrumentation to Examine Sensorimotor Integration and Corticomuscular Coupling

Esitetään Jyväskylän yliopiston liikuntatieteellisen tiedekunnan suostumuksella
julkisesti tarkastettavaksi yliopiston vanhassa juhlasalissa S212
tammikuun 16. päivänä 2025 kello 12.

Academic dissertation to be publicly discussed, by permission of
the Faculty of Sport and Health Sciences of the University of Jyväskylä,
in building Seminarium, auditorium S212, on January 16, 2025, at 12 o'clock noon.

JYVÄSKYLÄN YLIOPISTO
UNIVERSITY OF JYVÄSKYLÄ

JYVÄSKYLÄ 2025

Editors
Kasper Salin
Faculty of Sport and Health Sciences, University of Jyväskylä
Ville Korkiakangas
Open Science Centre, University of Jyväskylä



The cover picture is made by Alessandra Giangrande.



ISBN 978-952-86-0449-5 (PDF)
URN:ISBN:978-952-86-0449-5
ISSN 2489-9003

Permanent link to this publication: http://urn.fi/URN:ISBN:978-952-86-0449-5

# ABSTRACT

Giangrande, Alessandra
Advanced methods and instrumentation to examine sensorimotor integration and corticomuscular coupling
Jyväskylä: University of Jyväskylä, 2025, 127 p.
(JYU Dissertations
ISSN 2489-9003; 863)
ISBN 978-952-86-0449-5 (PDF)

The recording of biopotentials such as electroencephalographic (EEG) and electromyographic (EMG) signals during motor actions is an effective approach to non-invasively track the physiological processes concerning sensorimotor integration. The neural encoding of afferent and efferent information has been widely investigated by means of outcome measures such as corticomuscular (CMC) and corticokinematic (CKC) coherence, evoked and induced EEG responses to stimuli provided in quasi-static conditions. However, the study of brain signals during movements is still strongly limited by bulky and wired technology, thus hindering the comprehensive investigation of the EEG signal properties and characteristics in dynamic conditions. With the long-term aim to apply cortical research to real-world-like scenarios, i.e., in everyday situations, the aim of this dissertation was the design, characterization and experimental application innovative technologies for the study of biopotentials in the context of the sensorimotor integration studies. To this purpose, the current bottlenecks limiting the EEG signal acquisition during movements were firstly identified and modelled. This operation led to the definition of possible technological solutions that were subsequently prototyped to overcome the highlighted limitations. Specifically, a miniaturized system to enable the wireless, unconstrained recording of EEG signals was designed and successfully validated against a well-established system under conventional, static conditions. Additionally, original EEG electrodes systems were designed with the aim of investigating the contribution of connecting cables and electrodes technology to the genesis of motion artifacts compromising the EEG signals quality. In the second part of the thesis, the developed wireless EEG system was applied in both static and dynamic physiological contexts. Firstly, the effect of a voluntary muscular contraction on cortical processing of naturalistic proprioceptive stimulation was evaluated. Secondly, the brain-periphery coupling was investigated during walking, jogging and cross-country skiing. These studies were performed to explore the possibility to effectively monitor the processing of afferent and efferent information occurring at the level of the primary sensorimotor cortex during movements. Overall, the presented studies showed promising results to extend EEG research to wide contexts, opening new frontiers to examine the physiological and pathological human sensorimotor system during naturalistic conditions.

*Keywords*: wireless EEG, biopotential signal acquisition, proprioception, sensorimotor integration, motor cortex, the brain

# TIIVISTELMÄ (ABSTRACT IN FINNISH)

Giangrande, Alessandra
Uusien menetelmien instrumentaatio ihmisen liike- ja tuntojärjestelmän aivoperustan tutkimiseksi liikkumisen aikana
Jyväskylä: Jyväskylän yliopisto, 2025, 127 p.
(JYU Dissertations
ISSN 2489-9003; 863)
ISBN 978-952-86-0449-5 (PDF)

Biopotentiaalien, kuten elektroenkefalografisten (EEG) ja elektromyografisten (EMG) signaalien rekisteröinti motoristen toimintojen aikana on tehokas lähestymistapa ihmisen keskushermoston sensorimotorisen integraation ja siihen liittyvien neurofysiologisten prosessien kajoamattomaan seurantaan. Aivoihin kehosta saapuvan somatosensorisen palautteen ja aivoista kehoon lähtevän liikeohjauksen välistä hermostollista yhteistoimintaa on tutkittu laajasti eri mittarein, kuten EEG herätevasteiden, kortikomuskulaarisen (CMC) ja kortikokinemaattisen (CKC) koherenssin avulla lähes staattisissa mittausolosuhteissa, sillä aivosignaalien tutkimusta luonnonmukaisemman dynaamisen liikkumisen aikana on rajoittanut suuret painavat johdolliset mittalaitteet. Tämän väitöskirjan tavoitteena oli uusien innovatiivisten teknologioiden suunnittelu, rakentaminen ja kokeellinen soveltaminen aivojen aivokuoren EEG aktiivisuuden mittaamiseksi dynaamisissa luonnonmukaisissa tilanteissa. Tätä varten tunnistimme ensin nykyiset EEG-mittauksen pullonkaulat, ja ne mallinnettiin, jonka perusteella määritimme mahdolliset teknologiset ratkaisut, joiden toimivuus tunnistettujen rajoitusten voittamiseksi testattiin kokeellisesti. Onnistuimme validoimaan pienoiskokoisen langattoman EEG järjestelmän vertaamalla sitä vakiintuneeseen langalliseen EEG järjestelmään tavanomaisissa staattisissa olosuhteissa. Lisäksi suunnittelimme uusia ratkaisuja EEG-mittauselektrodijärjestelmille, joiden tavoitteena oli auttaa ymmärtämään johtimien ja elektrodien teknologian vaikutusta ei-toivottujen liikeartefaktien syntyyn EEG-signaaliin. Väitöskirjani toisessa osassa kehittämäämme langatonta EEG-järjestelmää sovellettiin sekä staattisisten että dynaamisten liikkeiden aikana neurofysiologisten perusmekanismien selvittämiseksi. Ensiksi tutkimme kuinka tahdonalainen lihassupistus vaikuttaa aivokuorelle saapuvan liikeaistipalautteen käsittelyyn. Toiseksi tutkimme aivojen ja ääreishermoston yhteistoimintaa kävelyn, juoksun ja maastohiihdon aikana. Yhteenvetona tutkimuksemme osoittivat, että EEG-mittaukset kyetään laajentamaan luonnonmukaisemman liikkumisen tutkimuksen konteksteihin, joka avaa täysin uusia mahdollisuuksia ihmisen sensorimotorisen järjestelmän neurofysiologisten ja patologisten prosessien tutkimiseksi mahdollisimman luonnollisissa olosuhteissa.

*Avainsanat*: langaton EEG, biosignaali, proprioseptiikka, sensorimotorinen integraatio, motorinen aivokuori, aivot

**Author**

Alessandra Giangrande, Biomedical Engineer
Faculty of Sport and Health Sciences | University of Jyväskylä
Department of Electronics and Telecommunications | Polytechnic of Turin
alessandra.x.giangrande@jyu.fi
alessandra.giangrande@polito.it
ORCID: https://orcid.org/0000-0002-1311-1389

**Supervisors**

Professor Harri Piitulainen, PhD
Faculty of Sport and Health Sciences
University of Jyväskylä, Finland

Professor Alberto Botter, PhD
Department of Electronics and Telecommunications
Polytechnic of Turin, Italy

Professor Giacinto Luigi Cerone, PhD
Department of Electronics and Telecommunications
Polytechnic of Turin, Italy

Professor Marco Knaflitz, PhD
Department of Electronics and Telecommunications
Polytechnic of Turin, Italy

**Reviewers**

Professor Pasi A. Karjalainen, PhD
Department of Technical Physics
University of Eastern Finland, Kuopio, Finland

Professor Danilo Pani, PhD
Department of Electrical and Electronic Engineering
University of Cagliari, Italy

**Opponent**

Professor Klaus Gramann, PhD
Department of Psychology and Ergonomics
Technische Universität Berlin

## ACKNOWLEDGEMENTS

Completing this thesis has been not only an academic challenge but also a profound journey of personal and philosophical growth. This thesis acknowledgement is a tribute to all the people who made my academic experience worthwhile.

First and foremost, I extend my deepest gratitude to my supervisors Professors Harri Piitulainen, Alberto Botter and Giacinto Luigi Cerone. Your professional expertise, support and continuous guidance have been pivotal in navigating the complexities of my research. Your insightful critiques and meticulous attention to detail have significantly contributed to shaping not only this dissertation, but also my attitude as a researcher and academic. I am deeply grateful for the time and effort you have invested in my professional growth.

Among the most memorable highlights of my PhD journey was the opportunity to visit the Vuokatti Sports Technology Unit, whose resources were invaluable for the completion of my dissertation. This enriching experience would not have been possible without the dedication and expertise of Professor Jarmo Piirainen. I am deeply grateful for the knowledge you shared and the connections developed during that time.

Moreover, I am also truly thankful to the entire Laboratory for Engineering of the Neuromuscular System (LISiN), especially to Professors Marco Gazzoni and Taian Vieira. Working with you provided me with countless learning opportunities. I am honored to have contributed, even in a small way, to the invaluable work you are doing.

Furthermore, I would like to express my sincere gratitude to Maurizio Martinez, Sirpa, and Jouni for their prompt technical assistance. Your knowledge and extensive expertise were crucial for my research and experiments. The kindness and readiness with which you assisted me went beyond your working duties. Thank you from the bottom of my heart. Speaking about technical assistance, I wish to acknowledge Sakari Vekki who helped me to set up my experiments more smoothly and efficiently. Your passionate approach and methodical problem-solving abilities have been inspirational in coping with the difficulties of this project. Thank you for sharing your expertise and for bringing your positive mindset to our shared lunch breaks.

My heartfelt thanks to my officemate Toni Mujunen. Working alongside you encouraged me and kept me motivated throughout this doctoral journey. A huge *kiitos* also to the rest of the JYU PhD crew: Joona Juurakko, Johanna Kotikangas, Feiyue Li, Junru Chen and Dr. Nijia Hu. Thank you for sharing all the PhD struggles and for making my survival in a foreign country easier. You all made my Finnish visits enjoyable and memorable. A special mention goes to my POLITO PhD colleagues as well: Diletta Balta and Rachele Rossanigo. Thank you for the shared time, the late-night talking in a silent Brixen monastery and the last minute lunch breaks often interrupted by unwanted guests. The time spent together was always refreshing and made me feel less alone.

I wish to extend my special thanks to all the wonderful friends I met along the way. Specifically, thanks to Georgia Larvik for having been the perfect roommate and for sharing the few rays of sunshine during a dark, long Finnish winter. We built moments that will last forever in my heart. Thanks, Claudia Mescolini, for the moral support through our never-ending carefree saunas, innumerable hikes and smoky barbecues. The way you transformed your weaknesses in strengths has been exemplary for me.
I am also indebted to a selected group of people from LISiN, who provided both distractions when needed and encouragement when it seemed hard to go on. Thanks to the crazy "fresh ones", starting from my golden flowers Asja, Federica, and Martina, and continuing with my beloved Marco, Marta, Elena, Francesca, and Andrès. Despite our boring lunch boxes, the thought of a lunch break with you pushed me to face the daily anxieties of my PhD journey. Thank you for always making me smile.
I could not have completed this journey without Dr. Marco Carbonaro, more than a mere desk mate. The best sounding board and provider of constructive feedback I could have asked for. I truly appreciate every conversation we had and every piece of moral support I received. Your constant encouragement was fundamental for my progress (almost as much as your memes or reels were).
A special mention goes to my dear Enrica Tricomi, esteemed colleague and loyal friend. Your ambition, resourcefulness, and inexhaustible dedication have been a source of inspiration to me throughout these years. Thank you, because we did it together once again as we did five years ago "when it seemed impossible alone, but together we were amazing". You have been the greatest gift the Polytechnic has ever given me.
My gratitude must also be extended to my lifelong friends Beatrice, Daria, Nora, and Marta. Thank you for the support you gave me despite the distance. I know you always have my back, and I could not be more grateful to have you in my life.
To my family members, pillars of strength. The energy and perseverance I kept throughout this challenging journey were a reflection of the firm support and boundless love I received from you. *Grazie di cuore*.
Finally, I owe my utmost gratitude to my partner in crime, Fabio. Thank you for your endless patience, unwavering support, and belief in me. Our countless countdowns before our reunions will be forever etched in our memories. Thank you for your daily commitment in keeping our romance alive, your love kept me warm also miles away with below-freezing temperatures. These years taught me that home is wherever I am with you.

From the bottom of my heart,
Thank you, *Kiitos*, *Grazie* to all who significantly contributed to make this possible.

Jyväskylä, December 2024
Alessandra Giangrande

## LIST OF ABBREVIATIONS

| | |
|---|---|
| **AD** | Analog-to-digital |
| **CKC** | Corticokinematic coherence |
| **CMC** | Corticomuscular coherence |
| **CMRR** | Common mode rejection ratio |
| **CNS** | Central nervous system |
| **EEG** | Electroencephalography |
| **EMG** | Electromyography |
| **EOG** | Electrooculogram |
| **ERP** | Event related potentials |
| **ICA** | Independent component analysis |
| **ISI** | Inter stimulus interval |
| **M1** | Primary motor cortex |
| **S1** | Primary sensory cortex |
| **MEG** | Magnetoencephalography |
| **MU** | Motor unit |
| **MUAP** | Motor unit action potential |
| **PCB** | Printed circuit on board |
| **PNS** | Peripheral nervous system |
| **PLI** | Power line interference |
| **RMS** | Root mean square |
| **SEP** | Somatosensory evoked potential |
| **SM1** | Primary sensorimotor system |
| **SNR** | Signal to noise ratio |
| **TMS** | Transcranial magnetic stimulation |
| **TSE** | Temporal-spectral evolution |
| **wBSN** | wireless Body Sensor Network |

## ORIGINAL PUBLICATIONS AND AUTHOR CONTRIBUTION

This thesis is based on the following original publications:

1. G. L. Cerone*, **A. Giangrande***, M. Ghislieri, M. Gazzoni, H. Piitulainen and A. Botter. "Design and validation of a wireless Body Sensor Network for integrated EEG and HD-sEMG acquisitions". *IEEE Transactions on Neural Systems and Rehabilitation Engineering*, 30: 61-71, 2022. doi: 10.1109/TNSRE.2022.3140220. (*shared 1st authorship).

2. **A. Giangrande**, G. L. Cerone, A. Botter, and H. Piitulainen. "Volitional muscle activation intensifies neuronal processing of proprioceptive afference in the primary sensorimotor cortex: an EEG study". *Journal of Neurophysiology*, 31: 28–37, 2024. doi: 10.1152/jn.00340.2023.

3. **A. Giangrande**, A. Botter, H. Piitulainen, G. L. Cerone. "Motion artifacts in dynamic EEG recordings: experimental observations, electrical modelling and design considerations". *Sensors,* 24: 6363, 2024. doi: 10.3390/s24196363.

4. **A. Giangrande**, T. Mujunen, G. L. Cerone, A. Botter, and H. Piitulainen. "Maintained volitional activation of the muscle alters the cortical processing of proprioceptive afference from the ankle joint". *Neuroscience*, 560: 314-325, 2024. doi: 10.1016/j.neuroscience.2024.09.049.

Results of *Studies I* and *III* are presented and thoroughly examined in publication n.3 (Giangrande, Botter, et al., 2024). Results of *Study II* are reported and fully discussed in publication n.1 (Cerone et al., 2022). *Study IV* is outlined and explored in detail in publication n.2 (Giangrande, Cerone, et al., 2024) and in publication n.4 (Giangrande, Mujunen, et al., 2024). The outcome of *Study V* has not been published.

The entire research team contributed to the achievement of all the publications and of this dissertation. The candidate is the principal author in the original publications listed above.

The candidate participated in the technological developments and in designing the experiments. She was, indeed, the main responsible for recruiting participants and performing the experiments. The candidate performed the signal processing by designing the analysis pipeline with the co-authors. The interpretation of the results was performed by the whole research team. The candidate was responsible for preparing the figures and writing the manuscripts with the guidance of the co-authors.

# CONTENTS

ABSTRACT
TIIVISTELMÄ (ABSTRACT IN FINNISH)
ACKNOWLEDGEMENTS
LIST OF ABBREVIATIONS
ORIGINAL PUBLICATIONS AND AUTHOR CONTRIBUTION
CONTENTS

1 INTRODUCTION ..... 13
1.1 Scientific rationale of the research ..... 13
1.2 Studies included in the thesis ..... 15
1.3 Structure of the thesis ..... 17

2 BACKGROUND AND STATE OF THE ART ..... 20
2.1 Anatomy and physiology of the human sensorimotor system ..... 20
2.1.1 The primary somatosensory and motor cortices ..... 21
2.1.2 The human musculoskeletal system ..... 22
2.2 Methods to investigate the sensorimotor system ..... 24
2.2.1 The brain: Electroencephalography (EEG) ..... 25
2.2.1.1 Basic characteristics of EEG signals ..... 26
2.2.1.2 Evoked EEG responses ..... 28
2.2.1.3 Induced EEG responses ..... 29
2.2.2 Recording movement: kinematic, kinetic and electromyographic recordings ..... 30
2.2.3 Corticospinal coupling: Coherence measurements ..... 32
2.3 Acquisition of biopotential signals ..... 34
2.3.1 Block diagram of biopotential acquisition system ..... 35
2.3.1.1 Transduction stage: electrodes ..... 36
2.3.1.2 Analog electronics: Front-end amplifier ..... 39
2.3.2 Power line interference in biopotential acquisition systems ..... 39
2.3.3 EEG acquisition systems: state of the art and open issues ..... 45

3 PURPOSE OF THE PROJECT ..... 48

4 ANALYTICAL STUDY: ANALYSIS OF THE CONSTRAINTS LIMITING EEG SIGNAL ACQUISITION IN LABORATORY ENVIRONMENT (*STUDY I*) ..... 50
4.1 The genesis of motion artifacts: experimental observations, electrical models and good practice recommendations ..... 50
4.1.1 Artifacts arising from phenomena at the electrode-skin interface ..... 52
4.1.1.1 Experimental observation ..... 52
4.1.1.2 Lumped parameters model ..... 53

4.1.1.3 Analysis of the model ..... 56
4.1.2 Artifacts related to the movement of connecting cables ..... 57
4.1.2.1 Experimental observation ..... 57
4.1.2.2 Lumped parameters model ..... 57
4.1.2.3 Analysis of the model ..... 61
4.1.3 Artifacts related to the electrode-amplifier system properties leading to PLI modulation ..... 62
4.1.3.1 Experimental observation ..... 62
4.1.3.2 Lumped parameters model ..... 63
4.1.3.3 Analysis of the model ..... 66
4.2 *Study I*: Conclusion ..... 67

5 TECHNOLOGICAL STUDIES: ADVANCEMENTS ENABLING THE STUDY OF SENSORIMOTOR INTEGRATION IN DYNAMIC CONDITIONS (*STUDIES II-III*) ..... 69
5.1 Design and validation of a wireless body sensor network for integrated EEG and EMG acquisitions (*Study II*) ..... 69
5.1.1 System architecture ..... 70
5.1.2 Units prototyping ..... 71
5.1.3 Bench characterization ..... 72
5.1.4 Experimental validation ..... 74
5.1.4.1 Participants ..... 74
5.1.4.2 Materials and methods ..... 74
5.1.4.3 Results ..... 75
5.1.4.4 Discussion ..... 77
5.1.5 *Study II*: Conclusion ..... 78
5.2 Design and experimental considerations on innovative EEG electrodes systems for the evaluation of motion artifacts sources (*Study III*) ..... 79
5.2.1 Design of EEG electrodes systems ..... 79
5.2.1.1 ET Cap: Textile-based EEG electrodes system ..... 79
5.2.1.2 Lobster Cap: Flexible PCB-based EEG electrodes system 80
5.2.2 Experimental tests ..... 81
5.2.2.1 Material and methods ..... 81
5.2.2.2 Results and Discussion ..... 84
5.2.3 *Study III*: Conclusion ..... 86

6 NEUROPHYSIOLOGICAL STUDIES (*STUDIES IV-V*) ..... 88
6.1 Investigating the effect of maintained volitional muscular activation on cortical proprioceptive processing (*Study IV*) ..... 88
6.1.1 Participants ..... 89
6.1.2 Materials and methods ..... 89
6.1.3 Results ..... 90
6.1.4 Discussion ..... 93
6.1.5 *Study IV:* Conclusion ..... 95

6.2 Assessment of the sensorimotor integration in dynamic contexts: a proof-of-concept study (*Study V*) ..... 96
6.2.1 Participants ..... 97
6.2.2 Materials and methods ..... 97
6.2.3 Results and Discussion ..... 99
6.2.4 *Study V:* Conclusion ..... 102

7 FINAL CONCLUSIONS ..... 104
7.1 Main findings ..... 105
7.2 Limitations and future perspectives ..... 106

SUMMARY IN ENGLISH ..... 107

SUMMARY IN FINNISH ..... 110

REFERENCES ..... 113

ORIGINAL PUBLICATIONS

# 1 INTRODUCTION

## 1.1 Scientific rationale of the research

In everyday physical activity, the human body reacts to the surrounding changing environment around us thanks to the integration of efferent (motor) and afferent (sensory) information performed by our brain (Lattari et al., 2010; Machado et al., 2010). The former comprises the descendent mechanisms directed towards the muscles to produce actions and control body movements. The latter encompasses the ascendent information that the brain receives from "the movement sensors" of our locomotor system (Proske & Gandevia, 2012). These sensors are also known as proprioceptors and they are receptors located in muscles, tendons and joints signaling the brain about changes in body position, or movement of body segments which is an essential property in the human motor control (Konczak et al., 2009). Indeed, an efficient motor output to the muscle producing smooth motor actions is achieved through the functional interactions between multiple areas of the brain, merging sensorimotor information with intentional motor planning (Lattari et al., 2010; Proske & Gandevia, 2012). Diseases or traumatic events may deteriorate this complex neural network resulting in motor impairments. Therefore, the relevance of the *sensorimotor integration* in all human actions has encouraged researchers over decades to investigate how the brain combines the sensorimotor information by analyzing the cascade of events within the two-way brain-periphery pathway not only in lab-controlled environments, but also in real-life settings.
The non-invasive recording of electrical signals generated by the physiological processes within the human body (i.e., biopotentials) could allow for an in-depth investigation of the abovementioned phenomena aimed at a better, comprehensive understanding of the mechanisms hindering the sensorimotor integration. Nevertheless, quantifying the cortical processing of afferent and efferent mechanisms in the sensorimotor cortex is not trivial because of the low signal to noise ratio of biopotential signal recordings and technological challenges related to their acquisition. Previous research has relied on recording

the brain activity using techniques such as magnetoencephalography (MEG) (Piitulainen, Bourguignon, et al., 2015; Piitulainen, Seipäjärvi, et al., 2018) and electroencephalography (EEG) (Alegre et al., 2002; Shibasaki et al., 1980) to map the human brain functions investigating cortical couplings both to muscular activity and somatosensory stimuli. Therefore, additionally to the recording of "central" (i.e., cortical) activity, "peripheral" activity has been tracked by means of the recording of electromyography (EMG), accelerometry, etc. (Piitulainen et al., 2013b; Piitulainen, Illman, et al., 2018; Smeds et al., 2017).

Cortical proprioceptive processing has been quantified by means of corticokinematic coherence (CKC) (Bourguignon et al., 2011), and evoked and induced responses to proprioceptive stimuli. CKC measures the degree of coupling between cortical activity (either MEG- or EEG- based) and kinematics of repetitive movements (i.e., passive movements of limbs, fingers or toes) elicited by custom-made stimulators (Nurmi et al., 2023; Piitulainen, Bourguignon, et al., 2015). Whereas evoked and induced responses reflect the strength of cortical activation and excitability (Hari & Puce, 2017). On the other hand, the degree of coupling between primary somatosensory cortex beta band oscillatory activity (13–30 Hz) and electrical activity of the muscle(s) has been quantified by means of the corticomuscular coherence (CMC) (Conway et al., 1995; Kilner et al., 1999; Piitulainen, Botter, et al., 2015; Riddle & Baker, 2006) which is computed between MEG- or EEG-based measurements and EMG signals.

However, although EEG and EMG techniques are well-established, their use is very limited in naturalistic conditions and movements, because of the current technological gap associated to both wired and wireless acquisition systems that are not optimized to collect high-quality data during movements. As a result, the study of brain signals is restricted to well-controlled and static conditions, leading to the lack of the knowledge not only of the physiological mechanisms occurring during daily movements or sports, but also of the signal properties and related technological issues during dynamic tasks (e.g. motion artifacts contamination). The physiological sensorimotor processes might change under particular circumstances due to the execution of specific tasks or as effect of ageing or neurological diseases. Therefore, there is an increasing demand for a wireless and robust recording instrumentation to monitor cortical brain activity during dynamic tasks in more naturalistic environments and conditions.

Recent advancements in the acquisition of electrophysiological signals have laid the basis to overcome barriers limiting the acquisition of high-quality electrophysiological signals during the dynamic tasks. Although these hardware and software innovations have resulted in the novel design of multi-channel, wireless, miniaturized and floating systems for signal acquisition of muscular electrical activity (Cerone et al., 2019; Cerone & Gazzoni, 2018), different considerations might be needed for the recording of brain activity. Therefore, the way to comprehensively study the brain activity in challenging contexts remains an open question.

The aim of this dissertation is to develop, validate and apply innovative technologies and methods for the acquisition of high-quality EEG signals not only during conventional, static tasks, but also in unconstrained movements to examine neurophysiological mechanisms related to cortical sensorimotor integration. By providing the foundations for innovative technological solutions for wireless EEG recordings in dynamic condition, this doctoral project aims at opening new frontiers to extend the tools to examine the physiological and pathological human sensorimotor system, to advance the research in the field of innovative rehabilitation and diagnostic solutions.

## 1.2 Studies included in the thesis

This PhD thesis delves into the investigation of the human neocortex functions to a new minimally restricted level by means of originally developed methods and technologies allowing combined EEG-EMG recordings in more naturalistic experimental conditions.
Chapter 2 provides a general view of the background knowledge needed to frame the context of the PhD thesis. It includes a *physiological background* on the anatomy and physiology of the human sensorimotor system, a *methodological background* on the methods for the assessment of sensorimotor system and a *technological background* examining the state of the art in the acquisition of biopotential signals.
Chapter 3 declares the purpose of the project and the specific research questions for each carried out study.
Chapter 4 provides the analysis of the technological restrictions limiting the recording of EEG biopotentials during tasks outside lab-environments in dynamic contexts. Custom-designed *analytical models* are proposed to hypothesize and describe the genesis of the causes of movement-related constraints (*Study I*).
Chapter 5 describes the *technological progresses* made in the context of the PhD project. An innovative wireless, miniaturized EEG amplifier with a wireless synchronization system was firstly prototyped to meet the requirements of system portability, modularity and integrability with other devices. Therefore, its design and experimental validation with respect to a wired EEG gold standard system during conventional tasks is hereby presented (*Study II*). Additionally, innovative design considerations on electrodes systems were proposed to deepen the study of the motion artifacts. The causes of this type of artifacts previously discussed in Chapter 4 are experimentally tested through ad-hoc developed electrode systems and their design and relative results are hereby presented in Chapter 5 (*Study III*).
Chapter 6 describes the performed neurophysiological studies investigating the brain-body interactions during static and dynamic conditions with the miniaturized EEG system. Specifically, the cortical proprioceptive processing with and without a maintained voluntary muscle activity during proprioceptive stimulation is investigated (*Study IV*). Finally, this section reports a proof-of-concept

study on the feasibility of the wireless EEG unit to extract neurophysiological outcome variables such as corticomuscular coupling and somatosensory responses in dynamic contexts (*Study V*).

This thesis is based on four original publications reported at the end of this dissertation and hereby summarized:

1. Cerone-Giangrande et al., 2022;
2. Giangrande, Cerone, et al., 2024;
3. Giangrande, Botter, et al., 2024;
4. Giangrande, Mujunen, et al., 2024.

Specifically, results of *Studies I* and *III* are presented and thoroughly examined in publication n.3 (Giangrande, Botter, et al., 2024). Results of *Study II* are reported and fully discussed in publication n.1 (Cerone-Giangrande et al., 2022). *Study IV* is outlined and explored in detail in publication n.2 (Giangrande, Cerone, et al., 2024) and in publication n.4 (Giangrande, Mujunen, et al., 2024). The outcome of *Study V* has not been published.

## 1.3 Structure of the thesis

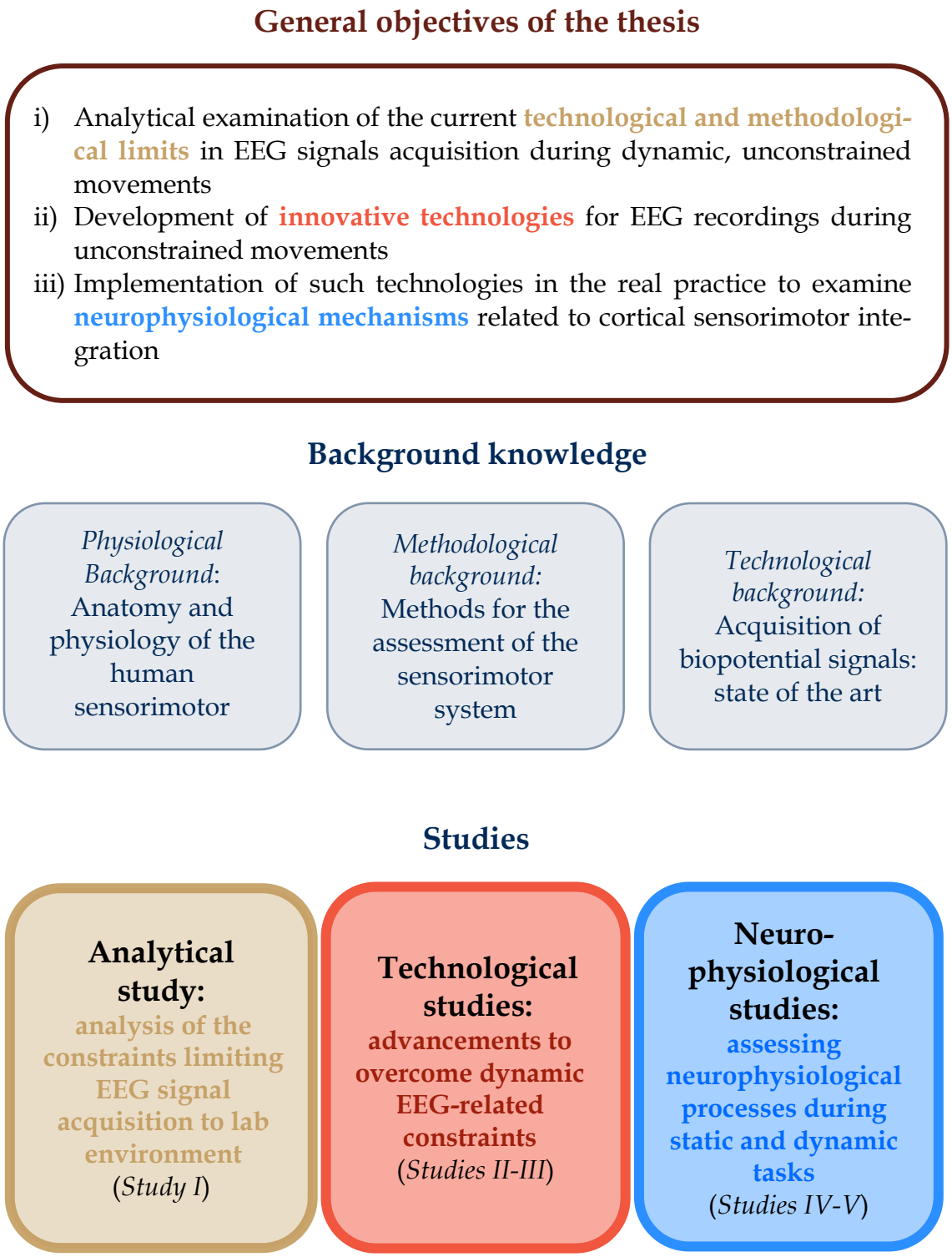

## SUMMARY OF THE STUDIES

| | *Study I* | *Study II* | *Study III* | *Study IV* | *Study V* |
|---|---|---|---|---|---|
| **TITLE** | **EEG motion artifacts assessment** | **Design and validation of a wireless-EEG system** | **EEG motion artifacts evaluation through innovative EEG electrodes systems** | **Assessment of cortical proprioceptive processing of ankle joint rotations** | **Proof-of-concept study: dynamic EEG recordings** |
| **RESEARCH QUESTION** | **Q1:** What are the phenomena leading to the genesis of motion artifacts in EEG signal acquisition? | **Q2:** How does an innovative wireless-EEG system perform when compared to a gold standard wired EEG system? | **Q3:** To what extent EEG electrodes systems with limited movements of cables and electrodes affect the recording of high quality EEG signals? | **Q4:** How does maintained volitional muscular activation affect the cortical processing of naturalistic continuous and intermittent ankle joint proprioceptive stimulation? | **Q5:** Is it feasible to extract physiological outcome measures from wireless EEG recordings during dynamic tasks? |
| **HYPOTHESES** | **H1:** Hypotheses and electrical models on the sources of motion artifacts at different levels: the skin-electrode interface, the connecting cables, and the electrode-amplifier system. | **H2:** Robust performance of the wireless EEG system is expected given its system architecture and design. | **H3:** High quality EEG signals during dynamic tasks are hypothesized when minimizing cables and electrodes movements. | **H4:** An enhanced cortical proprioceptive processing is hypothesized when a muscular contraction is performed as a result of a multi-level mechanism affecting from the muscular to the spinal and the cortical levels. | **H5:** Positive outcomes are expected being the EEG setup particularly optimized for dynamic EEG recordings. |

| | | | | | |
|---|---|---|---|---|---|
| **PARTICIPANTS** | No participants | 11 healthy subjects<br>24-40 y.o.<br>5 females, 6 males<br>height: 1.74 m ± 0.6 m<br>mass: 72.3 kg ± 4.5 kg | 1 healthy subject<br>34 y.o.<br>1 male<br>height: 1.7 m<br>mass: 90 kg | 25 healthy subjects<br>21-32 y.o.<br>11 females, 14 males<br>height: 1.71 m ± 0.8 m<br>mass: 71.6 kg ± 12.4 kg | *CMC study:*<br>5 healthy subjects<br>29-34 y.o.<br>2 females, 3 males<br>height: 1.68 m ± 0.2 m<br>mass: 77 kg ± 3 kg<br>*SEP study:*<br>5 healthy subjects<br>39-44 y.o.<br>1 female, 4 males<br>height: 1.79 m ± 0.9 m<br>mass: 74.3 kg ± 9.8 kg |
| **RESULTS** | **R1:** Suitability of the models to embody real experimental situations: the movements of the cables and electrodes are the main factors influencing the recording of EEG motion artifacts. | **R2:** Good agreement between the wireless and wired EEG system with no device-specific differences during a set of static experimental conditions. | **R3:** Negligible EEG motion artifacts when using EEG electrodes systems specifically developed to disentangle the possible causes of motion artifacts (i.e., connecting cables and electrodes technology). | **R4:** Volitional muscle activation intensifies neuronal processing of proprioceptive afference in the somatosensory cortex and EEG-based outcome measures can be used to track such changes. | **R5:** Feasibility to extract significant CMC during walking and jogging and reproducible SEPs during cross-country skiing. |
| **RESEARCH PAPER** | Publication n.3 (Giangrande, Botter et al. 2024). | Publication n.1 (Cerone-Giangrande et al. 2022). | Publication n.3 (Giangrande, Botter et al. 2024). | Publication n.2 (Giangrande, Cerone et al. 2024).<br>Publication n.4 (Giangrande, Mujunen et al. 2024). | |

# 2 BACKGROUND AND STATE OF THE ART

This Chapter aims at providing the basic knowledge for the general understanding of the present dissertation from both the physiological and technical point of views. It delves into the description of the anatomy and physiology of the body structures under investigation (i.e., the central nervous system and the musculoskeletal system) and of the main methodologies used to non-invasively extract information about brain-body interactions. Finally, an overview of the state of the art technologies for the assessment of sensorimotor integration is provided, highlighting the current needs and open issues on high-quality EEG signal acquisition in contexts other than laboratory environments.

## 2.1 Anatomy and physiology of the human sensorimotor system

The sensorimotor system is an extremely complex network playing an important role in human motor control. It is, indeed, responsible for: processing external stimuli, perceiving and processing internal sensations, and generating a motor response accordingly. Therefore, the sensorimotor system encompasses all the structures involved in the sensory, motor and central integration and information processing (Riemann & Lephart, 2002). FIGURE 1 shows a schematic representation of the sensorimotor system. It consists of a two-way pathway from the brain to the periphery: an efferent (motor) route and an afferent (sensory) one. The former comprises the descendent information (i.e., motor command) generated within the primary somatosensory (S1) and motor (M1) cortices of the brain and directed towards the muscles to produce actions. According to this pathway information travels along the pyramidal tract thanks to upper (from the cortex to the spinal cord) and lower (from the spinal cord to the muscles) motor neurons (Carpenter, 1994). The latter afferent pathway encompasses the ascendent information (i.e., somatosensory feedback) that is conveyed to the brain by the "the movement sensors" of the musculoskeletal system (e.g. receptors located in muscles, tendons and joints and peripheral afferences)

(Konczak et al., 2009). Afferent proprioceptive pathways to the brain travel primarily along the afferent dorsal column-medial lemniscus first to the spinal cord (through first-order neurons), then to the subcortical structures such as the thalamus (through second-order neurons) and finally to the cerebral cortex (through third-order neurons) (Purves et al., 2018; Tuthill & Azim, 2018). The integration of these two, already intricate, pathways through the functional interactions between multiple areas of the brain (including e.g. the cerebellum) is particularly important to produce an efficient motor output generating fine-tuned, well-balanced and smooth motor actions (Deiber et al., 2012; Lattari et al., 2010; Proske & Gandevia, 2012).

### 2.1.1 The primary somatosensory and motor cortices

The site where the basic integration between the sensory information and the intentional motor commands are integrated is the sensorimotor cortex (SM1). Information exchange is made possible within the brain due to specialized excitable cells called neurons. The communication between neurons and other cells is achieved by means of the transmission of action potentials generated by trans-membrane depolarization following a combination of electrical and chemical phenomena (Zhang, 2019). FIGURE 2 shows the anatomy of the SM1. It refers to the primary somatosensory (S1) and motor (M1) areas which are located

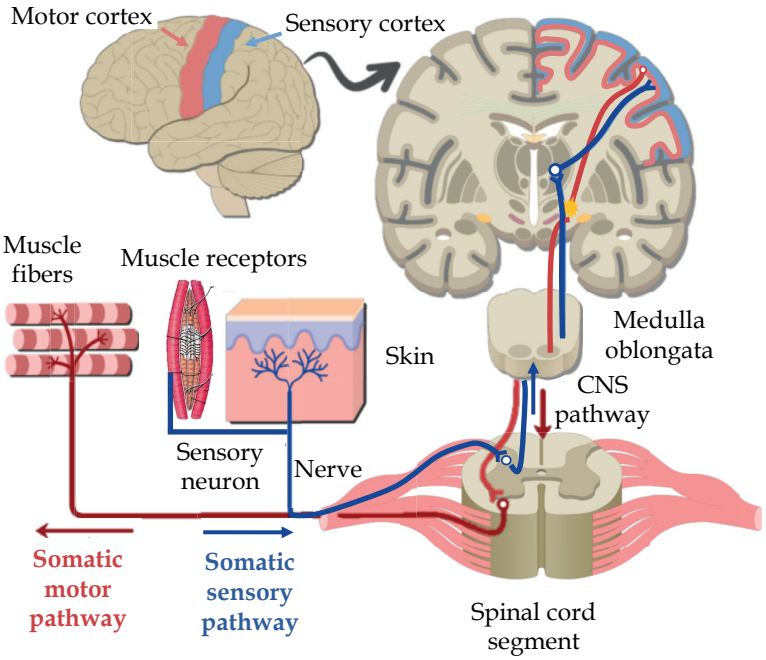


FIGURE 1 Schematic representation of motor (red) and somatosensory (blue) pathways. The former is generated within the motor cortex and directed to the muscle fibers of the muscles allowing for the performance of movements. The latter starts at peripheral level and regards the activity of sensory neurons innervating muscle spindle or skin receptors and it is directed towards the sensory cortex. Adapted from getbodysmart.com and kenhub.com.

over the central sulcus on both sides of the scalp, with the M1 placed anteriorly with respect to the S1 (Kelly & Dodd, 1991). The S1 is the target of the afferent sensory pathway arising from the contralateral body portions via the thalamus, while M1 represents the site where movements are initiated by sending the efferent information to the movement executors via the corticospinal tract (Martin & Jessel, 1991). Nevertheless, bilateral primary motor regions are not idle when no motor action is performed. Dense inter- and intra-hemispheric connections, instead, occur to properly combine information from different sensory modalities aimed at movements modulation and optimization (Carson, 2005; Deiber et al., 2012; Kandel et al., 2000). All the connections within the SM1 undergo continuous reorganizations and functional modifications according to the needs of prioritizing certain neural networks and this aspect, called brain plasticity, is an essential feature of the nervous system to adapt to changing situations (Vogels et al., 2011).
Clinical observations and experimental works demonstrated that the SM1 is functionally organized by following a somatotopic arrangement meaning that specific portions of the SM1 cortex are related to the activity of skeletal muscles of specific body parts (Kaas, 2005). As shown in FIGURE 2 C, the upper body portions and the face are mapped bilaterally in the cortices while the lower limbs (i.e., legs and feet) are represented more medially towards the longitudinal fissure. The cortical representation support of a specific body portion depends on the degree of needed tactile sensitivity and the density of motor efference of that body part. Therefore, wider represented cortical areas are associated to body regions with better tactile sensitivity and fine motor control (Hsiao, 2008).

### 2.1.2 The human musculoskeletal system

The human musculoskeletal (or locomotor) system comprises a series of anatomical structures as target of brain-muscles communication. The muscular

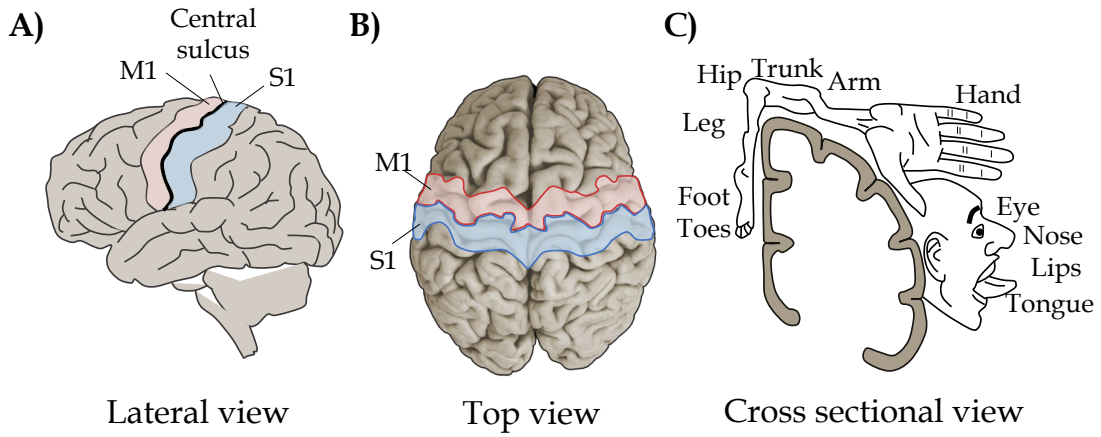


FIGURE 2 Anatomy of the sensorimotor cortex. A) Lateral and B) top view of the human cortex. Primary sensory (S1) and motor (M1) cortices are high-lighted respectively in light- blue and red colors. C) Cross sectional view of the sensorimotor cortex (right hemisphere) showing the somatotopic cortical arrangement. Modified from (Betts et al., 2013).

system includes skeletal contractile muscles and tendons, whereas the skeletal system includes the mechanical structures constituted by bones, joints and associated tissues providing a framework for the body. While the former structures are the movement actuators allowing for the movement performance or posture maintenance, the latter skeletal structures are equally important in the context of motor control as they are part of the somatosensory system providing information to the central nervous system (CNS) about the internal state of the musculoskeletal system itself (Sherrington, 1916).
Movements are caused by the contraction of skeletal muscles driven by neural commands generated within the motor cortex and travelling through spinal cord circuits and specialized neurons, called alpha motor neurons, towards the muscles (Davis & Kovac, 1981). The muscle fibers contraction is then caused by the muscle tissue depolarization following such stimuli. FIGURE 3 shows a schematic representation of anatomy and physiology of muscle activation. The basic functional unit of a skeletal muscle is referred to as motor unit (MU) and it is composed of a motor neuron and its innervated muscle fibers (ranging from 5 to 2000) (Duchateau & Enoka, 2011). Cell bodies of motor neurons are located in the ventral horn of the spinal cord and their axons exit the spinal cord through the ventral root projecting in spinal nerves to terminate on striated muscles. The transmission of the neural command is made possible by the excitable membrane composing the motor neurons which allows the electrical pulse (i.e., action potential) generated at cortical level to travel towards specific sites of the muscle fibers called neuromuscular junctions. Once the action potential reaches the neuromuscular junction, two action potentials are propagated in opposite directions along the innervated muscle fibers towards the tendon endings, triggering the fibers contraction. Therefore, the synchronous summation of the propagating action potentials of all the fibers innervated by the same motor neuron goes under the name of motor unit action potential (MUAP).

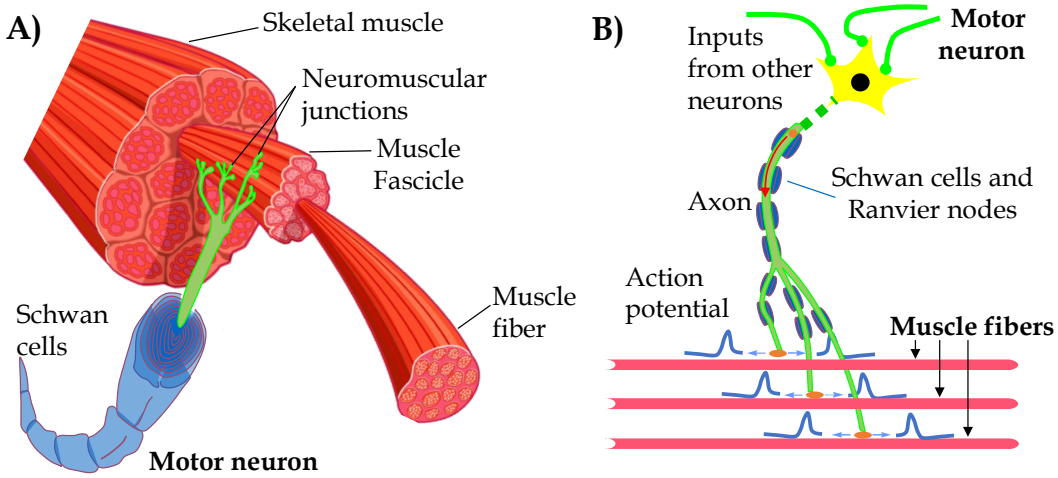


FIGURE 3 Anatomy and physiology of muscle activation. A) Cross sectional view of the muscle with its principal anatomical compartments: muscle fascicles and fibers innervated by a motor neuron. B) Motor unit transmitting the neural input to the innervated muscle fibers. Images courtesy of Laboratorio di Ingegneria del Sistema Neuromuscolare (LISiN), Dipartimento di Elettronica e Telecomunicazioni, Politecnico di Torino.

The regulatory feedback about movements and changes in position of body segments performed by the synergic activity of muscles and joints is continuously sent to the CNS thanks to specialized structures located in the muscles, joints, ligaments, and tissues surrounding the joints (Van Beers et al., 2002). These structures are peripheral mechanoreceptors known as proprioceptors. Proprioception is part of the somatosensory system, and it refers to the ability to inform the CNS about the internal state of the musculoskeletal system (Moon et al., 2021). Proprioceptors located in skeletal muscle include Golgi tendon organs, muscle spindles and joint receptors and they are represented in FIGURE 4. Golgi tendon organs (FIGURE 4 B) are responsible of sensing changes in muscle tension. They are made up of branches of afferent neurons located in the network of collagen fibers within the tendons (Benjamin et al., 2008). Muscle spindles (FIGURE 4 C) are, instead, in charge of signaling changes in muscle length. They consist in intrafusal muscle fibers surrounded by a capsule embedded within the fibers of skeletal muscles. When the muscle length varies, the stretch level of the intrafusal fibers changes accordingly, thus increasing the rate of discharge of the sensory afferents which promptly transmit the information about position and dynamics of the limb towards the brain (Matthews, 1964). Nevertheless, muscle spindles are additionally sensitized because of the firing of gamma motor neurons to the intrafusal muscle fibers. The role of the gamma motor neurons is not to add force to the muscle contraction, but rather to regulate the afferent input by adjusting the level of tension in the intrafusal muscle fibers of the muscle spindle allowing the spindles to deliver information centrally at all muscle lengths. Additionally, the activity of gamma motor neuron itself can also be modulated to fine adjust challenging and precise fine movements, independently from the motor drive sent through the lower motor neuron pool (Purves et al., 2018).

## 2.2 Methods to investigate the sensorimotor system

Studying biopotential electrical signals recorded from the skin surface is a valuable technique used to obtain information about how brain and muscles function and how they integrate their mutual activity. Biopotentials are electrical signals recorded as difference of electrical potentials between two or more points, called detection points and a reference site. Electrical activity is generated by excitable biological tissues such as the ones constituting the heart, the brain and muscles, where electrical current flows because of continuous ionic exchanges (Thakor, 1999). With the aim of examining the aspects related to sensorimotor integration mechanisms, central (i.e., brain-related) and peripheral (i.e., muscle-related) information should be combined to provide further insight into the human motor control and functioning. Thus, the following dissertation will be focused on biopotentials recorded from the brain (Electroencephalography - EEG) and the muscles (Electromyography - EMG) as well as other peripheral recordings concerning body kinematics and kinetics.

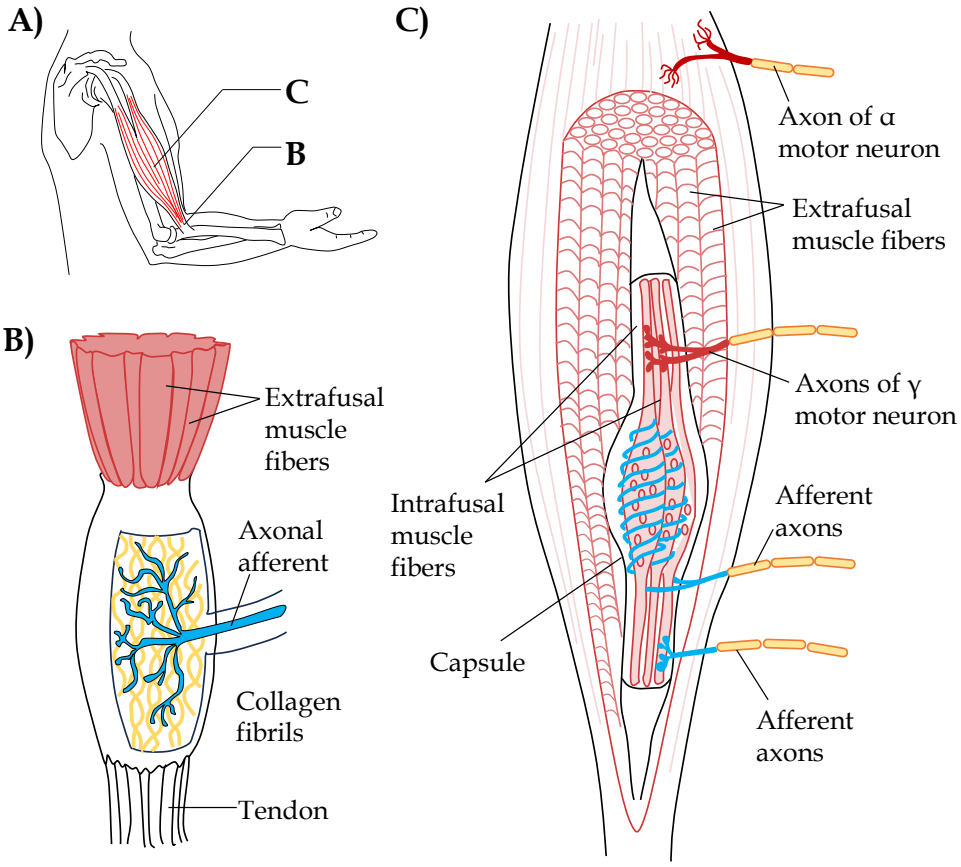


FIGURE 4 Proprioceptors in the musculoskeletal system. A) Lateral view of a muscle (biceps brachii) with two sites of mechanoreceptors specialized in proprioception. B) Golgi tendon organs and C) muscle spindles receptors schematic representation with their main constituents. Taken from (Purves et al., 2018).

### 2.2.1 The brain: Electroencephalography (EEG)

Electrical signal generated by the neuronal activity within the brain and recorded from the scalp surface is referred to as Electroencephalography (EEG). EEG signal detects the synchronous activity of large groups of neurons, belonging to several different neuronal populations (Schutter & Hortensius, 2011). FIGURE 5 provides a schematic representation of EEG signal source. Specifically, the EEG signal is given by the summation of excitatory and inhibitory post-synaptic potentials of pyramidal neuronal cells which are in turn the result of action potentials of depolarized pre-synaptic neurons. At a single neuron level (FIGURE 5 B), the net flow of ions within soma and dendrites generates current dipole (primary current). Since the currents cannot accumulate in any part of the brain, under the hypothesis that the brain is a conductive homogeneous medium, the primary current is always associated with return secondary currents (volume currents) closing the loop. As a result, an electric dipole is generated along the direction of the neuron itself (Hari & Puce, 2017). Therefore, EEG is most sensitive to electrical currents oriented radially to the cortex and close to the detection

points, but it can be also sensitive to tangential and strong deep currents (Da Silva, 2023) (FIGURE 5 A).
Brain activity could also be measured through other technologies such as Magnetoencephalography (MEG), or functional Near infrared spectroscopy. However, the present dissertation will be focused on electroencephalography because of its advantages with respect to the other methodologies in the view of enabling cortical measurements in minimally restricted naturalistic conditions. Firstly, EEG provides a good compromise of spatial and temporal resolution being able to discern sources in the centimeter range and to catch changes over milli-seconds. Secondly, EEG-instrumentation involves smaller acquisition systems than other brain technologies, thus it is easy to transport as, e.g. contrarily to MEG, it has not to be performed exclusively in ad-hoc rooms. Thirdly, EEG has low related costs both of implantation and usage and it is suitable to acquire brain signals from different groups e.g. ranging from newborns to the elderly, from sedentary participants to athletes, from healthy to clinical populations (Beniczky & Schomer, 2020).

#### 2.2.1.1 Basic characteristics of EEG signals

Recorded EEG signals are expressed in Volts (typical magnitude order of a few hundreds of microvolts), with a spectral content between 0.1 Hz and 100 Hz. EEG signals can be evaluated both in time and frequency domains. Specifically, the continuous, repetitive EEG activity occurring at defined frequency ranges is referred to as cortical rhythm. TABLE 1 shows the main physiological EEG cortical rhythms (Lattari et al., 2010).

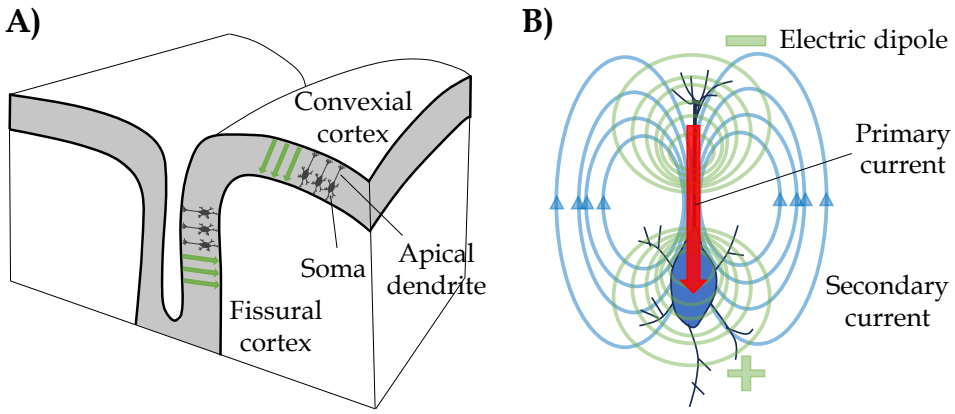


FIGURE 5 Schematic representation of EEG signal source. A) Sectional view of the cortical surface. Neurons are modelled in black with the current dipoles (red arrows). The current flow may point the opposite direction with respect to the depicted one according to the type of postsynaptic current (excitatory/inhibitory). B) Schematic representation of the current dipole generation in a single neuron. Figure adapted from (Hari & Puce, 2017).

TABLE 1 Summary of the EEG cortical rhythms.

**EEG cortical rhythms**

| Rhythm | Frequency | RMS Amplitude | State |
|---|---|---|---|
| Delta | 1 Hz – 3 Hz | 20 μV – 200 μV | Pathological conditions (e.g. coma), very deep sleep |
| Theta | 4 Hz – 7 Hz | 5 μV – 10 μV | Meditative or sleep state |
| Alfa | 8 Hz – 12 Hz | 15 μV – 45 μV | Relaxed state, boredom, eyes closed |
| Beta | 13 Hz – 30 Hz | 10 μV – 20 μV | Awake state, sensorimotor processing |
| Gamma | 30 Hz – 100 Hz | 1 μV – 20 μV | Peak concentration, positive mood, and creativity |

Several cortical rhythms have been recognized throughout the history of EEG signal analysis and they have been associated with specific states of the subject according to the signal amplitude and frequency content (Babiloni et al., 2006). Additionally to the abovementioned cortical rhythms, the *mu* rhythm has been introduced by H. J. Gastaut & Bert, 1954 dealing with the assessment of sensorimotor integration. Although it is party overlapped with alpha and beta rhythms in terms of the frequency content, it is thought to have different neural sources as it is differently distributed within the scalp (Salenius et al., 1997). Indeed, while alpha waves characterize the frontal or the occipital brain areas, the mu-rhythm specifically originates in the primary SM1 area. It has a typical arc-like shape and it has been associated to executed motor actions (H. Gastaut, 1952). The mu-rhythm consists of two different frequency sub-bands: the former around 10 Hz referred to as mu-alpha and the latter around 20 Hz referred to as mu-beta (Hari, 2006). Contrarily to the mu-alpha that did not demonstrate clear somatotopy, the mu-beta has been shown to be somatotopically organized (appearing lateral in the Rolandic cortex after mouth movements, more medial after finger movements, and close to midline after foot movements) (Hari, 2006; Salmelin et al., 1995). The mainly investigated frequency band considered to be involved in both somatosensory processing and motor control is the mu-beta which showed strong correlation with the human corticospinal excitability and therefore considered a reliable tool to monitor the functional state of the primary motor cortex (Diesburg et al., 2021; Hussain et al., 2019). However, the temporal and spectral content of EEG signals across cortical rhythms might change in response to external stimuli or performed tasks. Because of the abovementioned characteristics regarding the frequency and amplitude ranges, EEG signals have a relatively low Signal to Noise Ratio (SNR). This implies two important aspects in terms of both signal recording and processing. From a technological point of view, the recording of high quality EEG signals requires the design of high resolution acquisition systems with low input noise, while from an analytical perspective, averaging techniques are often needed to improve the SNR and obtain a clear response. The way how the brain activity is modulated in healthy and pathological populations has been widely investigated over decades by means of evoked and induced EEG responses, objectives of the following sections.

#### 2.2.1.2 Evoked EEG responses

Time-domain EEG signal analysis has been focused for decades on the evaluation of evoked EEG responses (i.e., potentials) to a multitude of external stimulus types which, in these contexts, are also known as event related potentials (ERP) (Hari & Puce, 2017). FIGURE 6 A shows the basic principles of extracting evoked EEG responses. These responses are obtained by applying a stimulus-triggered averaging technique on EEG signals because they occur time- and phase-locked with the provided stimuli. Specifically, continuous EEG signals are divided into segments (i.e., epochs) according to the number of the provided stimuli and then averaged to highlight the stimulus-related response with respect to the ongoing EEG activity. EEG epochs include a pre-stimulus (usually of 100 ms-200 ms) and a post-stimulus period ranging from 200 ms up to 700 ms according to the brain activity to be tracked. The pre-stimulus period is typically removed from the post-stimulus to get rid of the baseline status preceding the response (Hu et al., 2014) . Evoked responses appear as post-stimulus positive or negative deflections with respect to the baseline that are time-locked and phase-locked to the given stimuli. They have been characterized by introducing a specific nomenclature combining the peak polarity (*N* for negative, *P* for positive) and the value of the peak latency expressed in milliseconds. The polarity refers to the signal amplitude computed with respect to the pre-stimulus baseline (i.e., average of the EEG signal amplitude prior the stimulus). Whereas the latency is a time-domain measure as it is referred to the time taken to reach a local response peak after sending the stimulus. As an example, a P300 component refers to a positive deflection occurring at 300 ms after the stimulus onset. Typical peak amplitudes range from few to tens of microvolts with latencies spanning from tens to hundreds of milliseconds (Picton & Hink, 1974). Experimental paradigms designed to elicit robust evoked responses account for: (i) averaging a number of repetitions ranging from tens to hundreds of single stimuli to increase the SNR of the recorded response, (ii) a randomized Inter-Stimulus-Interval (ISI) to minimize the effect of cortical habituation, (iii) a proper stimulus intensity at least above the threshold of sensation (Hari & Puce, 2017), (iv) a high degree of synchronization between the recording systems. Evoked responses have been evaluated to assess cortical activity across various stimulation types such as sensory stimulation like auditory, visual, somatosensory (i.e., muscle/nerve electrical stimulation), but also during movement performance, dual task paradigms or motor imagery tasks (Babiloni et al., 1999; Lifshitz, 1966; Savers et al., 1974). These responses are typically highly reproducible both intra- and inter-subject and therefore suggested to be used as reliable tool to evaluate the integrity of the afferent sensory pathways (Ciganek, 1967; Virtanen et al., 1998). Nevertheless, specific experimental paradigms (e.g. cognitive state alterations) might be accompanied by a higher intra-trial response variability that can be taken into account by evaluating single-trial responses (Ratcliff et al., 2009).

#### 2.2.1.3 Induced EEG responses

Induced responses have been proposed as a measure to quantify the modulation of the SM1 cortex beta-band power (~ 14 Hz – 32 Hz) during a stimulation as they are thought to provide information on the degree of cortical inhibition-excitation (Illman et al., 2023; Mujunen et al., 2022; Parkkonen et al., 2017; Vinding et al., 2019). FIGURE 6B shows the basic principles of extracting induced EEG responses. They are stimulus-triggered modulations of the spectral EEG content, but they are not phase-locked to the stimulus and often not time-locked (Skosnik & Cortes-Briones, 2016). Therefore, the application of time-domain stimulus-triggered averaging does not allow to extract any response because of the random phase relationship (Adjamian, 2014). In this view, a specific method firstly introduced by Salmelin and Hari (Salmelin & Hari, 1994) has been proposed to evaluate induced EEG activity known as the Temporal-Spectral Evolution (TSE) method. It is applied to EEG signals filtered in the beta frequency band and then rectified applying a Hilbert transform. While evoked responses are concentrated within 1 s post-stimulus, induced responses typically occur after several seconds after the stimulus onset and they typically show reduced response strengths (Ramkumar et al., 2012). Thus, EEG signals are segmented into epochs whose length ranges from ~ −1 s to ~ 3 s with respect to the stimulus onset. The evoked responses are then subtracted from the post-stimulus period (David et al., 2006). Induced responses to somatosensory stimuli over the SM1 area are characterized by an early reduction of the beta power (suppression) and a delayed increase of the beta power (rebound) (Barone & Rossiter, 2021; Engel & Fries, 2010; Salmelin & Hari, 1994; Tan et al., 2016). The former deflection has been related to the degree of cortical activation due the somatosensory afference and it reflects the motor preparation or planning of movement (Barone & Rossiter, 2021; Engel & Fries, 2010; Tan et al., 2016). On the contrary, the latter beta rebound likely reflects intra- or intercortical inhibition occurring also at thalamic and sub-thalamic levels and it is related to the resting- or idle- state of the sensorimotor cortex (Bizovičar et al., 2014; Brittain et al., 2012). These beta modulations have been found bilaterally over the SM1 cortices during unilateral stimulation, but always following the somatotopic organization of the sensorimotor cortex. Beta suppression and rebound are characterized in terms of amplitude with respect to the baseline level and latency with respect to the stimulus onset. Although the not negligible inter-individual variation likely due to the variability of the individual functional anatomy (Illman et al., 2022; Mujunen et al., 2022), the reproducibility and robustness of the induced responses has been validated in the recent literature in various contexts and scenarios. SM1 induced responses have been found during proprioceptive stimulation (Alegre et al., 2002; Cassim et al., 2000; Parkkonen et al., 2015; Toledo et al., 2016), executed, observed or even imagined movements (Neuper et al., 2009; Pfurtscheller et al., 2005; Salmelin et al., 1995) even though eliciting different response strengths. As a result, induced EEG activity has been proposed as a biomarker to assess the sensorimotor cortical function and its adaptations to exercise, rehabilitation, and disease.

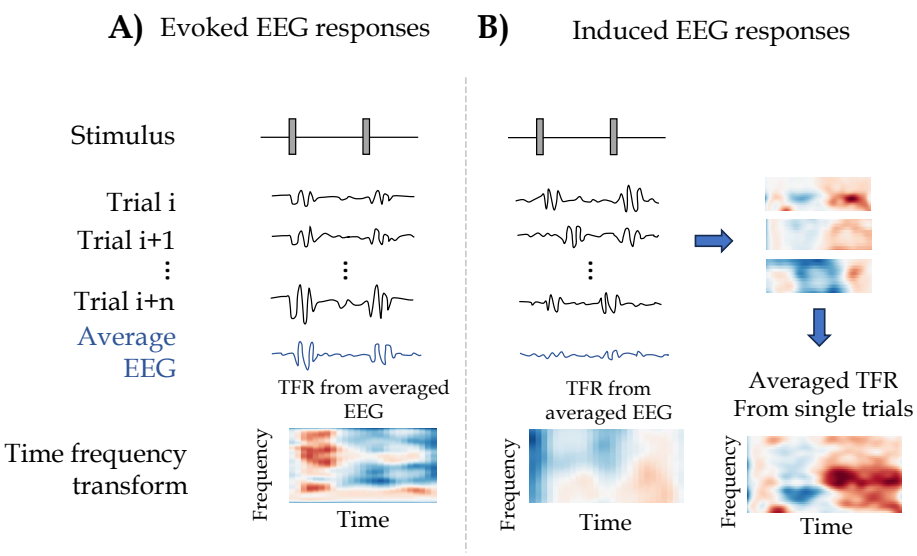


FIGURE 6 Basic principles of evoked and induced EEG responses. A) Evoked responses are time-locked and phase-locked to the stimuli. Stimulus-triggered averaging techniques allow to cancel out the non-phase locked oscillation and elicit the response. B) Induced responses are not phase-locked to the stimulus and often non-time-locked. Hence, an analysis in the time-frequency domain should be performed on single trials prior performing the average. Generated *de novo* by the authors inspired by (Skosnik & Cortes-Briones, 2016).

### 2.2.2 Recording movement: kinematic, kinetic and electromyographic recordings

Peripheral recordings are referred to the acquisition of information related to the musculoskeletal system during limb movements. Motion descriptors, therefore, include the recording of kinematic, kinetic and electromyographic activity measurements.

Kinematic recordings describe limb displacement, joint angles, velocity and acceleration over time. Sensors such as accelerometer, magnetometer, gyroscope, or joint goniometer can be adopted in the experimental design to track the body kinematics (Eckhouse et al., 1996). Kinetics regards the study of motion and it includes considerations on forces generated by or applied to the human body as well as torque interpreted as the interaction of forces associated with external loads and muscle activity. Therefore, example of sensors providing kinetic information mainly include force sensors (e.g. load cells) (Bachschmidt et al., 2001).

Muscular activity initiated within the cortex and travelling through the motor neurons towards the skeletal muscles can be recorded by means of Electromyography (EMG). Within the present dissertation EMG refers to the non invasive recording of biosignals from the skin surface, thus commonly known as (surface)EMG (sEMG). FIGURE 7 shows a schematic representation of the EMG signal source. When performing a muscle contraction, the brain recruits only a certain number of motor units (Clamann, 1993).

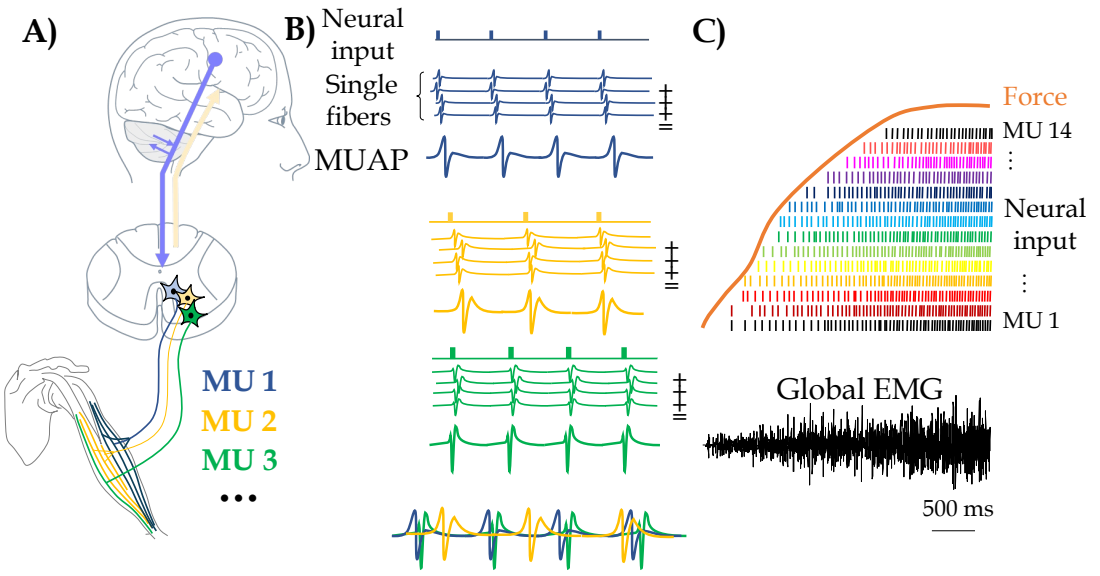


FIGURE 7 Schematic representation of EMG signal source. A) Motor drive generated within the motor cortex is directed towards different motor units. B) Summation principle of single fibers MUAP from separated motor units. C) Global EMG as a result of the neural input to several motor units.

Therefore, EMG signal is the result of the spatial and temporal summation of the single MUAP related to the activated muscle fibers (Farina et al., 2002; Merletti & Farina, 2016; D. F. Stegeman et al., 1997). Although EMG signal characteristics vary according to anatomical, physical, and detections system parameters (e.g. the length of the fibers, the thickness of the subcutaneous tissue layer, the depth of the investigated muscle, the shape and size of the detection system, etc.) (Dimitrova et al., 1999), recorded EMG signals peak amplitudes are around some milli-Volt , with a spectral content ranging from 10 Hz to 500 Hz. However, muscle contraction can be also elicited by neuromuscular electrical stimulation delivered to a nerve trunk or muscle belly (Doucet et al., 2012). This technique allows the activation not only of the motor pathway (i.e., increasing the alpha motor neurons discharge without involving the central nervous system), but also of the sensory pathway (i.e., increasing the firing of the primary afferences directed from the periphery to the brain) (Bergquist et al., 2011). Under this condition, EMG recordings track the so-called H-wave and M-wave pathways eliciting two distinguished waveforms in the collected signals. FIGURE 8 represents the two pathways initiated through the electrical stimulation of the muscle. With low intensity and short duration electrical stimuli, an action potential is generated at the level of the sensory afferences directed towards the spinal cord (blue arrow) which elicits in turns action potentials travelling through the motoneurons to the muscle. The MUAPs can be non-invasively recorded through sEMG as they generate an H-reflex occurring ~30 ms after the stimulus (Palmieri et al., 2004). With higher intensity stimulation, the electric pulse origins action potentials directly in the motoneurons (all or some according to the stimulation intensity) travelling in two directions: to the muscle and to the spinal cord.

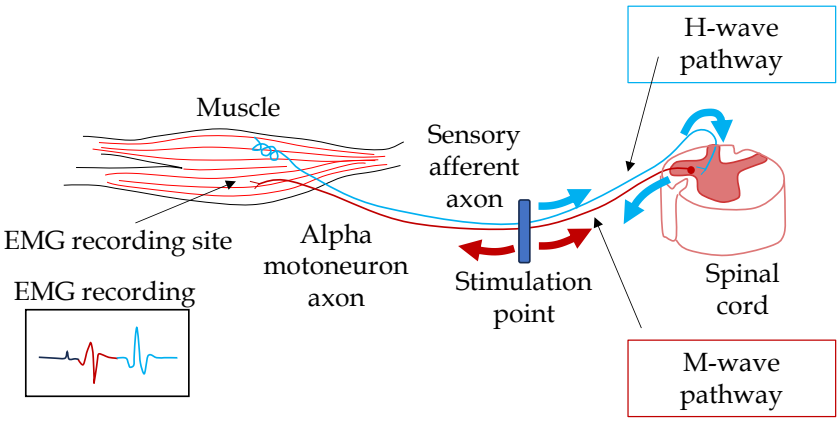


FIGURE 8 Hoffmann reflex (H-reflex) and muscle response (M-wave) pathways elicited by nerve or muscle electrical stimulation. Adapted from (Lienhard, 2015).

The former volley is responsible for the generation of the M-wave occurring at ~10 ms after the stimulus onset, while the latter causes the partial or total cancellation of the H-reflex. An electrophysiological variation of the H-reflex, known as V-wave, is measured during ongoing maximal muscle contraction and it also can be recorded by EMG (Duclay & Martin, 2005). These sensory signals are further relayed from the muscles to the cerebral cortex according to feedback loop involving the motor cortex (Marsden et al., 1973). Therefore, because of their functioning principles, H-reflexes and V-waves have been used to investigate the neural modulation of the efferent motoneuronal output under different conditions (Nevanperä et al., 2023).

### 2.2.3 Corticospinal coupling: Coherence measurements

Brain-body interactions occurring during sensorimotor processes have been primarily assessed through coherence measures quantifying the degree of coupling between central (e.g. EEG) and peripheral (e.g. EMG, kinematic) recordings. Two types of interactions have been highlighted: cortex-kinematic and cortex-muscles interactions. The former quantifies the degree of coupling between cortical information and the movement kinematics and it is referred to as corticokinematic coherence (CKC). The latter measures the coupling between cortical and muscular activity while performing a movement and it is known as corticomuscular coherence (CMC) (Bourguignon et al., 2019). As a result, these measures are thought to be powerful instruments to evaluate the integration of afferent and efferent information. FIGURE 9 represents a summary of corticokinematic and coherence analysis using the formulation of Halliday et al., 1995. Specifically, EEG, EMG/kinematic collected signals are pre-processed before carrying out the coherence analysis to ensure a proper signal quality and avoid any confounding factors on the observed results. To this end, Independent Component Analysis (ICA) and spatial filtering might be applied on EEG data to improve the SNR. In regards of peripheral recordings, an optional rectification and normalization is performed on EMG data, whereas 3-axes acceleration

signals are combined by computing the Euclidean norm (Piitulainen et al., 2013a). Afterwards, auto- and cross- power spectra are yielded with the purpose of extracting the coherence as follows:

$$Coh(f) = \frac{|P_{cross}(f)|^2}{P_{auto1}(f)P_{auto2}(f)}$$

( 2.1 )

where $P_{cross}$ is the cross-spectrum between the input signals, and $P_{auto1}$, $P_{auto2}$ are the individual auto-spectra of the brain and peripheral signals. From a mathematical point of view, as indicated in Eq. ( 2.1 ), coherence expressed in the frequency domain is analogous to the correlation computed in the time domain. Indeed, a coherence measurement is a non-dimensional number ranging from 0 (i.e., no coupling) to 1 (i.e., perfect matching) indicating the degree of linear dependence in terms of amplitude and phase coupling between the input signals (i.e., EEG and EMG or kinematic signals) (Bourguignon et al., 2019).

CKC has been proposed to track the processing of proprioceptive afferences to the SM1 cortex by quantifying the strength of the coherence spectrum (Nurmi et al., 2023; Piitulainen et al., 2013a; Smeds et al., 2017). Indeed, the neural basis of CKC has been predominantly associated to the afferent input generated by peripheral proprioceptors such as muscle spindles, Golgi tendon organs, skin receptors, with negligible contribution of the tactile inputs (Bourguignon et al., 2015; Piitulainen et al., 2013b). CKC studies typically involve rhythmic passive movements produced by movement actuators specifically designed to primarily elicit the stimulation of the proprioceptive afferent pathways (Lolli et al., 2019; Piitulainen, Bourguignon, et al., 2015; Piitulainen, Seipäjärvi, et al., 2018). Thus, the CKC spectrum computed between brain and any peripheral movement-related signal (e.g. acceleration, velocity, torque) finds its peak at the movement frequency and its harmonics, following the contralateral somatotopic SM1 cortex organization (Piitulainen et al., 2013a). As a result, CKC has been proposed as a tool for the functional motor mapping of the motor cortex and its robustness and repeatability have been widely demonstrated both in upper and lower limb studies (Bourguignon et al., 2011; De Tiège et al., 2020; Piitulainen et al., 2020; Piitulainen, Illman, et al., 2018). On the other hand, CMC evaluates the coupling between sensorimotor cortical rhythms and muscular activity (Conway et al., 1995). The neural generator of CMC is linked to the cortico-motoneuronal pathways originating above the M1 cortex contralateral to the muscle involved in the motor task, according to the cortical somatotopic organization (Brown et al., 2009; Maezawa et al., 2022; Murayama et al., 2001; Salenius et al., 1997). The majority of CMC studies involved the performance of a steady, not fatiguing isometric muscle contraction. In these cases, significant CMC peaks have been found to fall within the beta sensorimotor frequency bandwidth (i.e., 15 Hz – 35 Hz) above the contralateral brain area with respect ot the one involved in the task

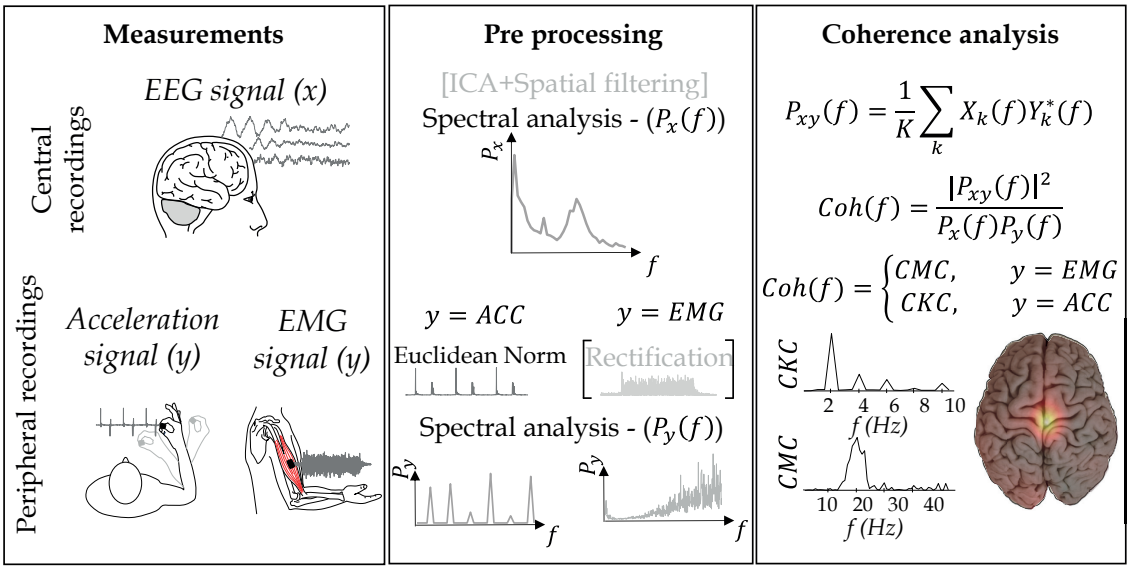


FIGURE 9 CKC and CMC computation to study brain-body interactions. Measurements, pre-processing and coherence analysis steps are indicated.

(Liu et al., 2019; Piitulainen, Botter, et al., 2015). However, when compared to CKC, CMC has shown globally weaker strengths, and a higher inter- and intra-individual variability. Different factors can influence the coherence strength. As examples, the regularity of the stimulus, the movement range, and the number of stimulated joints influence CKC strength (Hakonen et al., 2022; Mujunen et al., 2021; Nurmi et al., 2023). Whereas muscle characteristics such as the size of its cortical representation or its position (i.e., proximal/distal) affect the CMC output (Murayama et al., 2001; Ushiyama et al., 2010). Therefore, brain disorders affecting the efferent and afferent pathways might result in altered CKC and CMC measures, as shown by early evidence (Démas et al., 2022; Roeder et al., 2020; Smeds et al., 2017). As a result, the abovementioned coherence measures have a great potential to assess the relationship between motor efferences and proprioceptive afferences in humans and to provide further insights on the neural adaptations in altered conditions with respect to a relaxes, healthy state such as during exercise, rehabilitation or disorders.

## 2.3 Acquisition of biopotential signals

The recording of biopotential signals requires some crucial steps before they can be manipulated by the users. Indeed, biopotentials such as EEG or EMG are characterized by generally low signal amplitudes. As a result, they need to be properly amplified to improve the SNR and to reject the external interferences coming from both internal (from inside the body) or external (coming from outside the body) sources. In addition, a proper signal conditioning is needed to sample the continuous signals and to reject disturbances that are outside the frequency range of interest. Therefore, biopotential signals are filtered and

converted from an analog to a digital format to be consequently visualized on a digital support and eventually further processed. These intermediate stages are borne by ad-hoc designed instrumentation generally referred to as biopotential acquisition system (Merletti & Cerone, 2020; Yaziciouglu et al., 2009).

### 2.3.1 Block diagram of biopotential acquisition system

FIGURE 10 depicts a simplified diagram of a biopotential acquisition system as composed of three main blocks: the transduction stage, the analog electronics and the digital electronics. The transduction stage includes sensing electrodes placed on a specific site (i.e., either the scalp for EEG measurements, or the skin for EMG measurements) and work as transductor element. The analog electronics block delves into the amplification and conditioning of the acquired electrical potentials. In this stage, input signals are amplified according to the dynamic range of the acquisition system and filtered depending on the frequency band of the recorded biopotential. The first element of an analog acquisition system is often a differential amplifier which goes under the name of front-end. Its design is particularly important as it determines some key features of the device. Indeed, the analog electronic stage design is critical for the rejection of common-mode components leading to, e.g. power line interference falling within the frequency band of interest. Therefore, particular attention should be given to the design choices. Finally, the digital electronics block regards the sampling and discretization of the detected signals through a sample&hold circuit and an Analog-to-Digital (A/D) converter. Specifically, within the context of the present dissertation, high resolution A/D converter will be taken into account (typically 16 bit - 24 bit). This solution allows the use of front-end amplifier with a moderate amplification factor (e.g. 1-50) to minimize the risk of signal saturation at the amplifier input, still ensuring a high-resolution of the converted signal. This architecture is particularly convenient when designing miniaturized instrumentation with low power consumption (E. Spinelli & Guerrero, 2017). In the following sections, the main blocks of a biopotential acquisition system are described more in detail.

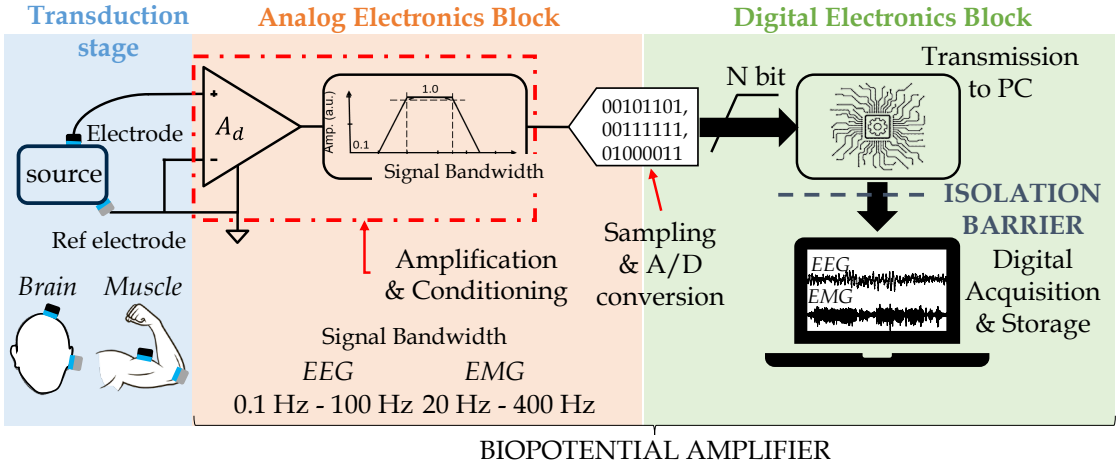


FIGURE 10 Block diagram of biopotential acquisition system. Main blocks: transduction stage, amplifying and conditioning circuit, processing and acquisition unit.

#### 2.3.1.1 Transduction stage: electrodes

The first block of the chain of a biopotential acquisition system is constituted by the electrodes. Their role is to act as ionic transducers as they translate the ionic currents occurring at the electrode-skin interface into electrical, measurable, potentials (i.e., due to electronic currents). Electrodes for biopotential acquisition are made mainly of metallic materials, eventually coated with metal salts. Therefore, when they are immersed in the electrolyte (i.e., an aqueous solution) containing ions of the metal, a net current crosses the electrode-electrolyte interface because of electron-ion exchanges at the interface through oxidation and reduction phenomena (Chan et al., 2013; Merletti & Cerone, 2020). These Red-Ox reactions reach the chemical equilibrium though the development of an electrical double layer at the electrodes-electrolyte interface with the appearance of a DC voltage, which is also known as half-cell potential and it depends on the properties of both electrode material and electrolyte. Often, Ag/AgCl electrodes are adopted to acquire biopotential signals because of their stable half-cell potential across different samples. FIGURE 11 shows different types of electrodes typically used in EEG and EMG recordings. Depending to the use of an additional electrolytic medium at the interface between the electrode and the skin, they are defined as dry or wet electrodes. The former do not include any electrolytic medium. Recent developments of dry electrodes include innovative conductive electrodes printed or sewn on textile supports (Cerone et al., 2021; Tseghai et al., 2021). Although dry electrodes are easy to wear because they do not require particular preparation, they are characterized by high electrical impedances at the electrode-skin interface, thus being prone to disturbances such as motion artifacts or power line interference (Cattarello & Merletti, 2016; Chi et al., 2010). On the contrary, wet electrodes imply the use of an electrolytic medium between the metal electrode and the skin such as gel or conductive paste. The role of the conductive medium is to improve the electrode-skin contact (i.e., lowering the electrical impedance) guaranteeing a higher quality of collected signals with respect to dry electrodes (Cattarello & Merletti, 2016). As a result, the choice of the type of electrodes to use during an experimental study is mainly carried out considering the specific application. However, EEG applications typically include caps with embedded electrodes (either wet or dry), whereas adhesive electrodes are generally used for EMG applications (either single electrodes or arranged in grids or arrays of electrodes) to reduce electrical impedances at the electrode-skin interface. This choice makes the acquisition system more robust towards power line noise and it allows to avoid possible relative movements of the electrodes with respect to the skin and, as a consequence, to reduce motion artifacts. Electrodes should be placed close to the signal source (i.e., the muscle for EMG, the brain for EEG recordings). When referring to EMG signal acquisition, electrodes are placed on top of the muscle belly, following, in the vast majority of cases, the SENIAM recommendations which define electrodes placement according to anatomical landmarks (D. Stegeman & Hermens, 2007).


FIGURE 11 Commonly used electrodes for the acquisition of biopotential signals: wet and dry electrodes (including textile solutions), and electrodes solutions typically adopted for EEG (electrodes cap), and EMG (adhesive arrays/grids or pre-gelled bipolar electrodes) recordings.

When referring to EEG signal acquisition, electrodes are often placed according to the international 10-20 system as shown in FIGURE 12. In this case, electrodes are placed at reciprocal 10% or 20% distance between anatomical landmarks (i.e., nasion, inion). Additionally, they are named according to specific labels indicating the cortical region and the hemisphere where they are placed (e.g. F3 electrode indicates an electrodes placed above the frontal area on the left hemisphere) (Mecarelli, 2019).

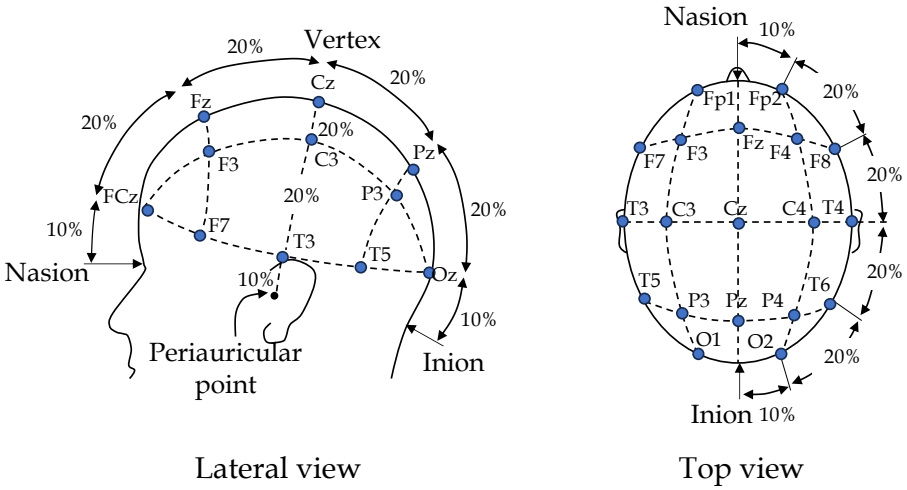


FIGURE 12 International 10-20 system to monitor EEG activity. Lateral and top view of the electrodes placement for the non-invasive measurements from the scalp surface.

The electrical properties of electrode-skin interface have been the subject of numerous studies (Burbank & Webster, 1978; Wu et al., 2020; L. Yang et al., 2022). FIGURE 13 shows the electric model of a biopotential electrode in contact with the skin. FIGURE 13 A reports the full model where: $E_{he}$ represents the half-cell potential given by the different electric potential of the metal electrode with respect to the rest of the solution, $C_d$ and $R_d$ make up the impedance associated with the electrode-electrolyte interface and polarization effects, $R_s$ refer to the effective resistance associated with interface effects, $E_{se}$ represents the electric

potential difference because of the different ionic concentrations across the stratum corneum, $C_e$ and $R_e$ make up the electric impedance of the epidermal layer. Minimizing the effect of the stratum corneum by its removal tends to short out $E_{se}, C_e$ and $R_e$ (Neumann et al., 1998). Additionally, when using systems acquiring electrophysiological signals that filter out the DC component, the $E_{he}$ can be also neglected. Finally, $R_s$ terms can be reasonably be neglected when dealing with biopotential signal acquisition due to their restrained values (i.e., tens to hundred Ohm). Therefore, the equivalent, simplified circuit for a biopotential electrode in contact with the skin is presented in FIGURE 13 B where the $R_d$ resistor represents the resistance linked to the phenomenon of direct charge transfer, and the capacitor $C_d$ accounts for the capacitance across the double layer of charges at the electrode-electrolyte interface (Webster, 1984). Considering Ag/AgCl electrodes placed on the skin, with a sensing area of 1 cm$^2$, in a frequency interval within 1 kHz: $R_d = 40$ kΩ and $C_d = 40$ nF (Neumann et al., 1998).

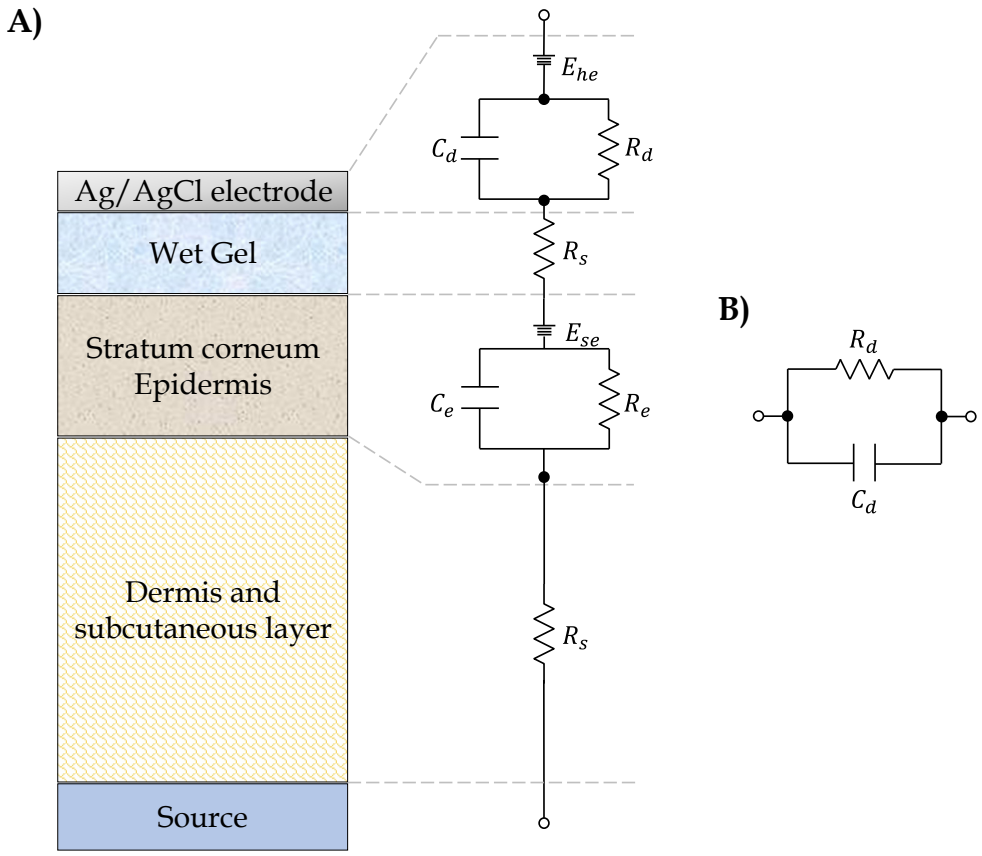


FIGURE 13 Electric model of a biopotential electrode in contact with the skin. A) Complete electric model: $E_{he}$ represents the half-cell potential, $C_d$ and $R_d$ make up the impedance associated with the electrode-electrolyte interface and polarization effects, $R_s$ refers to the effective resistance associated with interface effects, $E_{se}$ represents the electric potential difference because of the different ionic concentrations across the stratum corneum, $C_e$ and $R_e$ make up the electric impedance of the epidermal layer. B) Equivalent, simplified electric model.

#### 2.3.1.2 Analog electronics: Front-end amplifier

The analog electronics block of a biopotential acquisition chain includes a differential amplifier used as a front-end circuit along with possible multiple single-ended stages allowing for signal amplification and conditioning. When considering biopotential signal recordings through mains-powered systems, a standard, three-electrodes front-end amplifier is adopted with two exploring electrodes and a reference one aimed at detecting biopotentials in differential configuration (either monopolar or bipolar) (Wang et al., 2011). FIGURE 14 shows the electrical model of the subject-electrode-amplifier system considering a input common mode excitation due to the coupling between the subject and the power line. Considering a monopolar configuration, one is the exploring electrode $R_{e2}$ and the other is the monopolar reference electrode $R_{e1}$ which are hereinafter considered purely resistive under the assumption of using relatively large (~1 $cm^2$) Ag/AgCl electrodes with a gelled skin interface (i.e., the reactive component $C_d$ can be neglected). Therefore, the output voltage will be proportional to the voltage potential difference between the exploring and the monopolar reference points. Finally, the reference electrode ($R_r$) connects the biopotential amplifier reference to the subject, while the term $R_i$ represents the amplifier input resistance at 50 Hz (i.e., Power Line frequency, 60 Hz in some regions as in the United States) which is shown as a purely resistive for simplicity. When designing a front-end amplifier for biopotential acquisition, the general condition of $R_i \gg R_e$ is adopted by choosing high input impedances (from tens to hundreds of mega Ohm) to avoid any distortion of the signal to be amplified (Chi et al., 2011). In addition, another important parameter of a front-end amplifier is the CMRR (Common Mode Rejection Ratio) as it quantifies the ability of the amplifier to reject common-mode voltages (i.e., simultaneously appearing at both amplifier inputs such as those due to the coupling with power line). Typical values of CMRR adopted during the design of a front-end amplifier for biopotential signal acquisition are ~ 80 dB - 100 dB (E. M. Spinelli et al., 2003).

### 2.3.2 Power line interference in biopotential acquisition systems

One of the major concerns in biopotential signal acquisition is the rejection of the Power Line Interference (PLI) at 50/60 Hz. The source signals of PLI-related issues are mainly due the parasitic electrical capacitive coupling between the subject, the power line source and the ground which are reported in the simplified schematic of FIGURE 15.

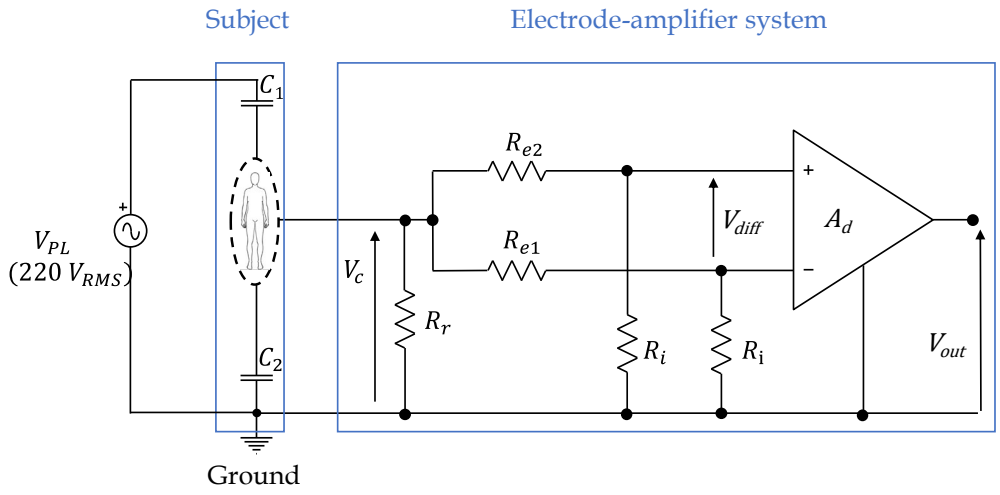


FIGURE 14 Electrical model of the subject-electrode-amplifier system of a three-electrodes biopotential acquisition system with the subject coupled to the power line and to the ground. From left to right, blue rectangles represent: the subject, the electrode-amplifier stage and the differential front-end amplifier.

The subject (considered as an equipotential node) is coupled to the active phase of the power line distribution through the capacitance $C_1$ typically ranging from 10 pF to 20 pF (E. Spinelli & Guerrero, 2017) and depending on the parasitic coupling between the subject and the active phase of the power line. Additionally, a second parasitic capacitive coupling ($C_2$) establishes between the subject and the power line ground and its numerical value can vary from 50 pF to 10 nF (Merletti & Cerone, 2020; Pallás-Areny & Webster, 1990). The voltage generator $V_{PL}$ refers to the power line source mains and, when capacitively coupled to the subject though $C_1$ and $C_2$, it represents a common mode excitation for the electrode-amplifier system. FIGURE 15B represents the electrical model (Thevenin equivalent circuit) modelling the abovementioned couplings, where $V_C$ is the resulting common mode potential on the subject and it will be dependent on $V_{eq}$ and $C_{eq}$:

$$V_{eq} = V_{PL}\frac{C_1}{C_1 + C_2}, \qquad C_{eq} = C_1 + C_2 \tag{2.2}$$

During the past years, mains-powered systems have been abandoned in favor of ground floating (i.e., battery powered) systems which are, instead, preferred because of higher rejection of power line interference and patient electrical safety. Indeed, the introduction of ground floating systems contribute to decouple the electrode-amplifier system from the power line mains.

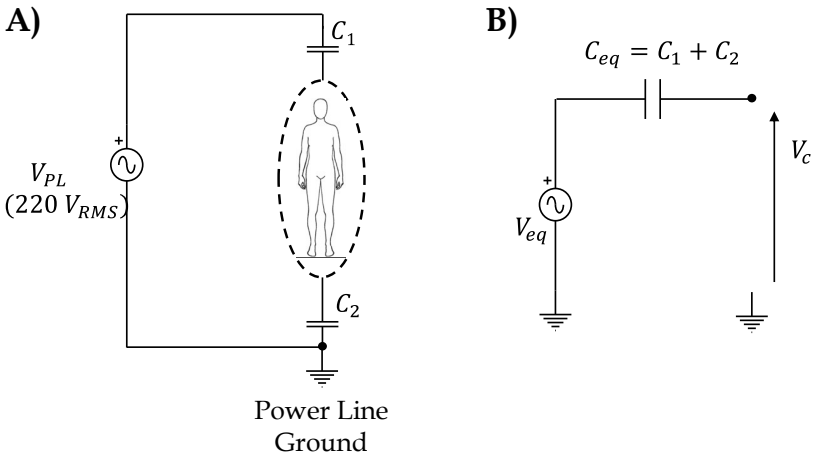


FIGURE 15 Coupling between the subject, the power line source and the ground. A) Schematic representation and B) Thevenin equivalent circuit of the power line-subject coupling: $C_1$ represents the coupling with the active phase of the power line, $C_2$ represents the coupling with the ground, $V_C$ is the resulting common mode potential on the subject.

Additionally, another important consideration should be made when referring to battery-powered systems to be used in the context of dynamic movements. Indeed, while it is true that adopting an additional physical ground-reference electrode $R_r$ would result in mitigating the common mode excitation $V_c$ also in presence of a capacitive coupling, it negatively affects the system encumbrance which is not optimal to perform biopotential signal acquisition in dynamics where miniaturized acquisition systems are desired. Therefore, an optimized floating system is not only decoupled with respect to the power-line ground, but it also uses a single monopolar reference electrode (i.e., no $R_r$ is involved). This two-electrodes front-end solution is preferred to the traditional three-electrodes configuration because it allows for system miniaturization, and more degree of freedom for the subject with no need to be physically connected to the recording system (D. Dobrev, 2002; D. Dobrev et al., 2005; D. P. Dobrev et al., 2008; Webster, 1984). However, completely decoupling the amplifier stage from the power line ground is only a pure ideal scenario which is never reproducible in the real world. FIGURE 16 shows the electrical model of the power line-electrode-amplifier system (ground floating) without the additional reference electrode connecting the biopotential amplifier reference to the subject. The front-end amplifier reference and the power line ground, which are supposed to be decoupled, are, instead, coupled through a parasitic coupling ($C_p$), highlighted in red, whose numerical value depends on the design of the amplifier itself, but it generally ranges from 10 pF to hundreds of picofarads (Metting van Rijn et al., 1990; Pallás-Areny & Webster, 1990). $R_{e1}$ and $R_{e2}$ are the electrode-skin impedances respectively of the monopolar reference and an exploring electrode, while $R_i$ represents the amplifier input resistance. The reactive components of the electrodes impedances were reasonably neglected according to the assumption of using Ag/AgCl gelled electrodes of 1 cm$^2$ at the power line frequency (i.e., 50 Hz).

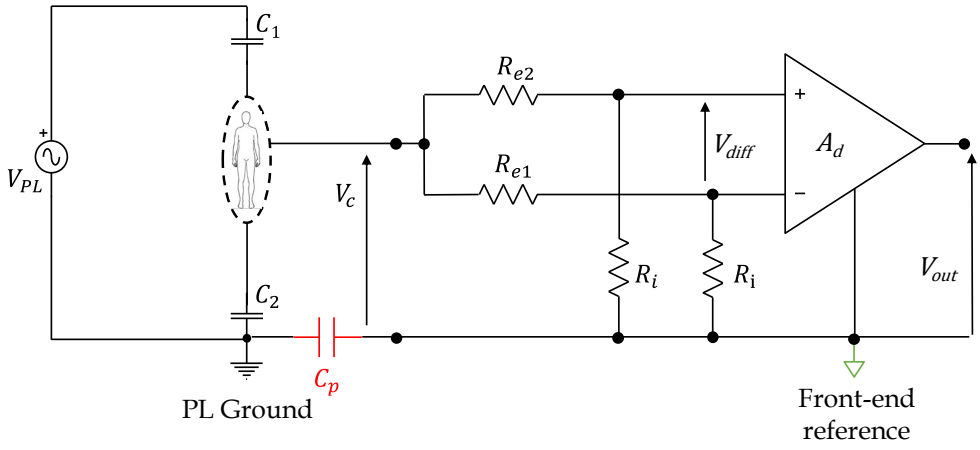


FIGURE 16 Electrical model of the power line-electrode-amplifier system when adopting ground floating instrumentation under a common mode excitation (power line source) using a two-electrodes configuration. The parasitic coupling ($C_p$) taking place between the front-end reference and the power line ground is highlighted in red.

Given the electrical model of FIGURE 16, considering that the input impedance of the front-end amplifier is at least three order of magnitude (mega Ohm) greater than the electrode-skin resistance (tens of kilo Ohm), the whole model can be simplified as in FIGURE 17 with:

$$V_{eq} = V_{PL}\frac{C_1}{C_1 + C_2},\quad C_{eq} = \frac{(C_1 + C_2)C_p}{C_1 + C_2 + C_p},\quad R_{eq} = (R_{e2} + R_i)\oplus(R_{e2} + R_i) \cong \frac{R_i}{2} \tag{2.3}$$

Where $\oplus$ indicates the parallel operator expressed by the product divided by the sum of the two elements (i.e., $(R_{e2} + R_i)$ and $(R_{e2} + R_i)$). Therefore, a common mode voltage amplitude ($V_C$) related to the power line interference applies at the input of the electrode-amplifier system. According to the electrical model of FIGURE 17, following the Eq. ( 2.3 ), the input common mode voltage amplitude can be derived as indicated in Eq. ( 2.4 ):

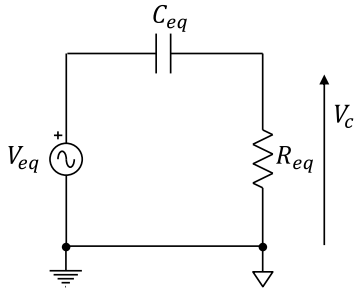


FIGURE 17 Thevenin equivalent circuit of the power line-electrode-amplifier system when adopting battery-powered instrumentation.

$$|V_C| = V_{PL} \frac{\omega R_{eq} C_{eq}}{\sqrt{1 + \left(\omega R_{eq} C_{eq}\right)^2}}$$

( 2.4 )

where $\omega$ is the pulsation of the line voltage, $\omega = 2\pi f_{PL}$ being $f_{PL}$ the 50 Hz/60 Hz PL frequency. However, it can be assumed that $C_{eq} \cong C_p$ because $C_p \ll (C_1 + C_2)$ since in the real practice it is generally possible to lower $C_p$ by designing battery powered, floating and miniaturized systems (Dellacorna, 2006) as the lower is the value, the lower the common mode input voltage will be.
However, it is worth noting that although the common mode voltage at the input of the electrodes-amplifier system ($V_C$) is the result of a common mode excitation ($V_{PL}$), the non idealities of the electrodes-amplifier system (i.e., non-infinite front-end amplifier input impedance and CMRR, non-zero electrode-skin impedance) lead to the conversion of this common mode excitation to a differential one (De Talhouet & Webster, 1996; Guermandi et al., 2016; Merletti & Cerone, 2020), leading to the so-called PLI. Therefore, this contribution of power line-related interference cannot be totally rejected by simply computing the differential input signal and the common mode excitation becomes a differential one. Specifically, considering that (i) the common mode rejection ratio ($CMRR$) and the amplifier input resistance of a real biopotential amplifier are non-infinite and that (ii) the electrode-skin impedances $R_{e2}$ and $R_{e1}$ are not exactly balanced although when adopting the same type of electrodes, the amplifier input-referred power line interference is given by Eq. ( 2.5 ).

$$V_{IRN\,50} = V_C \left(\frac{R_{e2} - R_{e1}}{R_i} + \frac{1}{CMRR}\right)$$

( 2.5 )

Thus, even a common mode excitation at the input amplifier will be translated into a differential mode excitation in case of an imbalance between electrode-skin impedances. Therefore, this input voltage can be amplified potentially causing the saturation of the amplifier itself, lowering the SNR.
Furthermore, the cables connecting the electrodes to the amplifier, are also coupled to the power line through a capacitive coupling implying a common and a differential mode voltage at the input of the amplifier. FIGURE 18 represents the electrical diagrams of the two main solutions proposed to deal with the mitigation of the effect of capacitive coupling of the connecting cables: the implementation of active electrodes (FIGURE 18A) and shielded cables (FIGURE 18B).
Active electrodes have been introduced during the Eighties and they dealt with mounting pre-amplifiers close to the sensing electrodes with the aim of transferring an input signal to the differential amplifier with a low input impedance. These amplifiers are, in the simpler version, voltage-followers (unit

amplification factor) with extremely high input impedance and extremely low output impedances ($R_0$). FIGURE 18A highlights in red color the resistance of the exploring electrode as seen at the input of the amplifier ($R_0$). With significantly low electrode resistance (e.g. $R_0 \cong 0$), the voltage divider of the input power line source will be null at the input of the main amplifier. Therefore, the use of active electrodes allows to reduce the effect of the capacitive coupling between connecting cables and power line mains mitigating the effect of the conversion of the power line excitation from a common to a differential mode by reducing the effects of high impedance (Laszlo et al., 2014; E. Spinelli & Haberman, 2010).

Cables shielding refers to the implementation of a layer of conductive metal around the cable connecting the electrodes to the amplifier. Similarly to the previous case, the effect of the shielding, when in presence of a common mode excitation with capacitive coupling downstream the electrodes is to provide a null partition of the common mode interfering signal at the input of the amplifier (Webster, 1984) by putting the cable surrounding insulator to ground.

Nevertheless, recent studies demonstrated that passive, non-shielded configurations do not always perform significantly worse than active, shielded ones (Laszlo et al., 2014; Oliveira et al., 2016; Scanlon et al., 2021). The result is not surprising as active electrodes are mainly effective to mitigate the effect of capacitive couplings occurring downstream of the electrodes. For this reason, they were particularly suitable solutions to mitigate disturbances related to power line interference, especially when using non floating biopotential acquisition systems. However, with the introduction of ground floating instrumentation the effectiveness of active electrodes and cable shielding started to wane with the simultaneous increase of the robustness of the electrode-amplifier systems to power line interference and the concurrent increased use of battery powered, floating, instrumentation. Furthermore, these solutions have severe drawbacks, especially when considering them for biopotential signal acquisition in dynamic conditions. Indeed, implementing active electrodes and cables shielding implies: (i) a sensible increase of the total encumbrance, weight and price of the recording system, (ii) an increase of the power consumption of the system because of the presence of additional circuits (e.g. pre-amplifiers), and (iii) a deterioration of the robustness of the system to the baseline noise, being the pre-amplifiers a noise source themselves. Therefore, the implementation of active electrodes and cable shielding must be handled with care when designing biopotential signal acquisition systems for dynamic applications.

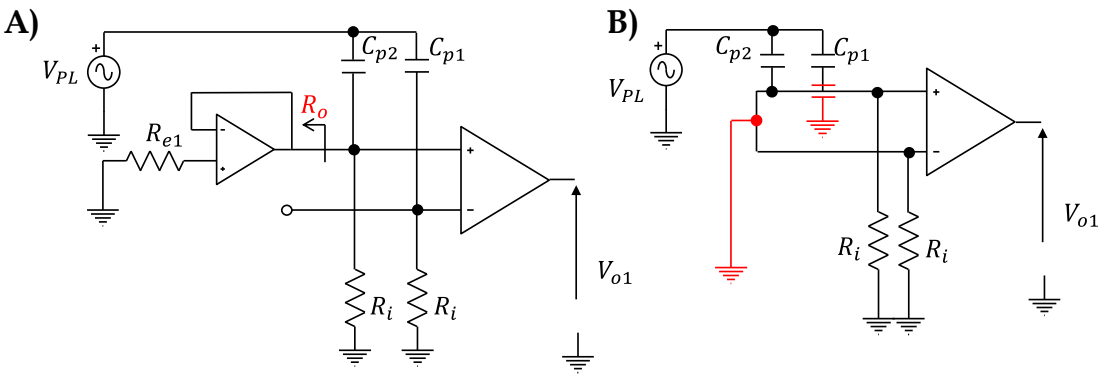


FIGURE 18 Electrical diagram of A) active electrodes and B) cables shielding. In both the models, $V_{PL}$ represents the power line source, $C_{p1}$ and $C_{p2}$ represent the capacitive coupling between the cables connecting the subject to the amplifier, and $R_i$ are the amplifier input resistance.

### 2.3.3 EEG acquisition systems: state of the art and open issues

To date, the emerging research and clinical need of investigating how the brain interacts with the external environment in real-world applications have raised the interest towards methodological and technological developments in the context of human EEG and EMG recordings. This increasing need allowed for making significant progresses over the last decades in terms of hardware miniaturization for EEG and EMG acquisition systems enabling dynamic recordings. FIGURE 19 summarizes three main types of biopotential acquisition systems according to the allowed degree of freedom:

- *Desktop systems*: typically including mains-powered systems. Although the high quality of collected signals, due to the system encumbrance they limit the recordings to static, well-controlled conditions and they increase the complexity of the experimental setup due to connecting cables that could hinder the subject during the execution of dynamic tasks.
- *Portable systems:* referring to battery-powered systems. Even though a higher degree of freedom is allowed with respect to the previous group of devices, their use is still limited in laboratory environments because of the short distances between the signal transmitter and receiver. Additionally, these systems might still include connecting cables and therefore being subjective to signal corruption from motion artifacts.
- *Wearable systems*: comprising all those devices allowing for biopotential signal recordings during naturalistic conditions (i.e., walking in the forest). Within this context, the term *wearable* does not refer to any 'self-fitting characteristic' of the device, but it rather stands for 'highly unobtrusive, near invisible, and comfortable to wear' (Niso et al., 2023). Wearable devices are commonly wireless systems (working either through Wi-Fi or Bluetooth connection) enabling a complete freedom of movement, strongly simplifying the experimental setup.

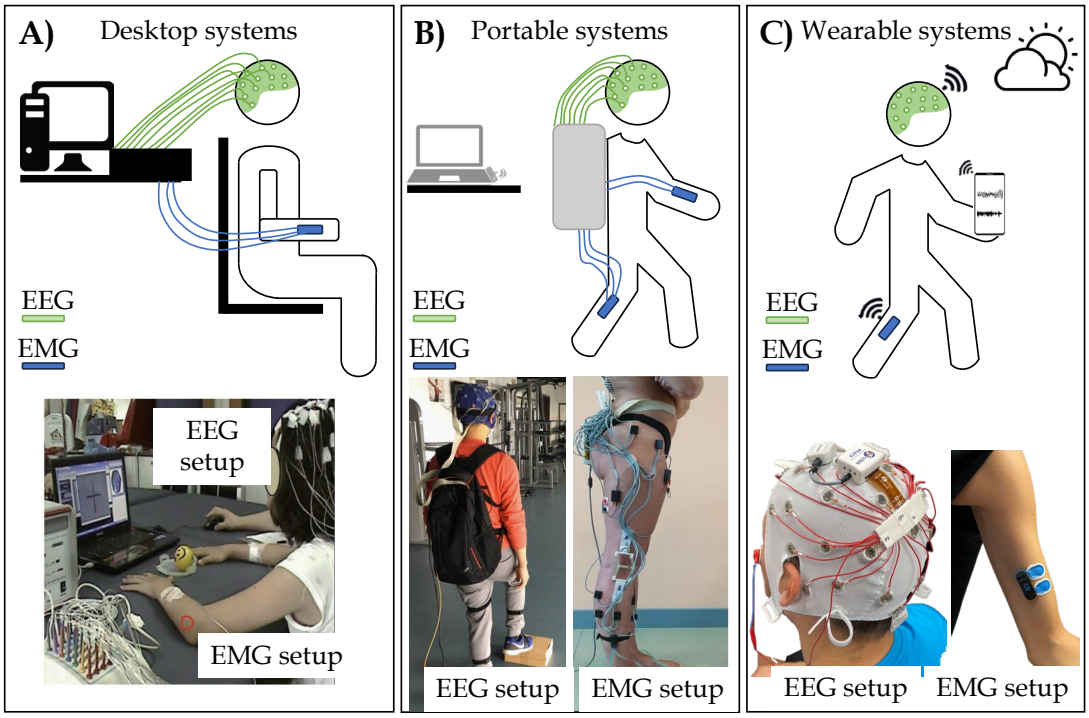


FIGURE 19 Schematic representation and real example pictures of A) desktop, B) portable and C) wearable systems adopted for the acquisition of EEG and EMG signals. Experimental setup pictures are taken from (Shin et al., 2012), (Long et al., 2018) or otherwise captured by the author.

Nevertheless, while several wearable devices for EMG acquisition have been proposed and extensively validated under a multitude of conditions including clinical studies, rehabilitation protocols, and sport applications (Casson, 2019; Cerone et al., 2019), the currently available EEG technology turns out not to be optimized to collect high-quality EEG signals during movements. As a result, the investigation of the functioning of the human brain is still limited to well controlled, static conditions. TABLE 2 offers a brief overview of the commercially available EEG devices and their main characteristics taken from (Niso et al., 2023). Exception made for the desktop and portable systems which are not suitable for EEG recordings during unconstrained conditions by default, some further considerations should be carried out for the listed wearable EEG systems. In view of enabling the comprehensive study of sensorimotor integration, EEG systems for dynamic recordings should be:

(i) miniaturized, wireless and lightweight to be used in unconstrained conditions. A Wi-Fi communication protocol should be preferred as it allows for maxima transmission distances, and it provides higher reliability in terms of packets delivered
(ii) configurable to acquire a sufficiently high number of signals (i.e., with an adequate number of channels to monitor the whole cortical surface)
(iii) modular, with the possibility of being easily synchronized with any other external device allowing for real-time data streaming.

To the best of our knowledge, none of the listed EEG systems in TABLE 2 simultaneously meets these three characteristics. Hence, current technological needs still concern the lack of suitable instrumentation optimized for dynamic EEG recordings. Furthermore, one of the biggest bottleneck still compromising the high-quality EEG recordings in real-world applications is the contamination of EEG traces from movement-related artifacts that are time-locked to the performed movements (i.e., motion artifacts).
Therefore, open issues regard the knowledge gap not only on the neurophysiological mechanisms occurring during daily movements or sports, but primarily on the signal properties and related technological issues during dynamic conditions (e.g. the genesis of motion artifacts contamination). Consequently, there is a demand for providing methods and suitable tools to drive the technical specification for the design of biopotential signal acquisition systems for monitoring cortical brain activity during dynamic tasks in more naturalistic conditions.

TABLE 2 Commercially available systems for EEG recordings with wet or gelled electrodes released on the market by 2020.

**Commercially available EEG systems**

| Company - System name | Type | Number of channels | Sampling frequency | Size, weight | Communication protocol | Modularity / Syn external device |
|---|---|---|---|---|---|---|
| Bittium - NeurOne | Desktop | Up to 160 | Up to 10 kHz | 16x12x8 cm 1300g | Wired | YES |
| TMSi - Apex | Portable | 32 | 1024 Hz | 15x7x3 cm 240 g | Bluetooth | NO |
| ANT Neuro – eego sports | Portable | 128 | 2048 Hz | 20x16x22 cm 500 g | Wi-Fi network | YES |
| Mentalab – Explore | Wearable | 8 | 1k Hz | 4x4x2 cm 27 g | Bluetooth (10 m distance) | NO |
| BitBrain – Versatile EEG | Wearable | 64 | 256 Hz | 10x7x7 cm 450 g | Bluetooth (10 m distance) | YES |
| Neuroelectrics - Enobio | Wearable | 32 | 500 Hz | 9x6x2 cm 81 g | Wi-Fi network | NO |
| g.tec – Nautilus PRO | Wearable | 32 | 500 Hz | 8*6*2 cm 110 g | ISM Proprietary (2.4GHz) | YES |
| mBrain Train PRO | Wearable | 64 | 4 kHz | Not available | Bluetooth | NO |
| Open BCI - Ganglion | Wearable | 4 | 200 Hz | 6x6x3 cm 30 g | Bluetooth Low Energy | NO |
| Brain Products – LiveAmp | Wearable | 64 | 1 kHz | 14x8x2 cm 120 g | ISM Proprietary (2.4GHz) | YES |

# 3 PURPOSE OF THE PROJECT

This dissertation is aimed:

(i) to analytically examine the current technological and methodological limits in EEG signals acquisition during dynamic, unconstrained movements, with a particular focus on investigating the causes of signal corruption

(ii) to develop and test innovative technologies suitable for the acquisition of high-quality EEG signals

(iii) to implement such technologies in the real practice to examine neurophysiological mechanisms related to cortical sensorimotor integration in both static and dynamic conditions.

Specific research questions (*Q)* and related hypotheses (*H*) of the separated studies were:

- *Study I* – EEG motion artifacts assessment.
  ***Q1)*** What are the phenomena leading to the genesis of motion artifacts in EEG signal acquisition?
  ***H1)*** Starting from experimental observations hypotheses and electrical models are developed analyzing the sources of motion artifacts at different levels: the skin-electrode interface, the connecting cables, and the electrode-amplifier system.
- *Study II* – Design and validation of an innovative, miniaturized wireless-EEG and synchronization system.
  ***Q2)*** How does the developed wireless-EEG system perform when compared to a gold standard wired EEG system?
  ***H2)*** Robust performance is expected given the wireless-EEG system architecture and design.
- *Study III* – Development of innovative EEG electrodes systems to deepen the study of EEG motion artifacts and related challenges in EEG signal acquisition outside the lab environment.

***Q3)*** To what extent EEG electrodes systems with limited movements of cables and electrodes affect the recording of high quality EEG signals?
***H3*)** Negligible motion artifacts on wireless EEG recordings are hypothesized when minimizing the cables length and the electrodes movements during dynamic tasks.

- *Study IV* – Assessment of cortical proprioceptive processing of ankle joint rotations.
  ***Q4)*** How does maintained volitional muscular activation affect the cortical processing of naturalistic continuous and intermittent ankle joint proprioceptive stimulation?
  ***H4)*** An intensified cortical proprioceptive processing is hypothesized when a muscular contraction is performed as a result of a multi-level mechanism affecting from the muscular to the spinal and the cortical levels.
- *Study V – P*roof-of-concept study: dynamic EEG recordings.
  ***Q5)*** Is it feasible to extract physiological outcome measures from wireless EEG recordings during dynamic tasks?
  ***H5*)** Positive outcomes are expected being the EEG setup particularly optimized for dynamic EEG recordings.

# 4 ANALYTICAL STUDY: ANALYSIS OF THE CONSTRAINTS LIMITING EEG SIGNAL ACQUISITION IN LABORATORY ENVIRONMENT (*Study I*)

This Chapter aims at analyzing the constraints currently limiting good-quality EEG signal acquisition exclusively in controlled lab-environments answering to the *Q1:* what are the phenomena leading to the genesis of motion artifacts in EEG signal acquisition? *Study I* focuses on the movement-related bottlenecks which are mainly attributable to the corruption of EEG signals from motion artifacts. The main phenomena behind motion artifacts generation have been electrically modelled starting from experimental observations. This analytical dissertation aims at providing the bases to drive the design of innovative technological solutions (e.g. biopotential amplifier, electrodes systems, etc.) to overcome the challenges currently hindering the acquisition of EEG in dynamic condition.

## 4.1 The genesis of motion artifacts: experimental observations, electrical models and good practice recommendations

Movements performed during EEG signal acquisition are likely to generate non-physiological artifacts, called motion artifacts, which are superimposed on the physiological cortical signals (Sörnmo & Laguna, 2005). Their amplitude ranges up to two orders of magnitude greater than the amplitude of the EEG signal of interest, thus the correct interpretation of brain signals is severely hindered. Motion artifacts can be observed both at low frequency (i.e., baseline shifts) and high frequencies (e.g. spike-like variations), therefore it is not trivial to distinguish the relative contribution of artifacts with respect to the true cortical signals (Tandle et al., 2015). One of the most common approaches to deal with motion artifacts contaminating EEG recordings is the removal of specific portions of the signals through visual inspection, but this approach is strictly subject-dependent, hardly automatable, ineffective for semi-periodic motion artifacts

(i.e., time-locked with the movement (Girton & Kamiya, 1972), and cannot be applicable when the occurrence of motion artifacts is almost continue, as in the case of dynamic, naturalistic, tasks. For this reason, also Wavelet- or moving average- based approaches are limited only to those cases where the main target is the analysis of cortical activity in non-movement related signal portions (e.g. dual paradigm tasks) (Shukla et al., 2020). More advanced filtering techniques such as ICA have also been developed to separate and isolate the unwanted sources from brain signals (Debener et al., 2005, 2007), but their effectiveness in the context of movement artifact removal cannot be generalized as movement-related artifacts remain in most of the independent components. Therefore, none of the currently available signal processing techniques resulted to be robust and reliable enough as it is obscure to what extent their implementation entirely preserves electrical brain activity. As a result, dynamic EEG would benefit from artifact-free raw signals recordings to ensure the possibility of preserving a high signal-to-noise ratio allowing to safeguard the cortical activity. For this goal to be achieved, an in-depth analysis of the genesis of artifact contamination of EEG recordings should be carried out to enable good-quality EEG signals collection. Sources of motion artifacts could be identified starting from the analysis of the phenomena taking place at each of the three main stages constituting a traditional biopotential acquisition chain:

i. *Skin-electrode interface (transduction stage)*: although it has been extensively demonstrated that this cause of artifact can be partially minimized through a proper electrode-skin interface preparation (i.e., abrading the body area under investigation and adding a conductive medium) (De Talhouet & Webster, 1996), the relative movement between the conductive part of the electrode (Ag/AgCl) and the skin still remains a point to be discussed as it alters the ions distribution at the electrode-skin interface that is in turn read as an additive phenomenon with respect to the electrophysiological one of interest.
ii. *Electrode-amplifier connecting cables*: due to triboelectric phenomena, the friction and deformation of cable insulator generated by the movement of the cables generate an additive input voltage potential. This additional voltage will be brought at the output stage and amplified additionally to the signal of interest (Wartzek et al., 2011).
iii. *Electrode-amplifier system (acquisition stage):* the electrodes-amplifier system is parasitically coupled with the surrounding electromagnetic environment. Specifically, although power-line related problems have been mitigated through the design of wireless and floating (e.g. battery powered) acquisition systems, the residual input-referred power line interference might be modulated during the movement performance. In case of bad contact at the electrode-skin interface and poor amplifier technology (e.g. low input impedance and CMRR) the abovementioned effect is even worse. Therefore, the modulation of residual power line

interference generates voltage potential differences displayed as motion artifacts.

The output signal will be affected by the mutual interaction and superimposition of all or some of the abovementioned factors. However, although it is unlikely to disentangle the sources of the motion artifacts in the experimental practice, a model-based approach for the understanding of the basic phenomena underlying the generation of motion artifacts is hereby proposed following the hypothesis of an additive model of the corruption of EEG recording from motion artifacts. Specifically, starting from the experimental observations of motion-artifacts, dedicated lumped-parameters models allowing to describe and synthesize the experimentally observed phenomena have been designed and analyzed.

### 4.1.1 Artifacts arising from phenomena at the electrode-skin interface

#### 4.1.1.1 Experimental observation

FIGURE 20 shows three examples of motion artifacts corrupting monopolar EEG signals recorded during overground walking by using the FCz electrode as a reference electrode. Considering this case-study, motion artifacts occur as relatively slow changes of the baseline voltage potential highly correlated to the gait frequency. It is hypothesized that motion artifacts are due to changes in voltage potentials acquired by the electrodes because of their relative movements during the motor performance. The hypothesis of excluding the movements of the cable as sources of these types of artifacts (FIGURE 20**)** is considered to be realistic in light of previous studies on motion artifacts affecting biopotential signal recording. Indeed, these studies show that cables-related artifacts typically generate spike-like variations of the recorded biopotentials (Merletti & Cerone, 2020). Additionally, it is assumed that the electrodes movements do not cause a complete detachment with respect to the scalp but exclusively a relative movement with respect to the underneath skin, otherwise a clear contamination from the power line source (i.e., sinusoidal signal at 50 Hz/60 Hz) would have been the predominant undesired contamination. Qualitatively, two distinct patterns of motion artifacts were identified when using as a reference electrode one of those embedded into an EEG cap hereinafter referred as *Type I* and *Type II*. Type I artifacts show up as an additive signal corrupting similarly all the EEG channels and it is reasonable to assume to be mainly driven by the monopolar reference electrode as its effect is reflected on all other electrodes (FIGURE 20B). Type II artifacts are instead localized at single channel sites and thus attributable to specific exploring electrodes (e.g. CP1 in FIGURE 20C). A combination of the two might also occur, thus increasing the degree of signal corruption (FIGURE 20A).

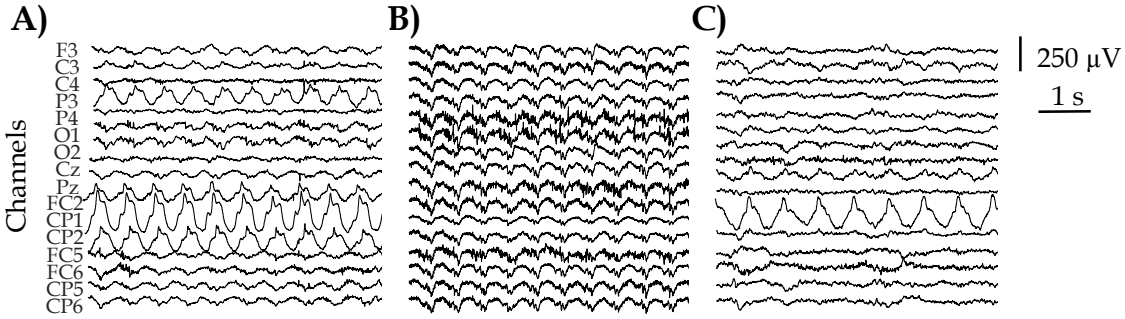


FIGURE 20 Examples of motion artifacts contamination on a subset of 16 EEG signals recorded during overground walking. A) Type I+II motion artifacts: related to both exploring- and reference- electrodes, B) Type I motion artifacts: related to reference electrode, and C) Type I motion artifacts: exploring electrode related. Modified from (Giangrande, Botter, et al., 2024).

#### 4.1.1.2 Lumped parameters model

FIGURE 21 represents the electrical model of motion artifacts (Type I+II, Type I and Type II) generated by electrode movements. For simplicity, a single pair of electrodes is considered in the following electrical models under a differential acquisition in a monopolar configuration, but the same considerations apply for the each exploring electrode used during EEG measurements.

**Type I+II motion artifacts.** In FIGURE 21A motion artifacts are modelled as affecting simultaneously, but distinctly, two exploring electrodes $e_1$ and $e_2$ (having impedances respectively of $Z_{e1}$ and $Z_{e2}$), and the reference electrode $e_r$ (having impedance $Z_r$). The three voltage generators ($V_{AE1}, V_{AE2}$ and $V_{AR}$) model three different voltage changes generated by the relative movements of three electrodes. The input-referred voltages representing the motion artifact modulation due to the voltage divider between the front-end amplifier input impedances and the electrodes impedances are:

$$\begin{cases} V_{O1ir} = V_{AE1}\dfrac{R_i}{R_i + Z_{e1}} - V_{AR}\dfrac{R_i}{R_i + Z_r} \\ V_{O2ir} = V_{AE2}\dfrac{R_i}{R_i + Z_{e2}} - V_{AR}\dfrac{R_i}{R_i + Z_r} \end{cases}$$

( 4.1 )

From Eq. ( 4.1 ) it is straightforward that, under the realistic hypothesis of amplifier input resistance greater than the impedance of the electrode ($R_i \gg |Z_e|$), the resultant output voltage for a single EEG channel is given by $V_{Oir} = V_{AE} - V_{AR}$. Therefore, the output voltage registered from a single exploring electrode ($V_{Oir}$) is independent from the electrode impedances, and it is the result of the difference between the artifact-related voltages affecting the exploring electrode ($V_{AE}$) and the reference electrode ($V_{AR}$). The provided result is particularly evident when electrodes are optimally prepared as the electrode impedance is considerably low ($|Z_e| \to 0$) with respect to the amplifier input impedance.

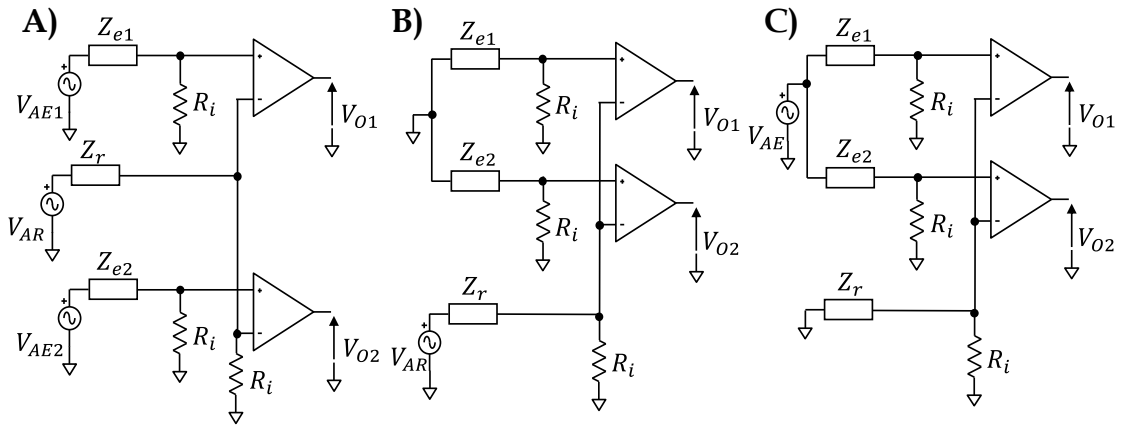


FIGURE 21 Electrical models of Type I+II, Type I and Type II motion artifacts. A) Type I+II artifacts are generated by electrode movements affecting two exploring electrodes ($Z_{e1}$ and $Z_{e2}$) and the reference electrode ($Z_r$). B) Type I artifacts involve movements of the sole reference electrode ($Z_r$). C) Type II artifacts exclusively regard the two exploring electrodes ($Z_{e1}$ and $Z_{e2}$). $R_i$ represents the amplifier input resistance. Modified from (Giangrande, Botter, et al., 2024).

Nevertheless, it remains valid also when electrodes are discretely prepared as well as the amplifiers input impedance is much greater than the electrode-skin impedances. Indeed, if that would not be the case (i.e., $R_i < |Z_e|$), the rejection of power line interference will not be effective and EEG traces will be strongly corrupted from Power Line Interference, which is not in line with the observations reported in FIGURE 20C.

**Type I motion artifacts.** FIGURE 21B represents the electrical model of motion artifacts affecting the reference electrode $e_r$ (with impedance $Z_r$) because of its movement modelled by the voltage generator ($V_{AR}$). The input-referred voltages representing the motion artifact modulation due to the voltage divider between the front-end amplifier input impedances and the electrodes impedances are:

$$\begin{cases} V_{O1ir} = -V_{AR}\dfrac{R_i}{R_i + Z_r} \\ V_{O2ir} = -V_{AR}\dfrac{R_i}{R_i + Z_r} \end{cases}$$

( 4.2 )

Therefore, the contribution of the motion artifact to the two recorded signals is identical from channel to channel and thus it can be easily attenuated by subtracting the common average from all the recorded EEG signals. However, this artifact removal is not always effective in the real practice because artifacts at the individual channel level are always superimposed to those affecting the reference electrode. Thus, the removal of the common average might introduce signal distortions. Therefore, the role of the reference electrode in EEG recordings should not be underestimated as if a movement-related voltage change occurs at

the level of the monopolar reference point, the result will be reported at the level of every collected EEG channels.

**Type II motion artifacts.** FIGURE 21B shows the electrical model of motion artifacts affecting two exploring electrodes $e_1$ and $e_2$ (having electrode-skin impedances respectively of $Z_{e1}$ and $Z_{e2}$) when no artifact contamination due to the reference electrode $e_r$ (with impedance $Z_r$) occurs. The voltage generator ($V_{AE}$) models the voltage change generated by the relative movements of two electrodes that is hypothesized to be the same, for simplicity. The input-referred voltages representing the motion artifact modulation due to the voltage divider between the front-end amplifier input impedances and the electrodes impedances are:

$$\begin{cases} V_{O1ir} = V_{AE} \dfrac{R_i}{R_i + Z_{e1}} \\ V_{O2ir} = V_{AE} \dfrac{R_i}{R_i + Z_{e2}} \end{cases}$$

( 4.3 )

To estimate how the same voltage change at the input is reflected at the amplifier output by two different recording electrodes, the difference between the two voltages $V_{O1ir} - V_{O2ir}$ can be derived as follows:

$$V_{O1ir} - V_{O2ir} = V_{AE} R_i \left( \frac{R_i}{R_i + Z_{e1}} - \frac{R_i}{R_i + Z_{e2}} \right) = V_{AE} R_i \left( \frac{Z_{e2} - Z_{e1}}{(R_i + Z_{e1})(R_i + Z_{e2})} \right)$$

( 4.4 )

Under the hypothesis that the input amplifier impedance is greater than the electrode impedances (i.e., $R_i \gg |Z_e|$), the Eq. ( 4.4 ) can be approximated as follows as indicated for the case of common-mode input i.e., capacitive coupling to the power line (Webster, 1984):

$$V_{O1ir} - V_{O2ir} \cong V_{AE} \frac{|\Delta Z_e|}{R_i}$$

( 4.5 )

Therefore, even with an identical artifact source, the difference between the output voltages registered through two exploring electrodes is non null, but rather dependent on the difference between the values of electrode impedances. Therefore, when considering the voltage difference between the two points $e_1$ and $e_2$, the artifact source applies as a common mode voltage which is, in turn, translated into a differential one because of the electrode impedance imbalance. As a result, the difference between the impedance values should be minimized as the greater the imbalance between the electrode impedances, the greater the

voltage differences (i.e., artifact signal amplitude) and the more difficult is to get rid of those motion artifacts.

#### 4.1.1.3 Analysis of the model

Eq. ( 4.5 ) can be used to numerically estimate the order of magnitude of the electrode impedance imbalance. Indeed, it is possible to consider a realistic input impedance value of a front-end amplifier of $R_i = 80$ MΩ, and the amplitude of an observed Type II movement artifact as $V_{AE} = 100$ mV with an inter-channel voltage difference of $V_{01ir} - V_{02ir} = 10$ μV (as example, refer to FIGURE 20C). In these conditions, from Eq. ( 4.5 ), it would result that such artifacts amplitude would be caused by electrodes impedance imbalance of $|\Delta Z_e| = 8$ kΩ . The obtained $\Delta Z_e$ is a plausible value, easily experimentally verifiable, thus giving further grounds to the theoretical models introduced above and suggesting that the relative movement of both exploring and reference electrodes may result in the contamination of EEG signals with motion artifacts (Type I+II, Type I and Type II). As shown, the magnitude order of the signal amplitude related to the recorded artifacts depends on the artifact-dependent voltage changes caused by the movements, but electrodes impedance mismatch is demonstrated to have an important effect in complicating the readability of the recorded signals as the signal corruption occurs with a different extent at single electrode level. In this view, ensuring a stable contact between the skin and the electrode either by performing an accurate electrode-skin preparation and by avoiding as much as possible relative movements becomes of paramount importance. This is particularly important when dealing with the reference electrode. Indeed, it is a critical electrode highly influencing the outcome of the recordings because it affects all other electrodes (i.e., the reference signal is subtracted from all other electrodes in a monopolar signal configuration). This result is in accordance to the good practice recommendations indicating the use of adhesive monopolar reference electrodes, preferably placed in body regions with limited movements to prevent its impact due to its relative movements to all channels Finally, demonstrating that the amplitude of the signal corrupted by artifact depends on electrodes impedance imbalances implies that implementing active electrodes in the system electronics does not provide an appreciable contribution to the mitigation of motion artifacts due to electrodes movement. In fact, their main contribution is to mitigate capacitive coupling downstream the electrodes in presence of a common mode input such as the electrical line noise (Metting van Rijn et al., 1990). Their use become ineffectual to mitigate electrodes impedance imbalances upstream the electrodes when the input voltage is changing rapidly, as the case of the relative movement of electrodes. This finding is in line to what shown by (Laszlo et al., 2014) who experimentally showed that during rapid voltage fluctuations active electrodes are equally affected by interelectrode impedance effects with respect to passive electrodes. On the contrary, the undesired result of using active electrodes in such situations is the increase of the system encumbrance and power consumption, and this is in contrast with the

need of developing miniaturized instrumentation allowing for a complete freedom of movements during EEG experiments.

### 4.1.2 Artifacts related to the movement of connecting cables

#### 4.1.2.1 Experimental observation

FIGURE 22A shows a set of EEG signals detected at rest while the experimenter wearing insulating gloves was manually shaking the cables connecting the electrodes to the amplifier. FIGURE 22B shows the power spectrum of a representative EEG signal collected when shaking the cables, while FIGURE 22C depicts the power spectrum of a representative EEG signal from the same subject at rest without cable shaking. It is clear that traditional signal processing techniques cannot be used to mitigate the effect of motion artifacts on EEG signals due to the overlap of the artifacts frequency spectrum to the EEG bandwidth (0,1 Hz – 100 Hz).

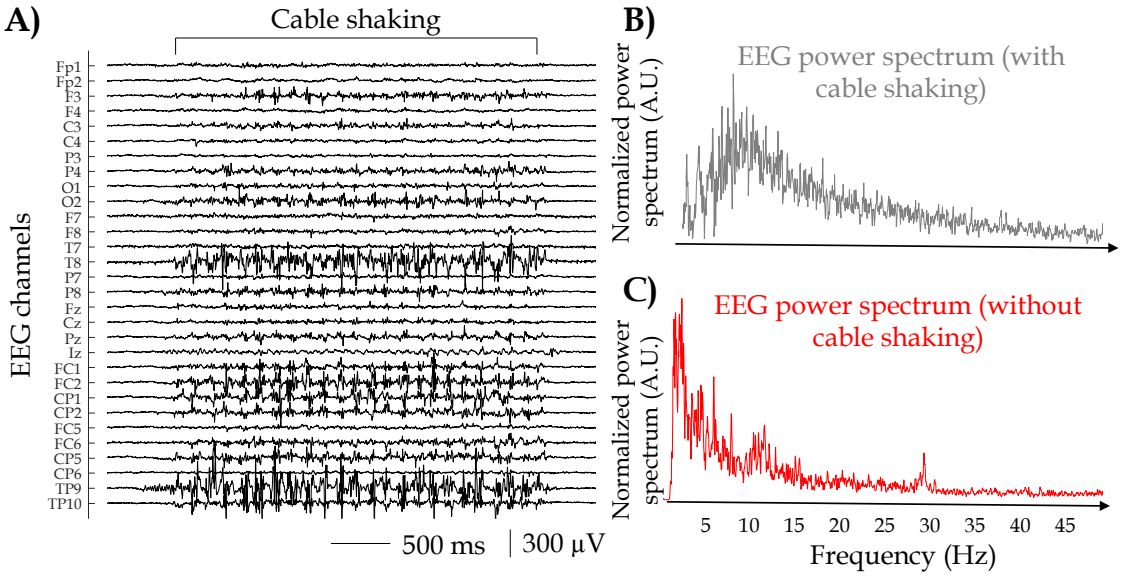


FIGURE 22 Motion artifacts caused by shaking the cables connecting the electrodes to the amplifiers. A) 30 EEG signals recorded with the subject at rest while the experimenter is shaking the cables wearing isolating gloves. B) Power spectrum of a representative EEG signal with cable shaking. C) Power spectrum of a representative EEG signal without cable shaking. Modified from (Giangrande, Botter, et al., 2024).

#### 4.1.2.2 Lumped parameters model

FIGURE 23 shows the schematic representation of typical cable structure used to connect electrodes and EEG amplifiers. They might be either individual cables (FIGURE 23A) or multicore cables (FIGURE 23B). The former is made of a conductive material (most often copper-*Cu*) embedded in a thin sheath of insulating material (e.g. silicone rubber), whereas the latter contains $N$ individual cables wrapped into an external layer of insulating material, with $N$ varying according to the number of electrodes to be connected (i.e., 10-256).

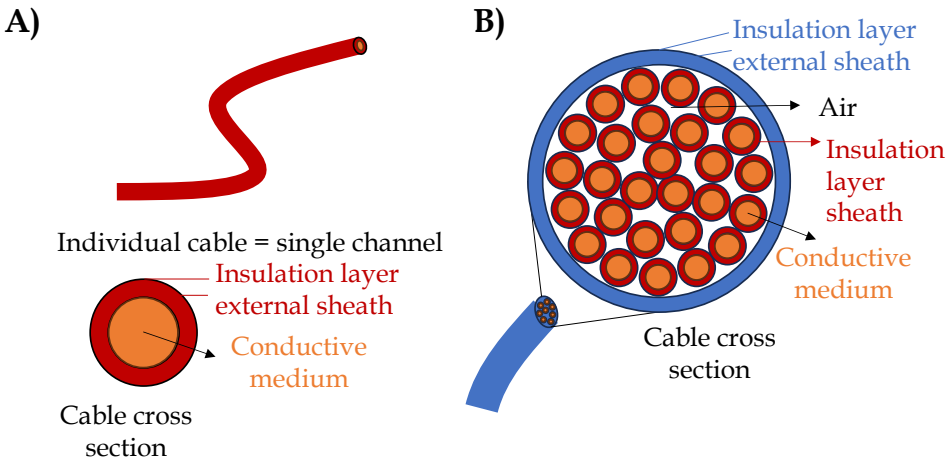


FIGURE 23 Schematic representation of connecting cables. A) single cable connecting the electrodes to the amplifier and B) a multi core cables.

FIGURE 24 represents the electrical model of two adjacent cables connecting two separated electrodes to the amplifier regardless the type of cable: $R_{c1}, R_{c2}$ are the cross-sectional electrical resistances of the copper cable (resistivity $\rho = 0.0168\ \Omega\text{mm}^2/\text{m}$), $C_{i1}, C_{i2}$ model the parasitic capacitance due to the cable dielectric, and $C_A$ is the electrical capacitance due to the dielectric (i.e., air) in between two conductive mediums. Some simplifications can be conveniently introduced. Firstly, the terms referring to the electrical resistance are reasonably negligible. Indeed, considering the resistivity of the copper and considering a small portion of the wire with a transversal section of 0.5 mm² and a length of 1 mm, the resulting cross sectional electrical resistance of a single cable will be with a magnitude order of tens of milli Ohm (e.g. $R_C = 36\ \text{m}\Omega$). Secondly, a single capacitance, hereinafter referred as $C^*$, can be used to model the dielectric layer separating the conductive portions of two adjacent cables. Therefore, the resulting simplified lumped parameters model can be represented as the electrical series of two capacitors: $C^*$ and $C_A$, that, under the hypothesis of considering a planar faces capacitor, are given by:

$$C^* = \varepsilon_r \varepsilon_0 \frac{S}{2d_i}, C_A = \varepsilon_A \varepsilon_0 \frac{S}{d_A}$$

( 4.6 )

being $\varepsilon_0$ the vacuum permittivity $\left(\varepsilon_0 = 8.854 \frac{pF}{m}\right)$, $S$ the facing portion of the cable, $d_i$ the thickness of the insulating layer wrapping a single cable, and $d_A$ the distance between two cables. As a result, the total capacitance of the whole model is given by:

$$C_{tot} = \frac{C^* C_A}{C^* + C_A}$$

( 4.7 )

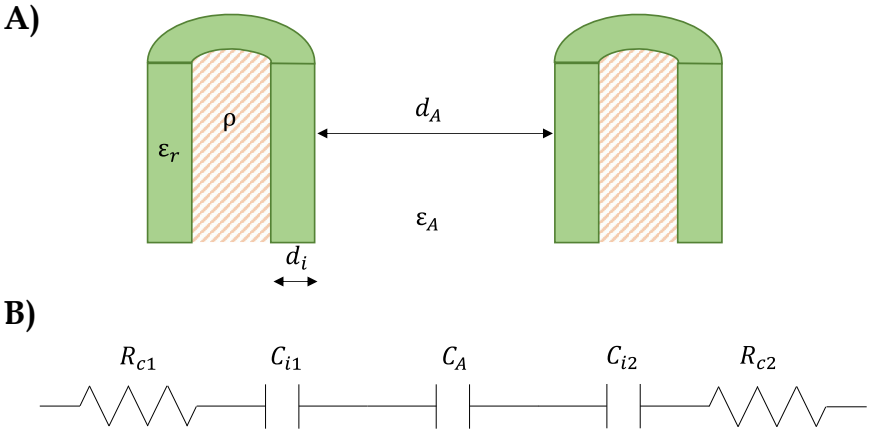


FIGURE 24 Adjacent cables used to connect two EEG electrodes to the amplifier. A) Schematic representation of the cross section of two unipolar cables separated by a distance $d_A$ in a medium (air, dielectric constant $\varepsilon_A$). Each cable is composed of a conductive wire (resistivity ρ) embedded in an insulator sheath (thickness $d_i$, dielectric constant $\varepsilon_r$) B) Equivalent electrical model of two adjacent cables, where $R_{c1,2}$ represent the electrical resistances of the conductive lead, $C_{i1,2}$ model the parasitic capacitances due to the cable insulator layer and $C_A$ depicts the electrical capacitance due to the dielectric $\varepsilon_A$. Modified from (Giangrande, Botter, et al., 2024).

It is important to note that the net charge accumulated on the capacitors modelling the cables is also strongly influenced by another non negligible phenomenon that has been shown to be a source of cable-related motion artifacts. This phenomenon goes under the name of *triboelectric effect* and it describes the transfer of electric charge between two objects when they slide against each other or even when they contact with any external materials (Klijn & Kloprogge, 1974; Ratz, 1969). When the distance between two objects is narrowed until the contact between the two, the atoms at the boundary layers start interacting each other by exchanging electrons (Helmholtz, 1879). As a result, a contact voltage between the adjacent surfaces due to the net charge accumulated between cables because of the triboelectric effect will appear and the two objects will remain charged when their reciprocal distance is increased (Wartzek et al., 2011). Considering the case of the cables adopted for biopotential signal acquisition, the triboelectric effect is expected to occur among the insulation layers of neighboring cables either within a multi-core cable or when considering single cables. Although the insulators are not prone to initiate electrons exchanges, they can still deliver or accumulate a small net electrostatic charge that is stored for a long period of time considering their low surface conductivity. Therefore, friction and deformation of the insulation layers of adjacent cables will be associated with triboelectricity and the resulting electrostatic voltage will be dependent on the materials, contact area, type of contact and speed of the varying reciprocal distance. With the aim of understanding and minimizing motion artifacts due to the movement of the cables, the phenomenon is studied according to the simplified model of two adjacent cables introduced above. The static voltage hypothesized to occur because of triboelectricity polarizes the capacitor $C_{tot}$ creating a voltage drop $V$

across its plates. The net charge $Q$ on the plates of the capacitor (planar faces approximation) is proportional to the potential difference across the two plates being the capacitance $C_{tot}$ the proportional constant. Therefore:

$$C_{tot} = \frac{Q}{V}$$

( 4.8 )

Different considerations can be carried out according to the type of cables connecting the electrodes to the amplifier (FIGURE 23). Indeed, when considering multicore cables, the dominating term in Eq. ( 4.7 ) is $C^*$. Under these circumstances, changes in the distance between two adjacent cables are reasonably limited because of the external containing sheath. Therefore, the main effect causing a voltage difference is mainly due to the friction and deformation of connecting cables driving the transfer of electric charge. However, this can be considered as a poorly representative case of a common EEG experimental practice, as the most common solutions include the use of individual cables. Indeed, in the case of freely-to-move cables, the motion artifacts phenomenon can be described by the inter-cable movements because of the varying distance between adjacent cables. Thus, with reference to the Eq. ( 4.6 ) and ( 4.7 ):

(i) $\varepsilon_r > \varepsilon_A$ since the involved dielectric constants of the insulating mediums are usually $\varepsilon_r \sim 4$ and $\varepsilon_A \sim 1$ for the cable insulator and air mediums respectively

(ii) $d_A > d_i$ since the distance between two adjacent cables is reasonably greater than the thickness of the insulating layer of the silicon rubber of a single wire. Indeed, in the common EEG practice, electrodes are embedded into caps with unipolar cables, at most embedded into an external sheath only for the ending edge. Therefore, adjacent cables cannot be in contact for the whole length of the cables (i.e., $d_A = 0$).

As a result, the dominating term in Eq. ( 4.6 ) is $C_A$ which is due to the contribution of the dielectric (i.e., air) in between two conductive media. This aspect is reflected also in the real practice as the $d_A$ distance is most likely to vary throughout the movement, thus modulating the value of $C_A$, and leading to a variation of the value of the total capacitance of the model influencing the electrical properties of the cables and generating motion artifacts. Due to the abovementioned considerations on $C_A$, the changing reciprocal distance among the cables ($\Delta d_A$) will lead to a change of the capacitance $C_A = C_{A1} - C_{A2}$. Under the reasonable assumption that the net charge $Q$ remains constant (i.e., because of the low leakages of the parasitic capacitance due to the high insultation degree of the insulators wrapping the cables), the changed capacitance will result in a voltage change $\Delta V = V_{A1} - V_{A2}$. FIGURE 25 reports a schematic representation of the phenomenon: $d_{A1}$ is the reciprocal distance between two adjacent cables at one time instant, resulting in a voltage potential $V_{A1}$ across the plate of the $C_A$ capacitor ($C_{A1}$), whereas $d_{A2}$ is the reciprocal distance between two adjacent cables at another time instant, resulting in the voltage potential $V_{A2}$ across the plate of the $C_A$ capacitor ($C_{A2}$).

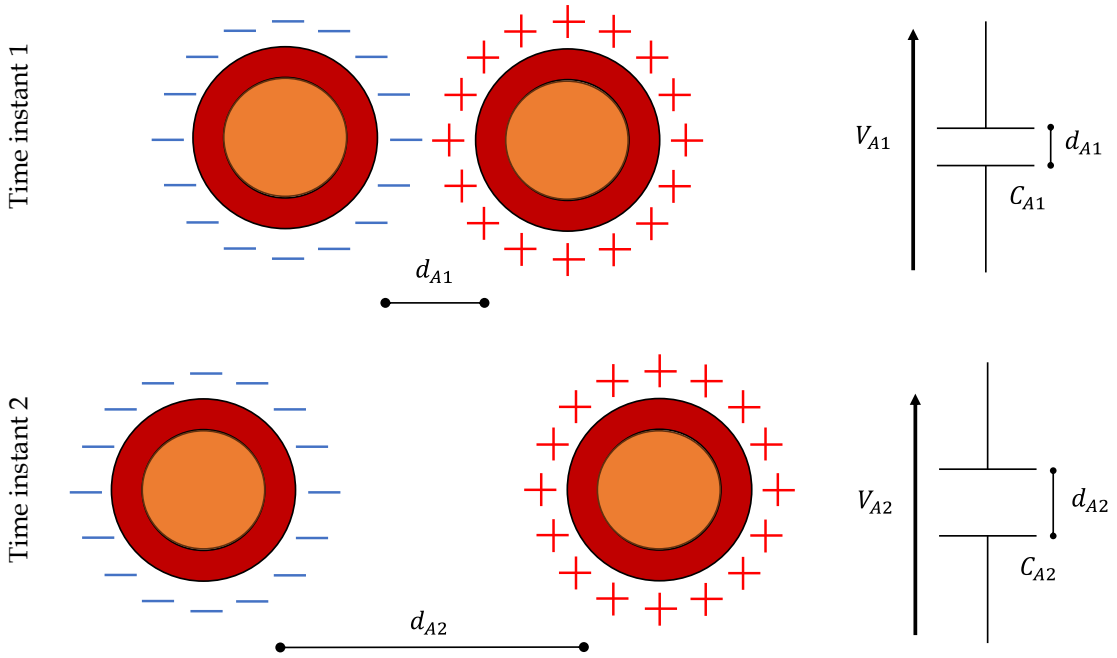


FIGURE 25 Schematic representation of changing reciprocal distance among two adjacent cables with the relative electrical models.

The voltage drop $\Delta V = V_{A1} - V_{A2}$ among adjacent cables is subjected to change throughout the movements, with varying $d_A$ and, therefore, it cannot be neglected when dealing with differential amplifiers involved for the biopotential signal acquisition. Indeed, the triboelectric-related voltage drop $\Delta V$ at the amplifier input will be an additive, pure differential mode, artifact to the biopotential signal of interest collected by means of the electrodes. Such differential-mode artifact is therefore amplified without possibilities of being rejected as in the case of common mode signals.

#### 4.1.2.3 Analysis of the model

The source of motion artifacts discussed in this section can be driven by both the triboelectric effect and the relative net charge accumulated on the surface of the cables connecting the electrodes to the amplifier. However, to numerically estimate the mentioned quantities $C, V$ and $Q$ it is convenient to separate two different cases according to the type of connecting cables adopted:

- Multicore cables: the rising of motion artifacts is supposed to be primarily driven by the direct transfer of electric charges occurring between adjacent cables when they slide or contact (i.e., $\Delta d_A = 0, \Delta Q \neq 0$).
- Unipolar cables: motion artifacts are mainly attributed to the varying distance between adjacent cables because of their movements (i.e., $\Delta d_A \neq 0, \Delta Q = 0$).

Considering the first case with respect to a recorded triboelectric-induced electrostatic voltage difference of $\Delta V \sim 2.5\ \mathrm{mV_{pp}}$, the electric charge can be quantified from Eq. ( 4.8 ). Indeed, considering a fixed distance between cables

($d_i \sim 0.5\ mm$) and being $\varepsilon_0 = 8.854 \frac{\text{pF}}{\text{m}}$, $\varepsilon_r \sim 1$, and $S \sim 0.5\ \text{mm}^2$, the capacitance of the cable is given by $C^* = \varepsilon_r \varepsilon_0 \frac{S}{2d_i}$, therefore resulting in $\Delta Q \sim 10^{-5}\ pC$. As a result, even with relatively small electrostatic charge exchange, the related recorded potentials might alter the correct interpretation of the EEG signals due to their non negligible amplitudes.

Regarding the second scenario, it is hypothesized that there are electrical charges accumulated on the insulators wrapping the cables because of triboelectricity accompanied with the movement of the cables. However, the net charge is assumed to remain constant (i.e., net charge transfer $\Delta Q = Q_1 - Q_2$) as the recorded voltage change (i.e., $\Delta V \sim 2.5\ \text{mV}_{\text{pp}}$) is attributed to the varying capacitance $C_A$, because of the varying distance among adjacent cables $d_A$. Under these circumstances, the Eq. ( 4.8 ) can be used to estimate the value of the net charge accumulated on the surface of the cables as $Q = \Delta V \frac{C_{A1} C_{A2}}{C_{A2} - C_{A1}}$. Thus, being $\Delta d_A \sim 1mm$ hypothesizing $d_{A_1} \sim 10mm$ and $d_{A_2} \sim 9mm$, the net charge results to be $Q \sim 10^{-6}\ pC$. The obtained results indicate that even with small cable movements (i.e., millimeters), it is possible to detect non negligible artifacts even with relatively small amounts of net charge accumulated on the cable insulator.

Even though triboelectric effect-induced artifacts are poorly reproducible in terms of amplitude and spectral content in different trials and quantitative considerations are difficult to carry out, the electrical model of the phenomenon and the performed experiments point in the same direction, suggesting that even small changes in the reciprocal distance between adjacent cables can be the source of motion artifact contamination on recorded EEG signals. In view of what analytically demonstrated, good practice recommendation to reduce the cable-induced motion artifacts during EEG recordings would therefore include the use of EEG electrodes cap with short cables, preferably fixed or embedded into the fabric of the cap itself.

### 4.1.3 Artifacts related to the electrode-amplifier system properties leading to PLI modulation

#### 4.1.3.1 Experimental observation

FIGURE 26 shows an example of the modulation of PLI at 50 Hz, contaminating EEG signals with different waveform morphologies and temporal supports. Being this effect localized on individual, single electrodes, it is hypothesized that an unstable contact at the electrode-skin interface together with non-optimal features of the frontend amplifier may induce the modulation of the residual input-referred power line interference during movement. This phenomenon is particularly interesting within the context of motion artifacts as the movements might influence the electrode-skin interface, thus contributing to the modulation of the PLI. Under static conditions, if a proper electrode-skin preparation is performed (i.e., restrained electrode impedance values through proper scrubbing and conductive gel injection), it is unlikely to assist to an unstable electrode-skin

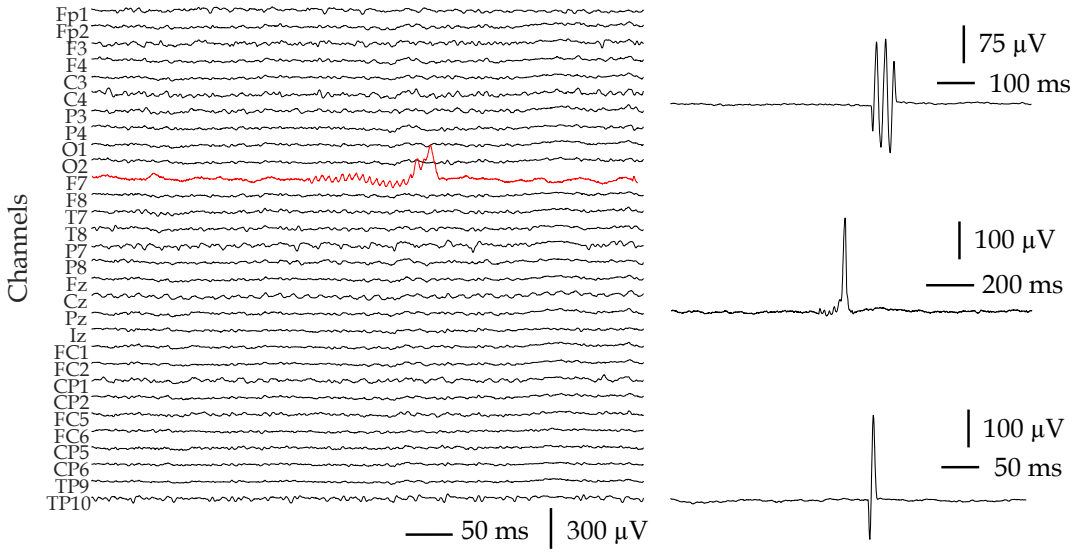


FIGURE 26 Examples of the effect of modulation of power line interference highlighted by the red trace during the recording of 30 EEG and 2 EOG signals during dynamic movement. On the right panel three single-case examples of possible artifact morphology due to the modulation of PL interference.

contacts and the modulation of the power line interference is not expected to occur. On the contrary, when performing movements temporary movement of the electrode with respect to the underneath skin, e.g. owing to a brisk movement, could generate a modulation of the residual PLI due to the variation of the electrode-skin imbalance as showed in the following section.

#### 4.1.3.2 Lumped parameters model

The source signal of PLI-related issues is mainly due to the common mode voltage originating from the parasitic electrical capacitive coupling between a subject, the power line source and the ground. With reference to FIGURE 16, Eq. ( 2.5 ) shows that a common mode excitation can be converted into a differential mode excitation in case of a mismatch between the electrode-skin impedances. When dealing with dynamic EEG recordings, the movement might cause a variation of the electrode-skin impedance e.g. due to a temporary detachment of the electrode with respect to the scalp. This impedance imbalance could vary for a limited temporal support, therefore resulting in a modulation of the residual PLI at the input of the electrode-amplifier system which does not appear on EEG traces with its traditional morphology (i.e., sinusoidal wave at 50/60 Hz). The shape of the resulting artifacts cannot be predicted, and sometimes even its visual identification is difficult. Therefore, post processing filtering techniques (e.g. adaptive filtering of (Botter & Vieira, 2015)) are not effective in removing these type of motion artifacts, thus complicating the signal analysis, post-processing, and consequent interpretation. FIGURE 27 shows a representation of the phenomenon. Specifically, the red sine wave represents the power line signal at 50 Hz frequency, whereas the blue waveform is the modulating signal due to the movement and it is depicted as an on-off signal (i.e., a binary signal where the

levels 0-1 represent respectively the absence-presence of movement). The movement is assumed to cause a skin-electrode imbalance thus resulting to a modulation of PLI. The output signal is shown as the black trace and it is the result of the combination of the previous signals under the assumption of recording exclusively the effect of modulation of power line interference.
To evaluate this phenomenon from an analytical perspective, the electrical model of FIGURE 16 can be taken as a reference, under the following simplifications:

- Electrode-skin impedances are purely resistive (only $R_e$ in the model). This is the case when relatively large (1 cm²) silver electrodes are used.
- Front-end amplifier input impedances are purely resistive (only $R_i$ in the model).
- Input impedance of the front-end amplifier circuit $R_i$ is at least three orders of magnitude (mega Ohm) greater than the electrode-skin impedance $R_e$ (tens of kilo Ohm if 1cm² Ag/AgCl are used). Therefore: $R_i \gg R_e$.
- $C_p \ll (C_1 + C_2)$ because in the real practice it is generally possible to lower $C_p$ by designing battery powered, floating and miniaturized systems (Dellacorna, 2006) as the lower is the value, the lower the common mode input voltage will be. Therefore, the equivalent capacitance of the model will be $C_{eq} \cong C_p$.

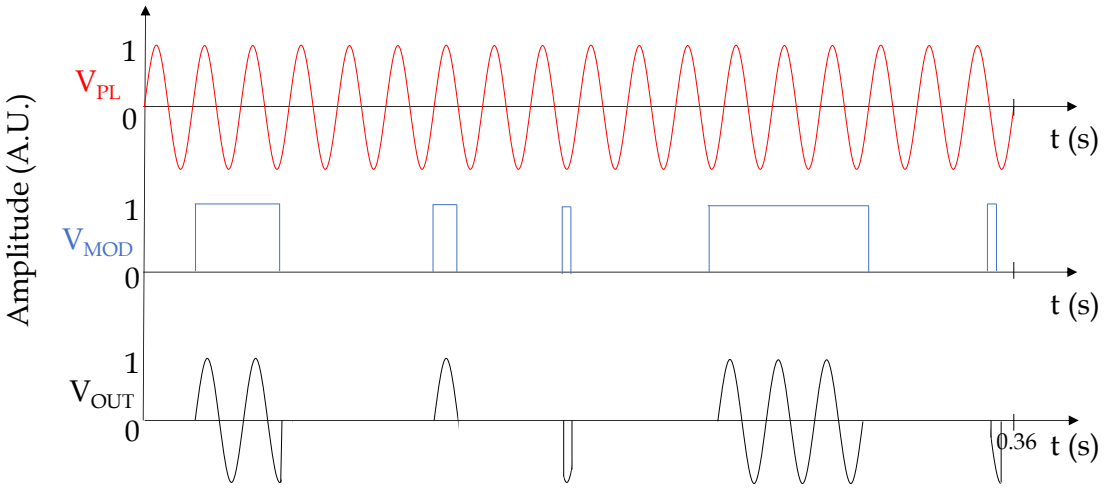


FIGURE 27 Schematic representation of the phenomenon of the modulation of power line interference. From top to bottom: power-line signal (red trace), modulating signal (blue trace), resulting detected signal (black trace). Modified from (Giangrande, Botter, et al., 2024).

However, the case should be adapted to a realistic EEG recording under a multichannel configuration (i.e., with more than two sensing electrodes), as shown in FIGURE 28. Therefore, the Thevenin equivalent circuit extracted from the electrical model of the power line-electrode-amplifier (ground floating) system considers the total resistance obtained as the electrical parallel of all the input resistances of each channel. FIGURE 29 shows the equivalent circuit of the common mode voltage at the input of the electrodes-amplifier system (monopolar configuration) in a multichannel recording where: $V_{PL}$ represents the

PL source being modulated, $C_p$ models the parasitic coupling between the front-end amplifier reference and the power line ground, $V_c$ is the
common mode voltage at the input of the electrodes-amplifier system, $R_e$ refer to electrode-skin impedances of exploring electrodes, $R_i$ represent the front-end amplifier input impedances, and $R_{er}$ refers to the electrode-skin impedance of the monopolar reference electrode. Under this consideration, approximating $C_{eq} \cong C_p$, the equivalent resistance of the electrical model reported above is given by: $R_{eq} = (R_{e1} + R_i) \oplus (R_{e2} + R_i) \oplus (R_{e3} + R_i) \ldots \oplus (R_{eN} + R_i)$ where $\oplus$ indicates the parallel operator of the electrical series of resistances. Thus, the equivalent resistance results in $R_{eq} = R_i/(N)$, where N is the number of channels (e.g. N=32, 64, 128, etc.). Therefore, Eq. ( 2.4 ) can be rewritten as follows:

$$|V_C| = \frac{V_{PL}}{2} \frac{\omega \frac{R_i}{N} C_p}{\sqrt{1 + \left(\omega \frac{R_i}{N} C_p\right)^2}}$$

( 4.9 )

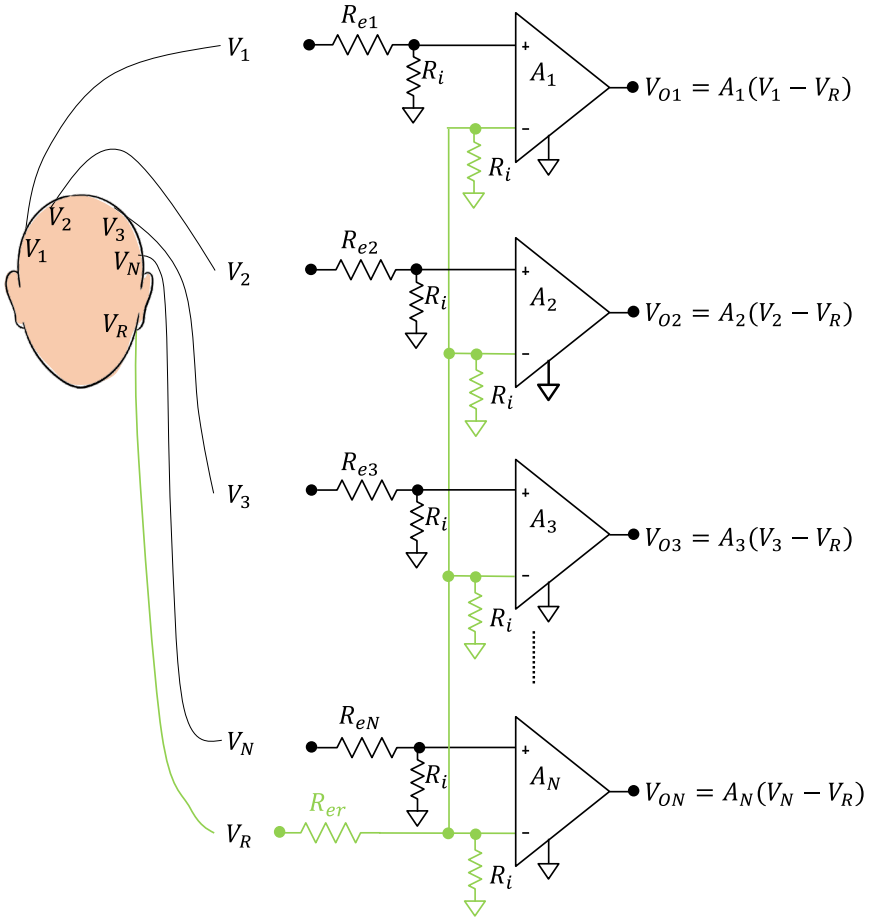


FIGURE 28 EEG multichannel recording schematization. $R_e$ refer to electrode-skin impedances of exploring electrodes, $R_i$ represent the front-end amplifier input impedances, $R_r$ depicts the electrode-skin impedance of the monopolar reference electrode (N = number of channels).

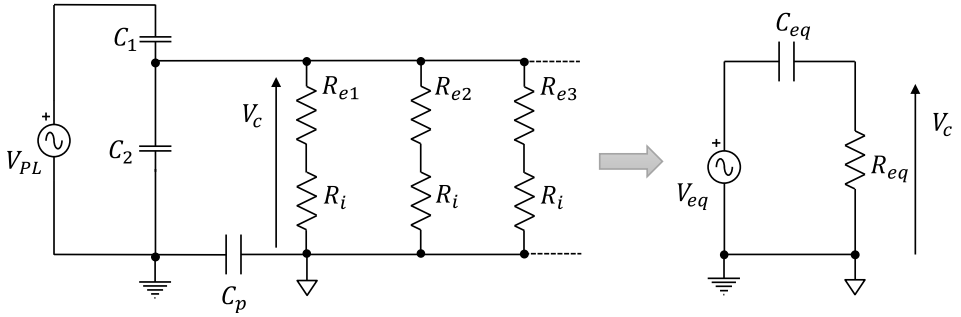


FIGURE 29 Thevenin equivalent circuit of the common mode voltage at the input of the electrodes-amplifier ($V_c$) with ground floating system in a multi-channel EEG recording configuration.

#### 4.1.3.3 Analysis of the model

The common mode voltage at the input of the electrodes-amplifier system $V_c$, can, therefore, be numerically estimated with the following reasonable assumptions, considering a worst-case scenario: $C_p = 10\ \text{pF}, \text{V}_{\text{eq}} = 110\ \text{V}_{\text{RMS}}, R_i = 80\ \text{M}\Omega, \text{N} = 32$, leading to a $V_C = 870{,}7\ \text{mV}_{\text{RMS}}$. With reference to Eq. ( 2.5 ), the input-referred power line interference can be numerically estimated considering an electrode-skin impedance mismatch between electrodes of $\Delta R_e = R_{e2} - R_{e1} = 3\ \text{k}\Omega$, and a $\text{CMRR} = 100\ \text{dB}$, thus leading to a value of $V_{IRN_{50}} = 32{,}65\ \mu\text{V}$ which is plausible to fall within the amplitude range commonly experimentally observed.
Practical considerations can be carried out on Eq. ( 2.5 ) to identify which are the main factors that is worth monitoring to mitigate the modulation of PLI. The outcome of these considerations might serve to draw up useful guidelines to optimize the experimental setup with the aim of reducing the influence of motion artifacts. Specifically, the value of the amplifier input-referred power line interference ($V_{IRN_{50}}$) depends on:

- The common mode voltage due to the power line source referred to the input of the electrodes-amplifier system ($V_C$). This parameter depends on both the design of the amplifier (i.e., design of $R_i$, three- or two-electrodes front-end solution, etc.) and on the experimental setup (i.e., electrodes preparation, coupling between the subject and the power line, etc.). Thus, it can vary according to the movements performed during the recordings. However, a varying common mode voltage is unlikely the cause of movement artifacts appearing at single channel level as its variation would have an effect, although potentially different, on all the channels.
- The common mode rejection ratio (CMRR) of the amplifier, which is, in turn, dependent on the design of the amplifier itself. As a result, no movement-dependent changes on the CMRR are expected to occur and therefore it cannot be the cause hindering the variation of the $V_{IRN_{50}}$.
- The input amplifier resistance ($R_i$) which depends on the design of the amplifier. The same considerations made for the CMRR apply.
- The electrodes-skin resistances imbalance ($\Delta R_e$). This parameter is strictly dependent on the specific experimental setup characteristics and it is the only one that can explain the observed PLI modulation on specific

channels. Indeed, at a single channel level, the electrodes-skin resistances imbalance is obtained from the relative difference between the resistance of the exploring electrode and the one taken as a reference for the monopolar signal acquisition $\Delta R_e = R_{e2} - R_{e1}$ . Additionally, when performing a movement, the single values of electrode impedances may be affected by the changes caused by alteration of the skin-electrode contact due to e.g. reciprocal movements between the electrode and the skin. When the impedance of reference electrode used in the monopolar configuration (i.e., $R_{e1}$) is altered, all the channels should be affected. Whereas if the impedance of a single exploring electrode changes due to an event (i.e., a movement), the effect of the electrode-skin impedance mismatch affects exclusively that channel.

It is therefore possible to conclude that, while an ad-hoc electrodes preparation is mandatory to ensure similarly low impedances among all the channels, it is also preferrable: (i) to adopt adhesive monopolar reference electrodes, preferably placed in body regions with limited movements as an effect is expected to occur at all channels, (ii) to ensure a stable skin contact of the exploring electrodes by avoiding temporary and brisk skin-electrodes detachments causing sudden electrodes impedance changes (i.e., downstream the electrodes). Since the electrodes impedance mismatch is once again demonstrated to play an important role in the context of motion artifacts, the use of active electrodes does not give significant contribution neither to mitigate the phenomenon of PLI modulation. Indeed, the same considerations made for the previously analyzed case of movement electrodes could be applied. Thus, implementing active electrodes becomes ineffectual as their role is to mitigate capacitive coupling downstream the electrodes in presence of a common mode input. Contrarily, the phenomenon of PLI modulation is driven by the electrodes impedance changes occurring downstream the electrodes because of the performed movement. In this regard, good skin-electrodes adhesion is encouraged, suggesting the use of conductive gel with an appropriate viscosity and amount according to the specific application to be performed.

## 4.2 *Study I*: Conclusion

According to the hypothesis of S*tudy I (H1)*, three main sources of motion artifacts affecting EEG recordings during dynamic tasks were identified starting from the experimental observations of Paragraphs 4.1.1.1, 4.1.2.1, and 4.1.3.1: (i) the interelectrode impedance changes, (ii) the triboelectric effect together with the movement of connecting cables, and (iii) the movement-triggered modulation of the power line interference. All these aspects have been analyzed through electrical models and the analytical considerations demonstrated the suitability of the model themselves to embody real experimental situations. Hence, it was possible to identify some good practice recommendations for dynamic EEG:

- Movements of the electrodes should be minimized. A stable electrode-skin contact should be ensured throughout the measurement with the purpose of minimizing the electrode-skin impedance mismatches. Therefore, electrodes sites should be well prepared ensuring an optimal contact and relatively low electrode-skin impedance with respect to the amplifier input impedance. In this regard, the use of wet electrodes with a sufficient amount of conductive gel guaranteeing a good skin-electrode contact throughout the measurements is therefore recommended. Additionally, the same considerations should be applied for the monopolar reference electrode. Indeed, with the aim of avoiding an impact on all the recorded EEG traces, the use of an adhesive reference electrode put in a region less prone to movements (i.e., ear lobe) is highly recommended. Finally, the choice of the cap size that best fits the scalp anatomy of the subject performing the task remains a good practice to be followed in this regard.
- Short and as much as possible fixed cables connecting the electrodes to the recording system are required to mitigate motion artifacts triggered by triboelectric phenomenon and cables movements. An ideal case would be, therefore, to keep electrodes fixed or directly embedded into the fabric of the electrodes cap.
- Whilst the implementation of active electrodes and cable shielding results to be a valuable solution to mitigate power line noise, especially when dealing with non-ground floating systems, their use become ineffectual to mitigate electrodes impedance imbalances upstream the electrodes when the input voltage is changing rapidly. On the contrary, their use may negatively affect the performance of the recording system by increasing the physical dimensions of the system, increasing the risk of noise contamination and the power consumption. Therefore, the choice of including active electrodes and cable shielding when design a wearable EEG acquisition system should be pondered.

The present dissertation highlighted that future studies are needed to investigate possible solutions to overcome the challenges of motion artifact during dynamic tasks. Further technological developments would allow to selectively investigate the abovementioned phenomena in the experimental practice. Thus, their design and application will be presented in the following sections.

# 5 TECHNOLOGICAL STUDIES: ADVANCEMENTS ENABLING THE STUDY OF SENSORIMOTOR INTEGRATION IN DYNAMIC CONDITIONS (*Studies II-III*)

This Chapter describes the design and development activities made to investigate the technological bottlenecks highlighted in Chapter 4 in terms of: EEG signal amplifier characteristics (*Study II*), and EEG electrodes system technology with particular focus on how to handle cables and electrodes features to record dynamic EEG (*Study III*). Therefore, the following dissertation aims at answering the specific research questions of *Studies II* and *III*:

*Q2)* How does the developed wireless-EEG system perform when compared to a gold standard wired EEG system? The design and experimental validation of a wireless, modular EEG synchronized acquisition system as part of a wireless body sensor network is presented.

*Q3)* To what extent EEG electrodes systems with limited movements of cables and electrodes affect the recording of high quality EEG signals? Custom-made EEG electrodes systems are specifically conceived to experimentally meet to the analysis of motion artifacts (Chapter 3) occurring during EEG recordings in dynamic tasks.

## 5.1 Design and validation of a wireless body sensor network for integrated EEG and EMG acquisitions (*Study II*)

Building upon previous technological advancements in the field of wireless EMG (Cerone et al., 2019), this study aims at developing and validating a wireless Body Sensor Network (wBSN) for the simultaneous and synchronous acquisition of biopotentials. The system architecture includes wireless EEG-EMG acquisition systems and a synchronization module allowing the sensor network to be interfaceable with third party devices (i.e., general-purpose instrumentation used

to provide multimodal stimulations or real-time biofeedback). Within the context of the present project, the EEG system and the synchronization units have been prototyped, characterized through bench tests and then experimentally validated in different experimental conditions. A summary of the implemented material and methods and the obtained results is reported.

### 5.1.1 System architecture

FIGURE 30 shows the system architecture. The proposed system implements a client-server wBSN where the clients of the sensor network are named Sensor Units (SU) and allow the collection of biopotentials (EEG or EMG signals) acquisition, while the server is a receiving device allowing for the signal visualization and storage. SUs perform the conditioning and sampling of 33 analog signals and their real-time transmission to the server by means of Wi-Fi connection though a dedicated access point. Additionally, a set of synchronization modules (SyncU) has been designed to serve as a trigger for the synchronous acquisition of the signals collected through the clients by using a communication protocol based on a dedicated, low-latency radio channel. The synchronization set was intended to be an external module. A modular design approach was preferred rather than integrating it in the SU design for three main reasons: (i) minimize the size of the SUs, (ii) use a single, configurable SyncU as a receiver or transmitter, (iii) use a SyncU with any other third party instrumentation involved in an experimental setup to be acquired simultaneously to the collected biopotential signals (i.e., electrical stimulator, movement actuators, etc.). A standalone software has been implemented allowing for the online visualization, acquisition and storage of the collected signals from the clients.

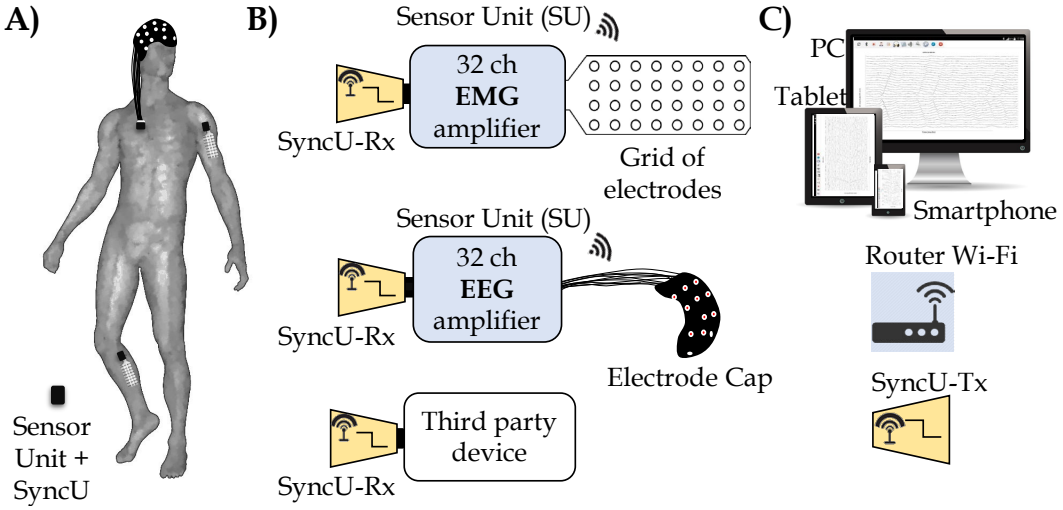


FIGURE 30 System architecture. A) Example of a wBSN (EEG and sEMG SUs). B) From top to bottom: sEMG SU connected to a grid of electrodes, EEG SU connected to an electrode cap, a third-party device. Each module is connected to a SyncU-Rx receiving the wireless synchronization pulse from the SyncU-Tx. C) Receiving mobile device through Wi-Fi. Modified from (Cerone et al., 2022).

### 5.1.2 Units prototyping

The prototyping stage concerned the design of two modules: the EEG SU and the synchronization units. Instead, the EMG SU has been already prototyped and widely adopted in other studies (Carbonaro et al., 2022; Cerone et al., 2019, 2023; Vieira et al., 2024).

***EEG Sensor Unit***. The EEG SU is a compact and wireless biosignal acquisition system aimed at the collection, sampling and transmission of 32 EEG signals and one auxiliary digital signal used for synchronization purposes. The design of the EEG SU follows what described for the EMG SU in (Cerone et al., 2019) with the technical specifications detailed in TABLE 3.
Three main blocks constitute a SU:

- *Acquisition unit* implementing the conditioning and quantization of 32 EEG signals (sampling frequency: 2048 Hz, A/D resolution: 16 bit)
- *Control unit* responsible for the sampling and transmission of the collected signals using a Wi-Fi network link (frequency 2.4 GHz)
- *Power management unit* providing a 3.3 V power supply and handling the battery charging process.

TABLE 3 Technical specifications of the EEG sensor unit.

| Description | Parameter | Value |
|---|---|---|
| Num. of analog channels | $N_A$ | 32 |
| Num. of digital channels | $N_D$ | 1 |
| Bandwidth (EEG mode) | $BW_{EEG}$ | 0.1 Hz – 500 Hz |
| Gain | G | 192 ± 1 V/V |
| Common Mode Rejection Ratio | CMRR | 82 dB |
| Input Impedance module | $\|Z_{In}\|$ | 1.3 GΩ (10 Hz)<br>13 MΩ (1 kHz) |
| Input Range | IR | 10 $mV_{pp}$ |
| Noise referred to input | $N_{RTI}$ | $< 3\ \mu V_{RMS}$ |
| A/D Resolution | Res | 16 bit |
| Sampling Frequency | $f_s$ | 2048 sps |
| Communication | ------- | Wi-Fi |
| Receiver Type | ------- | PC, Smartphone or Tablet |
| Max. Sync. delay | $\Delta t_{Sync}$ | ±5 µs |
| Max. time latency | $\Delta t_{Lat}$ | ±400 µs |
| Max. transmission distance | $d_{TX}$ | 22 m (<0.02% data loss) |
| Power Supply | ------- | 200 mAh 1-Cell LiPo Battery |
| Life time (transmitting) | $T_{TX}$ | 3h |
| Dimensions | ------- | 3.4 cm × 3 cm × 1.5 cm |
| Weight | ------- | 16.7 g |

Each SU is composed of a Printed Circuit on Board (PCB) (eight-layers, 0.8 mm thick, 30 x 25 mm) encapsulated into a 3D printed case leading to a total size of the system of 34 x 30 x 15 mm. The inner PCB contains an analog front-end

(RHD2132 chip, Intan Technologies, California, USA) that was selected for the SU prototyping because of its small size (9 mm × 9 mm, QFN package), low-power with fixed gain (192 V/V), programmable bandwidth (0.1 Hz - 20 kHz) and availability as pre-packaged component for standard pick and place mounting of the PCB.

***Synchronization Unit***. The SyncU module includes two or more units working together: SyncU-Tx for the transmission and a set of SyncU-Rx for the receiving of the synchronization signal. When the SyncU-Rx receives the synchronization pulse, it generates a digital signal that can be acquired by any system connected to it (i.e., either a SU or an external instrumentation). Therefore, a single SyncU-Tx is needed to transmit in broadcasting mode the same signal to all the Sync-Rx units involved in the measurements.
Two main blocks constitute the SyncU:

- *Transmission unit* managing the transmission/receiving of synchronization pulses
- *Antenna matching circuit* managing the wireless transmission of the signals.

Each SyncU consists of an inner PCB (two-layers, 0.8 mm thick, 25 x 22 mm, components mounted on both sides) encapsulated in a 3D printed plastic case leading to a total size of the synchronization unit of 28 x 24 x 12 mm. The inner PCB contains a CC1310 wireless MCU (Texas Instruments, USA) implementing a low-latency radio channel allows building a Personal Area Network with a low power consumption (i.e., 15mW during signal reception). This choice allowed for excellent performance of the receiver in terms of sensitivity (-124 dBm), selectivity (56 dB) and transmission carrier frequency (868 MHz).

### 5.1.3 Bench characterization

The EEG SU and Synchronization Units underwent bench characterization tests aimed at evaluating their compliance with the technical requirements and specifications. On the following, materials and methods used to carry out the bench tests are reported summarily.

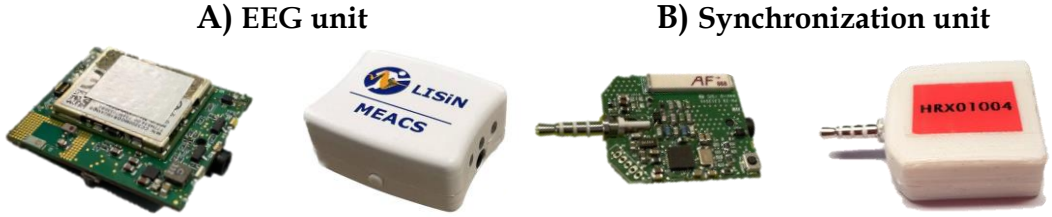


FIGURE 31 Prototypes of EEG and Synchronization modules. Top view of the inner PCB with mounted components and respective external case for the EEG sensor unit (A) and the Synchronization unit (B). Modified from (Cerone et al., 2022).

***EEG Sensor Unit***. The bench characterization of the EEG system included the estimation of the following outcome measures:

- the input-referred noise level measured by short circuiting the analog inputs of the RHD2132 chip and measuring the RMS value for each channel over a 30 s epoch of the collected signal
- the band-pass gain calculated by computing the output-input ratio (peak-to-peak amplitude) when applying a 40 Hz, 2 $mV_{pp}$ sinewave to the input of the RHD2132 front-end
- the robustness to the second order non linearities by means of quantifying the total harmonic distortion and the first-order IMD products. The former was measured in the 0.1 Hz – 100 Hz frequency band for different sinusoidal input (2 $mV_{pp}$, 4$mV_{pp}$, and 8$mV_{pp}$). The first-order IMD products were quantified by applying a linear combination of two sinusoidal inputs (amplitude 8 $mV_{pp}$, $f_1$ = 39 Hz and $f_2$ = 41 Hz).

The obtained outcome measures are reported in the following:

- input-referred noise level: 2 µV ± 0.2 µV RMS on average across channels
- band-pass gain: 192 V/V ± 1 V/V (CoV= 0.5%) within a 0.1 Hz - 500 Hz frequency band for each channel, with an inter-channel gain variability between 0.5% and 1%
- robustness to the second order non linearities: the total harmonic distortion was lower than 0.8% in the 0.1 Hz - 100 Hz frequency band and lower than 0.36% in the 20 Hz – 80 Hz frequency band. The first order IMD products located at 37 Hz and 43 Hz resulted in 135.5 dB ± 6.0 dB.

Therefore, the benchmark characterization of the wireless EEG sensor unit was successful due to the good agreement between the obtained values of the considered outcome variables and the values reported in the datasheet of the involved chip (RHD2132 front-end amplifier).

***Synchronization Unit***. The SyncU were characterized in terms of power consumption and wireless communication performance (i.e., time latency between the transmitted and the received synchronization signals and between the signals received by different SynU-Rx modules).

The SyncU-Tx was powered through a 5 V USB phone charger and the obtained power consumption was 32.5 mW (6.5 mA current consumption) during the synchronization signal transmission. The SyncU-Rx module resulted in a 21.45 mW power consumption (6.5 mA current consumption). When estimating the wireless performance of the SyncUs, an average time latency of 400 µs, with a maximum delay between receivers of 5 µs were obtained.

As a result, also the benchmark tests performed on the synchronization units were satisfying in terms of the obtained performance. The power consumption of the SyncU-Tx was 51% higher than that found for the SyncU-Rx. Nevertheless, the higher power consumption is not critical as the unit is designed to be powered by a USB port rather than a battery-powered device. For what concerns the average time latency and the maximum delay between the receiving units, the presented synchronization system offers a high degree of synchronization

(i.e., below one sample) considering the conventional biopotential signal acquisition systems which have a sampling frequency lower than 2 kHz.

### 5.1.4 Experimental validation

After demonstrating the compliance of the prototyped units with the technical specifications, an experimental validation study was carried out. A head-to-head comparison of the wireless EEG SU with a wired EEG system, taken as a benchmark, was performed during conventional experiment. The aim was to validate the on-field performance of the prototyped EEG system combined with the synchronization module in terms of EEG signal quality, inter-unit degree of synchronization and synchronization with third party instrumentation.

#### 5.1.4.1 Participants

The experimental validation was performed at the EEG Laboratory in the Department of Psychology - Centre for Interdisciplinary Brain Research (CIBR) of the University of Jyväskylä, Finland. For the purpose, eleven healthy subjects (age range: 24–40 yrs., 5 females) were recruited. Participants' handedness was assessed through the Edinburgh handedness inventory (R. C. Oldfield, 1971). All the participants were right-handed with a mean score range 92.37 on a scale from –100 to 100.

#### 5.1.4.2 Materials and methods

The experimental conditions included: (i) auditory, (ii) visual and (iii) somatosensory stimulation, (iv) proprioceptive stimulation and (v) an isometric contraction task. The tasks were repeated twice for a total of ten consecutive measurements by alternating two EEG systems in a randomized and balanced manner. The wireless EEG amplifier was compared to a wired one (Bittium, NeurOne Tesla, Oulu, Finland) considered as a benchmark. Eleven healthy participants were recruited. For both systems, 30 EEG signals were collected in monopolar configuration, online referenced to the FCz reference electrode of the cap. Scalp preparation was done before the measurements and the EEG cap was held in place between consecutive tasks with the sole EEG amplifier to be alternated. TABLE 4 reports a summary of the performed experimental protocols. An offline synchronization was performed on all the acquired signals by using the common external trigger signal transmitted by the synchronization modules. Separately for the EEG systems, according to the stimulation type:

i-iii. EEG evoked responses were computed for each stimulation type (i.e., auditory, visual, and somatosensory) and specific ERP components were identified for each sensory domain

iv. Corticokinematic coherence was computed between 30-EEG signals and the acceleration signal of the finger (Euclidean norm acceleration)

v. Corticomuscular coherence was computed between 30-EEG signals and the unrectified, RMS-normalized sEMG signals.

A Wilcoxon signed rank statistical test was carried out on the extracted variables with the purpose of comparing the results obtained using the two devices.

TABLE 4 Overview of Study II. Experimental protocol details, measurements and outcome variables extracted for the five tested experimental conditions.

| Experimental condition | Experimental Protocol | Acquired signals | Aim |
|---|---|---|---|
| Auditory stimulation | 100 right, 100 left ear acoustic tones (1 kHz, 60 dB, 100 ms duration, ISI: 2 s ± 0.25 s) | 30 EEG signals<br>2 EOG signals<br>Stimulation pattern | To validate the performance of the wireless EEG sensor unit in terms of shape (timing and amplitude) and topographic distribution of the evoked EEG cortical responses |
| Visual stimulation | 100 checkerboard flashes (100 ms duration, ISI: 2 s ± 0.25 s) | 30 EEG signals<br>2 EOG signals<br>Stimulation pattern | |
| Somatosensory stimulation | 100 electrical stimuli to the right median nerve (200 μs duration, intensity of 8.5 mA ± 2.1 mA, across participants, ISI: 2 s ± 0.25 s) | 30 EEG signals<br>2 EOG signals<br>Stimulation pattern | |
| Proprioceptive stimulation | 4 minutes of continuous movement (3 Hz) of the right index finger | 30 EEG signals<br>2 EOG signals<br>Stimulation pattern<br>Right index finger acceleration | To verify the synchronous wireless acquisition of multiple signals to quantify the cortico-kinematic and cortico-spinal coupling in terms of coherence spectra and topographic distribution of coherent sources |
| Isometric contraction task | 4 minutes of a steady isometric pinch contraction (10% ± 2% of maximum voluntary contraction) | 30 EEG<br>2 EOG<br>Stimulation pattern<br>Pinch force signal<br>32 sEMG signals (right flexor pollicis brevis) | |

### 5.1.4.3 Results

FIGURE 32 shows the results obtained from the comparison between EEG recording systems in the five tested experimental conditions. TABLE 5 summarizes the numerical results of the extracted outcome measures from the EEG recording systems in the five tested experimental conditions. Good agreement between the wireless and wired EEG devices was found in all the tested experimental conditions. Indeed, no statistically significant differences were found when comparing the extracted variables from the wireless- and wired-based recordings ($p>0.05$). ERPs studies (i-iii) provided similar results when extracting spatiotemporal information from the sensory stimulation responses. The three sensory stimulations elicited the activation of specific brain areas: bilateral temporal areas for the auditory, occipital area for the visual and contralateral SM1 for the somatosensory stimulation. The same brain areas

showed the strongest responses when comparing wireless- and wired- based EEG recordings. Additionally, coherence studies (iv, v) demonstrated highly concordant coherence spectra between the recording devices. As expected, CKC and CMC spectra were peaking at the expected frequencies (i.e., movement frequency for CKC, and β frequency band for CMC) with the most coherent source located above the sensorimotor cortex, contralaterally with respect to the side involved in the stimulation.

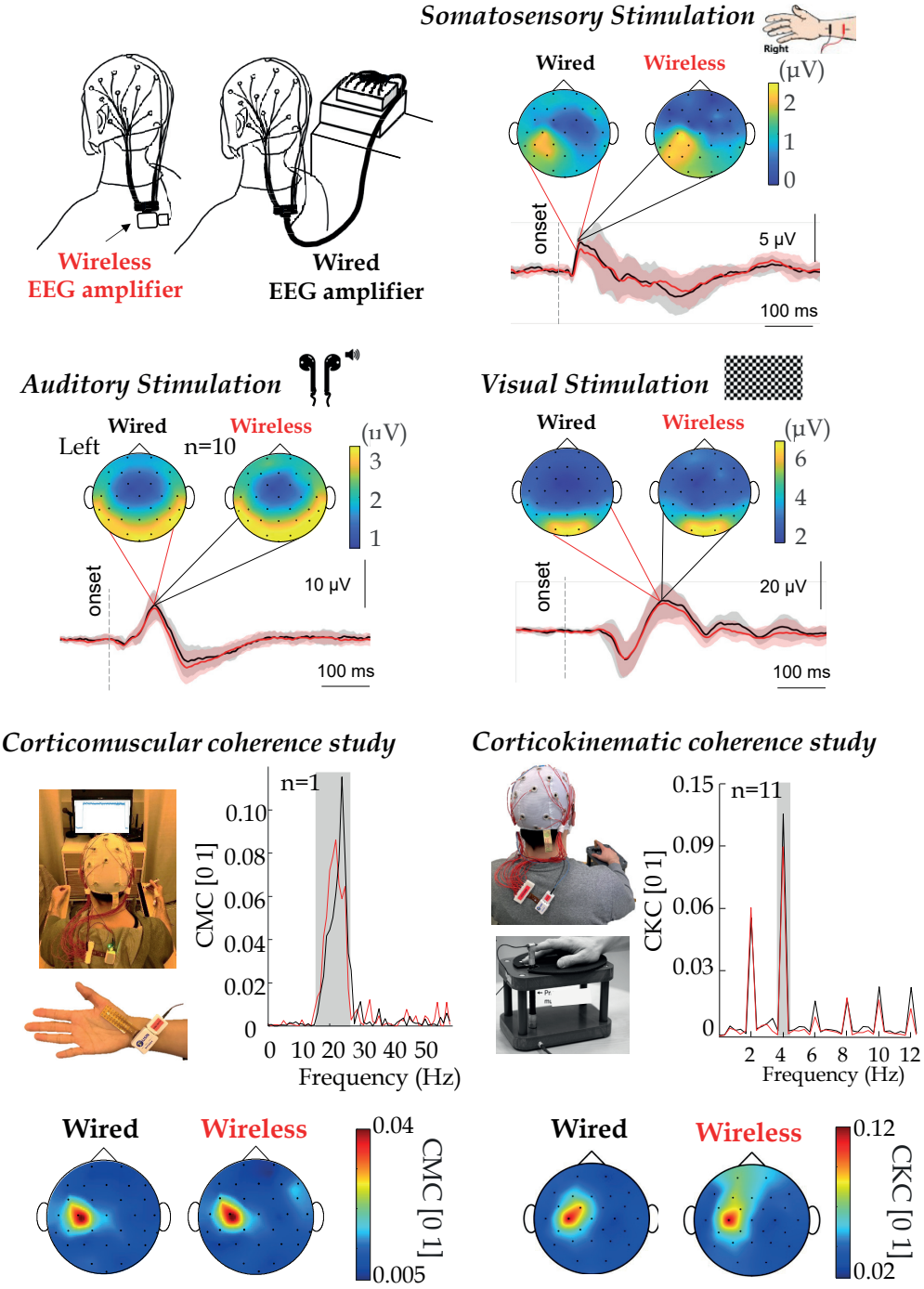


FIGURE 32 Results of Study II: comparison between the wireless and wired EEG systems. ERP to auditory, visual and somatosensory stimuli and CMC and CKC at group-level are shown. Modified from (Cerone et al., 2022).

TABLE 5 Results of Study II: estimated outcome measures (mean ± SD) from the recordings of wireless and wired EEG systems in the five tested experimental conditions.

| | | Peak Latency (ms) | | Peak Amplitude (μV) | |
|---|---|---|---|---|---|
| **Stim Type** | **ERP** | **Wired** | **Wireless** | **Wired** | **Wireless** |
| **Auditory** | P100 | 90.7 ± 6.8 | 86.1 ± 10.7 | 7.86 ± 2.99 | 7.22 ± 3.17 |
| | N170 | 179.8 ± 38.0 | 173.9 ± 29.5 | 5.98 ± 2.88 | 6.57 ± 3.29 |
| **Visual** | N100 | 113.2 ± 16.5 | 116.4 ± 10.2 | 15.79 ± 7.14 | 14.20 ± 7.51 |
| | P200 | 192.5 ± 15.6 | 191.9 ± 18.0 | 15.97 ± 6.87 | 14.50 ± 7.03 |
| **Somato sensory** | N20 | 12.9 ± 10.6 | 16.1 ± 9.8 | 0.97 ± 0.72 | 0.98 ± 0.85 |
| | P30 | 36.5 ± 13.9 | 38.3 ± 14.6 | 4.37 ± 1.95 | 3.06 ± 1.40 |
| | | **Peak coherence strength [0 1]** | | **Peak coherence frequency (Hz)** | |
| **Stim type** | | **Wired** | **Wireless** | **Wired** | **Wireless** |
| **CMC** | | 0.031 ± 0.019 | 0.030 ± 0.012 | 25.0 ± 1.2 | 23.4 ± 0.8 |
| **CKC** | | 0.15 ± 0.11 | 0.12 ± 0.07 | 3.0 ± 0.0 | 3.0 ± 0.0 |

#### 5.1.4.4 Discussion

The experimental findings demonstrated a high degree of overlap between the device under investigation and a gold standard, thus positively contributing to validate the performance, in terms of signal quality, of the designed EEG-based wireless body sensor network in various experimental scenarios. The proposed system architecture represents an advancement with respect to the current state of the art regarding the technological changes in biopotential signal acquisition (Lee & Song, 2019; Niso et al., 2023; Petkos et al., 2019). There are three main strengths with respect to the currently available technologies for the wireless EEG recordings:

i. Modularity: both Sensor and Synchronization Units are totally independent. Data are transferred to the PC and the sensor network allows the contemporary use of up to four units simultaneously.
ii. Portability: the server receiving the acquired signals can be whatever platform with Wi-Fi connectivity such as PC, smartphone, tablet, single board computer (e.g. Raspberry Pi). Therefore, thanks to the reduced size of the involved units, the body sensor unit is not only wireless (i.e., no implication of cables between electrodes and amplifier), but also portable in a way that it allows the acquisition of biopotential signals also in experimental scenarios other than the laboratory (e.g. naturalistic tasks).
iii. Synchronization: the use of external synchronization units allows to simultaneously record (i.e., with synchronization delays lower than the

sampling period) biopotentials with any external, third-party signals still preserving the wireless and floating nature of the whole architecture.

Therefore, the developed body sensor network represents an enabling technology in the field of biopotential signal acquisition, laying the foundations for future investigations of sensorimotor integration and corticospinal coupling not only in static, but also in dynamic and naturalistic tasks and naturalistic environments.

### 5.1.5 *Study II*: Conclusion

*Study II* described the design and characterization of an innovative wireless EEG system as part of a wBSN allowing the simultaneous acquisition of biopotentials and other external data with a high degree of synchronization. To this end, the prototype of the proposed body sensor network includes a set of Sensor Units and Synchronization Units allowing integrated measurement of EEG and sEMG signals. Additionally, the synchronization with external data acquired from third-party devices is allowed. Examples of third-party data include external stimulation patterns (e.g., for auditory, visual, tactile, transcranial magnetic stimulation, etc.), external signals (e.g., force, kinematics, etc.) or other auxiliary signals (e.g. trigger pulses).

Contrarily to the sEMG module that has been already fully described and extensively validated in a wide range of experimental scenarios, the wireless EEG unit and the synchronization modules have been purposely designed within the context of the current PhD project. Therefore, a validation study on the body sensor network performance, with a focus on the wireless EEG unit, was considered mandatory both in terms of bench and experimental characterization. All the performed bench tests were successful in demonstrating the compliance of the wireless EEG system to the technical project specifications. Moreover, according to the hypothesis of *Study II (H2)*, a good agreement between the wireless and wired EEG system was expected. In this view, the head-to-head comparison confirmed the hypothesis. Indeed, no specific device-related differences in signal properties and derived outcome variables were found between the developed wireless EEG unit with respect to the wired, well-established one combined with third-party devices under conventional experimental conditions (i.e., sensory stimulations, proprioceptive stimulation, isometric contraction task). The wireless body sensor network allowed to identify event-related potentials to sensory stimulation, and significant CKC and CMC, similarly to gold-standard EEG acquisition system. As a result, this initial validation performed in laboratory environment validated the use of the wireless body sensor network with respect to state-of-the-art devices, laying the foundations for future investigations of the human sensorimotor functions in naturalistic conditions and tasks.

## 5.2 Design and experimental considerations on innovative EEG electrodes systems for the evaluation of motion artifacts sources (*Study III*)

The analytical study presented in Chapter 4 highlighted that although the development of miniaturized and wireless acquisition systems allowed to enable the study of EEG also during movements, this opportunity is not fully exploited in practice as one of the biggest obstacles still compromising the high-quality of EEG recordings in real-world applications is the residual contamination of EEG traces from motion artifacts. Specifically, the main factors negatively influencing the quality of EEG electrodes are related to (i) the presence of cables connecting electrodes and the amplifier and (ii) the electrodes technology. Therefore, further technological developments are needed to selectively investigate the effect of cables and traditional electrodes in the real experimental practice and thus to experimentally test the advanced hypotheses on the genesis of EEG motion artifacts (Chapter 4).

### 5.2.1 Design of EEG electrodes systems

To better understand the role of cables and electrodes as sources of motion artifacts on EEG signal collection during dynamic tasks, we designed two customized EEG electrodes systems to be used with the developed wireless, miniaturized amplifier (Cerone et al., 2022). The former was named ET Cap and it is a textile-based system aimed at minimizing the effects of the cables. Indeed, it is based on electrodes-amplifier connections embedded into the fabric of an EEG cap. The latter EEG cap is named Lobster Cap and it consists of printed-circuits on a flexible support aiming at reducing the influence of both connecting cables and moving electrodes as they are intended to be attached to the scalp. These caps have been designed and prototyped with the specific aim of mitigating respectively the effects of the moving cables and the varying interelectrode impedances during movements.

#### 5.2.1.1 ET Cap: Textile-based EEG electrodes system

FIGURE 33 shows the ET Cap. FIGURE 33 A represents the construction details of the textile traces. A standard 30 head-mounted electrodes EEG cap (EasyCap GmbH, Gliching, Germany) was adapted to our purpose. Specifically, the connecting free to move wires have been substituted by conductive traces embedded in the fabric of the cap itself through a sewing machine. These traces are made of a conductive material coated with a thin insulating glaze. Their morphology has been chosen as a sinusoidal waveform to efficiently maximize the stretchability. The two edges of the conductive sinusoidal traces are then soldered on one side onto a small part of the electrode native cable (~0.5 cm), and to the other side onto the soldering pads of a printed-circuits flexible adaptor with a specific connector to be used as input for the acquisition system.

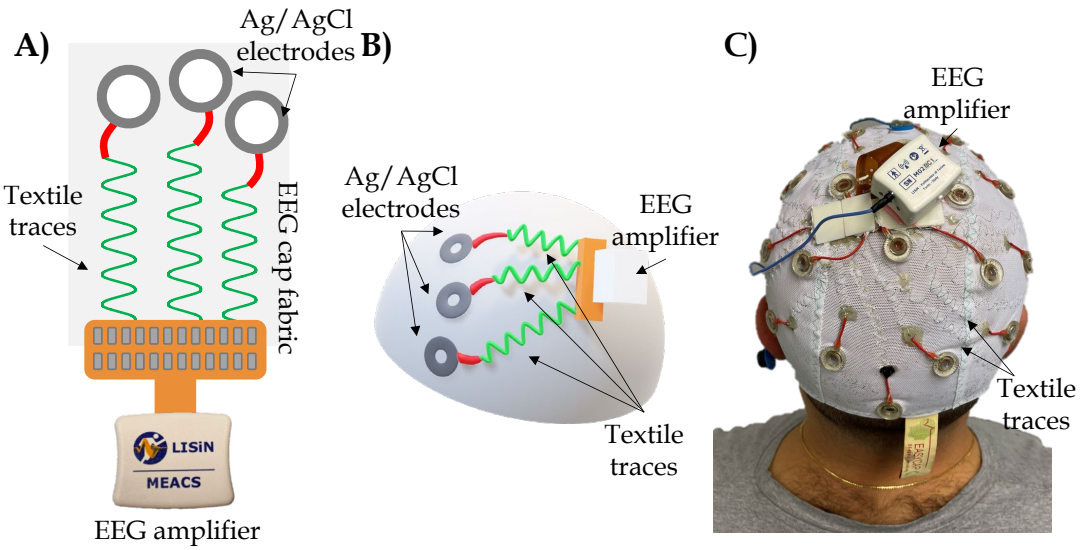


FIGURE 33 ET Cap: textile-based EEG electrodes system. A) Schematic representation of the textile traces sewed onto the EEG cap fabric and further connected to the exploring electrodes and the flexible connector constituting the input of the EEG amplifier. B) 3-D representation on a phantom. C) Picture of a subject wearing the textile-based electrodes system connected to the EEG amplifier. Modified from (Giangrande, Botter, et al., 2024).

Finally, the welding points from the electrodes side were further reinforced through an epoxy adhesive glue, while the soldering pads of the connector-side were covered with a thin layer of silicone. The flexible adaptor is fixed onto the cap itself to minimize the cable lengths with the aim of placing the acquisition system on top of the head (see FIGURE 33 B-C for details). Since the electrode technology has not changed with respect to the native one, the sites preparation follows gold standard practices.

#### 5.2.1.2 Lobster Cap: Flexible PCB-based EEG electrodes system

FIGURE 34 depicts the Lobster Cap. FIGURE 34 A shows the design of the two-dimensional flexible system of electrodes. It is characterized by the total absence of connecting cables as it includes printed circuits on a flexible support (Polyimid, 80 µm thick). The flexible PCB integrates 30 Ag ring electrodes (inner diameter Ø 0.8 mm) connected to the input connector of the EEG acquisition system. Each electrode site is labelled according to the 10-20 system as they are intended to be placed on the subject's scalp according to the standardized positions identified and marked prior the measurements. FIGURE 34 B reports the detail of a single exploring electrode (e.g. Cz) showing three main layers: a first double sided adhesive tape (1 mm thick) to allow for the other layers to be attached to the flexible support, a FR4 ring (1 mm thick) to give mechanical support and to facilitate its bonding to the scalp through a final layer of biocompatible glue (Histoacryl, Braun Medical, Germany) needed to fix the electrodes in the correct position and avoid their relative movement with respect to the scalp. The length of the different branches of the electrodes system were purposely designed to

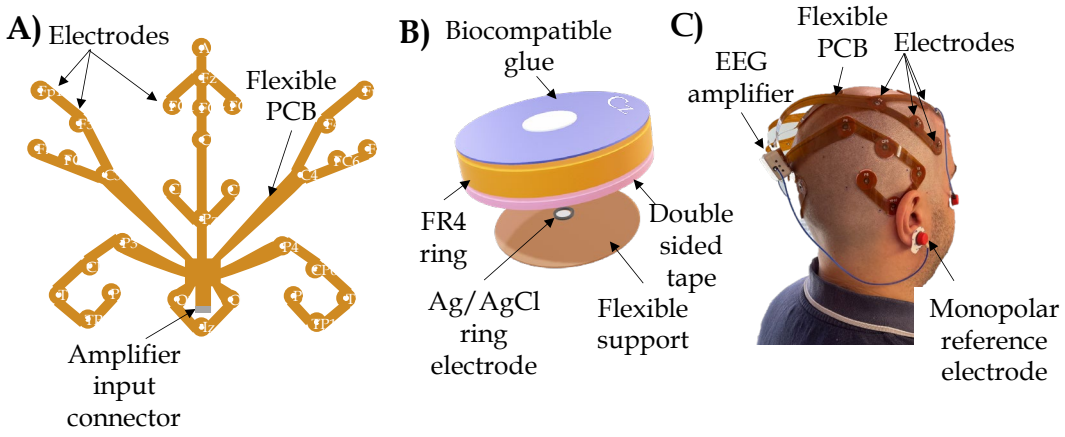


FIGURE 34 Lobster Cap: Flexible PCB-based EEG electrodes system. A) Design of the entire system based on printed circuits on a flexible support. B) Details of a single electrode preparation. A FR4 ring is attached on top of the electrode through a double sided tape. Electrodes are then attached to the scalp by means of a biocompatible glue. C) Picture of a subject wearing the adhesive-based electrodes system connected to the EEG amplifier. Modified from (Giangrande, Botter, et al., 2024).

have a small slack allowing for a correct placement according to the subjects' scalp anatomy. The electrodes design included a ring-shape allowing the user to inject the conductive gel after the electrodes placement. FIGURE 34 C shows the Lobster Cap put in place on a subject. It is important to underline that the designed solution is not intended to be used in wide context scenarios, as, due to its limited applicability (i.e., only bald subjects and time-consuming electrodes preparation), it could not be generalized to a heterogeneous population. Indeed, it was purposely designed to shed lights on the specific topic of the genesis of motion artifacts on EEG recordings during movements with the aim of simultaneously mitigating both cables- and electrodes- influence.

### 5.2.2 Experimental tests

Both standard (i.e., wet electrodes with connecting cables to the amplifier) and customized solutions (i.e., ET Cap with shortened cable connections or Lobster Cap with different electrode technology) were evaluated during dynamic motor tasks. Time- and frequency- domain variables were extracted to investigate the influence of cables and electrode technologies to give further grounds and experimentally investigate the hypothesis modelled in the previous sections.

#### 5.2.2.1 Material and methods

The study was conducted on a single, bald subject as our aim was to experimentally meet the advanced hypotheses on the genesis of motion artifacts on EEG dynamic acquisitions with particular focus on the effect of cables and electrodes. FIGURE 35 shows the four EEG electrodes systems involved in the study: A) *STN Cap* - a standard head-mounted electrodes cap (EasyCap GmbH, Gliching, Germany) with 50 cm of connecting cables, B) *ET Cap* - the textile-based

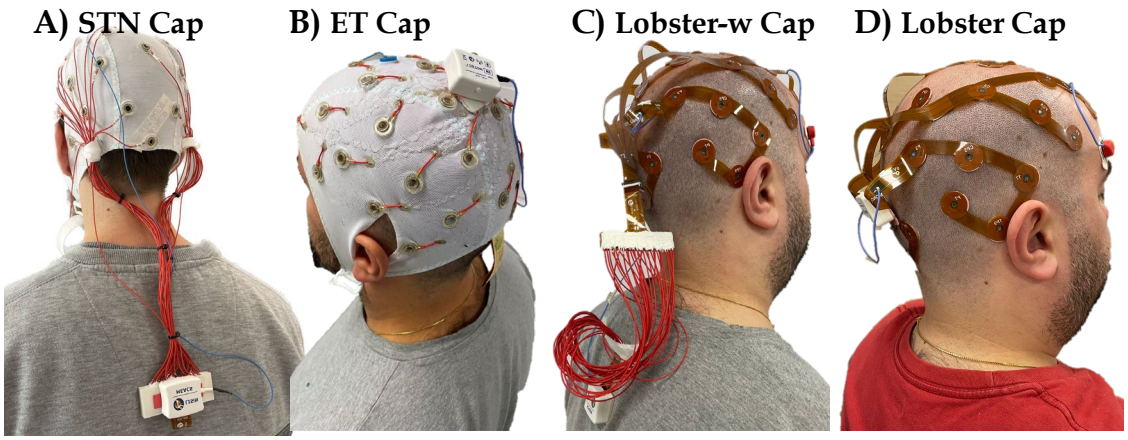


FIGURE 35 EEG electrodes systems used in the experimental case study of Study III. A) Standard head-mounted electrodes with connecting cables (STN Cap), B) textile-based system (ET Cap), C) modified Lobster with cables (Lobster-w Cap), D) flexible PCB-based system (Lobster Cap). Modified from (Giangrande, Botter, et al., 2024).

system, C) *Lobster-w Cap* - obtained from the Lobster Cap by adding a custom-made adaptor constituted by 50 cm long connecting cables, D) *Lobster Cap* – the flexible PCB-based EEG electrodes system with no additional cables. 30 EEG signals and 2 Electrooculograms (EOG) were recorded through the wireless EEG acquisition system described in Chapter 5.1 with a sampling frequency of 2048 Hz (Cerone et al., 2022). The experimental setup included a general purpose acquisition unit collecting magneto-inertial signals (100 Hz sampling frequency) placed on the head to track its acceleration, while a second unit (DuePro, OT Bioelettronica, Italy) was used to collect an additional analogue signal from a footswitch (force sensor-FlexiForce A201, Tekscan) placed under the right heel (2048 Hz sampling frequency). The experimental protocol included the repetition of three tasks: 60-s of standing balance considered as a rest condition, treadmill walking at 4.6 km/h and jogging at 6 km/h. Measurements were carried out in four different days (one EEG electrodes system per day) to avoid any influence of impedance changes related to the consecutive scalp preparations. Subject preparation was performed following the steps of electrodes sites abrasion and conductive gel injection. At first an abrasive paste (NuPrep, Weaver and Company, Aurora, USA) was used to gently scrab the scalp by abrading the entire surface. Afterwards, the EEG electrodes system was held in place and a conductive gel (NeurGel, SPES MEDICA, Genova, Italy) was inserted into the electrode cavities. Finally, two additional electrodes (30 mm × 22 mm Ambu s.r.l., Denmark) placed in the up-left and down-right corners were used to record EOG signals. A further adhesive electrode (Ø 24 mm, Kendall, Covidien, Minneapolis, USA) placed on the right ear lobe after a gentle skin abrasion served as the monopolar reference site for the EEG signals recordings. This choice was specifically made to minimize the relative movements of the reference electrode and, therefore, to avoid any additional confounding factor (i.e., possible artifacts other than cable- or exploring electrodes- related) on the collected signals.

EEG signals collected through the four electrodes systems were initially evaluated through visual inspection. Analyses in the time and frequency domains were carried out by using Matlab Software (Mathwork Inc, Natick, MA, USA). Statistical analyses were performed using R Statistical Software (v4.1.2; R Core Team 2021). First, EEG signals were band-pass limited through a 4$^{th}$ order Butterworth bandpass filter (0.1 Hz - 100 Hz). Then, the common average filter was applied by removing the average of all the 30 EEG signals at each channel level to remove the noise floor common to all the recorded signals. Under the hypothesis that signals corrupted by motion artifacts (either generated as cables- or electrodes- effect) are characterized by greater amplitudes with a more heterogeneous distribution among channels, we estimated the median Root-Mean-Square (RMS) value over 1-s epochs (50% overlap) at each electrode level. A one-way repeated measures ANOVA statistical test (Tukey's post-hoc correction) was applied on the RMS values to evaluate the effect of the EEG electrodes system on the recorded signal amplitudes. Then, the two types of motion artifacts displayed in FIGURE 36 were identified on the collected EEG signals. The former are characterized by spurious spike-like motion artifacts and they are mostly attributable to cables movements. Whereas the latter artifacts are displayed as low frequency variations correlated to the movement frequency. Therefore, further analyses were carried out aimed at specifically evaluating the effect of the (i) cables- and (ii) electrodes- triggered artifacts.

To investigate the influence of the cables, we compared the results of "cabled" electrodes systems (STN and Lobster-w caps from FIGURE 35) to those of "non-cabled" technological developments (ET and Lobster caps from FIGURE 35). The comparison was performed pairwise considering the electrodes systems with the same electrode technology (i.e., STN vs ET caps and Lobster-w vs Lobster caps). The effect of the cables was evaluated by assessing the median kurtosis value of the amplitudes of the recorded EEG signals over 1-s epochs (50% overlap), under the assumption that a more heterogeneous distribution of amplitude values among EEG channels is associated to the presence of the spike-like artifacts generated by cable movements. To quantify the heterogeneity of the kurtosis values within the 30-EEG channels of the different electrodes systems, the variation coefficient for each kurtosis distribution was extracted.

The effect of the electrodes was further evaluated by comparing the results of the two custom-made solutions including standard and original electrodes technology (ET vs Lobster caps from FIGURE 35) in a two steps procedure. We hypothesized to find repeatable artifacts time-locked to the heel strikes when using standard electrodes (i.e., strongly correlating with the gait frequency), while no strides-triggered artifacts were expected with electrodes attached to the scalp. As a result, at first, the coherence between cortical signals and the head acceleration signal was computed to isolate the 6 EEG signals (i.e., 20% of the total) showing the highest coherence value. Secondly, we extracted the average cortical response through spike triggered averaging technique (i.e., synchro average technique) with respect to the right heel strikes. Thus, the peak-to-peak

amplitude values of the averaged response are finally compared to quantify the effect of electrode-related motion artifacts.

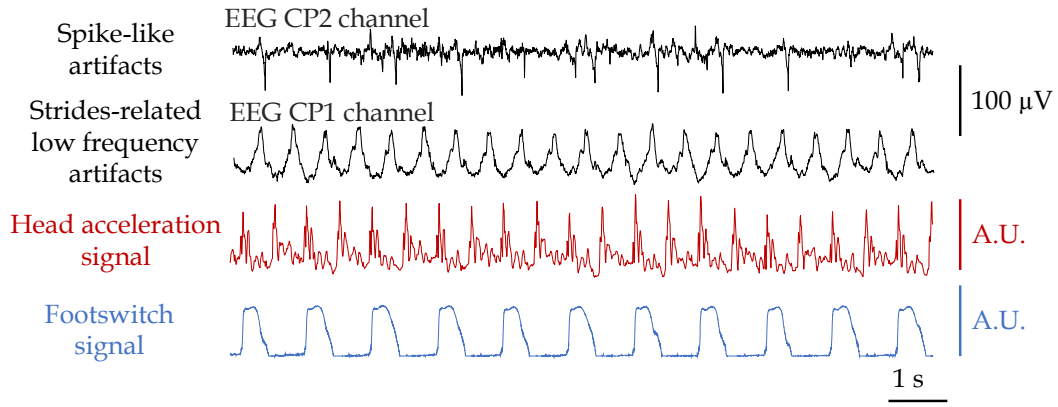


FIGURE 36 Examples of recorded EEG motion artifacts related to cables- and electrodes-movements recorded through a standard EEG electrodes system. The force signal collected from the right heel is also reported timewise.

#### 5.2.2.2 Results and Discussion

FIGURE 37 shows RMS amplitude values of the EEG signals recorded with the four electrodes systems during rest, treadmill walking and jogging. TABLE 6 reports the numerical values of RMS amplitudes (mean ± SD across channels) for each electrode system and condition. No statistically significant differences were found among RMS values of EEG signals recorded through the four electrodes systems with the subject at rest or performing a treadmill walking task, except for the comparison between the cabled and non-cabled adhesive-based electrodes system (i.e., Lobster-w vs Lobster caps). Results from the jogging task revealed, instead, statistically significant differences between RMS values obtained by cabled (STN and Lobster-w caps) versus non-cabled solutions (ET and Lobster caps). Additionally, further differences were highlighted between the standard, cabled electrodes technology (STN Cap) and the non-cabled, flexible PCB-based one (Lobster Cap). As expected, higher RMS values are obtained with the increasing dynamics of the performed task because of the rising of both motion and other movement-related physiological artifacts (e.g. muscular activity contamination from neck, or temporal regions). Furthermore, the cabled electrodes systems (STN and Lobster-w) showed on average higher RMS amplitude with a wider distribution according to the task dynamics.

TABLE 6 RMS amplitude values of the EEG signals recorded with the four electrodes systems during rest, treadmill walking and jogging (mean ± SD).

| **EEG electrodes system** | **RMS Amplitude (Mean ± SD, µV)** | | |
|---|---|---|---|
| | **Rest** | **Walking** | **Jogging** |
| STN | 5.52 ± 0.98 | 9.47 ± 5.47 | 17.3 ± 12.1 |
| ET Cap | 6.26 ± 1.35 | 9.53 ± 5.57 | 13.8 ± 10.2 |
| Lobster-w | 5.62 ± 0.85 | 10.3 ± 3.71 | 19.5 ± 13.1 |
| Lobster Cap | 6.04 ± 1.09 | 8.28 ± 2.73 | 10.2 ± 4.74 |

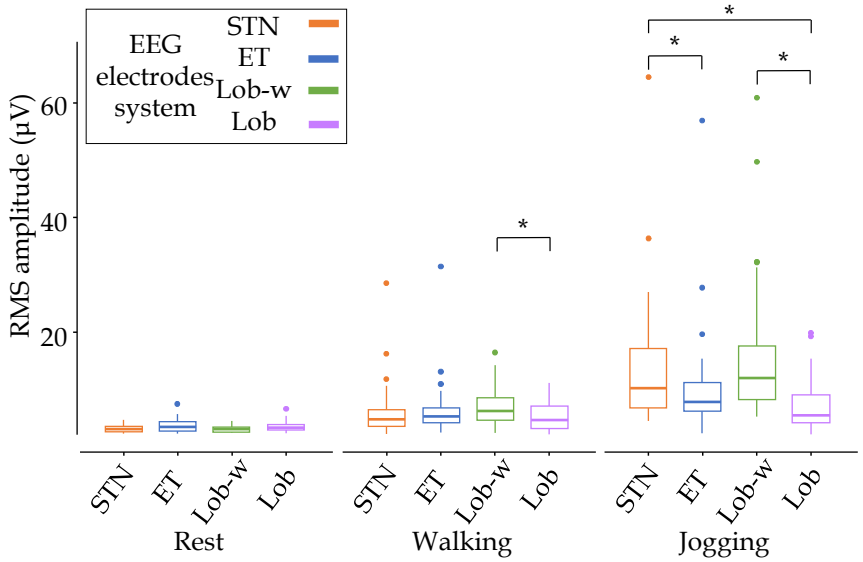


FIGURE 37 Results of Study III. Boxplot of RMS amplitude values of 30 EEG signals recorded with the four electrodes systems during rest, treadmill walking and jogging. *p<0.05 obtained with one-way ANOVA (Tukey post-hoc correction). From (Giangrande, Botter, et al., 2024).

FIGURE 38 represents the distributions of the kurtosis values extracted on the 30 EEG signals with the four electrodes systems in all the performed tasks. We obtained variation coefficients of: STN) 5%; ET) 8%; Lobster-w) 4%; Lobster) 5% during rest, STN) 14%; ET) 8%; Lobster-w) 16%; Lobster) 14% during walking, and STN) 47%; ET) 20%; Lobster-w) 34%; Lobster) 24% during jogging task.

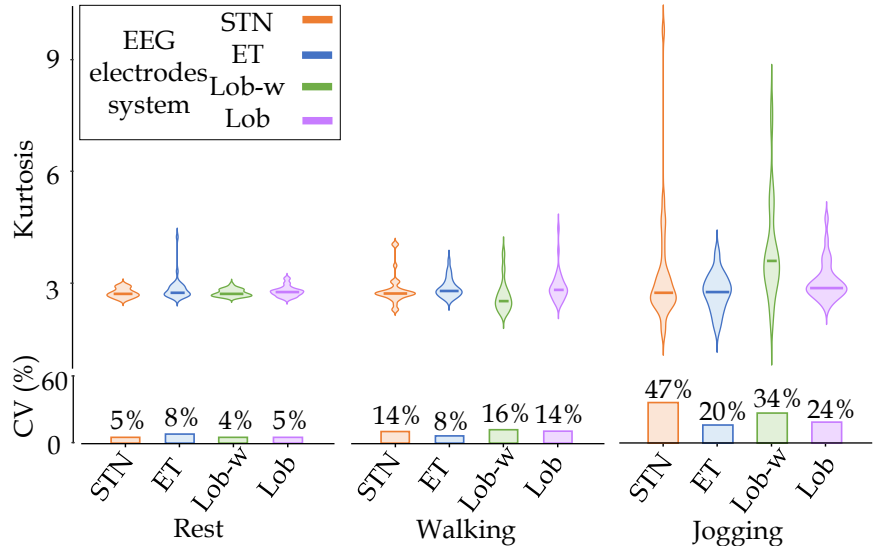


FIGURE 38 Results of Study III. Violin plots displaying the median values of kurtosis computed over 1-s epochs for 30 EEG signals recorded through the four electrodes systems in all the performed tasks. From (Giangrande, Botter, et al., 2024).

According to our hypotheses, the greater the task dynamics and the resulting cables movements, the more heterogeneous is the amplitude signal distribution mainly because of a higher occurrence of spike-like artifacts. Therefore, the greatest variation coefficients of the kurtosis values were expected for signals recorded through cabled electrodes system (STN and Lobster-w caps) during the jogging task. FIGURE 39 shows the cortical responses averaged with respect to the right heel strikes across strides (n=54 walking, n=70 jogging) considering the most coherent channels with head acceleration during walking and jogging. Although different morphologies of cortical responses (e.g. even showing different polarities) might occur at intra-electrode level, we found motion artifacts time-locked to the heel strikes, with high intra-electrode repeatability. In line with our assumptions, higher peak to peak amplitude values were obtained for the cortical responses recorded with textile-based electrodes system when compared to the flexible PCB-based one (24.70 µV vs 7.23 µV and 46.03 µV vs 7.64 µV respectively during walking and jogging). The STN and Lobster-w caps were not included in this analysis to minimize the contamination of cables-related artifacts as a potential confounding factor.

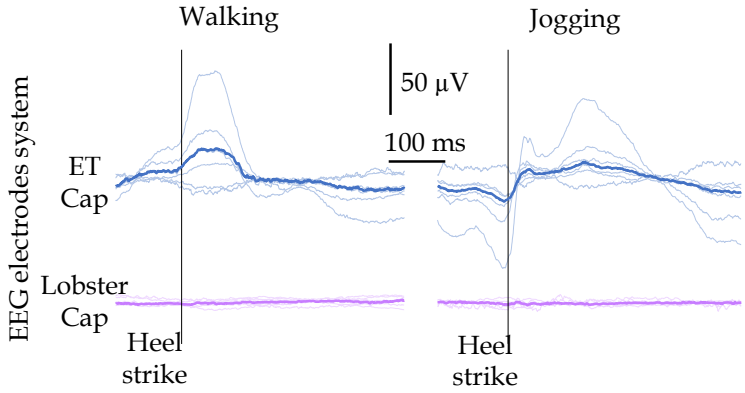


FIGURE 39 Results of Study III. Averaged cortical responses with respect to the right heel strike onset obtained from EEG signals recorded through textile-based (B, green traces) and adhesive-based (D, violet traces) electrodes systems during walking and jogging motor tasks. Only the most 6 coherent EEG signals with the head acceleration are displayed. From (Giangrande, Botter, et al., 2024).

### 5.2.3 *Study III*: Conclusion

According to the hypotheses of *Study III*, the obtained results contribute to endorse the analytical investigation of the phenomena related to the genesis of EEG motion artifacts (Chapter 4). Indeed, the purpose of developing EEG electrodes systems was not to propose a system intended to be used in the future experimental practice, but instead to prove that with little to no movements of electrodes and cables, EEG measurements are robust towards motion artifacts contamination. The hypothesis that also electrodes, and not only acquisition systems, need to be specifically designed and developed for dynamic applications is therefore verified. In particular, the experimental case study suggested that the choice of the EEG electrodes system is critical when planning

EEG recordings during dynamic tasks. While the ideal case would be to keep electrodes and cables fixed such as the case of the Lobster Cap, it cannot be always used as it is applicable only to bald subjects and it might require a longer preparation than a standard cap. However, considering the need for minimization of the connecting cables length and related reciprocal movements to mitigate the effects of triboelectric phenomenon, embedding the connecting cables into the fabric of the cap of electrodes such as in the ET Cap could be a good compromise between usability and performance needs. Moreover, while adhesive electrodes represent the optimal choice to avoid additional electrodes movements, specific experimental cautions can be taken to prevent the electrodes-related motion artifacts. In this regard, a good compromise can be found when adopting wet or dry electrodes embedded in EEG caps with a proper size that best fits the scalp anatomy of the subject. Firmly securing the EEG cap during the experiment prevents the electrodes movements and the related rising of motion artifacts. Further technological advancements should therefore focus on the transduction stage of the biopotentials amplification chain such as the electrode technology and its interfacing to the acquisition system.

# 6 NEUROPHYSIOLOGICAL STUDIES (*Studies IV-V*)

This section describes two applied studies (*Studies IV – V*) using the developed wireless EEG system as part of specific wireless body sensor networks. Physiologically-oriented studies aimed at evaluating sensorimotor integration phenomena have been carried out. Brain-body interactions are investigated by answering to specific research questions:

*Q4)* How does maintained volitional muscular activation affect the cortical processing of naturalistic continuous and intermittent ankle joint proprioceptive stimulation?

*Q5)* Is it feasible to extract physiological outcome measures from wireless EEG recordings during dynamic tasks?

## 6.1 Investigating the effect of maintained volitional muscular activation on cortical proprioceptive processing (*Study IV*)

The research aim underlying this study was to assess the neuronal proprioceptive processing in the human neocortex through the quantification of CKC, evoked and induced EEG responses to naturalistic ankle-joint proprioceptive stimuli. Specifically, the effect of a steady voluntary muscular activity on the processing of the afferences arising from the ankle joint was estimated by comparing active (i.e., isometric plantar-flexor torque) and passive (i.e., relaxed) conditions. Nevertheless, results would contribute to demonstrate not only whether and how the cortical processing is modulated because of an ongoing motor action, but also inherently show the validity and reliability of the applied technology to track alterations of the proprioceptive afferent pathway through the quantification of specific neurophysiological outcome measures during quasi-static conditions.

### 6.1.1 Participants

A group of 25 young, healthy adults (age 28.8 ± 7 y.o., mean ± SD, 11 females) was recruited for the study. According to the Waterloo footedness inventory (van Melick et al., 2017), 23 out of 25 participants were right-footed reporting an average score of 42 ± 32 on a scale from–100 to 100. All the participants declared their right hand as the writing one. The measurements were carried out at the Faculty of Sport and Health Sciences in the University of Jyväskylä, Jyväskylä, Finland.

### 6.1.2 Materials and methods

Naturalistic proprioceptive stimuli were delivered to the participants' ankle joint in two conditions: with steady 5-Nm plantar flexion (*active* condition) and with no plantar flexion torque exerted (*passive* condition) through a custom-made actuator. Two types of ankle movements were elicited by stimulating the ankle joint continuously and intermittently in two separated experimental sessions for each condition (i.e., *active* and *passive*). The wireless EEG system was adopted for the recording of 30 EEG and 2 EOG signals. Additionally, measurements involved the recording of EMG and kinematic signals to be used in the signal processing step. Measurements were performed on a group of 25 young, healthy adults who volunteered for the study. The experimental setup with an example of acquired signals is reported in FIGURE 40.
Data analysis was performed using MNE-Python (Gramfort et al., 2013) and in Matlab R2022b (MathWorks Inc, Natick, MA) software and the FieldTrip Matlab toolbox for the EEG analysis (Oostenveld et al., 2011). An offline signal synchronization was performed by means of the trigger signal handled with the

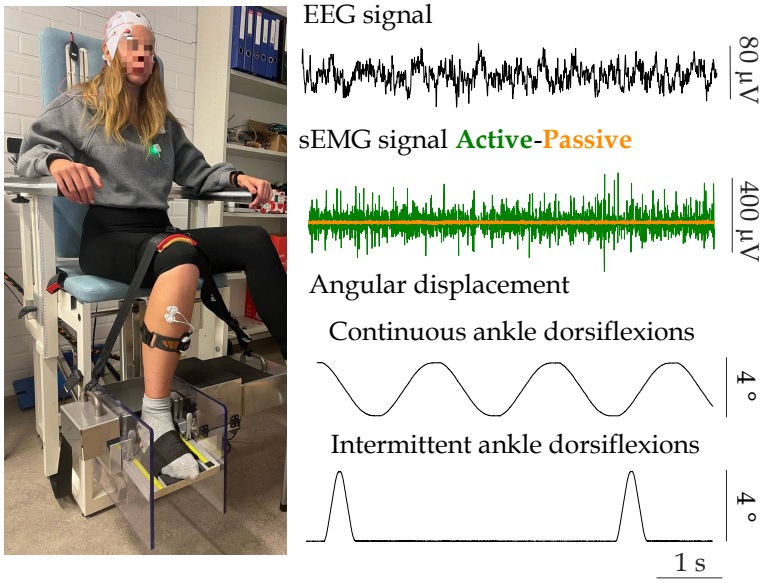


FIGURE 40 Experimental setup of Study IV. Example of acquired EEG, sEMG and foot angular displacement signals during continuous and intermittent dorsiflexions of the ankle joint.

external wireless synchronization module. Then EEG signals were visually inspected and ICA was applied to remove those components related to eye blinks or neck muscle contamination artifacts. Afterwards, CKC between EEG signals and foot angular displacement recorded during continuous ankle-joint stimulation was extracted following the procedure described in Chapter 2.2.3 (frequency resolution: 0.5 Hz). Additionally, evoked and induced EEG responses were analyzed from intermittent ankle-joint stimulation. The former were computed on signal epochs from −200 to 1000 ms with respect to the stimulus onset occurring at 0 s. The latter were quantified according to the temporal spectral evolution method introduced by Salmelin and Hari (Salmelin & Hari, 1994) on epochs from −1 s to 3 s with respect to the stimulus onset. The same analyses were performed for *active* and *passive* conditions to compare the outcome measures between conditions through a nonparametric test (Wilcoxon signed-rank test). TABLE 7 reports a brief overview of the experimental paradigm and extracted outcome measures for the type of proprioceptive stimulation.

TABLE 7 Overview of Study IV. Experimental protocol details, measurements and outcome variables extracted for the proprioceptive studies.

| **Proprioceptive stimulation type** | **Experimental Protocol** | **Acquired signals** | **Outcome measures** |
|---|---|---|---|
| Continuous stimuli | 3-min of ankle rotations at 2 Hz (range of motion: 8°, peak angular velocity: 25°/s) | 30 EEG signals<br>2 EOG signals<br>EMG: soleus medialis, tibialis anterior | Corticokinematic coherence |
| Intermittent stimuli | 100 stimuli (range of motion: 4°, ISI: 4 s ± 0.25 s,). | Foot angular displacement<br>Ankle joint torque signals | Evoked and induced EEG responses |

### 6.1.3 Results

***Corticokinematic coherence.*** FIGURE 41 shows CKC results. When above the statistical significance level, CKC peak was found at the 2 Hz movement frequency at Cz electrode site level (i.e., above the midline central scalp region as expected for ankle joint stimulation) in both conditions. At the group level, the proprioceptive stimulation during the *active* condition elicited robustly stronger CKC strength than the *passive* condition at the peaking electrode as demonstrated by the FIGURE 41 C ($p<0.01$).

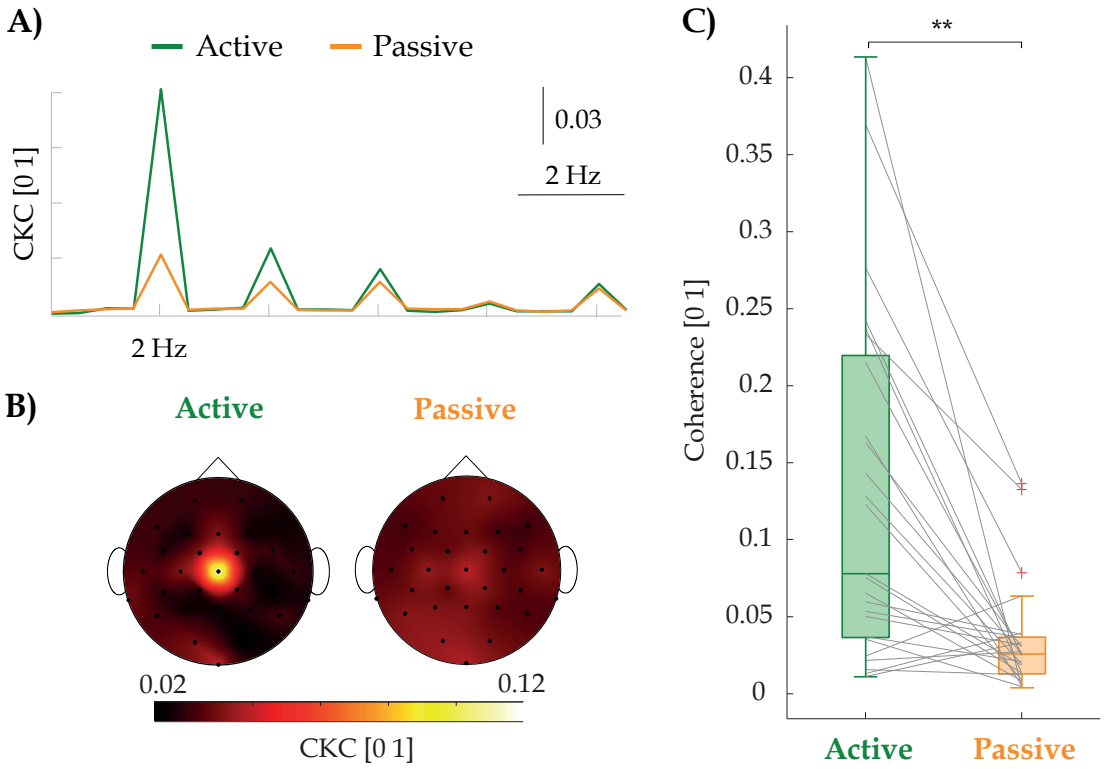


FIGURE 41 Results of Study IV. Corticokinematic coherence (CKC) results at Cz electrode level (n= 25 participants) for active (green) and passive (orange) conditions. A) Grand average CKC spectra, B) topographic representation of CKC strength at the movement frequency averaged across participants, C) boxplot representations of CKC strengths. Statistical analysis by Wilcoxon signed-rank test, (**p<0.01). Modified from (Giangrande, Cerone, et al., 2024).

***Evoked EEG responses.*** FIGURE 42 depicts the EEG evoked responses extracted from the intermittent proprioceptive ankle joint stimulation. ERPs were peaking at the Cz-electrode level corresponding to the foot sensorimotor area above the SM1 cortex. Two prominent ERP components were highlighted for both conditions: N100 and P200 respectively at ~100 ms and ~200 ms with respect to the movement onset. The *active* condition showed a consistently larger peak-to-peak ERP amplitude than the *passive* condition (~26%, p<0.001), with no difference in terms of ERP latencies.

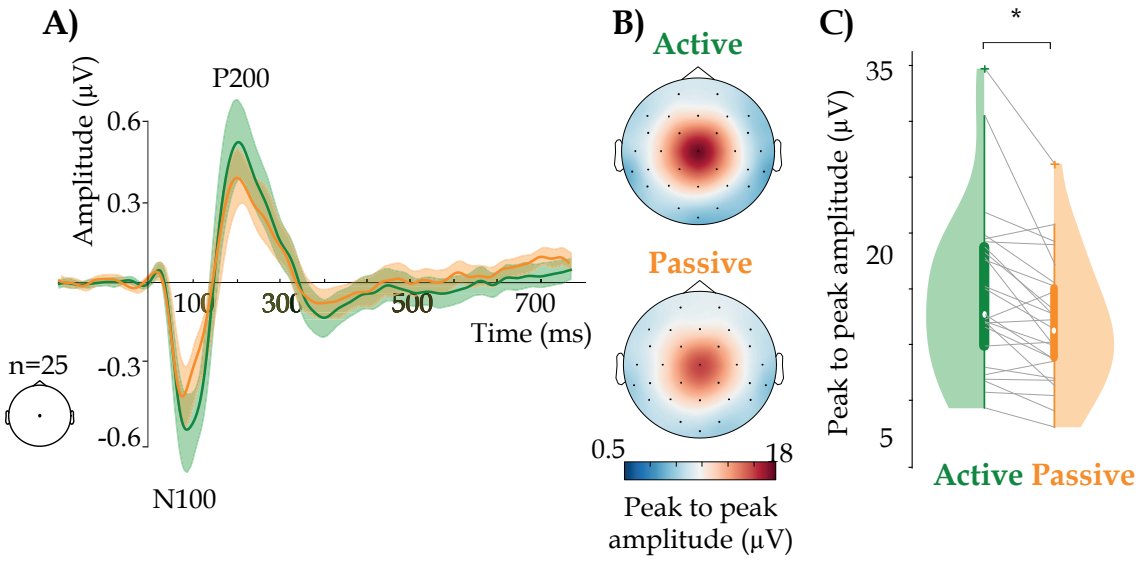


FIGURE 42 Results of Study IV: Evoked responses. A) Grand average of ERPs across participants for active (green) and passive (orange) conditions at Cz electrode level (n=25 participants). Shaded areas correspond to the standard deviations across participants. B) Grand average scalp topographies of the peak to peak ERP amplitude. C) Violin plots of peak to peak amplitude of evoked responses (Statistical analysis by Wilcoxon signed-rank test, *p<0.05). Modified from (Giangrande, Mujunen, et al., 2024).

***Induced EEG responses.*** FIGURE 43 summarizes results of the induced EEG responses for those participants who showed significant beta modulations at the level of Cz electrode over the SM1 cortex in both conditions (19 out of 25 participants). Results showed typical evolution of beta power content with prominent peak responses located above the foot sensorimotor area (i.e., Cz electrode) for both *active* and *passive* conditions. Induced responses demonstrated an initial power decrease (beta suppression) followed by a late post-movement increase (beta rebound). However, the *active* condition elicited a stronger peak beta suppression (~38%, $p<0.01$) and a weaker beta rebound (~–42%, $p<0.05$) with respect to the *passive* condition. Additionally, the significantly larger area-under-the-curve of the rebound ($p<0.001$) extracted from the *passive* condition demonstrated a more prolonged rebound recovery than the one elicited during *active* condition. Finally, no differences in terms of the peak-response (suppression and rebound) latencies were highlighted between conditions ($p>0.05$).

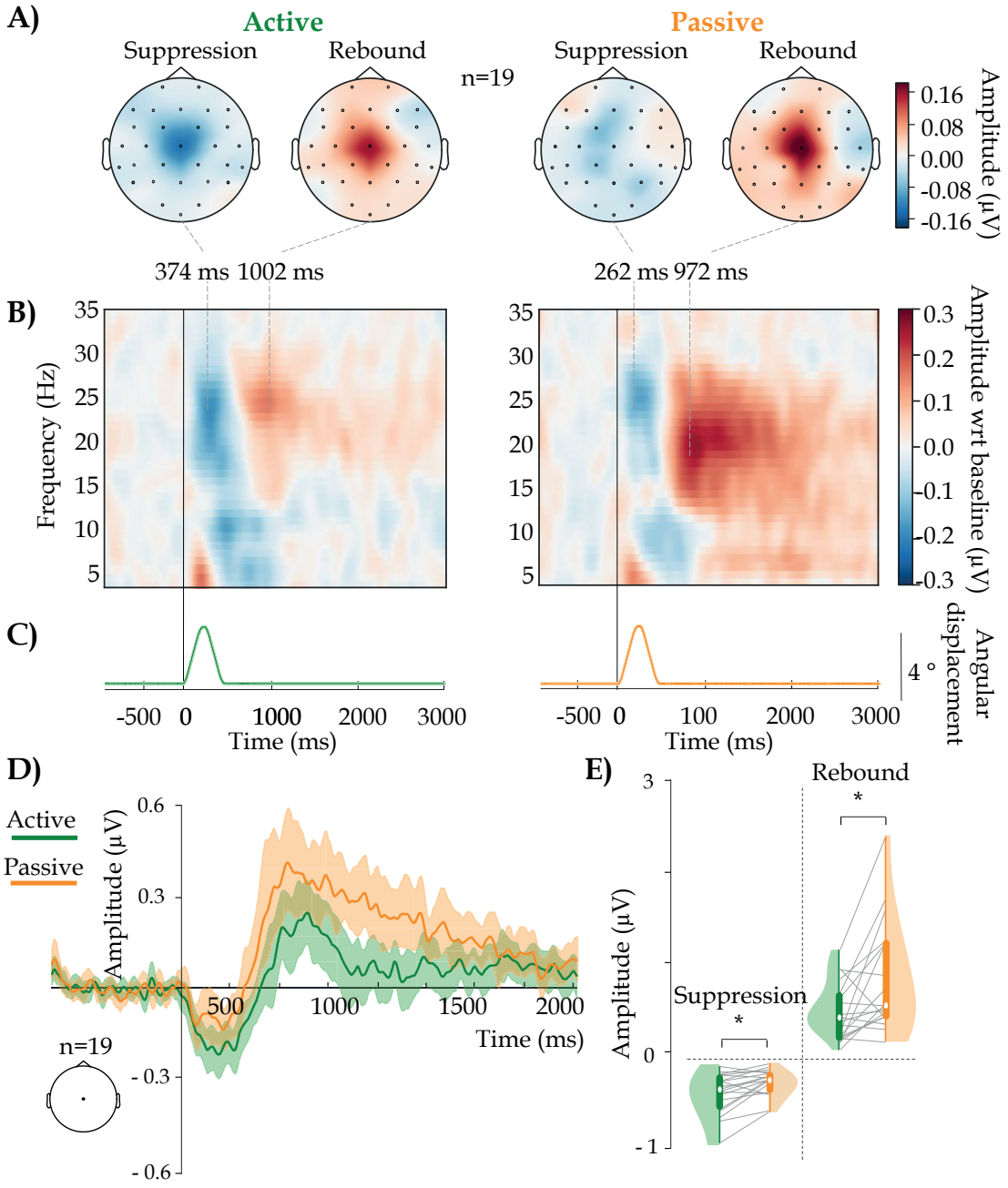


FIGURE 43 Results of Study IV: Induced responses (n=19 participants). A) Grand average topography at peak suppression and rebound and B) time-frequency representations based on z-score transformations, C) grand average foot angular displacement, D) induced EEG responses, and E) violin plots of beta suppression and rebound peak amplitudes for both active (green) and passive (orange) conditions (*p<0.05). Modified from (Giangrande, Mujunen, et al., 2024).

### 6.1.4 Discussion

The findings revealed that the proposed wireless EEG technology can be used as valuable tool to track the modulations of the cortical proprioceptive processing. Indeed, cortical, muscular and kinetic signals were collected simultaneously, and

the extracted outcome measures were in line with previous findings in the field, further demonstrating their robustness and reliability to be used as biomarkers of sensorimotor cortical function.

Specifically, results indicated that volitional muscular activation modulates the cortical processing of proprioceptive afferences in the SM1 cortex with respect to a relaxed condition. The main findings revealed that the voluntary motor output (i) intensifies the cortical processing of proprioceptive afferences in the SM1 cortex (stronger CKC strength), (ii) enhances the cortical activation (greater evoked responses and beta suppression amplitudes), and (iii) weakens the post-movement cortical inhibition (lower beta rebound amplitude). Different potential mechanisms occurring at various levels (i.e., peripheral, spinal, cortical) of the afferent somatosensory pathway might explain these observations.

At peripheral level, the state of the receptors (mainly muscle spindles) in charge of signaling the brain about proprioceptive input is altered in the *active* with respect to the *passive* condition. Indeed, muscle spindles are sensitized both mechanically and neuronally. The former sensitization depends on the increased muscle-tendon unit stiffness due to the constantly applied torque likely resulting in a reduction of the muscle-tendon unit slack with respect to a relaxed condition (Piitulainen et al., 2023). The latter sensitization is instead related to the increased firing rate of the muscle spindles because of the gamma motor neuron activity. They are efferent neurons innervating the intrafusal fibers of the muscle spindles of skeletal muscles and they take part into the muscle contraction by adjusting the sensitivity of the spindles throughout the motor task. Therefore, an increase in their firing because of the voluntary muscle activation results in a neuronal sensitization of the peripheral proprioceptors. The overall increased sensitization of the proprioceptors in the *active* condition thus enhances the readiness of peripheral proprioceptors likely leading to more synchronized afferent proprioceptive volleys to the SM1. This would, in turn, increase the degree of cortical activation with resulting stronger cortical responses in the SM1 cortex, as EEG is fundamentally a measure of synchrony among a large population of neurons.

At spinal level, modulations of the somatosensory afference from the peripheral receptors to the SM1 cortex are expected to occur during the *active* than the *passive* condition, especially at spinal, medullary, and thalamic circuits (McIlroy et al., 2003). During voluntary muscle actions, the somatosensory receptor input to the spinal cord converges in the spinal circuits which are also under control by the efferent motor output from the brain (Seki et al., 2003). Therefore, the brain itself can additionally contribute to modify the somatosensory feedback in case of an *active* voluntary muscle contraction intensifying the whole proprioceptive processing.

At cortical level, the *active* condition is characterized by an altered cortical state due to the activation of the motor cortices to maintain the isometric contraction. In fact, the SM1 cortical proprioceptive processing is likely influenced by the activated cortico-cortical connections taking place while performing a voluntary movement accompanied with stronger intra- and inter-hemispheric mechanisms

(Alitto & Usrey, 2003; Briggs & Usrey, 2008; SooHyun et al., 2008). Furthermore, the *active* condition was associated with active motor output and directed attention towards the visuomotor force precision task. Thus, the cortical sensorimotor processing may be impacted by the active engagement of different cortices (motor, visual, etc.) and sensorimotor integration processes to a higher extent with respect to the *passive* condition. The facilitation of the cortical responses might be also explained by the nature of the experimental paradigm itself as similar enhancement of the somatosensory afference have been identified in case of somatosensory stimulation relevant for the ongoing motor task (Gantchev et al., 1994; Staines et al., 2002). The ankle joint rotation was indeed very relevant, although distracting, for the current motor task.
These hypotheses endeavoring a stronger cortical activation during the *active* condition could, thus, explain the intensified neuronal processing as demonstrated by the enhanced CKC and evoked EEG responses obtained respectively for continuous and intermittent ankle joint proprioceptive stimulation. The strengthened SM1 activation during the *active* condition is further demonstrated by the marked beta power suppression elicited by the intermittent proprioceptive stimulation. Indeed, the beta suppression (i.e., reduction in the beta power) is thought to reflect the activation of the SM1 cortex and it has been found to occur, e.g., in response to active and passive movements, motor imagery, and action observation (Barone & Rossiter, 2021; Engel & Fries, 2010; Tan et al., 2016). Furthermore, the reduced post-movement beta rebound found for the *active* than *passive* condition points in the same direction. Indeed, since the amplitude of the rebound has been interpreted as an indicator of the cortical areas being at "rest" (Bizovičar et al., 2014), it is coherent to encounter a less inhibited cortical state as the SM1 cortex was not at the resting state during the *active* condition, but more so during the *passive* one. The reduced inhibition probably reflects some additional mechanisms occurring at sub cortical level (e.g. thalamus) (Pfurtscheller & Neuper, 1994). Indeed, sub cortical structures oversee the regulation of the activity of basal ganglia needed to suppress the thalamic facilitation of the motor cortices, and thus help to suppress the activation of competing motor programs in the motor cortex (Brittain et al., 2012). This suggestion is further reinforced by the faster rate of beta recovery of the *active* condition with respect to the *passive* one, highlighted by the smaller area under the rebound curve.

### 6.1.5 *Study IV:* Conclusion

*Study IV* was an applicative experimental study designed to investigate the cortical role of proprioception during volitional muscle activation. The choice of evaluating the effect of active muscular contraction on cortical proprioceptive processing was driven by the aim of applying cortical research to real-world-like scenarios to provide further insights into how the brain controls motor functions in everyday situations. However, before moving to highly dynamic contexts, a quasi-static condition was tested to inspect the suitability of the developed wireless EEG unit to investigate the neuronal processing of proprioceptive

afference in the primary sensorimotor cortex. Therefore, ankle-dorsiflexion movements were delivered by a custom-made movement actuator while recording cortical electrical activity in two conditions: with (*active*) and without (*passive*) a steady plantarflexion.
From both technological and methodological points of view, the findings showed that outcome measures such as CKC, evoked and induced EEG responses obtained by means of the proposed wireless technology are robust methods to track the modulations of cortical proprioceptive processing. From a physiological point of view, an intensified cortical proprioceptive processing is hypothesized (*H4*) when a muscular contraction is performed as a result of a multi-level mechanism affecting from the muscular to the spinal and the cortical levels. Results indicated that the active volitional motor task during naturalistic proprioceptive stimulation alters the cortical excitability and inhibition to proprioceptive stimulation with respect to the sole passive condition. Specifically, with a maintained motor output, the SM1 cortical activation is intensified, and its post-movement inhibition is reduced with respect to a relaxed condition. Possible mechanisms behind these differences might involve several levels of the proprioceptive pathway: from the peripheral (i.e., altered firing rate of proprioceptors) to the central (i.e., spinal, sub-cortical and cortical) one. A broader exploitation of the research outcome involves the investigation of the effects of altered motor functions on cortical proprioception due to ageing, neurological or developmental diseases.

## 6.2 Assessment of the sensorimotor integration in dynamic contexts: a proof-of-concept study (*Study V*)

*Study V* was designed as a proof-of-concept to explore the possibility of extracting relevant neurophysiological variables in the field of sensorimotor integration by applying wireless technologies to record biopotential signals during moderate to highly dynamic conditions. Specifically, the study is divided into two experimental designs. The former deals with overground walking and jogging tasks aimed at quantifying CMC between cortical and muscular signals (*CMC study*). The second experimental design consists in a two-sessions study to quantify the possibility to induce and reproduce EEG somatosensory evoked potentials (SEPs) during treadmill cross-country skiing (*SEPs study*). Both experiments were aimed at answering the *Q5* research question about the feasibility of extracting physiological outcome measures from wireless EEG recordings during dynamic tasks. Demonstrating the possibility to extend the use of such measures also to dynamic applications would, indeed, pave the way to new studies on the role of the cortex and its interactions with the peripheral nervous system during real-world activities and tasks.

### 6.2.1 Participants

The two experiments were carried out on a relatively small sample size population. Two different groups of five young, healthy adults (first group: age 31 ± 3 years, 2 females, second group: age 41 ± 3 years, 4 males) were recruited respectively for the CMC- and SEPs- experimental paradigms. The former measurements were carried out at the Faculty of Sport and Health Sciences in the University of Jyväskylä, Jyväskylä, Finland. The skiing measurements were performed in the Skiing lab of Vuokatti Sport Center (Vuokatti, Finland).

### 6.2.2 Materials and methods

***CMC study.*** Participants were asked to perform 5 minutes of overground walking and jogging at their preferred moderate speed (4.42 ± 1.58 km/h and 7.51 ± 0.95 km/h, mean ± SD, respectively). FIGURE 44 shows the experimental setup used for the study. EEG, EMG and kinematics signals were collected throughout the task by means of a wBSN including: (i) a 32-channel EEG acquisition unit, (ii) a set of bipolar sEMG acquisition units (DuePro, OT Bioelettronica, Italy) placed on the right Tibialis Anterior (TA), Gastrocnemius medialis (GM) and Soleus (SOL) muscles, and (iii) a general-purpose custom-made acquisition unit collecting magneto-inertial signals from the foot and an additional signal from the right heel through a force sensor detecting the ground reaction force (Flexiforce, Tekscan, Norwood, USA). The wBSN was based on a hybrid wireless network simultaneously managing Bluetooth, Bluetooth Low Energy and Wi-Fi communication protocols. Data analysis was performed in Matlab R2022b (MathWorks Inc, Natick, MA). EEG and EMG signals were offline band-pass filtered according to their specific frequency bandwidth ($4^{th}$ order Butterworth filter, [0.5 - 45] Hz and [20 - 400] Hz, respectively). Artifactual independent components of EEG signals (e.g. due to eye movements and neck or temporal muscular contamination) were extracted and further rejected (FieldTrip Matlab toolbox (Oostenveld et al., 2011)). Afterwards, EEG channels characterized by an unstable contact or showing residual movement artifacts were interpolated by computing the average of the neighbor channels. The coupling between cortical and muscular signals was finally quantified by extracting CMC. To this end, activation intervals were specifically extracted by evaluating EMG signal portions exceeding a single threshold on EMG envelopes ($2^{nd}$ order Butterworth low-pass filter). Then, the chosen portions of EEG and EMG signals were divided into 512 ms long epochs (70% overlap) leading to a spectral resolution of 2 Hz (Bortel & Sovka, 2006). For CMC analysis, only the active phases of TA, GM and SOL muscles were considered. Coherence spectra were computed between 30-channels EEG and EMG signals (unrectified, RMS-normalized (Negro et al., 2015)) from TA, GM and SOL pairwise. CMC strength was identified as the peak of the coherence spectra in the beta frequency band (10 Hz – 30 Hz) over the 30 EEG channels. Results were displayed as coherence spectra in the frequency domain and through scalp topographies representing the CMC strengths at channel level.

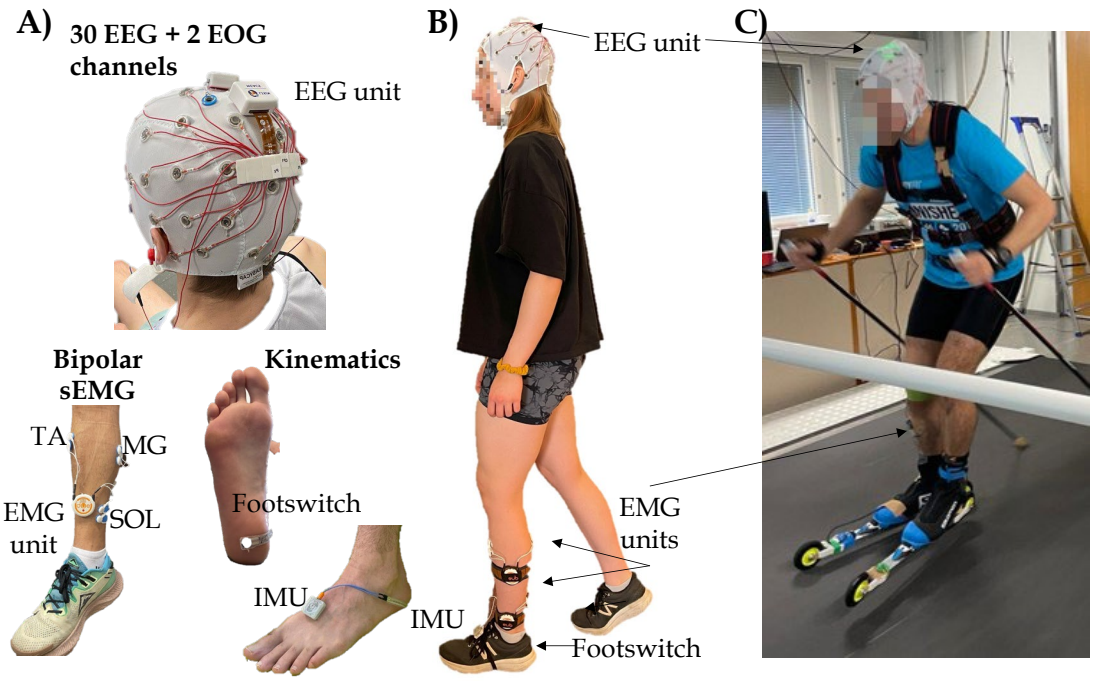


FIGURE 44 Experimental setup of Study V. From left to right: A) details of sensors and instrumentation used. B) Example picture taken from a participant performing overground walking/jogging task, C) Example picture taken from a participant during cross-country skiing.

***SEPs study.*** Participants performed three minutes of simulated cross-country skiing on a treadmill (Rodby, Sweden, elevation degree: 2°, technique: V2, speed: 70% of the maximal heart rate) while receiving electrical stimulation of the right tibial nerve. FIGURE 44 shows the experimental setup used for the study. EEG, EMG and kinematic signals were recorded with a wBSN composed of: (i) a 32-channel EEG acquisition unit, (ii) a set of bipolar sEMG acquisition units (Noraxon, USA) placed on the right Tibialis Anterior (TA), Gastrocnemius medialis (GM), and Soleus (SOL) muscles, and (iii) 2D ground reaction forces from the right ski. A constant-current stimulator (DS7A, Digitimer, Hertfordshire, UK) was used to deliver a total of 15 electrical stimuli (rectangular pulses with 200 μs duration) to the common tibial nerve every three skiing cycles. To this purpose, a circular cathode (Unilect short-term ECG Electrodes, Ag/AgCl, Unomedical Ltd., Great Britain) placed over the tibial nerve in the popliteal fossa, and an oval shaped (5.08 cm x 10.16 cm) anode (V-trodes neurostimulation electrodes, Mattler Electronics corp., USA) placed above the patella were used. Supramaximal nerve stimulation was performed by setting a current intensity of 125% of the current that induced a maximal M-wave (43 ± 12 mA in session 1, 37 ± 16 mA in session 2 among participants). Electrical stimuli were delivered after 255 ms with respect to the onset of the gliding phase. This choice was made to avoid any contamination from a naturalistic proprioceptive response possibly elicited by the ski-ground contact (i.e., eventually occurring at 0 ms with respect to the onset of the ski-ground contact). Measurements were repeated twice, 24 hours apart to evaluate the reproducibility of the SEPs between sessions. Data

analysis was performed in Matlab R2022b (MathWorks Inc, Natick, MA). Preprocessing steps followed what performed for the CMC experiment (i.e., band-pass filtering, ICA, channels interpolation). Afterwards, SEPs were extracted by averaging EEG signal epochs (−100 to 500 ms with respect to the stimulus onset occurring at 0 s, n=15 epochs). A baseline correction was additionally performed by subtracting the average of the pre-stimulus (i.e., -100 to 0 ms with respect to the stimulus onset) at each channel level. SEPs were characterized in terms of peak amplitude and latency of the earliest evoked components.

### 6.2.3 Results and Discussion

***CMC study.*** The wBSN succeeded to simultaneously record multiple signals (i.e., biopotential and kinematic signals), handling different communication protocols with a high degree of synchronization among sensor units. FIGURE 45 shows individual examples of recorded signals over time. The quality of the collected signals assessed through visual inspection was consistent with the findings reported in the present dissertation. Nevertheless, as highlighted in the right panel of FIGURE 45, some EEG channels still suffered from residual motion artifacts contamination. However, this contamination was only limited to a small number of channels (on average, less than one channel per recording) mainly affected by the movements of electrodes because of a non-optimal contact with the scalp surface either due to a massive hair density or to anatomical scalp characteristics (i.e., Iz electrode). Therefore, it did not interfere with the overall study outcome as it was possible to proceed with the interpolation of the bad channels because of their low number. FIGURE 46 shows single examples of CMC results demonstrating its individual variability within the tested population. Significant coupling from 15 Hz to 30 Hz was observed for two out of five participants for both TA and SOL muscles peaking over the leg SM1 area (i.e., Examples 1 of FIGURE 46 of walking ang jogging tasks). This finding points in the same directions of latest evidence on the role of a supraspinal control of human locomotion along with the spinal one (Moshonkina et al., 2021). Indeed, although walking can be considered as an automatic task, thus involving cortical circuits to a lesser extent with respect to the performance of a precision task, recent research underlined a non-negligible cortical contribution to the spinal ones in the regulation of the human walking behavior (Arauz et al., 2024; Petersen et al., 2012; J. F. Yang & Gorassini, 2006).

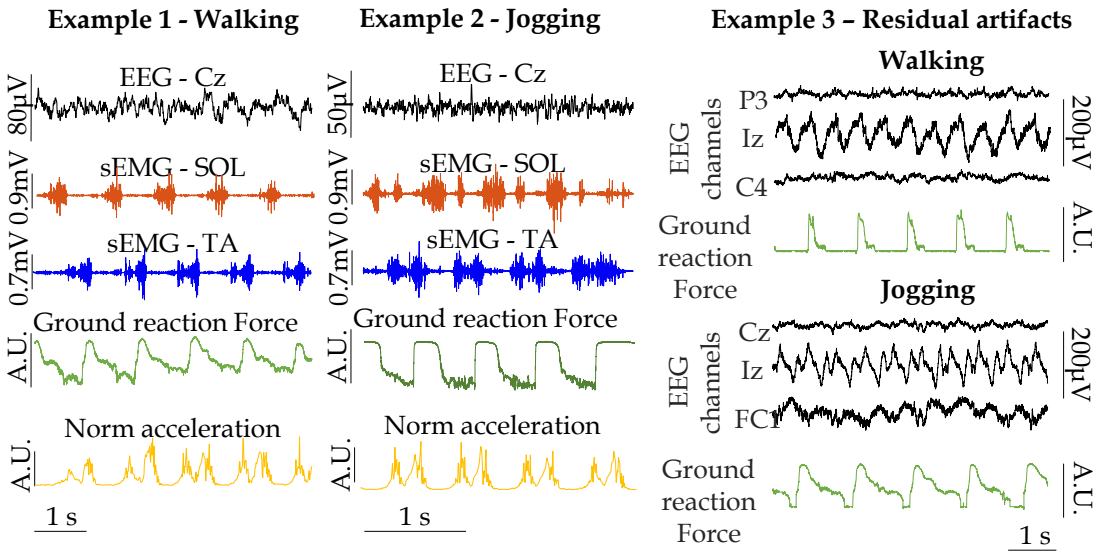


FIGURE 45 Recorded signals of Study V: CMC protocol. From left to right: the first two panels show examples of recorded EEG, EMG and kinematic signals from two participants performing overground walking and jogging. The third panel depicts EEG signals and ground reaction forces from two additional participants experiencing EEG signal motion artifact contamination.

In this view, coherence analysis showing the presence of a rhythmic coupling between cortical and muscular activity, seems to support the idea of a complex dialog between cortical, subcortical and spinal networks in gait control. However, CMC results were highly variable in the tested population (see Examples 2 of FIGURE 46). Moreover, the overall CMC strength was relatively low (generally below 0.01), and only in a single case it reached a value of 0.3 on a scale from 0 to 1. Nevertheless, this finding was not surprising as CMC is not even detectable in some individuals. Moreover, CMC strengths are generally weak values, sometimes lower than the significance level even during steady isometric contraction tasks in MEG-studies (usually the preferred technology dealing with coherence analysis because of its high SNR) (Pohja et al., 2005). Nonetheless, the present study was conceived as a proof-of-concept. Therefore its results should be approached cautiously, and further extensive studies are needed to deepen the investigation on functional connectivity between the cerebral cortex and muscles during human locomotion.

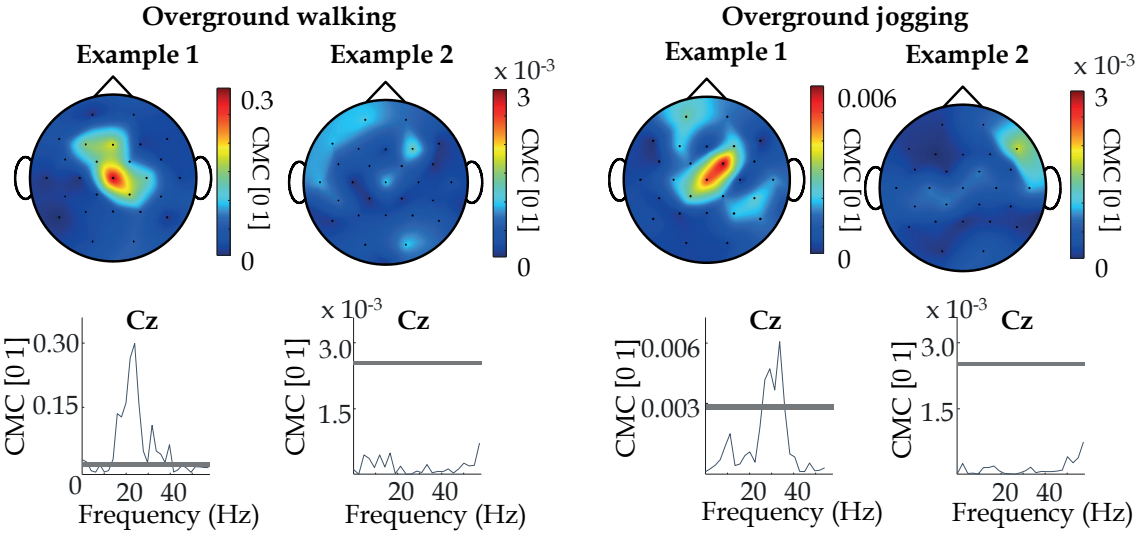


FIGURE 46 Results of Study V: CMC protocol. Scalp topography and coherence spectra of the most coherent channel (Cz electrode). From left to right: significant and non-significant CMC between EEG-EMG (SOL muscle) during walking task, and significant and non-significant CMC between EEG-EMG (TA muscle) during jogging task.

***SEPs study.*** Although a proof-of-concept, this is the first study investigating somatosensory evoked potentials during dynamic, sport applications as cross-country skiing. FIGURE 47 depicts an example of the recorded signals and obtained individual results from the study. Also in this second experimental design, the dedicated wBSN succeeded to simultaneously record EEG, EMG and kinematic signals with good signal quality, as shown in the right panel of FIGURE 47. Physiological artifacts on EEG signals such as eye blinks and neck muscle activity contamination are purposely displayed in the EEG traces of FIGURE 47, but they were isolated and removed during the signal pre-processing. Additionally, promising results were obtained in terms of the extracted physiological cortical responses to the electrical stimulation during such a dynamic task as cross-country skiing. It was indeed feasible to elicit robust SEPs with a high degree of reproducibility between sessions, indicating good somatosensory feedback in four out of five participants. The elicited SEPs showed two main components: N100 and P200, and in one case an earlier, positive component P50 was also visible. Cortical responses were additionally highly reproducible in terms of: (i) electrode location (peak response above the Cz electrode corresponding to the leg motor area of the primary somatosensory cortex), (ii) peak amplitude (28 ± 5 μV session 1, 27 ± 6 μV session 2) and (iii) peak latencies (N1: 131 ± 16 ms session 1, 132 ± 9 ms session 2; P2: 227 ± 21 ms session 1, 237 ± 14 ms session 2). Therefore, these results suggest that SEPs can be used to effectively track the processing of somatosensory afferent input also under dynamic conditions. However, it is important to underline that EEG responses might be modulated according to the individual task-related skills of the tested participants. As an example, weaker SEPs are expected for skilled athletes as it is reasonable to hypothesize that such population activates a smaller number of neurons to initiate and control the movement with respect to amateur or non-

skiers. Therefore, specific studies should be carried out to further clarify eventual SEPs modulations according to individual cross-country skiing skills. Additionally, further analyses are also needed to deepen the study of the cortical somatosensory processing and its integration with the ongoing descending motor output. Indeed, although the analysis of EMG responses (i.e., V-waves) is out of the scope of the present proof-of-concept study, further combined investigations on both brain and muscle signals might shed lights on the role of spinal and supraspinal motor control during cross-country skiing and on the related sensorimotor gating phenomena.

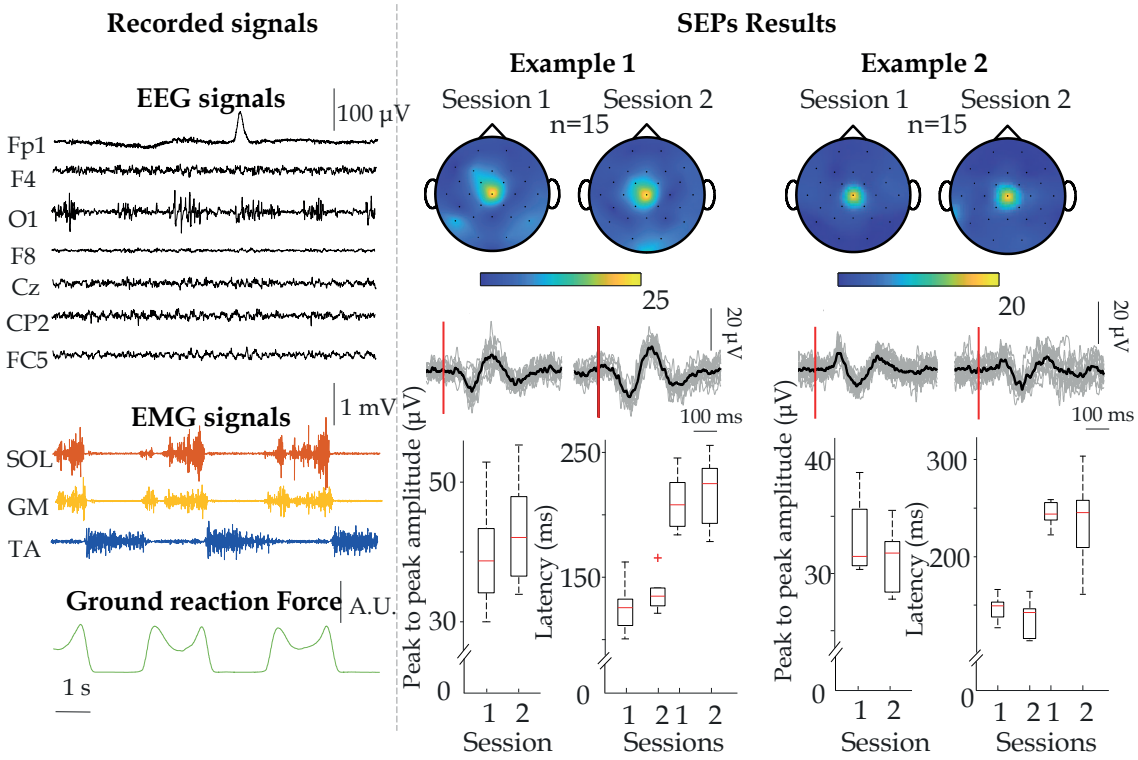


FIGURE 47 Results of Study V: SEPs protocol. Left panel: examples of recorded raw EEG, EMG and kinematic signals from a representative subject. Right panel: SEPs results in terms of scalp topography, average SEP over the peak channel (i.e., Cz electrode) for both sessions, and boxplot representations of SEPs amplitudes and latencies for individual stimuli of the two recording sessions from two representative subjects.

### 6.2.4 *Study V:* Conclusion

Despite the limited number of participants being tested, this proof-of-concept study demonstrates encouraging results supporting preliminary hypotheses (*H5*) about the feasibility of employing the developed wireless EEG system within experiment-specific body sensor networks aimed at simultaneously record cortical, muscular, and kinematic/kinetic signals during dynamic tasks. Indeed, overall results are considered promising in several respects. Firstly, the proposed wireless EEG system demonstrated to be versatile to be part of customized wBSN aimed at the simultaneous recording of different signals. Secondly, the quality of EEG signals when following the good practice recommendations discussed in the

previous Chapter 4 showed to be robust to the performed movements although particular attention should be still put to additional factors potentially affecting the results such as hair density or participants' scalp anatomy. Thirdly, the described observations demonstrate the feasibility of extracting meaningful variables such as corticomuscular coherence, and somatosensory evoked responses to track phenomena related to the sensorimotor integration during dynamic tasks. Starting from this experimental evidence it is possible to conclude that the developed technologies demonstrated to have a great potential to enable the study of brain-body interactions in unconstrained, naturalistic conditions.

# 7 FINAL CONCLUSIONS

This PhD thesis investigated and proposed new technological solutions related to the acquisition and interpretation of EEG signals during dynamic and naturalistic tasks. As a starting point, this dissertation delved into the examination of the current bottlenecks limiting the recording of brain signals mainly to static tasks in lab-environments (*Study I*). To this end, the design, the technological description and the experimental application of innovative tools for the assessment of the human sensorimotor functions during motor control have been described (*Study II – III*). The outcome of the studies in static and dynamic conditions (*Study IV – V*) reveals the potentiality of the proposed solutions to be applied in a wide range of contexts, opening new frontiers to examine the physiological and pathological human sensorimotor system. Indeed, it is now possible to record high-quality brain signals also during dynamic tasks thanks to the designed technologies along with the implementation of the identified good practice recommendations. With particular reference to the aims described in Chapter 3, the illustrated research:

i) expands the general knowledge on dynamic biopotential signal recording, with particular regard on the modelling and understanding of the main sources of motion artifacts affecting dynamic EEG acquisitions
ii) advances the state of art technology related to the acquisition of EEG signals
iii) provides the foundations for innovative research lines on sensorimotor integration during naturalistic (i.e., close to the real-world) conditions, sport contexts, rehabilitation treatments and diagnostic solutions.

On the following, the main findings of the PhD project are summarized together with the study limitations and possible future research lines.

## 7.1 Main findings

The high-quality EEG signal collection is currently limited exclusively to quasi-static lab environments because of technological bottlenecks.
Firstly, the lack of miniaturized and lightweight instrumentation, easily integrable with third-party devices used e.g. to provide external stimuli limited the acquisition of EEG signals only in static laboratory environments. In this view, an innovative wireless EEG system was designed in compliance with these specifications to overcome the current technological barriers and to allow the recording of cortical signals during unconstrained conditions. Additionally, an external, modular, synchronization unit was prototyped allowing for the simultaneous acquisition of EEG signals with third-party devices. The bench tests and the experimental validation in a various use-case scenarios in comparison to a well-established, wired EEG system showed that the developed acquisition system can be reliably used to investigate cortical functions.
Secondly, dynamic EEG recordings are also affected by the contamination of EEG signals by motion artifacts time-locked with the performed movements. Three main phenomena are hypothesized to hinder the genesis of motion artifacts including: (i) varying interelectrode impedance due to electrodes movements, (ii) moving connecting cables and (iii) modulation of power line interference fostered by the performed movement. For each hypothesized source of motion artifact an electrical model was described and analyzed to analytically evaluate to what extent these phenomena can influence dynamic EEG recordings. Further experimental tests made by means of innovative customized EEG electrodes systems (i.e., textile- and adhesive- based solutions) allowed to investigate experimentally this aspect and supported the theoretical analysis on the genesis of motion artifacts, which highlighted the relevant contribution of cables and electrodes movements. Therefore, good practice recommendations to be implemented in the design of EEG recordings instrumentation and related experimental acquisition include minimizing the cables length and the electrodes movements during the measurements.
The developed wireless EEG technology allowed for a in depth investigation of sensorimotor processes in different contexts ranging from static to dynamic tasks. Specifically, proprioception-related studies demonstrated the possibility to track the modulations of the cortical processing of proprioceptive afferences from the ankle joint due to a steady voluntary contraction. According to the initial hypotheses, an early stronger cortical activation accompanied by a late weaker inhibition were found in active *vs* passive condition. These changes at the level of the SM1 cortex are the result of the mechanisms occurring both at peripheral (i.e., proprioceptors) and central (i.e., cortical, sub-cortical and spinal) levels. Although preliminarily, studies on sensorimotor integration further revealed the potentiality to track the corticomuscular coupling and cortical somatosensory responses during moderate to highly dynamic movements. As proof of this, overground walking and jogging tests showed significant corticomuscular

coupling between cortical and muscular recorded signals giving further grounds to the cortical role in gait control. Finally, the highly reproducible somatosensory evoked potentials during treadmill cross-country skiing open up new possibilities of more advanced investigations on the integration of afferent and efferent pathways occurring at cortical level during movements.

## 7.2 Limitations and future perspectives

Despite the novelty of the discussed topics, some limitations can be pointed out. First, in the recent five years new wireless EEG systems have been released on the market (Niso et al., 2023). Therefore, an additional comparison to correlate the performance of the proposed miniaturized device with respect to those of other commercially available systems could further stress the potentialities and eventually the weaknesses of the present technological work.
Second, regarding the EEG motion artifacts contamination, whilst the electrical models and analytical considerations hereby demonstrated that further improvements from the hardware point of view (e.g. implementation of active electrodes) does not necessarily imply a reduction of artifacts contamination, no direct comparison of EEG systems with/without active electrodes has been performed to quantitatively estimate the absence of benefits of using active electrodes in the real experimental practice. Moreover, further efforts should be put towards the optimization of EEG electrodes technology that might still limit the applicability of the wireless EEG recordings to specific conditions (e.g. low to medium hair density, highly dynamic tasks, etc.).
Third, due to the lack of previous studies on the topic, additional extensive research is needed to deepen the investigation of the role of the brain and related sensorimotor integration processes occurring during the movement performance. Indeed, the last described proof-of-concept study only included a limited number of participants. However, the neurophysiological mechanisms related to cortical sensorimotor integration during gait or skiing should be further examined. Future investigations would span measurements of physiological and pathological human sensorimotor interactions in minimally restricted naturalistic dynamic experimental conditions in sport and health sciences.
Finally, further technological developments might be performed towards the compatibility with transcranial magnetic stimulation (TMS) to make the wireless EEG system robust towards the presence of electromagnetic artifacts. This would enable new studies to evaluate the functional causality and state of the corticospinal pathway as well as the cortical causal reactivity and connectivity by looking respectively at EMG and EEG responses to TMS.

## SUMMARY IN ENGLISH

The recording of brain signals outside laboratory environments is limited by technological constraints. They are related to the need of wireless, miniaturized and portable devices allowing to simultaneously record several physiological signals, including EEG and sEMG. Furthermore, also the quality of the collected signals (especially EEG signals) is critical during dynamic recordings because of the corruption of motion artifacts. This dissertation delved into the investigation of the human neocortex functions to a new minimally restricted level by means of originally developed methods and technologies allowing combined EEG-EMG recordings in more naturalistic experimental conditions.

The first study (*Study I*) illustrates the description of three possible phenomena leading to motion artifacts in dynamic EEG recordings. The approach used to model motion artifacts generation was to study this phenomenon behind the genesis of motion artifacts are hypothesized to occur at three different levels of a traditional biopotential acquisition chain: the skin-electrode interface, the connecting cables between the electrodes and the acquisition systems, and the electrode-amplifier system. Indeed, the relative movements between the electrode and the skin creates a consequent alteration of the electrical impedance modifying the recorded voltage scalp potential. Secondly, the movement of the cables is hypothesized to cause an additive input voltage potential because of the accumulated charge on the surface of the cables because of the triboelectric effect. Thirdly, the residual input-referred power line interference might be modulated in case of poor electrode-skin contact (e.g. due to a brisk, partial detachment of the electrodes) generating a distortion of the visualized EEG signals. The three phenomena are described by means of lumped parameters electrical models synthesized starting from experimental observations.

The second study (*Study II*) describes the design and validation of an innovative wireless, miniaturized EEG acquisition system for the integrated acquisition of EEG and sEMG signals. The developed system has a modular architecture, it is portable as it transmits data through a Wi-Fi network to different platforms such as PC, Smartphone, Tablet, etc., and it allows for a high degree of synchronization with external, third-party devices (e.g. used for the study of evoked potentials) still maintaining a fully wireless system architecture. The EEG system underwent to an experimental validation towards a wired, commercially available EEG amplifier, taken as a benchmark. The on-field performance of the two EEG systems in conventional, static tasks were evaluated to assess the robustness of the miniaturized, wireless EEG system to experimentally extract EEG evoked responses (i.e., auditory, visual, and somatosensory), corticokinematic and corticomuscular coherence. The excellent agreement between the performance of both the EEG systems allowed for a full validation of the proposed technology in laboratory environments.

The third study (*Study III*) illustrates innovative design considerations on electrodes systems were developed to deepen the effect of the movement of the cables and electrodes in a real experiment. Two EEG electrodes systems were

specifically designed: i) a textile-based system with the electrical connections embedded into the fabric to minimize the effects of cables movement and ii) a flexible-PCB based EEG electrode system aimed at reducing the effect of both connecting cables and electrodes movement. The experimental results demonstrated that when the movements of both cables and electrodes are minimized, it is possible to record high-quality EEG signals even during highly dynamic tasks. Therefore, good practice recommendations are drawn up regarding: the development of miniaturized EEG amplifier, the use of preferably adhesive electrodes (especially when dealing with the monopolar reference one), and the minimization of the connecting cables length and related reciprocal movements to mitigate the effects of cable motion sourced by e.g. electrical charges accumulated on their surface by triboelectric phenomena.

The fourth study (*Study IV*) deals with the application of the previously described technologies into a real-case experiment aimed at assessing the neuronal proprioceptive processing in the human neocortex. To this end, CKC, evoked and induced EEG responses to naturalistic ankle-joint proprioceptive stimuli were quantified. Specifically, the purpose of the study was to evaluate whether the steady volitional activation of the ankle plantar-flexor muscles affects the cortical processing of naturalistic proprioceptive afference arising from the respective muscles and joints. Results demonstrated a stronger cortical activation and a weaker inhibition in response to naturalistic proprioceptive stimulation of the ankle joint during active steady volitional motor task when compared to passive condition. Three major mechanisms are hypothesized to occur at different levels (i.e., at receptor, muscle, spinal, and central levels). Firstly, the enhanced sensitivity of the peripheral proprioceptors both from a mechanical and a neural point of view. The muscle-tendon unit is, indeed, more tensed when the muscle is activated and the intrafusal fibers of the muscle spindles are actively innervated by gamma motor neurons which increase their firing to keep the muscle contracted. Secondly, the intra and intercortical processing of the proprioceptive stimulation might be modulated differently between the two conditions because of the different functional state of the SM1 cortex differs between active volitional and resting passive states. Finally, also subcortical and spinal modulations cannot be neglected as influencing factors of the overall sensorimotor processing. These results endeavor the robustness of the extracted measures of cortical proprioception to be used as neurophysiological markers to study the mechanisms and adaptations of cortical proprioceptive processing in different settings. This is a significant finding as it may extend the use of wireless, dynamic EEG during active tasks to further evaluate the motor efference-proprioceptive afference relationship and the related adaptations to exercise, rehabilitation, and disease.

The fifth study (*Study V*) reports a proof-of-concept of dynamic EEG to study the brain-body interactions in moderate to highly dynamic conditions by applying the developed technologies. Specifically, corticomuscular coupling during overground walking and somatosensory evoked responses during cross-country skiing were quantified. The obtained results were considered promising both

from a technical and physiological points of view. Indeed, the implemented experimental design allowed for the synchronous recording of multiple signals with consistent high quality allowing post-processing and signals elaboration. Furthermore, encouraging results in terms of corticomuscular coupling and somatosensory evoked responses were obtained. Although with weak values and a relevant variability, significant CMC was found at single participant level giving further grounds to the latest evidence on the role of a supraspinal control of human locomotion. Additionally, repeatable somatosensory evoked potentials to electrical stimulation during cross-country skiing were elicited and robustly extracted. Therefore, the results obtained from the extracted neurophysiological variables demonstrated the possibility to extend the use of such measures also to dynamic applications. These findings would, indeed, pave the way to new studies on the role of the cortex and its interactions with the peripheral nervous system during real-world activities and tasks. Nevertheless, these findings should be approached cautiously as a wider sample size population should undergo to a deeper investigation to further explore the functional connectivity between the cerebral cortex and muscles during human movement and sport.

The positive, encouraging outcome of static and dynamic studies reveals the potentiality of the proposed technologies and methodologies to be widely applied to different contexts and to open new frontiers in the examination of the physiological and pathological human sensorimotor system. The illustrated research line can be considered as a pioneer study with respect to the state of art not only in terms of technological developments, but also in terms of expanding the knowledge on biopotential signal recording during dynamics and related experimental aspects. The proposed work, thus, eventually provides the foundations for innovative research lines on sensorimotor integration during naturalistic conditions, sport contexts, rehabilitation treatments, and diagnostic solutions.

## SUMMARY IN FINNISH

Aivosignaalien mittaamista laboratorion ulkopuolella teknologiset rajoitteet. Olisi erityisesti tarve kehittää langattomia, pienikokoisia ja kannettavia laitteita, jotka mahdollistavat useiden neurofysiologisten ja biomekaanisten signaalien, kuten EEG- ja EMG-signaalien, samanaikaisen tallentamisen. Erityisesti liike- ja muille ulkoisille häiriöille herkkä EEG-mittaus on kriittinen, jotta mittaus onnistuu dynaamisen liikkeen aikana. Tämä väitöskirja tutki ihmisen aivokuoren toimintaa uudella, langattomalla EEG-EMG-mittauslaitteistolla, joka mahdollisti mittaukset dynaamisen liikkeen aikana. Ensimmäinen tutkimus (*Tutkimus I*) kuvasi kolmea tärkeintä ilmiötä, jotka johtavat liikehäiriöihin dynaamisissa EEG-mittauksissa. Mallinsimme liikehäiriöiden syntyä kolmella eri tasolla: (1) ihon ja elektrodin rajapinta, (2) elektrodien ja tallennusjärjestelmien väliset johtimet, ja (3) elektrodi-vahvistinjärjestelmä. Ensimmäiseksi, elektrodin ja ihon välinen liike aiheuttaa sähköisen impedanssin muutoksen, mikä muuttaa päänahan jännitepotentiaalia. Toiseksi, johtimien välinen liike kasvattaa jännitepotentiaalia niiden pinnalle kertyneen varauksen vuoksi, joka johtuu tribosähköisestä ilmiöstä. Kolmanneksi jäännösteho moduloituu herkästi, jos elektrodin ja ihon välinen kontakti on huono (esim. elektrodien osittaisen irtoamisen vuoksi), mikä aiheuttaa EEG-signaalin vääristymän. Nämä kolme ilmiötä kuvattiin koetuloksista johdetuilla koontiparametrien sähkömalleilla.
Toinen tutkimus (*Tutkimus II*) kuvasi innovatiivisen langattoman, pienoiskokoisen EEG-signaalin mittausjärjestelmän suunnittelua ja validointia yhtäaikaiseen EEG- ja sEMG-signaalien mittaamiseen. Järjestelmällämme on modulaarinen arkkitehtuuri, se on kannettava, koska se välittää langattomasti dataa Wi-Fi-verkon kautta eri alustoille, kuten PC, älypuhelin, tabletti jne., ja se mahdollistaa korkean synkronointiasteen ulkoisten, kolmannen osapuolen laitteiden kanssa (esim. EEG herätevasteiden mittaamiseksi) säilyttäen silti täysin langattoman järjestelmäarkkitehtuurin. EEG-järjestelmä validoitiin kokeellisesti langalliseen, kaupallisesti saatavilla olevaan korkealaatuiseen EEG-vahvistimeen verrattuna. Mittaukset suoritettiin tavanomaisissa, staattisissa tehtävissä, joilla arvioimme uuden langattoman EEG-järjestelmämme luotettavuutta EEG-herätevasteiden (kuulo-, näkö- ja somatosensoriset vasteet), sekä kortikokinemaattisen (CKC) ja kortikomuskulaarisen (CMC) koherenssin mittaamiseksi. EEG-järjestelmien suorituskyvyt olivat yhtenevät, joka osoitti vahvasti, että uuden langattoman teknologiamme validiuden laboratorioympäristössä.
Kolmas tutkimus (*Tutkimus III*) havainnollistaa innovatiivisia EEG-elektrodijärjestelmiä elektrodien liikkeen vaikutuksen vähentämiseksi todellisissa EEG-mittauksissa, jotka olivat (1) tekstiilipohjainen järjestelmä, jossa johtimet on upotettu kankaaseen johtimien liikkeen vaikutuksen minimoimiseksi, ja (2) joustavalla piirilevyllä (PCB) varustettu EEG-elektrodijärjestelmä, jonka tarkoituksena on minimoida sekä johtimien, että elektrodien liikkeen vaikutusta. Kokeelliset tulokset osoittivat, että kun johtimien ja elektrodien liikkeet minimoidaan, on mahdollista tallentaa korkealaatuisia EEG-signaaleja jopa erittäin dynaamisten tehtävien aikana. Ehdotimmekin hyviä käytäntöjä koskevia suosituksia, jotka liit-

tyvät EEG-vahvistimen miniaturisointiin, tiukasti liimautuvien elektrodien käyttöön (etenkin monopolaaristen referenssielektrodien osalta) ja johtimien pituuden ja liikkeen minimointiin, jotta voidaan vähentää tribosähköisten ilmiöiden vaikutusta.
Neljäs tutkimus (*Tutkimus IV*) käsitteli aiemmin kuvatun langattoman EEG-järjestelmän soveltamista todelliseen neurofysiologiseen kokeeseen, jonka tarkoituksena oli arvioida aivokuoren proprioseptiivista (liikeaistin) käsittelyä, jonka mittareina toimi luonnolliseen nilkan proprioseptiivisen stimulaation (nilkan rotaatiot) aikaansaamat CKC sekä heräte- ja indusoidut (rytmiset) EEG-vasteet. Tutkimuksen tarkoituksena oli arvioida, vaikuttaako nilkan plantaarifleksorilihasten tahdonalainen aktivointi aivokuorelle saapuvan liikeaistipalautteen käsittelyyn aivoissa. Tulokset osoittivat voimakkaampaa aivokuoren aktivaatiota ja heikompaa inhibitiota tahdonalaisen lihasaktiivisuuden aikana verrattuna passiiviseen proprioseptiiviseen stimulointiin. Havaintojamme selittävät kolme päämekanismia liikejärjestelmän eri tasoilla (reseptori/lihas-, selkäydin- ja keskushermostotasolla). Ensinnäkin liikeaistinsolujen (proprioseptorien) herkkyys on lisääntynyt sekä mekaaniselta että hermostolliselta kannalta. Lihasjänne-yksikkö on aktiviisessa tilanteessa jännittyneempi ja lihassukkuloiden intrafusaaliset säikeet ovat aktivoituneet gamma-motoneuronien kautta. Molemmat tekijä herkistävät lihassukkuloita verrattuna passivitilanteeseen. Toiseksi, aivokuoren toiminnallinen tila eroaa aktiivisten ja passiivisten tilan välillä, jolloin liikeasitinpalautteen intra- ja interkortikaalinen käsittely voi moduloitua aivokuorella näiden tilanteiden välillä. Kolmanneksi, myös aivokuorenalainen ja selkäytimen hermoverkostot voivat moduloida sensorimotorista prosessointia. Nämä tulokset vahvistavat aivokuoren proprioseptiikan mittausten luotettavuuden neurofysiologiaa määrällistävinä mittareina, joita voidaan hyödyntää aivokuoren proprioseptiivisen käsittelyn mekanismien ja adaptaatioiden tutkimuksessa eri yhteyksissä. Tämä on merkittävä löytö, sillä se saattaa laajentaa langattoman, dynaamisen EEG käyttöä aktiivisten tehtävien aikana aivojen liikeohjauksen ja sensorimotorisen integraation ymmärtämiseksi, sekä niihin liittyvien adaptaatioiden tutkimiseksi harjoittelun, kuntoutuksen ja sairauden yhteydessä.
Viides tutkimus (*Tutkimus V*) oli uuden dynaamisen EEG-järjestelmme "proof-of-concept" koe, jossa tutkimme aivojen ja kehon vuorovaikutuksia hyvin dynaamisissa olosuhteissa. Määrällistimme onnistuneesti kortikospinaalinen yhteistoiminnan (CKC ja CMC) kävelyn aikana, sekä EEG herätevasteet maastohiihdon aikana. Tulokset ovat lupaavia sekä tekniseltä että neurofysiologiselta kannalta. Uusi EEG-EMG järjestelmä mahdollisti useiden signaalien yhtäaikaisen tallentamisen korkealaatuisesti. CMC arvot olivat odotetun suuruisia ja vaihtelua esiintyi odotetusti koehenkilöiden välillä. Ääreishermon sähköisen stimulaation aiheuttamat EEG herätevasteet olivat toistettavia ja saatiin esiin selkeästi maastohiihdon aikana. Tuloksemme osoittavat, että uusi EEG-järjestelmämme soveltuu liikkumisen aivoperustan tutkimiseen laajalti dynaamisiin suorituksiin. Löydöksemme voivat avata uusia tutkimusmahdollisuuksia aivokuoren roolista ja sen vuorovaikutuksesta ääreishermoston kanssa luonnonmukaisissa tehtävissä. Tuloksia on kuitenkin lähestyttävä varoen, koska otoskokomme oli tässä

osiossa suppea. Yhteenvetona voimme todeta, että staattisiin ja dynaamisiin EEG tutkimuksiin liittyvien rohkaisevien tulosten perusteella, ehdotettu uusi EEG teknologia on potentiaalinen ja sovellettava laajalti eri yhteyksiin ihmisen sensorimotorisen järjestelmän ja etenkin aivoperustan tutkimuksessa. Kuvattua tutkimuslinjaa voidaan pitää uraauurtavana tutkimuksena suhteessa nykyiseen tietämykseen, ei vain teknologian kehityksen, vaan myös biosignaalin mittaamisen ja siihen liittyvien kokeellisten näkökulmien laajentamisen suhteen dynaamisissa olosuhteissa. Työ luo siten perustan innovatiivisille tutkimuslinjoille, jotka koskevat sensorimotorista integraatiota luonnonmukaisissa olosuhteissa, urheilussa, kuntoutuksessa ja diagnostiikkaratkaisuissa.

## REFERENCES


Adjamian, P. (2014). The application of electro- and magneto-encephalography in tinnitus research-methods and interpretations. *Frontiers in Neurology*, *5*(NOV), 1–24. https://doi.org/10.3389/fneur.2014.00228

Alegre, M., Labarga, A., Gurtubay, I. G., Iriarte, J., Malanda, A., & Artieda, J. (2002). Beta electroencephalograph changes during passive movements: Sensory afferences contribute to beta event-related desynchronization in humans. *Neuroscience Letters*, *331*(1), 29–32.

Alitto, H. J., & Usrey, W. M. (2003). Corticothalamic feedback and sensory processing. *Current Opinion in Neurobiology*, *13*(4), 440–445. https://doi.org/10.1016/S0959-4388(03)00096-5

Arauz, P. G., Chavez, G., Reinoso, V., Ruiz, P., Ortiz, E., Cevallos, C., & Garcia, G. (2024). Influence of a passive exoskeleton on kinematics, joint moments, and self-reported ratings during a lifting task. *Journal of Biomechanics*, *162*(November 2023), 111886. https://doi.org/10.1016/j.jbiomech.2023.111886

Babiloni, C., Binetti, G., Cassarino, A., Dal Forno, G., Del Percio, C., Ferreri, F., Ferri, R., Frisoni, G., Galderisi, S., Hirata, K., Lanuzza, B., Miniussi, C., Mucci, A., Nobili, F., Rodriguez, G., Romani, G. L., & Rossini, P. M. (2006). Sources of cortical rhythms in adults during physiological aging: A multicentric EEG study. *Human Brain Mapping*, *27*(2), 162–172. https://doi.org/10.1002/hbm.20175

Babiloni, C., Carducci, F., Cincotti, F., Rossini, P. M., Neuper, C., Pfurtscheller, G., & Babiloni, F. (1999). Human movement-related potentials vs desynchronization of EEG alpha rhythm: A high-resolution EEG study. *NeuroImage*, *10*(6), 658–665. https://doi.org/10.1006/nimg.1999.0504

Bachschmidt, R. A., Harris, G. F., & Simoneau, G. G. (2001). Walker-assisted gait in rehabilitation: A study of biomechanics and instrumentation. *IEEE Transactions on Neural Systems and Rehabilitation Engineering*, *9*(1), 96–105. https://doi.org/10.1109/7333.918282

Barone, J., & Rossiter, H. E. (2021). Understanding the Role of Sensorimotor Beta Oscillations. *Frontiers in Systems Neuroscience*, *15*(May), 1–7. https://doi.org/10.3389/fnsys.2021.655886

Beniczky, S., & Schomer, D. L. (2020). Electroencephalography: basic biophysical and technological aspects important for clinical applications. *Epileptic Disorders*, *22*(6), 697–715. https://doi.org/10.1684/epd.2020.1217

Benjamin, M., Kaiser, E., & Milz, S. (2008). Structure-function relationships in tendons a review. *Journal of Anatomy*, 211–228. https://doi.org/10.1111/j.1469-7580.2008.00864.x

Bergquist, A. J., Clair, J. M., Lagerquist, O., Mang, C. S., Okuma, Y., & Collins, D. F. (2011). Neuromuscular electrical stimulation: Implications of the electrically evoked sensory volley. *European Journal of Applied Physiology*, *111*(10), 2409–2426. https://doi.org/10.1007/s00421-011-2087-9

Betts, J. G., Young, K. A., Wise, J. A., Johnson, E., Poe, B., Kruse, D. H., Korol, O., Johnson, J. E., Womble, M., & DeSaix, P. (2013). *Anatomy and Physiology*. OpenStax.

Bizovičar, N., Dreo, J., Koritnik, B., & Zidar, J. (2014). Decreased movement-related beta desynchronization and impaired post-movement beta rebound in amyotrophic lateral sclerosis. *Clinical Neurophysiology*, *125*(8), 1689–1699. https://doi.org/10.1016/j.clinph.2013.12.108

Bortel, R., & Sovka, P. (2006). EEG-EMG coherence enhancement. *Signal Processing*, *86*(7), 1737–1751. https://doi.org/10.1016/j.sigpro.2005.09.011

Botter, A., & Vieira, T. M. (2015). Filtered virtual reference: A new method for the reduction of power line interference with minimal distortion of monopolar surface EMG. *IEEE Transactions on Biomedical Engineering*, *62*(11), 2638–2647. https://doi.org/10.1109/TBME.2015.2438335

Bourguignon, M., De Tiège, X., de Beeck, M. O., Pirotte, B., Van Bogaert, P., Goldman, S., Hari, R., & Jousmäki, V. (2011). Functional motor-cortex mapping using corticokinematic coherence. *NeuroImage*, *55*(4), 1475–1479. https://doi.org/10.1016/j.neuroimage.2011.01.031

Bourguignon, M., Jousmäki, V., Dalal, S. S., Jerbi, K., & De Tiège, X. (2019). Coupling between human brain activity and body movements: Insights from non-invasive electromagnetic recordings. *NeuroImage*, *203*(February). https://doi.org/10.1016/j.neuroimage.2019.116177

Bourguignon, M., Piitulainen, H., De Tiège, X., Jousmäki, V., & Hari, R. (2015). Corticokinematic coherence mainly reflects movement-induced proprioceptive feedback. *NeuroImage*, *106*, 382–390. https://doi.org/10.1016/j.neuroimage.2014.11.026

Briggs, F., & Usrey, W. M. (2008). Emerging views of corticothalamic function. *Current Opinion in Neurobiology*, *18*(4), 403–407. https://doi.org/10.1016/j.conb.2008.09.002

Brittain, J. S., Watkins, K. E., Joundi, R. A., Ray, N. J., Holland, P., Green, A. L., Aziz, T. Z., & Jenkinson, N. (2012). A role for the subthalamic nucleus in response inhibition during conflict. *Journal of Neuroscience*, *32*(39), 13396–13401. https://doi.org/10.1523/JNEUROSCI.2259-12.2012

Brown, K., Kachelman, J., Topp, R., Quesada, P. M., Nyland, J., Malkani, A., & Swank, A. M. (2009). Predictors of functional task performance among patients scheduled for total knee arthroplasty. *The Journal of Strength & Conditioning Research*, *23*(2), 436–443.

Burbank, D. P., & Webster, J. G. (1978). Reducing skin potential motion artefact by skin abrasion. *Medical and Biological Engineering and Computing*, *16*(1), 31–38. https://doi.org/10.1007/BF02442929

Carbonaro, M., Meiburger, K. M., Seoni, S., Hodson-Tole, E. F., Vieira, T., & Botter, A. (2022). Physical and electrophysiological motor unit characteristics are revealed with simultaneous high-density electromyography and ultrafast ultrasound imaging. *Scientific Reports*, *12*(1), 1–14. https://doi.org/10.1038/s41598-022-12999-4

Carpenter, M. B. (1994). Upper and Lower Motor Neurons. In *The Physiological Basis of Rehabilitation Medicine* (Second Edi). Butterworth-Heinemann. https://doi.org/10.1016/b978-1-4831-7818-9.50007-1

Carson, R. G. (2005). Neural pathways mediating bilateral interactions between the upper limbs. *Brain Research Reviews*, *49*(3), 641–662. https://doi.org/10.1016/j.brainresrev.2005.03.005

Cassim, F., Szurhaj, W., Sediri, H., Devos, D., Bourriez, J. L., Poirot, I., Derambure, P., Defebvre, L., & Guieu, J. D. (2000). Brief and sustained movements: Differences in event-related (de)synchronization (ERD/ERS) patterns. *Clinical Neurophysiology*, *111*(11), 2032–2039. https://doi.org/10.1016/S1388-2457(00)00455-7

Casson, A. J. (2019). Wearable EEG and beyond. *Biomedical Engineering Letters*, *9*(1), 53–71. https://doi.org/10.1007/s13534-018-00093-6

Cattarello, P., & Merletti, R. (2016). Characterization of dry and wet Electrode-Skin interfaces on different skin treatments for HDsEMG. *2016 IEEE International Symposium on Medical Measurements and Applications, MeMeA 2016 - Proceedings*, *ii*, 1–6. https://doi.org/10.1109/MeMeA.2016.7533808

Cerone, G. L., Botter, A., & Gazzoni, M. (2019). A modular, smart, and wearable system for high density sEMG detection. *IEEE Transactions on Neural Systems and Rehabilitation Engineering*, *66*(22), 3371–3380.

Cerone, G. L., Botter, A., Vieira, T., & Gazzoni, M. (2021). Design and Characterization of a Textile Electrode System for the Detection of High-Density sEMG. *IEEE Transactions on Neural Systems and Rehabilitation Engineering*, *29*, 1110–1119. https://doi.org/10.1109/TNSRE.2021.3086860

Cerone, G. L., & Gazzoni, M. (2018). A wireless, minaturized multi-channel sEMG acquisition system for use in dynamic tasks. *2017 IEEE Biomedical Circuits and Systems Conference, BioCAS 2017 - Proceedings*, *2018-Janua*, 1–4. https://doi.org/10.1109/BIOCAS.2017.8325129

Cerone, G. L., Giangrande, A., Ghislieri, M., Gazzoni, M., Piitulainen, H., & Botter, A. (2022). Design and Validation of a Wireless Body Sensor Network for Integrated EEG and HD-sEMG Acquisitions. *IEEE Transactions on Neural Systems and Rehabilitation Engineering*, *30*, 61–71. https://doi.org/10.1109/TNSRE.2022.3140220

Cerone, G. L., Nicola, R., Caruso, M., Rossanigo, R., Cereatti, A., & Vieira, T. M. (2023). Running speed changes the distribution of excitation within the biceps femoris muscle in 80 m sprints. *Scandinavian Journal of Medicine and Science in Sports*, *33*(7), 1104–1115. https://doi.org/10.1111/sms.14341

Chan, Y. Y., Yue, Y., Li, Y., & Webster, R. D. (2013). Electrochemical/chemical oxidation of bisphenol A in a four-electron/two-proton process in aprotic organic solvents. *Electrochimica Acta*, *112*, 287–294.

Chi, Y. M., Jung, T. P., & Cauwenberghs, G. (2010). Dry-contact and noncontact biopotential electrodes: Methodological review. *IEEE Reviews in Biomedical Engineering*, *3*, 106–119. https://doi.org/10.1109/RBME.2010.2084078

Chi, Y. M., Maier, C., & Cauwenberghs, G. (2011). Ultra-high input impedance, low noise integrated amplifier for noncontact biopotential sensing. *IEEE*

*Journal on Emerging and Selected Topics in Circuits and Systems*, *1*(4), 526–535. https://doi.org/10.1109/JETCAS.2011.2179419

Ciganek, L. (1967). A comparative study of visual, auditory and somatosensory EEG responses in man. *Experimental Brain Research*, *4*, 118–125.

Clamann, H. P. (1993). Motor unit recruitment and the gradation of muscle force. *Physical Therapy*, *73*(12), 830–843. https://doi.org/10.1093/ptj/73.12.830

Conway, B. A., Halliday, D. M., Farmer, S. F., Shahani, U., Maas, P., Weir, A. I., & Rosenberg, J. R. (1995). Synchronization between motor cortex and spinal motoneuronal pool during the performance of a maintained motor task in man. *The Journal of Physiology*, *489*(3), 917–924. https://doi.org/10.1113/jphysiol.1995.sp021104

Da Silva, F. L. (2023). EEG: origin and measurement. In *EEG-fMRI: physiological basis, technique, and applications* (pp. 23–48). Springer.

David, O., Kilner, J. M., & Friston, K. J. (2006). Mechanisms of evoked and induced responses in MEG/EEG. *NeuroImage*, *31*(4), 1580–1591. https://doi.org/10.1016/j.neuroimage.2006.02.034

Davis, W. J., & Kovac, M. P. (1981). The command neuron and the organization of movement. *Trends in Neurosciences*, *4*, 73–76.

De Talhouet, H., & Webster, J. G. (1996). The origin of skin-stretch-caused motion artifacts under electrodes. *Physiological Measurement*, *17*(2), 81–93. https://doi.org/10.1088/0967-3334/17/2/003

De Tiège, X., Bourguignon, M., Piitulainen, H., & Jousmäki, V. (2020). Sensorimotor Mapping With MEG: An Update on the Current State of Clinical Research and Practice With Considerations for Clinical Practice Guidelines. *Journal of Clinical Neurophysiology*, *37*(6).

Debener, S., Strobel, A., Sorger, B., Peters, J., Kranczioch, C., Engel, A. K., & Goebel, R. (2007). Improved quality of auditory event-related potentials recorded simultaneously with 3-T fMRI: Removal of the ballistocardiogram artefact. *NeuroImage*, *34*(2), 587–597. https://doi.org/10.1016/j.neuroimage.2006.09.031

Debener, S., Ullsperger, M., Siegel, M., Fiehler, K., Von Cramon, D. Y., & Engel, A. K. (2005). Trial-by-trial coupling of concurrent electroencephalogram and functional magnetic resonance imaging identifies the dynamics of performance monitoring. *Journal of Neuroscience*, *25*(50), 11730–11737. https://doi.org/10.1523/JNEUROSCI.3286-05.2005

Deiber, M. P., Sallard, E., Ludwig, C., Ghezzi, C., Barral, J., & Ibañez, V. (2012). EEG alpha activity reflects motor preparation rather than the mode of action selection. *Frontiers in Integrative Neuroscience*, *6*(JULY 2012), 1–11. https://doi.org/10.3389/fnint.2012.00059

Dellacorna. (2006). *ELECTROMYOGRAPH FOR THE DETECTION OF ELECTROMYOGRAPHIC SIGNALS ON MOVING SUBJECTS - Pub. No.: US 2006/0287608 A1*.

Démas, J., Bourguignon, M., De Tiège, X., Wens, V., Coquelet, N., Rovai, A., Bouvier, S., Bailly, R., Brochard, S., Dinomais, M., & Van Bogaert, P. (2022). Assessing spino-cortical proprioceptive processing in childhood unilateral

cerebral palsy with corticokinematic coherence. *Neurophysiologie Clinique*, *52*(1), 33–43. https://doi.org/10.1016/j.neucli.2021.12.003

Diesburg, D. A., Greenlee, J. D. W., & Wessel, J. R. (2021). Cortico-subcortical β burst dynamics underlying movement cancellation in humans. *ELife*, *10*, 1–25. https://doi.org/10.7554/eLife.70270

Dimitrova, N. A., Dimitrov, G. V., & Chihman, V. N. (1999). Effect of electrode dimensions on motor unit potentials. *Medical Engineering and Physics*, *21*(6–7), 479–485. https://doi.org/10.1016/S1350-4533(99)00069-7

Dobrev, D. (2002). Two-electrode non-differential biopotential amplifier. *Medical and Biological Engineering and Computing*, *40*(5), 546–549. https://doi.org/10.1007/BF02345453

Dobrev, D., Neycheva, T., & Mudrov, N. (2005). Simple two-electrode biosignal amplifier. *Medical and Biological Engineering and Computing*, *43*(6), 725–730. https://doi.org/10.1007/BF02430949

Dobrev, D. P., Neycheva, T., & Mudrov, N. (2008). Bootstrapped two-electrode biosignal amplifier. *Medical and Biological Engineering and Computing*, *46*(6), 613–619. https://doi.org/10.1007/s11517-008-0312-4

Doucet, B. M., Lam, A., & Griffin, L. (2012). Neuromuscular Electrical Stimulation for Skeletal Muscle Function. *Yale Journal of Biology and Medicine*, *85*(2), 201–215.

Duchateau, J., & Enoka, R. M. (2011). Human motor unit recordings: Origins and insight into the integrated motor system. *Brain Research*, *1409*, 42–61. https://doi.org/10.1016/j.brainres.2011.06.011

Duclay, J., & Martin, A. (2005). Evoked H-reflex and V-wave responses during maximal isometric, concentric, and eccentric muscle contraction. *Journal of Neurophysiology*, *94*(5), 3555–3562. https://doi.org/10.1152/jn.00348.2005

Eckhouse, R. H., Penny, M. A., & Maulucci, R. A. (1996). A comparison of kinematic recording instruments. *Journal of Medical Systems*, *20*(6), 439–456. https://doi.org/10.1007/BF02257287

Engel, A. K., & Fries, P. (2010). Beta-band oscillations-signalling the status quo? *Current Opinion in Neurobiology*, *20*(2), 156–165. https://doi.org/10.1016/j.conb.2010.02.015

Farina, D., Cescon, C., & Merletti, R. (2002). Influence of anatomical, physical, and detection-system parameters on surface EMG. *Biological Cybernetics*, *86*(6), 445–456. https://doi.org/10.1007/s00422-002-0309-2

Gantchev, G., Gavrilenko, T., & Concek, V. (1994). Somatosensory evoked potentials modification related to isometric voluntary contraction. *International Journal of Psychophysiology*, *17*(3), 191–196. https://doi.org/10.1016/0167-8760(94)90062-0

Gastaut, H. (1952). Electrocorticographic study of the reactivity of rolandic rhythm. *Revue Neurologique*, *87*(2), 176–182.

Gastaut, H. J., & Bert, J. (1954). EEG changes during cinematographic presentation (Moving picture activation of the EEG). *Electroencephalography and Clinical Neurophysiology*, *6*, 433–444.

Giangrande, A., Botter, A., Piitulainen, H., & Cerone, G. L. (2024). Motion Artifacts in Dynamic EEG Recordings: Experimental Observations, Electrical Modelling, and Design Considerations. *Sensors*, *24*(19), 1–20. https://doi.org/10.3390/s24196363

Giangrande, A., Cerone, G. L., Botter, A., & Piitulainen, H. (2024). Volitional muscle activation intensifies neuronal processing of proprioceptive afference in the primary sensorimotor cortex: an EEG study. *Journal of Neurophysiology*, *131*(1), 28–37. https://doi.org/10.1152/JN.00340.2023

Giangrande, A., Mujunen, T., Luigi Cerone, G., Botter, A., & Piitulainen, H. (2024). Maintained volitional activation of the muscle alters the cortical processing of proprioceptive afference from the ankle joint. *Neuroscience*, *560*(September), 314–325. https://doi.org/10.1016/j.neuroscience.2024.09.049

Girton, D., & Kamiya, J. (1972). A simple on-line technique for removing eye movement artifacts from the EEG. *Electroencephalography and Clinical Neurophysiol*, *34*(2), 212–216. https://doi.org/https://doi.org/10.1016/0013-4694(73)90052-7

Gramfort, A., Luessi, M., Larson, E., Engemann, D. A., Strohmeier, D., Brodbeck, C., Goj, R., Jas, M., Brooks, T., Parkkonen, L., & Hämäläinen, M. (2013). MEG and EEG data analysis with MNE-Python. *Frontiers in Neuroscience*, *7*(7 DEC), 1–13. https://doi.org/10.3389/fnins.2013.00267

Guermandi, M., Scarselli, E. F., & Guerrieri, R. (2016). A Driving Right Leg Circuit (DgRL) for Improved Common Mode Rejection in Bio-Potential Acquisition Systems. *IEEE Transactions on Biomedical Circuits and Systems*, *10*(2), 507–517. https://doi.org/10.1109/TBCAS.2015.2446753

Hakonen, M., Nurmi, T., Vallinoja, J., Jaatela, J., & Piitulainen, H. (2022). More comprehensive proprioceptive stimulation of the hand amplifies its cortical processing. *Journal of Neurophysiology*, *128*(3), 568–581. https://doi.org/10.1152/jn.00485.2021

Halliday, D. M., Rosenberg, J. R., Amjad, A. M., Breeze, P., Conways, B. A., & Farmer, S. F. (1995). A framework for the analysis of mixed time series/point process data - theory ad application to the study of physiological tremor, single motor unit discharges and electromyograms. *Progr. Biophys. Molec. Biol.*, *64*(2–3), 237–278. https://doi.org/https://doi.org/10.1016/S0079-6107(96)00009-0

Hari, R. (2006). Action-perception connection and the cortical mu rhythm. *Progress in Brain Research*, *159*(06), 253–260. https://doi.org/10.1016/S0079-6123(06)59017-X

Hari, R., & Puce, A. (2017). MEG-EEG Primer. In *MEG-EEG Primer*.

Helmholtz, H. von. (1879). Studien über electrische Grenzschichten. *Annalen Der Physik*, *243*(7), 337–382.

Hsiao, S. (2008). Central mechanisms of tactile shape perception. *Current Opinion in Neurobiology*, *18*(4), 418–424. https://doi.org/10.1016/j.conb.2008.09.001

Hu, L., Xiao, P., Zhang, Z. G., Mouraux, A., & Iannetti, G. D. (2014). Single-trial time-frequency analysis of electrocortical signals: Baseline correction and

beyond. *NeuroImage*, *84*, 876–887. https://doi.org/10.1016/j.neuroimage.2013.09.055

Hussain, S. J., Cohen, L. G., & Bönstrup, M. (2019). Beta rhythm events predict corticospinal motor output. *Scientific Reports*, *9*(1), 1–10. https://doi.org/10.1038/s41598-019-54706-w

Illman, M., Jaatela, J., Vallinoja, J., Nurmi, T., Mäenpää, H., & Piitulainen, H. (2023). Altered excitation-inhibition balance in the primary sensorimotor cortex to proprioceptive hand stimulation in cerebral palsy. *Clinical Neurophysiology*, *157*, 25–36. https://doi.org/10.1016/j.clinph.2023.10.016

Illman, M., Laaksonen, K., Jousmäki, V., Forss, N., & Piitulainen, H. (2022). Reproducibility of Rolandic beta rhythm modulation in MEG and EEG. *Journal of Neurophysiology*, *127*(2), 559–570. https://doi.org/10.1152/jn.00267.2021

Kaas, J. H. (2005). The functional organization of somatosensory cortex in Primates. *Thromb. Haemostasis*, *94*, 907–915.

Kandel, E. R., Schwartz, J. H., Jessell, T. M., Siegelbaum, S., Hudspeth, A. J., & Mack, S. (2000). *Principles of neural science* (Vol. 4). McGraw-hill New York.

Kelly, J. P., & Dodd, J. (1991). Anatomical organization of the nervous system. *Principles of Neural Science. 3rd Ed. New York: Elsevier*, 276–292.

Kilner, J. M., Baker, S. N., Salenius, S., Jousmäki, V., Hari, R., & Lemon, R. N. (1999). Task-dependent modulation of 15-30 Hz coherence between rectified EMGs from human hand and forearm muscles. *Journal of Physiology*, *516*(2), 559–570. https://doi.org/10.1111/j.1469-7793.1999.0559v.x

Klijn, J. A. J., & Kloprogge, M. J. G. M. (1974). Movement artefact suppressor during ECG monitoring. *Cardiovascular Research*, *8*(1), 149–152. https://doi.org/10.1093/cvr/8.1.149

Konczak, J., Corcos, D. M., Horak, F., Poizner, H., Shapiro, M., Tuite, P., Volkmann, J., & Maschke, M. (2009). Proprioception and Motor Control in Parkinson's Disease. *Journal of Motor Behavior*, *41*(6), 543–552. https://doi.org/10.3200/35-09-002

Laszlo, S., Ruiz-Blondet, M., Khalifian, N., Chu, F., & Jin, Z. (2014). A direct comparison of active and passive amplification electrodes in the same amplifier system. *Journal of Neuroscience Methods*, *235*, 298–307. https://doi.org/10.1016/j.jneumeth.2014.05.012

Lattari, E., Velasques, B., Paes, F., Cunha, M., Budde, H., Basile, L., Cagy, M., Piedade, R., De Carvalho Machado, S. E., & Ribeiro, P. (2010). Corticomuscular coherence behavior in fine motor control of force: A critical review. *Revista de Neurologia*, *51*(10), 610–623.

Lee, C. J., & Song, J. I. (2019). A Chopper Stabilized Current-Feedback Instrumentation Amplifier for EEG Acquisition Applications. *IEEE Access*, *7*, 11565–11569. https://doi.org/10.1109/ACCESS.2019.2892502

Lienhard, K. (2015). Analysis of whole-body vibration exercise effect on lower limb muscle activity using surface electromyography : methodological considerations and practical applications. *Researchgate*, *November 2014*, 1–247.

Lifshitz, K. (1966). The averaged evoked cortical response to complex visual stimuli. *Psychophysiology*, *3*(1), 55–68.

Liu, J., Sheng, Y., & Liu, H. (2019). Corticomuscular coherence and its applications: A review. *Frontiers in Human Neuroscience*, *13*(March), 1–16. https://doi.org/10.3389/fnhum.2019.00100

Lolli, V., Rovaï, A., Trotta, N., Bourguignon, M., Goldman, S., Sadeghi, N., Jousmäki, V., & De Tiège, X. (2019). MRI-compatible pneumatic stimulator for sensorimotor mapping. *Journal of Neuroscience Methods*, *313*(December 2018), 29–36. https://doi.org/10.1016/j.jneumeth.2018.12.014

Long, X., Liu, D. X., Liang, S., Yan, Z., & Wu, X. (2018). An EEG-Based BCI System for Controlling Lower Exoskeleton to Step over Obstacles in Realistic Walking Situation. *2018 15th International Conference on Control, Automation, Robotics and Vision, ICARCV 2018*, *2*, 1609–1614. https://doi.org/10.1109/ICARCV.2018.8581094

Machado, S., Cunha, M., Velasques, B., Minc, D., Teixeira, S., Domingues, C. A., Silva, J. G., Bastos, V. H., Budde, H., Cagy, M., Basile, L., Piedade, R., & Ribeiro, P. (2010). Sensorimotor integration: basic concepts, abnormalities related to movement disorders and sensorimotor training-induced cortical reorganization. *Revista de Neurologia*, *51*(7), 427–436. https://doi.org/10.33588/rn.5107.2010228

Maezawa, H., Fujimoto, M., Hata, Y., Matsuhashi, M., Hashimoto, H., Kashioka, H., Yanagida, T., & Hirata, M. (2022). Functional cortical localization of tongue movements using corticokinematic coherence with a deep learning-assisted motion capture system. *Scientific Reports*, *12*(1), 1–11. https://doi.org/10.1038/s41598-021-04469-0

Marsden, C. D., Merton, P. A., & Morton, H. B. (1973). Is the Human Stretch Reflex Cortical Rather Than Spinal ? *The Lancet*, *301*(7806), 759–761. https://doi.org/10.1016/S0140-6736(73)92141-7

Martin, J., & Jessel, T. (1991). Modality coding in the somatic sensory system. *Principles of Neural Science*.

Matthews, P. B. C. (1964). Muscle spindles and their motor control. *Physiological Reviews*, *44*(2), 219–288.

McIlroy, W. E., Bishop, D. C., Staines, W. R., Nelson, A. J., Maki, B. E., & Brooke, J. D. (2003). Modulation of afferent inflow during the control of balancing tasks using the lower limbs. *Brain Research*, *961*(1), 73–80. https://doi.org/10.1016/S0006-8993(02)03845-3

Mecarelli, O. (2019). Electrode placement systems and montages. *Clinical Electroencephalography*, 35–52.

Merletti, R., & Cerone, G. L. (2020). Tutorial. Surface EMG detection, conditioning and pre-processing: Best practices. *Journal of Electromyography and Kinesiology*, *54*, 102440. https://doi.org/10.1016/j.jelekin.2020.102440

Merletti, R., & Farina, D. (2016). *Surface Electromyography: Physiology, Engineering, and Applications*. 30–53.

Metting van Rijn, A. C., Peper, A., & Grimbergen, C. A. (1990). High-quality recording of bioelectric events. *Medical & Biological Engineering & Computing*, *28*(5), 389–397. https://doi.org/10.1007/bf02441961

Moon, K. M., Kim, J., Seong, Y., Suh, B. C., Kang, K. J., Choe, H. K., & Kim, K. (2021). Proprioception, the regulator of motor function. *BMB Reports*, *54*(8), 393–402. https://doi.org/10.5483/BMBRep.2021.54.8.052

Moshonkina, T., Grishin, A., Bogacheva, I., Gorodnichev, R., Ovechkin, A., Siu, R., Edgerton, V. R., & Gerasimenko, Y. (2021). Novel Non-invasive Strategy for Spinal Neuromodulation to Control Human Locomotion. *Frontiers in Human Neuroscience*, *14*(January), 13–16. https://doi.org/10.3389/fnhum.2020.622533

Mujunen, T., Nurmi, T., & Piitulainen, H. (2021). Corticokinematic coherence is stronger to regular than irregular proprioceptive stimulation of the hand. *Journal of Neurophysiology*, *126*(2), 550–560. https://doi.org/10.1152/jn.00095.2021

Mujunen, T., Seipäjärvi, S., Nurminen, M., Parviainen, T., & Piitulainen, H. (2022). Reproducibility of evoked and induced MEG responses to proprioceptive stimulation of the ankle joint. *Neuroimage: Reports*, *2*(3), 100110. https://doi.org/10.1016/j.ynirp.2022.100110

Murayama, N., Lin, Y.-Y., Salenius, S., & Hari, R. (2001). Oscillatory interaction between human motor cortex and trunk muscles during isometric contraction. *Neuroimage*, *14*(5), 1206–1213.

Negro, F., Keenan, K., & Farina, D. (2015). Power spectrum of the rectified EMG: When and why is rectification beneficial for identifying neural connectivity? *Journal of Neural Engineering*, *12*(3). https://doi.org/10.1088/1741-2560/12/3/036008

Neumann, E., Toensing, K., Kakorin, S., Budde, P., & Frey, J. (1998). Mechanism of electroporative dye uptake by mouse B cells. *Biophysical Journal*, *74*(1), 98–108. https://doi.org/10.1016/S0006-3495(98)77771-9

Neuper, C., Scherer, R., Wriessnegger, S., & Pfurtscheller, G. (2009). Motor imagery and action observation: Modulation of sensorimotor brain rhythms during mental control of a brain-computer interface. *Clinical Neurophysiology*, *120*(2), 239–247. https://doi.org/10.1016/j.clinph.2008.11.015

Nevanperä, S., Hu, N., Walker, S., Avela, J., & Piirainen, J. M. (2023). Modulation of H-reflex and V-wave responses during dynamic balance perturbations. *Experimental Brain Research*, *241*(6), 1599–1610. https://doi.org/10.1007/s00221-023-06625-6

Niso, G., Romero, E., Moreau, J. T., Araujo, A., & Krol, L. R. (2023). Wireless EEG : A survey of systems and studies. *NeuroImage*, *269*(November 2022). https://doi.org/10.1016/j.neuroimage.2022.119774

Nurmi, T., Hakonen, M., Bourguignon, M., & Piitulainen, H. (2023). Proprioceptive response strength in the primary sensorimotor cortex is invariant to the range of finger movement. *NeuroImage*, *269*(December 2022), 119937. https://doi.org/10.1016/j.neuroimage.2023.119937

Oliveira, A. S., Schlink, B. R., Hairston, W. D., König, P., & Ferris, D. P. (2016). Induction and separation of motion artifacts in EEG data using a mobile phantom head device. *Journal of Neural Engineering*, *13*(3). https://doi.org/10.1088/1741-2560/13/3/036014

Oostenveld, R., Fries, P., Maris, E., & Schoffelen, J. (2011). *FieldTrip : Open Source Software for Advanced Analysis of MEG , EEG , and Invasive Electrophysiological Data*. *2011*. https://doi.org/10.1155/2011/156869

Pallás-Areny, R., & Webster, J. G. (1990). Composite instrumentation amplifier for biopotentials. *Annals of Biomedical Engineering*, *18*(3), 251–262. https://doi.org/10.1007/BF02368441

Palmieri, R. M., Ingersoll, C. D., & Hoffman, M. A. (2004). The Hoffmann reflex: Methodologic considerations and applications for use in sports medicine and athletic training research. *Journal of Athletic Training*, *39*(3), 268–277.

Parkkonen, E., Laaksonen, K., Piitulainen, H., Parkkonen, L., & Forss, N. (2015). Modulation of the~20-Hz motor-cortex rhythm to passivemovement and tactile stimulation. *Brain and Behavior*, *5*(5), 1–11. https://doi.org/10.1002/brb3.328

Parkkonen, E., Laaksonen, K., Piitulainen, H., Pekkola, J., Parkkonen, L., Tatlisumak, T., & Forss, N. (2017). Strength of ~20-Hz Rebound and Motor Recovery after Stroke. *Neurorehabilitation and Neural Repair*, *31*(5), 475–486. https://doi.org/10.1177/1545968316688795

Petersen, T. H., Willerslev-Olsen, M., Conway, B. A., & Nielsen, J. B. (2012). The motor cortex drives the muscles during walking in human subjects. *Journal of Physiology*, *590*(10), 2443–2452. https://doi.org/10.1113/jphysiol.2012.227397

Petkos, K., Koutsoftidis, S., Guiho, T., Degenaar, P., Jackson, A., Greenwald, S. E., Brown, P., Denison, T., & Drakakis, E. M. (2019). A high-performance 8 nV/√Hz 8-channel wearable and wireless system for real-time monitoring of bioelectrical signals. *Journal of NeuroEngineering and Rehabilitation*, *16*(1). https://doi.org/10.1186/s12984-019-0629-2

Pfurtscheller, G., & Neuper, C. (1994). Event-related synchronization of mu rhythm in the EEG over the cortical hand area in man. *Neuroscience Letters*, *174*(1), 93–96. https://doi.org/10.1016/0304-3940(94)90127-9

Pfurtscheller, G., Neuper, C., Brunner, C., & Lopes Da Silva, F. (2005). Beta rebound after different types of motor imagery in man. *Neuroscience Letters*, *378*(3), 156–159. https://doi.org/10.1016/j.neulet.2004.12.034

Picton, T. W., & Hink, R. F. (1974). Evoked potentials: how? what? and why? *American Journal of EEG Technology*, *14*(1), 9–44. https://doi.org/10.1080/00029238.1974.11080979

Piitulainen, H., Botter, A., Bourguignon, M., Jousmäki, V., & Hari, R. (2015). Spatial variability in cortex-muscle coherence investigated with magnetoencephalography and high-density surface electromyography. *Journal of Neurophysiology*, *114*(5), 2843–2853. https://doi.org/10.1152/jn.00574.2015

Piitulainen, H., Bourguignon, M., De Tiège, X., Hari, R., & Jousmäki, V. (2013a). Coherence between magnetoencephalography and hand-action-related

acceleration, force, pressure, and electromyogram. *NeuroImage*, *72*, 83–90. https://doi.org/10.1016/j.neuroimage.2013.01.029

Piitulainen, H., Bourguignon, M., De Tiège, X., Hari, R., & Jousmäki, V. (2013b). Corticokinematic coherence during active and passive finger movements. *Neuroscience*, *238*, 361–370. https://doi.org/10.1016/J.NEUROSCIENCE.2013.02.002

Piitulainen, H., Bourguignon, M., Hari, R., & Jousmäki, V. (2015). MEG-compatible pneumatic stimulator to elicit passive finger and toe movements. *NeuroImage*, *112*, 310–317.

Piitulainen, H., Illman, M., Jousmäki, V., & Bourguignon, M. (2020). Feasibility and reproducibility of electroencephalography-based corticokinematic coherence. *Journal of Neurophysiology*, *124*(6), 1959–1967. https://doi.org/10.1152/jn.00562.2020

Piitulainen, H., Illman, M., Laaksonen, K., Jousmäki, V., & Forss, N. (2018). Reproducibility of corticokinematic coherence. *NeuroImage*, *179*(June), 596–603. https://doi.org/10.1016/j.neuroimage.2018.06.078

Piitulainen, H., Seipäjärvi, S., Avela, J., Parviainen, T., & Walker, S. (2018). Cortical proprioceptive processing is altered by aging. *Frontiers in Aging Neuroscience*, *10*(JUN), 1–13. https://doi.org/10.3389/fnagi.2018.00147

Piitulainen, H., Sukanen, M., Finni, T., & Cenni, F. (2023). Proprioceptive-perception threshold is impaired in cerebral palsy and is associated with worse balance performance. *Gait & Posture*, *106*, S165–S166. https://doi.org/10.1016/j.gaitpost.2023.07.199

Pohja, M., Salenius, S., & Hari, R. (2005). Reproducibility of cortex–muscle coherence. *NeuroImage*, *26*(3), 764–770. https://doi.org/10.1016/J.NEUROIMAGE.2005.02.031

Proske, U., & Gandevia, S. C. (2012). The proprioceptive senses: Their roles in signaling body shape, body position and movement, and muscle force. *Physiological Reviews*, *92*(4), 1651–1697. https://doi.org/10.1152/physrev.00048.2011

Purves, D., Augustine, J. G., Fitzpatrick, D., Hall, C. W., LaMantia, A.-S., Mooney, D. R., Platt, L. M., & White, E. L. (2018). Neuroscience. In *Oxford University Press Inc.* (6th ed.). Oxford University Press Inc.

R. C. Oldfield. (1971). The assessment and analysis of handedness: the Edinburgh inventory. In *Neuropsychologia* (pp. 97–113). https://doi.org/10.1007/978-0-387-79948-3_6053

Ramkumar, P., Parkkonen, L., Hari, R., & Hyvärinen, A. (2012). Characterization of neuromagnetic brain rhythms over time scales of minutes using spatial independent component analysis. *Human Brain Mapping*, *33*(7), 1648–1662. https://doi.org/10.1002/hbm.21303

Ratcliff, R., Philiastides, M. G., & Sajda, P. (2009). Quality of evidence for perceptual decision making is indexed by trial-to-trial variability of the EEG. *Proceedings of the National Academy of Sciences of the United States of America*, *106*(16), 6539–6544. https://doi.org/10.1073/pnas.0812589106

Ratz, A. G. (1969). Triboelectric noise(Triboelectric noise in mechanically flexed low level signal cables for piezoelectric transducers with high gain amplifiers). *ISA TRANSACTIONS*, *9*(2), 154–158.

Riddle, C. N., & Baker, S. N. (2006). Digit displacement, not object compliance, underlies task dependent modulations in human corticomuscular coherence. *NeuroImage*, *33*(2), 618–627.

Riemann, B. L., & Lephart, S. M. (2002). The sensorimotor system, part I: The physiologic basis of functional joint stability. *Journal of Athletic Training*, *37*(1), 71–79.

Roeder, L., Boonstra, T. W., & Kerr, G. K. (2020). Corticomuscular control of walking in older people and people with parkinson's disease. *Scientific Reports*, *10*(2980). https://doi.org/10.1038/s41598-020-59810-w

Salenius, S., Portin, K., Kajola, M., Salmelin, R., & Hari, R. (1997). Cortical control of human motoneuron firing during isometric contraction. *Journal of Neurophysiology*, *77*(6), 3401–3405. https://doi.org/10.1152/jn.1997.77.6.3401

Salmelin, R., Hämäläinen, M., Kajola, M., & Hari, R. (1995). Functional segregation of movement-related rhythmic activity in the human brain. In *NeuroImage* (Vol. 2, Issue 4, pp. 237–243). https://doi.org/10.1006/nimg.1995.1031

Salmelin, R., & Hari, R. (1994). Spatiotemporal characteristics of rhythmic neuromagnetic activity related to thumb movement. *Neuroscience*, *60*(94), 537–550.

Savers, B. M., Beagley, H. A., & Henshall, W. R. (1974). The mechanism of auditory evoked EEG responses. *Nature*, *247*(5441), 481–483.

Scanlon, J. E. M., Jacobsen, N. S. J., Maack, M. C., & Debener, S. (2021). Does the electrode amplification style matter? A comparison of active and passive EEG system configurations during standing and walking. *European Journal of Neuroscience*, *54*(12), 8381–8395. https://doi.org/10.1111/ejn.15037

Schutter, D. J. L. G., & Hortensius, R. (2011). Brain oscillations and frequency-dependent modulation of cortical excitability. *Brain Stimulation*, *4*(2), 97–103. https://doi.org/10.1016/j.brs.2010.07.002

Seki, K., Perlmutter, S. I., & Fetz, E. E. (2003). Sensory input to primate spinal cord is presynaptically inhibited during voluntary movement. *Nature Neuroscience*, *6*(12), 1309–1316. https://doi.org/10.1038/nn1154

Sherrington, C. (1916). The integrative action of the Nervous System. In *Annals of internal medicine* (Vol. 34, Issue 6, pp. 150–180). https://doi.org/10.7326/0003-4819-34-6-1311

Shibasaki, H., Barrett, G., Halliday, E., & Halliday, A. M. (1980). Cortical potentials following voluntary and passive finger movements. *Electroencephalography and Clinical Neurophysiology*, *50*, 201–213.

Shin, Y. K., Lee, D. R., Hwang, H. J., You, S. H., & Im, C. H. (2012). A novel EEG-based brain mapping to determine cortical activation patterns in normal children and children with cerebral palsy during motor imagery tasks.

*NeuroRehabilitation*, *31*(4), 349–355. https://doi.org/10.3233/NRE-2012-00803

Shukla, S., Roy, V., & Prakash, A. (2020). Wavelet based empirical approach to mitigate the effect of motion artifacts from EEG signal. *Proceedings - 2020 IEEE 9th International Conference on Communication Systems and Network Technologies, CSNT 2020*, 323–326. https://doi.org/10.1109/CSNT48778.2020.9115761

Skosnik, P. D., & Cortes-Briones, J. A. (2016). Electroencephalography and Cannabis: From Event-Related Potentials to Oscillations. In *Neuropathology of Drug Addictions and Substance Misuse Volume 1: Foundations of Understanding, Tobacco, Alcohol, Cannabinoids and Opioids* (Vol. 1). Elsevier Inc. https://doi.org/10.1016/B978-0-12-800213-1.00080-8

Smeds, E., Vanhatalo, S., Piitulainen, H., Bourguignon, M., Jousmäki, V., & Hari, R. (2017). Corticokinematic coherence as a new marker for somatosensory afference in newborns. *Clinical Neurophysiology*, *128*(4), 647–655.

SooHyun, L., George, E. C., & Daniel, J. S. (2008). Motor modulation of afferent somatosensory circuits. *Nature Neuroscience*, *11*(12), 1430–1438. https://doi.org/10.1038/nn.2227.Motor

Sörnmo, L., & Laguna, P. (2005). *Bioelectrical signal processing in cardiac and neurological applications*. Academic press.

Spinelli, E., & Guerrero, F. N. (2017). *the Biological Amplifier*. 463–500. https://doi.org/10.1142/9789813147263_0012

Spinelli, E., & Haberman, M. (2010). Insulating electrodes: A review on biopotential front ends for dielectric skin-electrode interfaces. *Physiological Measurement*, *31*(10). https://doi.org/10.1088/0967-3334/31/10/S03

Spinelli, E. M., Pallàs-Areny, R., & Mayosky, M. A. (2003). AC-coupled front-end for biopotential measurements. *IEEE Transactions on Biomedical Engineering*, *50*(3), 391–395. https://doi.org/10.1109/TBME.2003.808826

Staines, W. R., Graham, S. J., Black, S. E., & McIlroy, W. E. (2002). Task-relevant modulation of contralateral and ipsilateral primary somatosensory cortex and the role of a prefrontal-cortical sensory gating system. *NeuroImage*, *15*(1), 190–199. https://doi.org/10.1006/nimg.2001.0953

Stegeman, D. F., Dumitru, D., King, J. C., & Roeleveld, K. (1997). Near-and far-fields: source characteristics and the conducting medium in neurophysiology. *Journal of Clinical Neurophysiology*, *14*(5), 429–442.

Stegeman, D., & Hermens, H. (2007). *Standards for surface electromyography: The European project Surface EMG for non-invasive assessment of muscles (SENIAM)*. http://www.seniam.org/%5Cnhttp://www.med.uni-jena.de/motorik/pdf/stegeman.pdf

Tan, H., Wade, C., & Brown, P. (2016). Post-movement beta activity in sensorimotor cortex indexes confidence in the estimations from internal models. *Journal of Neuroscience*, *36*(5), 1516–1528. https://doi.org/10.1523/JNEUROSCI.3204-15.2016

Tandle, A., Bhakti Vedanta Marg Vile Parle, S., -, M., & Jog, N. (2015). Classification of Artefacts in EEG Signal Recordings and Overview of Removing Techniques. *International Journal of Computer Applications*, *Icct*, 46.

Thakor, N. V. (1999). Biopotentials and electrophysiology measurement. *The Measurement, Instrumentation, and Sensors Handbook*, *74*.

Toledo, D. R., Manzano, G. M., Barela, J. A., & Kohn, A. F. (2016). Cortical correlates of response time slowing in older adults: ERP and ERD/ERS analyses during passive ankle movement. *Clinical Neurophysiology*, *127*(1), 655–663. https://doi.org/10.1016/j.clinph.2015.05.003

Tseghai, G. B., Malengier, B., Fante, K. A., & Van Langenhove, L. (2021). the Status of Textile-Based Dry Eeg Electrodes. *Autex Research Journal*, *21*(1), 63–70. https://doi.org/10.2478/aut-2019-0071

Tuthill, J. C., & Azim, E. (2018). Proprioception. *Current Biology*, *28*(5), R194–R203. https://doi.org/10.1016/j.cub.2018.01.064

Ushiyama, J., Takahashi, Y., & Ushiba, J. (2010). Muscle dependency of corticomuscular coherence in upper and lower limb muscles and training-related alterations in ballet dancers and weightlifters. *Journal of Applied Physiology*, *109*(4), 1086–1095. https://doi.org/10.1152/japplphysiol.00869.2009

Van Beers, R. J., Baraduc, P., & Wolpert, D. M. (2002). Role of uncertainty in sensorimotor control. *Philosophical Transactions of the Royal Society B: Biological Sciences*, *357*(1424), 1137–1145. https://doi.org/10.1098/rstb.2002.1101

van Melick, N., Meddeler, B. M., Hoogeboom, T. J., Nijhuis-van der Sanden, M. W. G., & van Cingel, R. E. H. (2017). How to determine leg dominance: The agreement between self-reported and observed performance in healthy adults. *PLoS ONE*, *12*(12), 1–9. https://doi.org/10.1371/journal.pone.0189876

Vieira, T. M., Cerone, G. L., Bruno, M., & Bachero-Mena, B. (2024). Myoelectric manifestations of fatigue of the finger flexor muscles and endurance capacity in experienced versus intermediate climbers during suspension tasks. *Journal of Sports Sciences*, *42*(8), 655–664. https://doi.org/10.1080/02640414.2024.2357470

Vinding, M. C., Tsitsi, P., Piitulainen, H., Waldthaler, J., Jousmäki, V., Ingvar, M., Svenningsson, P., & Lundqvist, D. (2019). Attenuated beta rebound to proprioceptive afferent feedback in Parkinson's disease. *Scientific Reports*, *9*(1), 1–11. https://doi.org/10.1038/s41598-019-39204-3

Virtanen, J., Ahveninen, J., Ilmoniemi, R. J., Näätänen, R., & Pekkonen, E. (1998). Replicability of MEG and EEG measures of the auditory N1/N1m-response. *Electroencephalography and Clinical Neurophysiology - Evoked Potentials*, *108*(3), 291–298. https://doi.org/10.1016/S0168-5597(98)00006-9

Vogels, T. P., Sprekeler, H., Zenke, F., Clopath, C., & Gerstner, W. (2011). Inhibitory Plasticity Balances Excitation and Inhibition in Sensory Pathways and Memory Networks. *Science*, *334*, 1569–1574.

Wang, W. S., Huang, H. Y., Wu, Z. C., Chen, S. C., Wang, W. F., Wu, C. F., & Luo, C. H. (2011). Wireless biopotential acquisition system for portable healthcare monitoring. *Journal of Medical Engineering and Technology*, *35*(5), 254–261. https://doi.org/10.3109/03091902.2011.580038

Wartzek, T., Lammersen, T., Eilebrecht, B., Walter, M., & Leonhardt, S. (2011). Triboelectricity in capacitive biopotential measurements. *IEEE Transactions on Biomedical Engineering*, *58*(5), 1268–1277. https://doi.org/10.1109/TBME.2010.2100393

Webster, J. G. (1984). Reducing Motion Artifacts and Interference in Biopotential Recording. *IEEE Transactions on Biomedical Engineering*, *31*(12), 823–826. https://doi.org/10.1109/TBME.1984.325244

Wu, H., Yang, G., Zhu, K., Liu, S., Guo, W., Jiang, Z., & Li, Z. (2020). Materials Devices and Systems of On-Skin Electrodes for Electrophysiological Monitoring.pdf. In *Advanced Science*.

Yang, J. F., & Gorassini, M. (2006). Spinal and brain control of human walking: Implications for retraining of walking. *Neuroscientist*, *12*(5), 379–389. https://doi.org/10.1177/1073858406292151

Yang, L., Gan, L., Zhang, Z., Zhang, Z., Yang, H., Zhang, Y., & Wu, J. (2022). Insight into the Contact Impedance between the Electrode and the Skin Surface for Electrophysical Recordings. *ACS Omega*, *7*(16), 13906–13912. https://doi.org/10.1021/acsomega.2c00282

Yaziciouglu, R. F., Van Hoof, C., & Puers, R. (2009). Introduction to Biopotential Acquisition. In *Biopotential Readout Circuits for Portable Acquisition Systems* (pp. 5–19). Springer Netherlands. https://doi.org/10.1007/978-1-4020-9093-6_2

Zhang, J. (2019). *Basic Neural Units of the Brain: Neurons, Synapses and Action Potential*. 1–38.

# ORIGINAL PUBLICATIONS

# I

## DESIGN AND VALIDATION OF A WIRELESS BODY SENSOR NETWORK FOR INTEGRATED EEG AND HD-SEMG ACQUISITIONS

by

G. L. Cerone, A. Giangrande, M. Ghislieri, M. Gazzoni, H. Piitulainen and A. Botter

*IEEE Transactions on Neural Systems and Rehabilitation Engineering*, 30: 61-71, 2022.

https://doi.org/10.1109/TNSRE.2022.3140220

# Design and Validation of a Wireless Body Sensor Network for Integrated EEG and HD-sEMG Acquisitions

G. L. Cerone, *Member, IEEE*, A. Giangrande, M. Ghislieri, *Member, IEEE*, M. Gazzoni, *Member, IEEE*, H. Piitulainen, and A. Botter, *Member, IEEE*

***Abstract*— Sensorimotor integration is the process through which the human brain plans the motor program execution according to external sources. Within this context, corticomuscular and corticokinematic coherence analyses are common methods to investigate the mechanism underlying the central control of muscle activation. This requires the synchronous acquisition of several physiological signals, including EEG and sEMG. Nevertheless, physical constraints of the current, mostly wired, technologies limit their application in dynamic and naturalistic contexts. In fact, although many efforts were made in the development of biomedical instrumentation for EEG and High Density-surface EMG (HD-sEMG) signal acquisition, the need for an integrated wireless system is emerging. We hereby describe the design and validation of a new fully wireless body sensor network for the integrated acquisition of EEG and HD-sEMG signals. This Body Sensor Network is composed of wireless bio-signal acquisition modules, named sensor units, and a set of synchronization modules used as a general-purpose system for time-locked recordings. The system was characterized in terms of accuracy of the synchronization and quality of the collected signals. An in-depth characterization of the entire system and an head-to-head comparison of the wireless EEG sensor unit with a wired benchmark EEG device were performed. The proposed device represents an advancement of the State-of-the-Art technology allowing the integrated acquisition of EEG and HD-sEMG signals for the study of sensorimotor integration.**

***Index Terms*— Biopotential acquisition systems, EEG, evoked potentials, High Density-surface EMG (HD-sEMG), sensorimotor integration, wireless body sensor network.**

Manuscript received June 15, 2021; revised September 8, 2021 and November 29, 2021; accepted December 2, 2021. Date of publication January 4, 2022; date of current version January 28, 2022. This work was supported by the University of Jyväskylä "Brain changes across the life-span" under Grant 311877. The work of H. Piitulainen was supported in part by the Academy of Finland under Grant 296240 and Grant 327288 and in part by the Jane and Aatos Erkko Foundation under Grant 602.274. *(G. L. Cerone and A. Giangrande contributed equally to this work.) (Corresponding author: G. L. Cerone.)*

This work involved human subjects or animals in its research. Approval of all ethical and experimental procedures and protocols was granted by the Ethics Committee of the University of Jyväskylä under Approval No. 369/13.00.04.00/2020, March 27, 2020.

G. L. Cerone, M. Gazzoni, and A. Botter are with the Laboratory for Engineering of the Neuromuscular System (LISiN) and the PoliToBIOMed Laboratory, Department of Electronics and Telecommunications, Politecnico di Torino, 10128 Turin, Italy (e-mail: giacintoluigi.cerone@polito.it).

A. Giangrande is with the Laboratory for Engineering of the Neuromuscular System (LISiN) and the PoliToBIOMed Laboratory, Department of Electronics and Telecommunications, Politecnico di Torino, 10129 Turin, Italy, and also with the Faculty of Sport and Health Sciences, University of Jyväskylä, 40014 Jyväskylä, Finland.

M. Ghislieri is with the Biolab and the PoliToBIOMed Laboratory, Department of Electronics and Telecommunications, Politecnico di Torino, 10129 Turin, Italy.

H. Piitulainen is with the Faculty of Sport and Health Sciences, University of Jyväskylä, 40014 Jyväskylä, Finland.

Digital Object Identifier 10.1109/TNSRE.2022.3140220

## I. Introduction

IN EVERYDAY activities our body interacts with the ever-changing environment in smooth manner thanks to sensory feedback from the external environment (e.g. visual, auditory, tactile, etc.) and internal state of our body (e.g. proprioceptive) to the central nervous system. The brain is responsible for integrating these feedbacks with intentional motor planning to generate efficient motor output to the muscles [1]. The ability of the brain to properly combine external information to assist motor program execution is called sensorimotor integration [2]. The deterioration of this function due to ageing, traumatic events, or pathologies may lead to a wide range of motor impairments affecting the quality of life [3]–[5]. Although the neural control of movement in healthy and pathological individuals has been widely investigated during the last few decades, the way humans control their interactions with the environment remains one of the unsolved neuroscience research questions, because it often requires performing dynamic tasks in naturalistic conditions [6]. Corticomuscular (CMC) and corticokinematic (CKC) coherence analyses are widely used to study the cortical control of movement [1], [7]–[9]. The two methods require the simultaneous recording of brain activity using electroencephalography (EEG) or magnetoencephalography (MEG) simultaneously with muscular activities (EMG) in case of CMC or limb kinematics in case of CKC. Recently, High-Density surface EMG (HD-sEMG) has been used in CMC analysis [9], [10]. By recording EMG activity from multiple detection points over the muscle, HD-sEMG allows to describe the spatiotemporal pattern of the muscle activation and to extract relevant information on central and peripheral properties of the neuromuscular system such as the motor unit behavior (investigated through motor unit decomposition algorithms), [11]–[13].

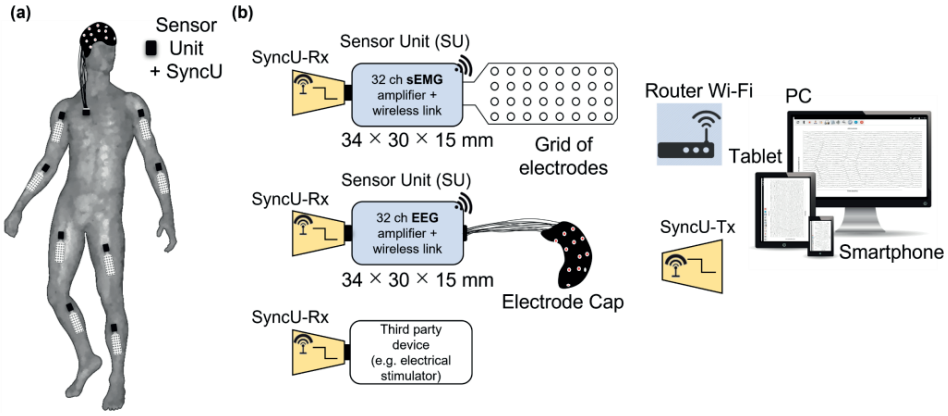


Fig. 1. System architecture. (a) Example of a wireless body sensor network composed of one EEG and 8 HD-sEMG sensor units. (b) From top to bottom: HD-sEMG sensor unit connected to a grid of electrodes, EEG sensor unit connected to an electrode cap, a third-party device (e.g., electrical stimulator, motion capture devices, force sensors). Each module is connected to the receiver module of a Synchronization unit (SyncU-Rx) receiving the wireless synchronization pulse from the transmitter (SyncU -Tx). Each sensor unit transmits the acquired signals to either a mobile device (smartphone or tablet with Wi-Fi connectivity) or a Personal Computer for real-time visualization and storage.

As compared to single-channel surface EMG, HD-sEMG provides a more accurate estimation of neural input issued to the muscle [11], [14], [15], thus improving the detected CMC [16]. Although all these techniques underwent significant advancements in the last 20 years, several bottlenecks limiting their integration and their concurrent application in naturalistic conditions outside the research lab still exist. One of the main issues concerns the physical constraints associated with the wired technology of the devices, which makes the experimental setups bulky, and thus unsuitable for dynamic/naturalistic tasks. Furthermore, wired acquisitions are usually more prone to interference and artifacts. To extend the usability and applicability of the devices towards naturalistic contexts, wireless devices for electrophysiological or biomechanical signal detection have been proposed [17], [18] and are now available on the market. However, these devices typically do not provide the possibility to readily integrate the acquisition of mixed signals (EMG, EEG, biomechanical variables) required to investigate sensorimotor integration. This leads to complex and unpractical setups often limiting the conditions in which data acquisition can be performed. It is not trivial to ensure the appropriate degree of synchronization between devices collecting different types of signals and not natively designed to be integrated with other, third-party devices (e.g., force transducers, inertial sensors, external trigger generators, transcranial magnetic stimulation device etc.). This is because standard wireless technologies based on high-throughput communication protocols (e.g., Bluetooth and Wi-Fi) cannot guarantee a sufficient degree of synchronization, often within one sample (i.e., few hundreds of $\mu$s), between data streamed by different transmitters without compromising the performances in terms of quality and affordability of the transmitted data. The emerging need for system integration requires modular systems natively conceived as part of an integrated wireless architecture but also sufficiently flexible to be synchronized with general-purpose, external devices. To the best of our knowledge, commercially available systems lack of all the requirements described before at the same time: wireless link, modularity, miniaturization, possibility to wirelessly synchronize each module with time delays within one sample, possibility to easily connect and integrate third-party instrumentation.

In this study, building upon the work described in [19], we developed a wireless system for the simultaneous and synchronous acquisition of HD-sEMG and EEG. Moreover, the system can interface with general-purpose instrumentation (third party devices, e.g., for real-time biofeedback or sensory multimodal stimulation providing, e.g., visual or auditory stimuli). Specifically, we hereby: (i) present the overall system architecture and the main design choices related to the HD-sEMG/EEG acquisition module, (ii) describe the design of the synchronization system for time-locked recordings, (iii) validate the performances of the wireless EEG device using a conventional wired EEG system as a benchmark, (iv) show a use-case validation study.

## II. Hardware Design and Prototyping

### A. System Architecture

The proposed system implements a client-server wireless Body Sensor Network (wBSN) (Fig. 1) composed of a set of Sensor Units (SU, clients) for the acquisition of HD-sEMG or EEG signals and one device (server) for signal visualization and storage. A synchronization system allows the synchronization of signals coming from different SUs. The entire set of sensors and the connected synchronization modules constitutes a wireless Body Sensor Network (wBSN).

Each SU has 32 analog and one digital input. The SUs perform the input signals conditioning, sampling and transmission to the receiver (a mobile device or a personal computer) through a Wi-Fi access point acting as a router for real-time visualization and storage.

The synchronization system is composed of a set of modules (SyncU) communicating over a dedicated, low-latency radio channel. One SyncU is configured as transmitter (SyncU-Tx) while the others are configured as receivers (SyncU-Rx) and connected to the SUs that must be synchronized. The

SyncU-Tx transmits a synchronization signal. The signal received by the SyncU-Rx is sampled throughout the SU digital input and transmitted to the wBSN server. The choice of designing an external synchronization module instead of integrating it into the SU module allows to: (i) reduce the size of the SUs when no synchronization is needed (e.g. when a single HD-sEMG or EEG SU is used), (ii) use a single, configurable, SyncU either as receiver and transmitter, (iii) provide the synchronization signal to any device with a digital input available (e.g., footswitches, auditory stimuli used to provide EP response, etc.), thus enabling the possibility to extend the wBSN with external, third-party instrumentation. Furthermore, using an external synchronization device reduces the total cost of the system as the same system can be used for both the SU and third-party devices. However, future developments requiring a higher degree of miniaturization of the whole system could integrate both the sensor and synchronization units into a single device. Apparently similar synchronization systems are commercially available (e.g. SyncSE, OT Bioelettronica, Italy) but they have a time latency above one sample (33.2 ms) that may not be adequate for studying short-latencies responses. Other open-source software synchronization systems [20], [21] are based on timestamp recording, which makes them unsuitable for real time applications as they require offline post processing.

TABLE I
TECHNICAL SPECIFICATIONS OF THE SYSTEM

| Description | Parameter | Value |
|---|---|---|
| Num. of analog channels | $N_A$ | 32 |
| Num. of digital channels | $N_D$ | 1 |
| Bandwidth (EMG mode) | $BW_{EMG}$ | 10 Hz – 500 Hz |
| Bandwidth (EEG mode) | $BW_{EEG}$ | 0.1 Hz – 500 Hz |
| Gain | G | 192 ± 1 V/V |
| Common Mode Rejection Ratio | CMRR | 82 dB |
| Input Impedance module | $\|Z_{In}\|$ | 1.3 GΩ (10 Hz)<br>13 MΩ (1 kHz) |
| Input Range | IR | 10 $mV_{pp}$ |
| RTI Noise | $N_{RTI}$ | $< 3\ \mu V_{RMS}$ |
| A/D Resolution | Res | 16 bit |
| Sampling Frequency | $f_s$ | 2048 sps |
| Communication | ------- | Wi-Fi |
| Receiver Type | ------- | PC, Smartphone or Tablet |
| Max. Sync. delay | $\Delta t_{Sync}$ | ±5 µs |
| Max. time latency | $\Delta t_{Lat}$ | ±400 µs |
| Max. TX distance | $d_{TX}$ | 22 m (<0.02% data loss) |
| Power Supply | ------- | 200 mAh 1-Cell LiPo Battery |
| Life time (transmitting) | $T_{TX}$ | 3h |
| Dimensions | ------- | 3.4 cm × 3 cm × 1.5 cm |
| Weight | ------- | 16.7 g |

### B. Hardware Design and Bench Characterization

*1) Sensor Unit:* The SU design was based on the design of the HD-sEMG SU described in [19]. The SU consists of three main building blocks:

i. The Bio-signals Acquisition Unit implementing the conditioning and quantization of 32 EMG/EEG signals at 2048 sps with 16 bit resolution;
ii. The Control Unit implementing the sampling and wireless transmission of the collected signals through a 2.4 GHz Wi-Fi link;
iii. The Power Management Unit providing a regulated 3.3 V power supply and handling the wireless battery charging.

The SU is powered through a 600 mAh single-Cell LiPo Battery. The detection systems (grid of electrodes for HD-sEMG or EEG caps) connect to the SU analog inputs through a ZIF connector (Molex 54104-3231, Illinois, USA). The RHD2132 chip [22] (Intan Technologies, California, USA) was selected for both the HD-sEMG and EEG analog front-end because of the following main characteristics: (i) compact size (9 mm × 9 mm, QFN package), (ii) low-power, 32 monopolar AC-coupled analog front-ends with fixed gain (192 V/V), (iii) programmable bandwidth (0.1 Hz - 20 kHz) compatible with both EEG and sEMG signals, (iv) availability of non-conditioned auxiliary channels for synchronization, and (v) availability as pre-packaged component for standard pick and place mounting of the PCB.

Table I shows the main features of the HD-sEMG and EEG SUs. With respect to the SU described in [19], the SU herein designed:

i. implements a mixed-signal bipotential acquisition system, sampling and transmitting 32 analog signals and one auxiliary digital signal (used to acquire the synchronization signal received by the SyncU-Rx modules).
ii. allows to dynamically select the bandwidth of the analog front-end during the SU startup to adapt to the acquisition of both EEG (0.1 Hz - 500 Hz) and HD-sEMG (10 Hz – 500 Hz) signals.

*2) Synchronization Unit:* A multi-function wireless synchronization module has been designed and prototyped. We chose to develop a single module for both transmission (SyncU-Tx) and receiver operations (SyncU-Rx) to simplify the design and reduce costs.

The transmitter is powered through a cable by a common USB phone charger containing a 3.3 V step-down DC/DC converter (LM3671MF-3.3, Texas Instruments, USA) and it is equipped with a configuration button that allows selecting the synchronization pulse transmission mode between (i) *automatic*: a programmable pulse train (e.g., 100 ms long pulse with 2 s period) is internally generated and transmitted, (ii) *external*: a synchronization signal generated by an external device (e.g., a push button, a footswitch, a signal generator, or a third-party device that acts as a synchronization/trigger signal source) is acquired and transmitted. The synchronization pulses are transmitted in broadcasting mode to all the SyncU-Rx modules. A 2.5 mm audio jack (50-00407, Tensility Int. Corp. USA) allows, when connected to the SU, to power the module and communicate the received synchronization pulse to the SU. When the SyncU-Rx receives the synchronization pulse, it generates a digital signal that can be acquired by any system connected to it via the 2.5 mm audio

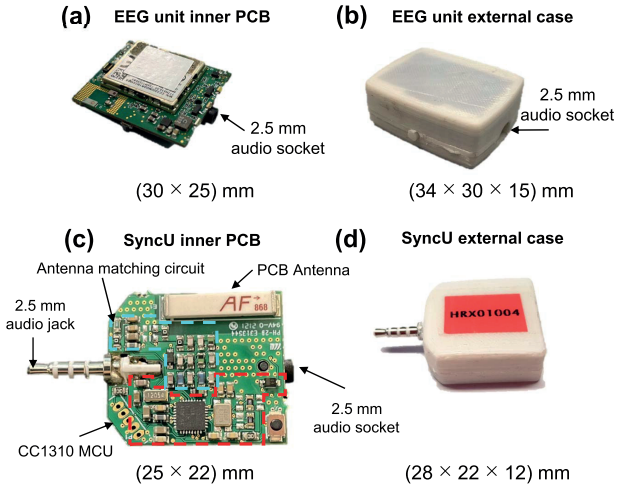


Fig. 2. Acquisition and Synchronization modules. (a) and (c) show the top view of the inner PCB with mounted components respectively for the EEG sensor unit (SU) and the synchronization unit (SyncU) with its main blocks. The PCB dimensions are: (a) 30mm × 25mm and (c) 25mm × 22mm. (b) and (d) show respectively the EEG SU and the SyncU in a 3D printed PLA case leading to a total encumbrance of (b) 34mm × 30mm × 15mm and (d) 28mm × 24mm × 12mm.

jack. A 2.5 mm audio socket (SJ2-25964A-SMT-TR, CUI Device, USA) positioned on the opposite side of the jack connector (Fig. 2a) is used for the connection to the external generator in *external mode*. The SyncU design was kept as simple as possible, minimizing the number, size, and cost of the components. The SyncU consists of two main hardware blocks: i) the wireless MCU, managing the wireless transmission/reception of synchronization pulses, and ii) the antenna matching circuit, used to effectively transmit wireless signals. The CC1310 wireless MCU (Texas Instruments, USA) [23] was selected as transceiver to implement a low-latency radio channel characterized by excellent performance of the receiver in terms of sensitivity (-124 dBm) and selectivity (56 dB) and a transmission carrier frequency of 868 MHz. The CC1310 wireless MCU implements a proprietary wireless protocol based on an IEEE 802.15.4 physical layer (the same as the ZigBee wireless protocol) that allows building a Personal Area Network (PAN) with a low power consumption of about 15 mW during signal reception. The adoption of a wireless protocol different from that used for the SU communication (Wi-Fi) [19] was motivated by the need of guaranteeing the required performance in terms of synchronization delays and latencies between different SyncU modules. Therefore, the system architecture relies on two different communication protocols used for SUs-receiver data exchange (Wi-Fi, characterized in [19]), and SUs synchronization through the SyncU modules (IEEE 802.15.4). The ANT-868-CHP-T (Linx Technologies, USA) 868 MHz ceramic chip antenna was selected and the antenna's impedance matching circuit was designed accordingly to the LAUNCHXL-CC1310 reference design (Texas Instruments, USA).

*3) Prototyping:* Commercially available Off-The-Shelf (COTS) components were used for the design of SyncU PCB. The minimization of the system's encumbrance was one of the primary objectives of the design. The SU PCB (Fig. 2a) consists of an eight-layers, 1 mm thick PCB (dimensions: 3.0 cm × 2.5 cm), and was encapsulated into a 3D-printed (Fig. 2b) case [19]. Fig. 2c shows the SyncU PCB. It consists of a two-layers, 0.8 mm thick PCB (dimensions: 2.5 cm × 2.2 cm) with components mounted on both sides. Fig. 2d shows the SyncU final prototype encapsulated in a 3D-printed plastic case. The total encumbrance of the SyncU module resulted in 2.8 cm × 2.4 cm × 1.2 cm (thickness). Two EMG/EEG SUs and four SyncU modules were built and prototyped.

*4) Bench Characterization:* The bench characterization of the system was mainly focused on the synchronization performances and the test of the EEG SU analog front-end since the HD-sEMG SU was previously characterized in [19]. The reader is redirected to [19] for a complete characterization of the SU module.

*a) EEG SU:* The input-referred noise level of the front-end amplifier was measured by shorting and connecting to the reference pin the analog inputs of the RHD2132 chip and calculating the RMS voltage for each channel over a 30 s long epoch of signal. The mean noise level across channels was $2\,\mu V_{RMS} \pm 0.2\,\mu V_{RMS}$. The band-pass gain of each channel was measured by applying a 40 Hz, 2 $mV_{pp}$ sinewave to the input of the RHD2132 front-end and calculating the ratio between the output and the input peak-to-peak amplitude. The bandwidth of each monopolar front-end was measured by applying a 2 $mV_{pp}$ sinewave to the input of the EEG SU and varying, for each channel, the input frequency to find the $-3$ dB attenuation with respect to the amplifier's nominal gain. The measured in-band gain for each channel was 192 V/V ± 1 V/V (CoV= 0.5%) within a 0.1 Hz - 500 Hz frequency band. The measured inter-channel gain variability was between 0.5% and 1% and results comparable with that observed in [19]. The minimum input voltage range was 10 $mV_{pp}$ ($\pm 5$ $mV_{pp}$) across all the analog acquisition channels. The total harmonic distortion was calculated in the 0.1 Hz - 100 Hz frequency band for three sinusoids of different amplitude (2 $mV_{pp}$, 4 $mV_{pp}$, and 8 $mV_{pp}$) and resulted less than 0.8%, in agreement with the values reported in the RHD2132 datasheet [24]. The total harmonic distortion was lower than 0.36% in mid-band frequencies (20 Hz and 80 Hz). The robustness of the EEG SU to the second-order non linearities of the RHD2132 front-end amplifier (Intan Technologies, USA) was evaluated by computing the first-order IMD products. A linear combination of two similar tones (amplitude 8 $mV_{pp}$, $f_1 = 39$ Hz and $f_2 = 41$ Hz) was applied to the inputs of the EEG SU through an analog mixer circuit. The first order IMD products, located at 37 Hz and 43 Hz, resulted in a 135.5 dB ± 6.0 dB attenuation with respect to the input signals.

*b) SyncU bench characterization:* Four SyncU modules (1 SyncU-Tx and 3 SyncU-Rx) were characterized in terms of power consumption and wireless performance. The SyncU-Tx was powered through a 5 V USB phone charger and the measured power consumption during the trigger signal transmission was 32.5 mW (6.5 mA current consumption). The measured power consumption of the SyncU-Rx module was

21.45 mW (6.5 mA current consumption). The higher power consumption of the SyncU-Tx module is not critical as it is intended to be used connected to a power line source or a USB port and not to a battery-powered device (as opposed to SyncU-Rx that is connected to a SU). The wireless performances of the synchronization unit were characterized by measuring the latency between transmitted and received signals and the time delay between the signal received by different SU modules. The SyncU-Tx module was configured in *automatic mode*. The output of all the SyncUs was acquired through a mixed-signal oscilloscope (MSO-X-2024A, Keysight Technologies, USA). We observed an average time latency of 400 $\mu$s, with a maximum delay between receivers of 5 $\mu$s. Considering that most of the HD-sEMG/EEG signal acquisition systems have a sampling frequency lower than 2 kHz (500 $\mu$s period), our synchronization system enables applications requiring latencies below one sample.

## III. Experimental Validation

### A. Material and Methods

Evaluating new devices and technologies by on-field experimental tests is of paramount importance dealing with the design and development of biomedical instrumentation. Although bench characterization allowed us to deterministically quantify the compliance of our device with the proposed technical specifications, the actual experimental use includes several variables (e.g., patient's capacitive coupling to the power line [25]–[27], electrode-skin impedance unbalance [26], [28] etc.) which are difficult to estimate. Hence, we performed a head-to-head (i.e. on the same subject, day, condition) quantitative comparison with a commercially available EEG system because the EEG signal features and the interference/noise levels affecting bio-signals depend on factors that may change substantially when recordings are performed in different labs/sessions. Four experimental protocols were designed to validate the on-field performances of our system in terms of quality of detected signals, inter-module synchronization, and synchronization with external devices. All tests were performed with our system (Device Under Test - DUT) and with a Benchmark Device (BD). The selected BD was Bittium (NeurOne Tesla, Oulu, Finland) because: (i) it is a commercially available medical device, (ii) it is a good test-bench for our wireless synchronization, due to its wired link which ensures negligible latencies, (iii) it is fully integrated with standard software for sensory stimulations. EEG signals were collected using three different but commonly used sensory stimulation designs in the field of EEG: auditory, visual, and somatosensory stimulations. The aim was to validate the wireless EEG module through the comparison of DUT vs. BD in the shape (timing and amplitude) and in the topographic distribution of the respective evoked cortical EEG responses. The DUT *versus* BD comparison of the cortical responses latencies during sensory stimulations was used to experimentally verify the possibility to synchronize the EEG SU with third-party devices used to provide the stimulation patterns. The fourth experiment represents an active task to quantify the corticospinal coupling between coherent cortical (EEG) and muscular (HD-sEMG) activities: a protocol to compute CMC. EEG, HD-sEMG, and an external signal (force) were collected simultaneously to verify the concurrent and synchronous wireless acquisition of multiple biological signals in this relevant experimental context. The details of the four validation tests are reported in the following sections.

*1) Participants:* A group of ten healthy subjects (6 males, 4 females, age range: 24–40 yrs) was recruited for the experimental validation of the designed system. All the participants were right-handed (mean score range 92.37 on a scale from –100 to 100, according to the Edinburgh handedness inventory [29]). Participants did not report any neurological or motor disorder. The study was approved by the Ethics Committee of the University of Jyväskylä before starting the measurements (approval number: 369/13.00.04.00/2020). The study was conducted in accordance with the Declaration of Helsinki and written informed consent was obtained from all participants after having provided them with a detailed explanation of the study procedure itself.

*2) Validation Protocols:* The four experiments (auditory, visual, and somatosensory stimulations and active isometric contraction for CMC) were carried out in the EEG Laboratory in the Department of Psychology, University of Jyväskylä (Jyväskylä, Finland).

Scalp signals were recorded during all four experiments with a 30 head-mounted electrodes cap (EasyCap GmbH, Gliching, Germany) kept in place between consecutive tasks (for BD-DUT comparison). The Ag/AgCl electrodes embedded into the cap were in accordance with the international 10-20 system. An abrasive paste (NuPrep, Weaver and Company, Aurora, USA) was used to gently scrab each electrode site with a cotton swab after having placed the cap on the scalp. Every cavity was then filled with a conductive gel (NeurGel, SPES MEDICA, Genova, Italy). In addition, EOG was recorded with two electrodes (30 mm $\times$ 22 mm Ambu s.r.l., Denmark) placed in the up-left and down-right corners to detect and further remove eye movements and blinks. EEG signals were referenced to the FCz electrode of the cap for both devices.

A detailed description of the four experimental protocols is reported hereafter.

*a) Auditory stimulation:* Acoustic tones (1 kHz, 60 dB, 100 ms duration including 10-ms rise and fall ramps) were presented alternatively to the right and left ear of the subjects through shielded earphones (ER-3C, 50 Ohm, Etymotic Research). In the meanwhile, participants were asked to gaze at a fixation cross showed on a screen in front of them. Tones were randomly delivered to the left and the right earphone every 2 s with a random jitter of $\pm$ 250 ms [30]. One hundred stimuli per ear were delivered to each participant. (Fig. 3a). The stimulation pattern was programmed using the stimulus delivery software Presentation (Neurobehavioral Systems, Berkeley, CA). This experiment required an EEG SU and two SyncU modules. A SyncU-Tx module was configured to acquire an external signal for each stimulus (driven by the software) and to transmit it to the SyncU-Rx.

*b) Visual stimulation:* Flashes of a black-and-white checkerboard pattern (14.6 deg $\times$ 8.2 deg, check size

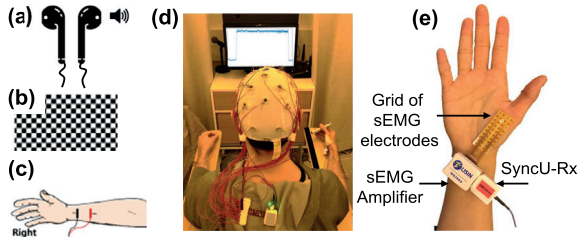


Fig. 3. Experimental protocol and setup. (a) Auditory stimulation; (b) Visual stimulation; (c) Electrical stimulation of the median nerve. (d) Isometric contraction task: visual force feedback during isometric pinch grip of the right hand at 10% of MVC for 4 minutes; (e) Experimental setup during the isometric contraction: high-density surface electromyography grid (8 × 4 electrodes, inter-electrode distance: 5 mm), wireless HD-sEMG amplifier and SyncU-Rx modules.

0.7 deg × 0.7 deg) were presented on a screen placed at 1.5 m in front of the subjects every 2 s with a random jitter of ± 250 ms (100 stimuli, duration 100 ms) [30]. (Fig. 3b). One EEG SU was connected to a SyncU-Rx module. The visual stimulation pattern was provided through a screen controlled by the Presentation software. The same software was used to deliver a synchronization pulse to the SyncU-Tx at the start of each stimulus.

*c) Somatosensory stimulation:* The right median nerve was electrically stimulated using two surface electrodes (30 mm × 22 mm, Ambu s.r.l., Denmark) placed 2 cm proximal to the wrist according to the course of the nerve, 1 cm apart. A neuromuscular electrical stimulator (DS7AH, Digitimer Ltd, UK) was used to deliver 0.2 ms long constant current monophasic pulses. The pulse intensity was adjusted according to the participants' motor threshold, defined as the lowest current level inducing a visible mechanical response of the thumb (I = 8.5 mA ± 2.1 mA, mean ± SD across participants). One hundred stimuli were delivered every 2 s with a random jitter of ± 250 ms [30] (Fig. 3c). The wBSN included an EEG SU and a SyncU-Rx. The electrical stimulator was used as a third-party device and connected to a SyncU-Tx.

*d) Isometric contraction for CMC:* This experiment was included to demonstrate the feasibility and straightforward configuration of a hybrid EEG/HD-sEMG recordings synchronous wBSN through the proposed system. Participants were seated with their right hand on the armrest of the chair, maintaining a steady isometric pinch contraction by the thumb and index fingers (flexion) on a force transducer (FS 6 N - model 1004; Vishay Precision Group, Malvern, PA). Before EEG recordings, subjects performed a maximum voluntary contraction (MVC) test lasting 3–4 s. A rigid load cell (FS 30 N - model 1042, Vishay Precision Group, Malvern, PA) was used to measure the MVC during the same pinch task. Participants were then asked to maintain a constant force level at 10% ± 2% of their MVC for 4 minutes. A visual, real-time force feedback (Fig. 3d) was provided on the screen in front of them. Force signals were sampled at 1 kHz and stored using a data acquisition unit (Micro1401-4, Cambridge, England, UK). The wBSN used during the motor task included one EEG SU, one HD-sEMG SU, and two SyncU-Rx modules connected to each SU. The data acquisition unit was used as a third-party device to synchronously record EEG, HD-sEMG, and force signals. EMG activity from the right flexor pollicis brevis muscle was collected using a grid of 32 Ag/AgCl electrodes (4 rows by 8 columns, inter-electrode distance (IED) of 10 mm - LISiN, Politecnico di Torino, Torino, Italy). The skin was gently scrubbed with an abrasive paste (Nuprep, Weaver and Company, Aurora, USA) and the grid was attached to the skin with the columns aligned according to the fibers orientation of the right thenar muscles [9]. Monopolar HD-sEMG signals were detected, conditioned (Bandwidth 10 Hz – 500 Hz, Gain 46 dB), and sampled at 2048 Hz with 16-bit resolution through the HD-sEMG SU [19].

*3) Data Analysis:* Time and frequency domain variables were analyzed to compare the quality of EEG signals detected by our system and by the BD and to assess the feasibility of an integrated detection of EEG/HD-sEMG measurements using our system. Specifically, the amount of Power Line Interference (PLI) during experimental conditions and the distribution of power across different EEG frequency bands were evaluated. Event-Related Potentials (ERP) and CMC provided information about the spatiotemporal alignment of the synchronized EEG/HD-sEMG recordings. All the analyses were performed offline using the Matlab Software (Mathwork Inc, Natick, MA, USA).

*a) Power spectral density:* The Power Spectral Density (PSD) of EEG signals acquired during the isometric contraction (0.5 Hz – 60 Hz) was computed using a non-overlapped flattop window over a 30-s window. Relative EEG power of the signals recorded with the BD and the DUT was separately computed for different frequency bands (Delta 0.5 Hz – 4 Hz, Theta 4 Hz – 8 Hz, Alpha 8 Hz – 14 Hz, Beta-1 14 Hz – 21 Hz, Beta-2 21 Hz – 30 Hz, Gamma 30 Hz – 45 Hz) normalized with the total absolute EEG power (0.5 Hz – 45 Hz). The median band power of all the 30 EEG channels was extracted for each participant, separately for each frequency band. The comparison between the DUT and BD was then performed evaluating the mean and standard deviation of the band power in each frequency band across participants.

*b) Power line interference and signal to interference ratio:* The power line contribution to the detected EEG signals was estimated computing the RMS value of the 50 Hz component and the Signal-to-Interference Ratio (SIR) of the collected signals. Estimations were performed on a 3-min long epoch of filtered EEG signals ($4^{th}$ order Butterworth, bandpass filter 0.5 Hz – 60 Hz) collected during the isometric contraction task. The RMS value of the 50-Hz contribution to the detected signals was computed by filtering, for each channel, the raw EEG signals with a 48 Hz – 52 Hz bandpass filter ($4^{th}$ order Butterworth filter). The median RMS value across all EEG channels (n = 30) was extracted for each participant. The mean and standard deviation across all participants (n = 10) was then used as a measure of comparison between the BD and the DUT. For each subject, the SIR was calculated according to (1). The EEG variance ($\sigma_{sig}$) was used to estimate the power of the collected signals without interference (Notch filter at 50 Hz, $4^{th}$ order Butterworth band-stop filter) across

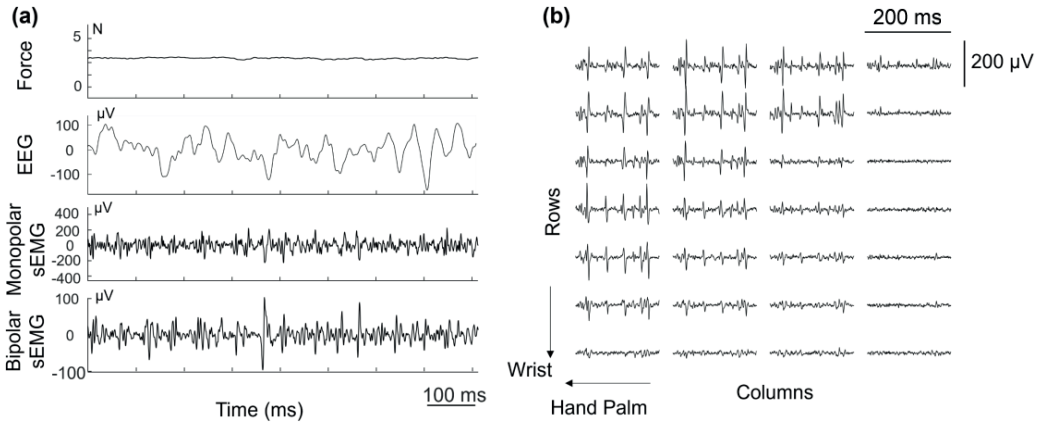


Fig. 4. (a) Examples of measured signals during the isometric contraction task of a single subject (800-ms epoch). From top to bottom: 10-Hz low-pass filtered force signal (10% of maximum voluntary contraction), wireless EEG signal (channel C3), one monopolar and one bipolar EMG signal (passband 20 Hz – 400 Hz). The selected EMG and EEG signals are those showing the highest peak of corticomuscular coherence. (b) Single differential HD-sEMG signals of a representative participant during a 200 ms epoch of the isometric contraction task. Firings of individual motor units are clearly visible.

channels. The EEG spectral components in the 48 Hz – 52 Hz band were considered negligible with respect to the total signal power. Mean and standard deviations were calculated from the variability across participants to compare the performances of standard and wireless EEG recording systems.

$$SIR = 20log\frac{\sigma_{sig}}{RMS_{int}} \quad (1)$$

*c) EEG preprocessing:* EEG noisy channels, due e.g. to a bad electrode-skin contact, etc., were identified by visual inspection and replaced with the average of all their neighboring channels by using FieldTrip Matlab toolbox for both the BD and the DUT. [31]. On average, 2 channels out of 30 were replaced among all the participants. The EEG signals were spatially filtered using the average reference of all EEG channels for further analyses. Independent Component Analysis using FieldTrip Matlab toolbox was used to separate the EEG components and reject the ones related to the eye blink artifacts chosen as those matching the EOG pattern (i.e., showing the highest correlation with the EOG) recorded time-locked with the EEG [32].

*d) EEG event-related potential (ERP) computation:* For each stimulation type (i.e., auditory, visual, and somatosensory), the EEG signals were averaged with respect to the stimulus onsets for 700-ms epoch (from –100 to 600 ms) to obtain the ERPs for each EEG channel separately. Three regions of interest (ROI) were identified from the 30 EEG channels depending on the stimulus type. The ROI included (contralateral to the stimulated right hand) motor cortex (C3, T7, FC5, CP5) for the auditory, visual, and somatosensory stimulations, respectively. The EEG responses of the ROI were then averaged for each participant and stimulation type separately. Finally, the ERPs were grand averaged across all participants. Peak latencies and amplitudes were extracted by considering the common ERP components specific for each sensory domain (i.e., auditory N100-P100, visual N100-P200, somatosensory N20-P30) [30], [33], [34]. EEG electrodes located in the auditory cortex (left: T7, TP9; right: T8, TP10), the visual cortex (O1, O2, Iz), the left (contralateral to the stimulated right hand) motor cortex (C3, T7, FC5, CP5) for the auditory, visual, and somatosensory stimulations, respectively. The EEG responses of the ROI were then averaged for each participant and stimulation type separately. Finally, the ERPs were grand averaged across all participants. Peak latencies and amplitudes were extracted by considering the common ERP components specific for each sensory domain (i.e., auditory N100-P100, visual N100-P200, somatosensory N20-P30) [30], [33], [34].

*e) Corticomuscular coherence (CMC) computation:* HD-sEMG signals were offline bandpass filtered (20 Hz – 400 Hz) [35]. Single Differential signals were first derived from the monopolar ones along the four columns of the EMG electrode grid. The location of the innervation zone (IZ) was identified, by visual inspection, as the single differential channel showing the lowest amplitude and inversion of the signal polarity with respect to its proximal either distal neighbors [36]. Then, the monopolar signals located over the IZ (i.e. showing the highest monopolar signal amplitude) were used to compute the CMC [9]. Fig. 4a and Fig. 4b show examples of the measured signals of a presentative participant performing the isometric contraction task. HD-sEMG and EEG signals were divided into 512 ms long epochs with 400 ms epoch overlap. The corresponding spectral resolution was 2 Hz. This spectral resolution has been used by many experiments as a good compromise between time and frequency resolution [8], [37], [38], ensuring sufficient number of epochs in the CMC analysis and capturing the coherent physiological event (bandwidth of ∼10–15 Hz). EEG epochs exceeding 200 mV were rejected to avoid contamination of the EEG data by eye movements, muscle activity, and other artifacts. Power spectra were calculated between EEG and unrectified, RMS-normalized sEMG signals [39]. The coherence spectra between EEG signals (30 channels) and the sEMG pair previously identified were computed according to Halliday *et al.*, 1995 [40]. The chosen coupling measure was the magnitude of the squared coherence

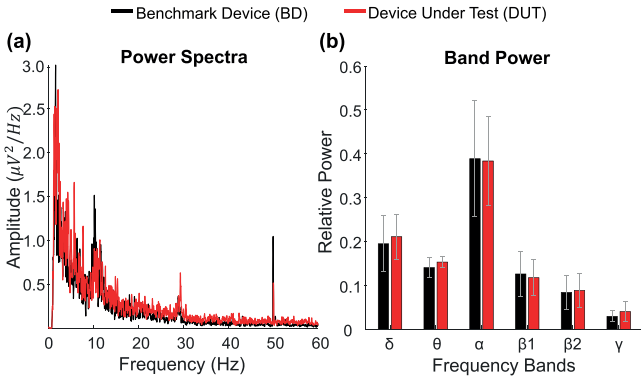


Fig. 5. (a) Power spectral densities of a channel (C3) of signals recorded with the benchmark device (BD - black color) and the device under test (DUT - red color) of a subject performing the isometric contraction task. (b) Mean values of relative band power at each band for the benchmark device (BD - black color) and the device under test (DUT - red color) normalized with respect to the total absolute power in the frequency band 0.5 Hz – 45 Hz. Error bars indicate the variability (standard deviation) across channels subjects (n = 10) during the isometric contraction. (Wilcoxon signed rank test showed no significant differences between the two systems for all frequency bands).

as previously done in similar studies [9], [41], [42]. CMC strength was defined as the maximum coherence value in the 10 Hz – 30 Hz frequency band across the midline and contralateral channels to the side involved in the task (i.e. Nc = 20). Furthermore, scalp topographies were obtained by means of the computation of the root mean square value over the frequency bands of interest (alpha 8 Hz – 14 Hz, beta 13 Hz – 30 Hz, gamma 30 Hz – 45 Hz). The CMC RMS values were interpolated to a standardized 30-channels electrode layout to visualize the topographic distributions of CMC across the scalp EEG electrodes.

*4) Statistical Analysis:* A Wilcoxon signed rank test was used to examine differences between the EEG recording systems (BD and DUT) on the following features: EEG power at specific frequency bands, SIR, primary ERP components amplitude and latency. The choice of carrying out non-parametric statistical tests was determined by the limited number of participants and the non-normal distribution of the considered variables (Shapiro-Wilk statistical test). Spearman correlation coefficients were computed across the participants to judge the agreement in the quantified ERP features between the EEG recording systems (BD and DUT). The statistical significance of individual CMC (peak value across the EEG signals of interest) was assessed under the hypothesis of linear independence of Fourier coefficients from epoch to epoch at each frequency of interest, taking into account the use of overlapping epochs [40], [43]. The $\alpha$-level was set to 0.05/Nc, where Nc = 20 (number of midline and contralateral channels to the side involved in the task) was chosen to correct for multiple comparisons among subjects.

## B. Results and Discussion

*1) Power Spectral Density:* Fig. 5a shows the PSD of the C3 electrode of EEG signals collected through the BD and DUT. The EEG signal power is mainly concentrated at physiological frequency ranges, predominantly in the 0.5 Hz – 30 Hz band. Fig. 5b shows that both devices detect an expected prominent alpha rhythm that is the most dominant rhythmic activity in the human brain [17] even during active isometric task and in the primary motor cortex. No statistically significant differences were observed in the relative mean EEG power between the EEG systems in any of the bands ($p > 0.54$ across the bands).

*2) EEG Signal Interference:* The RMS of powerline interference at 48 Hz – 52 Hz band did not differ significantly between the BD and the DUT (1.70 $\mu$V $\pm$ 0.31 $\mu$V vs. 1.47 $\mu$V $\pm$ 0.46 $\mu$V (mean $\pm$ SD across participants, $p = 0.28$ Wilcoxon rank-sum statistical test). These RMS values are comparable to the noise floor of the device, demonstrating the good performance of the EEG SU in terms of rejection of power line interference. Similarly, no significant effect of the recording system was found on the SIR of the BD and the DUT (25.40 dB $\pm$ 3.26 dB vs. 29.76 dB $\pm$ 6.22 dB, (mean $\pm$ SD across participants, $p = 0.15$, Wilcoxon signed-rank statistical test). Therefore, we conclude that the 50-Hz component of the power line interface affected similarly the quality of both the EEG recordings in the experimental conditions considered. This evidence is particularly important given the high relevance of PLI-related problems in biopotential recordings [25], [44], [45]. Although several hardware and signal processing techniques aimed to remove power line interference were proposed in the last twenty years [46]–[48], it is required to design biopotential amplifiers with high PLI rejection to avoid saturation at the input/output of the amplifier and improve the overall SNR of the collected signals [15], [49].

*3) ERP to Sensory Stimulations:* Fig. 6a shows the grand average of auditory, visual and somatosensory ERPs recorded with the two devices. ERPs components were similar for both EEG systems in each stimulation modality (Spearman correlation coefficients: auditory r = 0.89 $\pm$ 0.03, visual r = 0.96 $\pm$ 0.01 and somatosensory r = 0.85 $\pm$ 0.09; mean $\pm$ SD across participants). Table II reports a summary of ERP latencies and amplitudes. No significant changes were observed between the two recording systems for both ERP variables ($p > 0.38$ for ERP latencies and $p > 0.08$ for ERP amplitudes across the sensory stimulations). Results suggest that the two recording systems provide the same amount of spatiotemporal information under the same type of stimulation, consistently with previous ERP studies [30], [33], [34]. A high intra- and inter-individual reproducibility of the evoked responses was observed for auditory and visual stimulations. Somatosensory ERPs showed higher intra- and inter-subject variability, but it was not atypical. Despite the observed variability, we were able to detect reproducibly the typical short-latency components (i.e., N20 and P30, see Table II). Moreover, the degree of intra- and inter-subject variability shown by the standard deviation of the grand average ERPs of Fig. 6a was similar between the two EEG systems, indicating that there was no relevant effect of the used device. The source of this variability could be associated with different factors. In fact, the somatosensory responses are typically more variable across individuals due to a higher degree of anatomical and functional variations in the sensorimotor cortices compared to the visual and auditory ones. Another factor is that the electrical stimulation is more difficult to perform and standardize across the participants

TABLE II
PEAK LATENCIES AND AMPLITUDES (MEAN ± SD) OF SENSORY STIMULATIONS ERPS

| Stimulation Type | ERP Component | Peak Latencies (ms) | | | Peak Amplitudes (μV) | | |
|---|---|---|---|---|---|---|---|
| | | BD | DUT | p(*) | BD | DUT | p(*) |
| Auditory | P100 | 90.70 ± 6.82 | 86.13± 10.73 | 0.38 | 7.86 ± 2.99 | 7.22 ± 3.17 | 0.62 |
| | N170 | 179.75 ± 38.01 | 173.92 ± 29.55 | 0.91 | 5.98 ± 2.88 | 6.57 ± 3.29 | 0.68 |
| Visual | N100 | 113.20 ± 16.52 | 116.43 ± 10.21 | 0.62 | 15.79 ± 7.14 | 14.20 ± 7.51 | 0.62 |
| | P200 | 192.55 ± 15.61 | 191.85 ± 17.99 | 0.85 | 15.97 ± 6.87 | 14.50 ± 7.03 | 0.52 |
| Somatosensory | N20 | 12.85 ± 10.59 | 16.06 ± 9.74 | 0.42 | 0.97 ± 0.72 | 0.98 ± 0.85 | 0.16 |
| | P30 | 36.55 ± 13.92 | 38.33 ± 14.63 | 0.71 | 4.37 ± 1.95 | 3.06 ± 1.40 | 0.08 |

(*) Wilcoxon signed rank test.

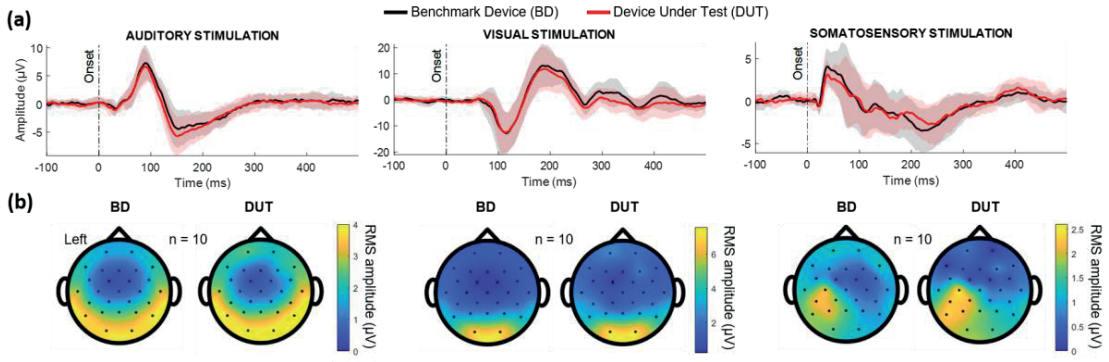


Fig. 6. Grand averages (a) ERPs and (b) scalp topographies across all subjects (n = 10) during conventional stimulations – from left to right: auditory, visual and somatosensory stimulation. (a) ERPs were recorded through the benchmark device (BD - black traces) and the device under test (DUT - red traces). Only a subgroup of channels was averaged for each subject over 600-ms epochs, according to the scalp region involved in the response to the stimulations. The shaded intervals indicate the standard deviations over all the subjects. From top to bottom: auditory, visual and somatosensory responses. (b) Topographies of the averaged visual responses (n = 100 stimuli) recorded with both devices (BD and DUT) (rms values of EEG signals on a 250 ms-window after the stimulus).

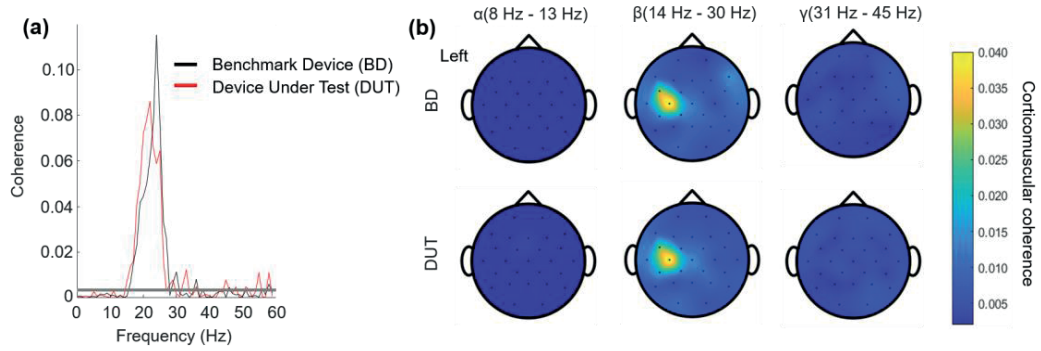


Fig. 7. CMC results from a representative participant. (a) Coherence spectra between sEMG and EEG (most coherent EEG channel: C3). Gray horizontal line indicates the threshold for statistical significance ($p < 0.05$). Black traces (BD) and red traces (DUT) are superimposed. (b) EEG/EMG coherence scalp topographies at alpha, beta and gamma bands (from left to right). On the upper panel topographies obtained from the benchmark device recordings, on the lower panel topographies obtained from the device under test recordings.

(e.g., in terms of definition of the stimulus intensity and/or electrode placement on the wrist).

*4) Corticomuscular Coherence (CMC):* All participants completed the flexion of the thumb at the requested force level (3.91 N ± 1.95 N) without reporting discomfort or perceptible fatigue. Three out of 10 participants showed significant CMC in the beta rhythm with both devices. This result was not atypical. In fact, even under magnetoencephalographic studies (usually the preferred technology dealing with coherence analysis) weak CMC strength, sometimes lower than the significance level, is often reported [50]. Due to the limited number of participants showing significant coherence, no statistical tests were carried out on peak CMC strength or its corresponding frequency in the current study. The most

coherent EEG electrode sites across participants were: F3, F7, C3, FC5, FC1, and CP5. Coherence spectra yielded from the BD and DUT systems were highly concordant in terms of peak CMC strength and frequency, and width of the significant CMC. In fact, overall CMC strength was quantitatively similar between the two measurements. The significant coherence peaks occurred in the expected beta band at a mean frequency of 25.0 Hz $\pm$ 1.2 Hz for wired (BD) and 23.4 Hz $\pm$ 0.8 Hz for wireless (DUT) EEG systems across the aforementioned EEG electrodes, whereas the CMC strength was of 0.031 $\pm$ 0.019 for the BD and 0.030 $\pm$ 0.012 for the DUT, in agreement with previous studies [9], [16]. Fig. 7a shows the DUT- and BD-based CMC spectra for a single subject performing the isometric contraction. The spectra appeared very similar in terms of amplitude and spectral width. Both spectra peaked around 23 Hz, (within the beta frequency band) with comparable strengths even though the exact peak frequency differed by 2 Hz. In fact, minor inter-session variations (e.g. steadiness of the isometric contraction or alertness) within the non-simultaneous recordings may impact on the CMC spectra but appeared to fall within a normal physiological variation in the current data. Fig. 7b shows EEG scalp topographies for the CMC peaking above the primary sensorimotor cortex contralateral to the contracting hand. As expected, the CMC was focused on EEG channels over the contralateral sensorimotor cortex, peaking at C3 electrode in both EEG systems.

## IV. Conclusion

The aim of this work was to design and develop a wireless Body Sensor Network allowing the synchronous acquisition of cortical (EEG) and muscular (HD-sEMG) activity for the assessment of the sensory evoked cortical responses and corticospinal coupling. The proposed system architecture is characterized by a set of Sensor Units and Synchronization Unit modules allowing to collect HD-sEMG and EEG signals in an integrated way. The developed synchronization unit allows also to integrate into the sensor network third-party devices used to provide stimuli (e.g., auditory, visual, tactile, transcranial magnetic stimulation, etc.), signals or to synchronously acquire other relevant variables (e.g., force, kinematics, etc.). The bench and experimental characterization of the system confirmed the agreement with the technical project specifications and the experimental performances observed through a wired benchmark device. Indeed, no device-specific differences were found in signal properties in terms of technical and experimental performances during conventional experimental conditions. The described experimental setups were fully wireless and did not imply any additional cabling to the subject, allowing to implement a completely wireless Body Sensor Network. Three main advantages of our system architecture with respect to the State of the Art technology for EEG and sEMG acquisition [51], [52] (MuoviPro, OT Bioelettronica, Italy) (SAGA, TMSi, The Netherlands) can be identified: (i) Modular architecture: Sensor Units do not require the use of a custom-made receiver to transfer data to the PC. Indeed, each SUs directly and independently transfer data to the receiver. Also the SyncU modules are completely independent from the receiver as they act only as a transmitter/receiver of synchronization pulses. (ii) Portability to different platforms such as PC, Smartphone, Tablet, Single Board Computers (e.g. Raspberry PI). Most of the previously cited systems transfer data exclusively to a PC through an ad-hoc receiver wired-connected to it, thus limiting the use of such devices to laboratory environments and standard protocols (e.g. walking on treadmill). On the contrary, the possibility to use a portable receiver allows the biopotential acquisition also during naturalistic tasks (e.g. free walking etc.). (iii) Synchronization: the proposed synchronization system ensures synchronization delays lower than the sampling period. Furthermore, our synchronization modules allow to synchronize the SUs with external, third-party devices (e.g. used for the study of evoked potentials) still maintaining a fully wireless system architecture. Other devices do have the possibility to interface with third party devices, but only through a cabled connection between the ad-hoc receiver and the device to be synchronized. Given the particular system architecture and the good quality of the collected signals, the proposed device represents an advancement of the State-of-the-Art technology regarding the simultaneous acquisition of EEG and HD-sEMG. Furthermore, the developed wBSN, thanks to its modularity and reduced size, represents an enabling technology to extend the investigation of the sensorimotor integration and of corticospinal coupling in addition to static conditions during more dynamic and naturalistic tasks and environments.

## Acknowledgment

The authors would like to thank Phoenix PCB S.r.l. (Ivrea, Italy) for the support in PCBs production and mounting.

## References

[1] E. Lattari *et al.*, "Corticomuscular coherence behavior in fine motor control of force: A critical review," *Rev. Neurol.*, vol. 51, no. 10, pp. 610–623, 2010.
[2] G. Abbruzzese and A. Berardelli, "Sensorimotor integration in movement disorders," *Movement Disorders*, vol. 18, no. 3, pp. 231–240, Mar. 2003.
[3] H. Piitulainen, S. Seipäjärvi, J. Avela, T. Parviainen, and S. Walker, "Cortical proprioceptive processing is altered by aging," *Frontiers Aging Neurosci.*, vol. 10, pp. 1–13, Jun. 2018.
[4] E. Seiss, P. Praamstra, C. Hesse, and H. Rickards, "Proprioceptive sensory function in Parkinson's disease and Huntington's disease: Evidence from proprioception-related EEG potentials," *Exp. Brain Res.*, vol. 148, no. 3, pp. 308–319, Feb. 2003.
[5] C. Pizzolato *et al.*, "Non-invasive approaches to functional recovery after spinal cord injury: Therapeutic targets and multimodal device interventions," *Exp. Neurol.*, vol. 339, May 2021, Art. no. 113612.
[6] A. Herwig, W. Prinz, and F. Waszak, "Two modes of sensorimotor integration in intention-based and stimulus-based actions," *Quart. J. Exp. Psychol.*, vol. 60, no. 11, pp. 1540–1554, Oct. 2007.
[7] M. De Tommaso, E. Vecchio, K. Ricci, A. Montemurno, D. De Venuto, and V. F. Annese, "Combined EEG/EMG evaluation during a novel dual task paradigm for gait analysis," in *Proc. 6th IEEE Int. Work. Adv. Sensors Interface (IWASI)*, Jun. 2015, pp. 181–186.
[8] R. Bortel and P. Sovka, "EEG–EMG coherence enhancement," *Signal Process.*, vol. 86, no. 7, pp. 1737–1751, 2006.
[9] H. Piitulainen, A. Botter, M. Bourguignon, V. Jousmäki, and R. Hari, "Spatial variability in cortex-muscle coherence investigated with magnetoencephalography and high-density surface electromyography," *J. Neurophysiol.*, vol. 114, no. 5, pp. 2843–2853, 2015.
[10] J. Ibáñez, A. Del Vecchio, J. C. Rothwell, S. N. Baker, and D. Farina, "Only the fastest corticospinal fibers contribute to $\beta$ corticomuscular coherence," *J. Neurosci.*, vol. 41, pp. 1–42, Jun. 2021.

[11] D. Farina, A. Holobar, R. Merletti, and R. M. Enoka, "Decoding the neural drive to muscles from the surface electromyogram," *Clin. Neurophysiol.*, vol. 121, no. 10, pp. 1616–1623, Oct. 2010.

[12] R. Merletti, A. Holobar, and D. Farina, "Analysis of motor units with high-density surface electromyography," *J. Electromyogr. Kinesiol.*, vol. 18, pp. 879–890, Dec. 2008.

[13] D. F. Stegeman, B. U. Kleine, B. G. Lapatki, and J. P. Van Dijk, "High-density surface EMG: Techniques and applications at a motor unit level," *Biocybern. Biomed. Eng.*, vol. 32, no. 3, pp. 3–27, 2012.

[14] R. Merletti, M. Aventaggiato, A. Botter, A. Holobar, H. Marateb, and T. M. M. Vieira, "Advances in surface EMG: Recent progress in detection and processing techniques," *Crit. Rev. Biomed. Eng.*, vol. 38, no. 4, pp. 305–345, 2010.

[15] R. Merletti and G. L. Cerone, "Tutorial. Surface EMG detection, conditioning and pre-processing: Best practices," *J. Electromyogr. Kinesiol.*, vol. 54, Oct. 2020, Art. no. 102440.

[16] C. van de Steeg, A. Daffertshofer, D. F. Stegeman, and T. W. Boonstra, "High-density surface electromyography improves the identification of oscillatory synaptic inputs to motoneurons," *J. Appl. Physiol.*, vol. 116, no. 10, pp. 1263–1271, 2014.

[17] S. Debener, F. Minow, R. Emkes, K. Gandras, and M. De Vos, "How about taking a low-cost, small, and wireless EEG for a walk?" *Psychophysiology*, vol. 49, no. 11, pp. 1617–1621, 2012.

[18] Y. Xie *et al.*, "Novel wearable sensors for biomechanical movement monitoring based on electromagnetic sensing techniques," *IEEE Sensors J.*, vol. 20, no. 2, pp. 1019–1027, Jan. 2020.

[19] G. L. Cerone, A. Botter, and M. Gazzoni, "A modular, smart, and wearable system for high density sEMG detection," *IEEE Trans. Biomed. Eng.*, vol. 66, no. 12, pp. 3371–3380, Dec. 2019.

[20] A. Delorme *et al.*, "EEGLAB, SIFT, NFT, BCILAB, and ERICA: New tools for advanced EEG processing," *Comput. Intell. Neurosci.*, vol. 2011, pp. 1–12, Oct. 2011.

[21] A. Ojeda, N. Bigdely-Shamlo, and S. Makeig, "MoBILAB: An open source toolbox for analysis and visualization of mobile brain/body imaging data," *Frontiers Hum. Neurosci.*, vol. 8, p. 121, Mar. 2014.

[22] R. R. Harrison and C. Charles, "A low-power low-noise CMOS amplifier for neural recording applications," *IEEE J. Solid-State Circuits*, vol. 38, no. 6, pp. 958–965, Jun. 2003.

[23] *CC1310 SimpleLink TM Ultra-Low-Power Sub-1 GHz Wireless MCU*, Texas Instrum., Dallas, TX, USA, 2018, vol. 68.

[24] *RHD2000 Series Digital Electrophysiology Interface Chips-Datasheet*, Intan Technol. LLC, Los Angeles, CA, USA, 2013, pp. 1–38.

[25] A. C. Metting van Rijn, A. Peper, and C. A. Grimbergen, "High-quality recording of bioelectric events—Part 1 interference reduction, theory and practice," *Med. Biol. Eng. Comput.*, vol. 28, no. 5, pp. 389–397, Sep. 1990.

[26] E. M. Spinelli, M. A. Mayosky, and R. Pallas-Areny, "A practical approach to electrode-skin impedance unbalance measurement," *IEEE Trans. Biomed. Eng.*, vol. 53, no. 7, pp. 1451–1453, Jul. 2006.

[27] M. Haberman, A. Cassino, and E. Spinelli, "Estimation of stray coupling capacitances in biopotential measurements," *Med. Biol. Eng. Comput.*, vol. 49, no. 9, pp. 1067–1071, Sep. 2011.

[28] G. Piervirgili, F. Petracca, and R. Merletti, "A new method to assess skin treatments for lowering the impedance and noise of individual gelled Ag–AgCl electrodes," *Physiol. Meas.*, vol. 35, no. 10, pp. 2101–2118, Oct. 2014.

[29] R. C. Oldfield, "The assessment and analysis of handedness: The Edinburgh inventory," *Neuropsychologia*, vol. 9, no. 1, pp. 97–113, Mar. 1971.

[30] R. Hari and A. Puce, *MEG-EEG Primer*. Oxford, U.K.: Oxford Univ. Press, 2017.

[31] R. Oostenveld, P. Fries, E. Maris, and J.-M. Schoffelen, "FieldTrip: Open source software for advanced analysis of MEG, EEG, and invasive electrophysiological data," *Comput. Intell. Neurosci.*, vol. 2011, pp. 1–9, Oct. 2011.

[32] A. Gramfort, "MEG and EEG data analysis with MNE-Python," *Frontiers Neurosci.*, vol. 7, pp. 1–13, Dec. 2013.

[33] T. Allison, G. McCarthy, C. C. Wood, P. D. Williamson, and D. D. Spencer, "Human cortical potentials evoked by stimulation of the median nerve. II. Cytoarchitectonic areas generating long-latency activity," *J. Neurophysiol.*, vol. 62, no. 3, pp. 711–722, Sep. 1989.

[34] B. A. Brett-Green, L. J. Miller, W. J. Gavin, and P. L. Davies, "Multisensory integration in children: A preliminary ERP study," *Brain Res.*, vol. 1242, pp. 283–290, Nov. 2008.

[35] T. M. Vieira, R. Merletti, and L. Mesin, "Automatic segmentation of surface EMG images: Improving the estimation of neuromuscular activity," *J. Biomech.*, vol. 43, no. 11, pp. 2149–2158, Aug. 2010.

[36] H. Piitulainen, T. Rantalainen, V. Linnamo, P. Komi, and J. Avela, "Innervation zone shift at different levels of isometric contraction in the biceps brachii muscle," *J. Electromyogr. Kinesiol.*, vol. 19, no. 4, pp. 667–675, 2009.

[37] J. T. Gwin and D. P. Ferris, "Beta- and gamma-range human lower limb corticomuscular coherence," *Frontiers Hum. Neurosci.*, vol. 6, p. 258, Sep. 2012.

[38] V. M. McClelland, Z. Cvetkovic, and K. R. Mills, "Modulation of corticomuscular coherence by peripheral stimuli," *Exp. Brain Res.*, vol. 219, no. 2, pp. 275–292, Jun. 2012.

[39] F. Negro, K. Keenan, and D. Farina, "Power spectrum of the rectified EMG: When and why is rectification beneficial for identifying neural connectivity?" *J. Neural Eng.*, vol. 12, no. 3, Jun. 2015, Art. no. 036008.

[40] D. M. Halliday, J. R. Rosenberg, A. M. Amjad, P. Breeze, B. A. Conways, and S. F. Farmer, "A framework for the analysis of mixed time series/point process data—Theory ad application to the study of physiological tremor, single motor unit discharges and electromyograms," *Prog. Biophys. Mol. Biology.* vol. 64, pp. 237–278, Oct. 1995.

[41] M. Illman, K. Laaksonen, M. Liljeström, V. Jousmäki, H. Piitulainen, and N. Forss, "Comparing MEG and EEG in detecting the ~20-Hz rhythm modulation to tactile and proprioceptive stimulation," *NeuroImage*, vol. 215, Jul. 2020, Art. no. 116804.

[42] H. Piitulainen, M. Bourguignon, X. De Tiège, R. Hari, and V. Jousmäki, "Coherence between magnetoencephalography and hand-action-related acceleration, force, pressure, and electromyogram," *NeuroImage*, vol. 72, pp. 83–90, May 2013.

[43] M. Bourguignon *et al.*, "Functional motor-cortex mapping using corticokinematic coherence," *NeuroImage*, vol. 55, no. 4, pp. 1475–1479, Apr. 2011.

[44] R. Merletti, M. Aventaggiato, A. Botter, A. Holobar, H. Marateb, and T. M. M. Vieira, "Advances in surface EMG: Recent progress in detection and processing techniques," *Crit. Rev. Biomed. Eng.*, vol. 38, no. 4, pp. 45–305, 2010.

[45] B. B. Winter and J. G. Webster, "Driven-right-leg circuit design," *IEEE Trans. Biomed. Eng.*, vol. BME-30, no. 1, pp. 62–66, Jan. 1983.

[46] M. R. Keshtkaran and Z. Yang, "A fast, robust algorithm for power line interference cancellation in neural recording," *J. Neural Eng.*, vol. 11, no. 2, pp. 1–14, 2014.

[47] D. T. Mewett, K. J. Reynolds, and H. Nazeran, "Reducing power line interference in digitised electromyogram recordings by spectrum interpolation," *Med. Biol. Eng. Comput.*, vol. 42, no. 4, pp. 524–531, Jul. 2004.

[48] A. Botter and T. M. Vieira, "Filtered virtual reference: A new method for the reduction of power line interference with minimal distortion of monopolar surface EMG," *IEEE Trans. Biomed. Eng.*, vol. 62, no. 11, pp. 2638–2647, Nov. 2015.

[49] J. G. Webster, *Medical Instrumentation: Application and Design*. Hoboken, NJ, USA: Wiley, 2013.

[50] M. Pohja, S. Salenius, and R. Hari, "Reproducibility of cortex–muscle coherence," *NeuroImage*, vol. 26, no. 3, pp. 764–770, Jul. 2005.

[51] K. Petkos *et al.*, "A high-performance 8 nV/$\sqrt{}$Hz 8-channel wearable and wireless system for real-time monitoring of bioelectrical signals," *J. NeuroEng. Rehabil.*, vol. 16, no. 1, pp. 1–24, Dec. 2019.

[52] W. Song *et al.*, "Design of a flexible wearable smart sEMG recorder integrated gradient boosting decision tree based hand gesture recognition," *IEEE Trans. Biomed. Circuits Syst.*, vol. 13, no. 6, pp. 1563–1574, Dec. 2019.

# II

# VOLITIONAL MUSCLE ACTIVATION INTENSIFIES NEURONAL PROCESSING OF PROPRIOCEPTIVE AFFERENCE IN THE PRIMARY SENSORIMOTOR CORTEX: AN EEG STUDY

by

**A**. Giangrande, G. L. Cerone, A. Botter, and H. Piitulainen

*Journal of Neurophysiology*, 31: 28–37, 2024.

https://doi.org/10.1152/jn.00340.2023

*J Neurophysiol* 131: 28–37, 2024.
*First published November 15, 2023; doi:10.1152/jn.00340.2023*

american physiological society

JNP JOURNAL OF NEUROPHYSIOLOGY

RESEARCH ARTICLE

*Sensory Processing*

# Volitional muscle activation intensifies neuronal processing of proprioceptive afference in the primary sensorimotor cortex: an EEG study

**Alessandra Giangrande,[1,2] Giacinto Luigi Cerone,[2] Alberto Botter,[2] and Harri Piitulainen[1]**

[1]*Faculty of Sport and Health Sciences, University of Jyväskylä, Jyväskylä, Finland and* [2]*Laboratory of Neuromuscular System and Rehabilitation Engineering, DET, Politecnico di Torino, Turin, Italy*

## Abstract

Proprioception refers to the ability to perceive the position and movement of body segments in space. The cortical aspects of the proprioceptive afference from the body can be investigated using corticokinematic coherence (CKC). CKC accurately quantifies the degree of coupling between cortical activity and limb kinematics, especially if precise proprioceptive stimulation of evoked movements is used. However, there is no evidence on how volitional muscle activation during proprioceptive stimulation affects CKC strength. Twenty-five healthy volunteers (28.8 ± 7 yr, 11 females) participated in the experiment, which included electroencephalographic (EEG), electromyographic (EMG), and kinematic recordings. Ankle-joint rotations (2-Hz) were elicited through a movement actuator in two conditions: *passive* condition with relaxed ankle and *active* condition with constant 5-Nm plantar flexion exerted during the stimulation. In total, 6 min of data were recorded per condition. CKC strength was defined as the maximum coherence value among all the EEG channels at the 2-Hz movement frequency for each condition separately. Both conditions resulted in significant CKC peaking at the Cz electrode over the foot area of the primary sensorimotor (SM1) cortex. Stronger CKC was found for the *active* (0.13 ± 0.14) than the *passive* (0.03 ± 0.04) condition ($P < 0.01$). The results indicated that volitional activation of the muscles intensifies the neuronal proprioceptive processing in the SM1 cortex. This finding could be explained both by peripheral sensitization of the ankle joint proprioceptors and central modulation of the neuronal proprioceptive processing at the spinal and cortical levels.

**NEW & NOTEWORTHY** The current study is the first to investigate the effect of volitional muscle activation on CKC-based assessment of cortical proprioception of the ankle joint. Results show that the motor efference intensifies the neuronal processing of proprioceptive afference of the ankle joint. This is a significant finding as it may extend the use of CKC method during active tasks to further evaluate the motor efference-proprioceptive afference relationship and the related adaptations to exercise, rehabilitation, and disease.

*corticokinematic coherence; electroencephalography; proprioception; somatosensory*

## INTRODUCTION

Motor control in humans relies on the combination of a multitude of senses regulated by sensory systems such as the visual, vestibular, and somatosensory systems that are responsible for informing the central nervous system (CNS) about the environment and the body itself (1, 2). Proprioception is part of the somatosensory system and it measures the internal state of the musculoskeletal system being responsible for providing information to the CNS about the position, movement, and dynamics of the musculoskeletal system (3). Proprioception encompasses various senses related to changes in the internal state of the locomotor system and it is restricted to the ones that can be consciously perceived. These include, e.g., the sense of movement, the sense of balance, the sense of joint position, and the sense of force and heaviness (i.e., the sense of effort) (4). These sensations arise from peripheral signals generated by various types of receptors (i.e., proprioceptors) located in the muscles, joints, ligaments, and soft tissues around the joints (5). Proprioceptors are mechanoreceptors whose activity is modulated by bodily movements

Correspondence: A. Giangrande (alessandra.giangrande@polito.it).
Submitted 8 September 2023 / Revised 18 October 2023 / Accepted 9 November 2023

changing the muscle length (muscle spindles) or muscle tension (Golgi tendon organs). Proprioceptive signals can be further integrated with closely related information from cutaneous tactile mechanoreceptors sensitive to stretch of the skin during joint rotation (e.g., Pacinian corpuscles), thus providing specific "fingerprints" of certain movements to the CNS (4, 6).

Afferent proprioceptive pathways to the brain travel primarily along the afferent dorsal column-medial lemniscus first to the thalamus where the signals are further relayed to the cortex (7). Here, the brain integrates the proprioceptive afference with inputs from other senses, such as vision or touch, carrying information from the external environment (4). Specifically, the primary sensorimotor cortex (SM1) is the site where the basic sensorimotor integration (i.e., the integration of sensory information from multiple sources aimed at producing task-specific motor output) occurs.

Proprioception has a crucial role in motor control as it provides essential rich regulatory feedback about the internal state of the locomotor system to the CNS (1). First, it is fundamental for joint stabilization in postural control and balance (8). Second, it is crucial to motor planning (feedforward strategy) rapidly signaling the brain allowing for anticipation, preparation, and response planning (9). Third, recent evidence supported the view that proprioceptive afference is one of the key sensory modalities supporting motor learning (10, 11). Through proprioception, it is also possible for the CNS to fine-tune the ongoing motor command or action and thus produce smooth, appropriate motor actions, which is especially important for targeted movements of the limbs (feedback strategy) (12).

The relevance of proprioception in all human actions has encouraged researchers over decades to investigate the proprioceptive sense at the cortical level (7, 8, 13–15). The majority of studies have used electroencephalography (EEG) or magnetoencephalography (MEG) in combination with stimulation of the proprioceptors using evoked joint rotations while the participant is at rest (14). The temporal and amplitude features of the neuronal cortical processing of the proprioceptive afference can then be examined by means of the averaged cortical activity time-locked with movements (i.e., evoked responses) (16, 17). In addition to the evoked responses, a recent approach proposed a robust quantification of the degree of cortical proprioceptive processing using corticokinematic coherence (CKC) (18, 19). Jerbi et al. (20) first demonstrated using MEG that hand movement velocity and SM1 cortex activity are correlated at the movement frequency (20). The CKC term was later introduced by Bourguignon et al. (21) and they proposed CKC as a tool for functional motor mapping of the hand region (i.e., locating the cortical origin for the coupling) using MEG and volitional continuous rhythmic movements. Later, it was demonstrated that CKC primarily reflects cortical proprioceptive processing by comparing CKC between active volitional and passive evoked movements. The contribution of corticospinal motor efference to CKC was negligible with respect to the somatosensory afference to the SM1 cortex (22–24). In addition, it was suggested that the strength of CKC can be used to quantify the degree of cortical proprioceptive processing. CKC strength ranges from 0 (no coupling) to 1 (perfect coupling) peaking at the frequency of the movement and its harmonics, following the somatotopy (25). CKC can be quantified using any peripheral signal (e.g., acceleration, force, electromyography, etc.) picking the rhythmicity of the movement (26).

To date, several CKC studies have examined proprioception using movement actuators in passive (resting) conditions (27, 28). CKC strength has been shown to be influenced by factors such as the directed attention to the stimulus (29), the regularity of the stimulation (30), the movement range (18), the number of joints stimulated simultaneously (31), aging (32), or neurological disabilities (e.g., cerebral palsy) (33). Furthermore, the reproducibility of CKC is high across experimental sessions both for MEG- and EEG- based measurements (28, 34) although MEG provides somewhat stronger CKC, because of the higher signal-to-noise-ratio (35).

Despite the broad spectrum of studies attempting to understand the mechanisms behind CKC, there is no evidence of how volitional muscle activation during proprioceptive stimulation affects CKC strength. The motor efference is expected to alter the somatosensory afference to the brain via input to the muscles but also more generally to the spinal neuronal circuits (6). In addition, even light volitional muscle contraction can alter the muscle-tendon unit mechanics with respect to the relaxed passive condition. During volitional muscle contraction, the intrafusal fibers of the muscle spindles are also activated by the gamma motor neurons and thus the stretch sensitivity of the spindle afferents is enhanced (6, 36, 37). Finally, the volitional muscle contraction also modifies the functional state of the SM1 cortex with respect to the passive condition that may likely alter the cortical processing of the proprioceptive afference.

With the present study, we aimed to examine the effect of volitional muscle activation on neuronal processing of proprioceptive afference in the human neocortex when quantified using CKC and EEG. We hypothesized that volitional plantarflexion during proprioceptive stimulation (i.e., continuous actuated ankle-joint rotations at 2 Hz) of the ankle joint would strengthen CKC when compared with a condition in which the ankle remains passive. The mechanisms are expected to be due to *1*) motor efference-related sensitization of the peripheral proprioceptors through mechanical and neuronal factors and to *2*) alterations in the neuronal proprioceptive processing in the spinal and cortical levels. Assessing the sensitivity of CKC to volitional muscle activation is relevant to better understand methodological aspects of CKC and to provide new insight into the neurophysiological processes underlying the complex interactions between the periphery and the brain.

## MATERIALS AND METHODS

### Participants

A total of 25 young, healthy adults (age 28.8 ± 7 means ± SD, 11 females) were recruited for the study. The majority of the participants were right-footed (only 2 out of 25 were left-footed) based on Waterloo footedness inventory score that was on average 42 ± 32 on a scale from −100 to 100. All participants reported their right hand as the writing hand. Participants were provided with a complete description of the study procedure after which they were asked to sign a

written informed consent. The study was conducted in accordance with the Declaration of Helsinki and its approval was obtained by the Ethics Committee of the University of Jyväskylä before starting the measurements (Approval No.: 369/13.00.04.00/2020).

### Experimental Design and Recordings

The measurements were conducted at the Faculty of Sports and Health Sciences of the University of Jyväskylä, Jyväskylä, Finland. Proprioceptive perception ability of the ankle joint was tested first (38, 39). Then, a short (i.e., 30 s) resting state recording was performed and further taken as a baseline. Finally, CKC during ankle joint rotations was quantified for two conditions of the plantar flexor muscles: *1*) *active* condition with steady 5-Nm plantar flexion and *2*) *passive* condition with no plantar flexion torque exerted. The mechanical rotations (i.e., perturbations) were identical between the conditions. The two conditions were measured in four 3-min trials (two trials per condition) with a short break in between in random order, to avoid effects from any systematic time-dependent effects during the recording session.

### Experimental Setup

Figure 1 shows the experimental setup adopted for the study. Participants were sitting in a chair with the forearms lying on the armrests and the left foot relaxed on a separate footstool. The right foot was placed on the rotating platform of a motorized ankle-movement actuator. The anatomical ankle-joint rotation axis was identified according to Isman and Inman (40) and it was aligned with the axis of the rotating platform. Ankle and knee joint angles were set to 90°.

During the experiment, EEG and electromyographic (EMG) signals were recorded synchronously with foot angular displacement and torque. Participants were instructed to completely relax their left leg throughout the recordings. In addition, they wore shielded earplugs (ER-3C, 50 Ohm, Etymotic Research) playing 60-dB Brownian noise to ascertain masking of any, although minute, auditory noise caused by the ankle-movement actuator. No vibrations were generated either at rest or during the stimulations. Visual contact with the stimulated foot was blocked by using a brown cardboard panel while a screen was placed 1.5 m in front of the participants.

### Movement Actuator

Proprioceptive stimuli (i.e., ankle rotations) were produced using a custom-made silent ankle-movement actuator. It was composed of a rotating platform driven by a servomotor controlling the rotations according to the desired angular velocity (full operational range: 0–200°/s) managed by a control unit. The platform was equipped with torque and angular displacement sensors that were interfaced to a control unit generating analog output signals in the range of 0–5 V. The stimulation patterns were controlled using a custom-made Graphical User Interface (Matlab R2022b, MathWorks Inc, Natick, MA) that was configured to handle real-time visualization and storage of the data. A data acquisition unit (USB-6216 AD-board, National Instrument, Austin, TX) was, indeed, configured as an I/O board communicating with the proprioceptive stimulator and it was set through Matlab software to deliver the stimulation patterns and to acquire analog torque and joint angle signals (sampling frequency of 1 kHz).

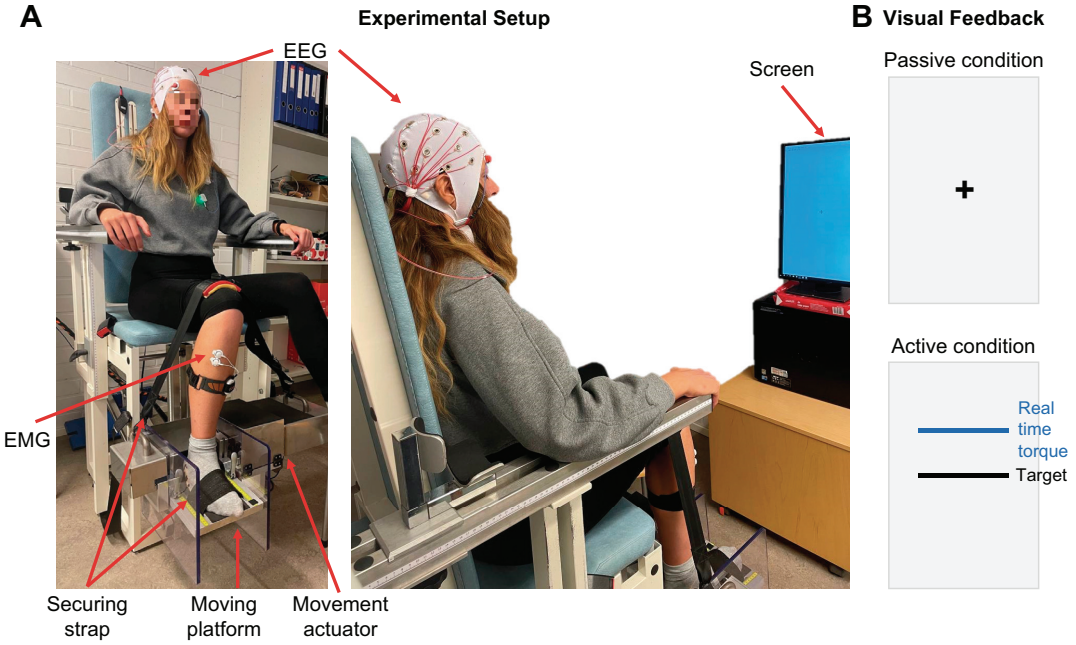


**Figure 1.** Experimental setup. *A*: participant's right foot was placed on the rotating platform with knee and ankle joints at 90°; 30 EEG, 2 EOG channels, and EMG from right soleus and tibialis anterior were recorded. *B*: visual feedback varied between the conditions. A fixation cross was shown during the passive condition, and the real-time torque with 5 Nm target level was shown during the active condition. EEG, electroencephalographic; EMG, electromyographic signals; EOG, electro-oculogram.

### EEG Recordings

A wireless light-weight EEG amplifier (41–43) was used to record EEG signals with a 30 Ag/AgCl electrode cap (EasyCap GmbH, Gliching, Germany) following the international 10–20 system. To ensure a good skin-electrode contact, each electrode site has been gently scrubbed through a cotton swab with an abrasive paste (NuPrep, Weaver and Company, Aurora) and then filled with a conductive gel (NeurGel, SPES MEDICA, Genova, Italy). In addition, electro-oculogram (EOG) signals were acquired through two surface electrodes (30 mm × 22 mm Ambu s.r.l., Denmark) placed in the up-left and down-right corners of the eye region. EEG and EOG signals were acquired in a monopolar derivation, using the FCz electrode of the cap as the reference with a sampling frequency of 2,048 Hz and a bandwidth of 0.1–500 Hz. EEG signals were collected synchronously with EMG and they were offline synchronized with kinematic signals according to a common external trigger by using the synchronization unit introduced in Ref. 41.

### EMG Recordings

EMGs were recorded from the tibialis anterior muscle and right medial part of the soleus muscle using a pair of Ag/AgCl electrodes (Ø 24 mm Kendall, Covidien, Dublin, Ireland) placed on each muscle according to the SENIAM recommendations (44) after a gentle skin abrasion of the interested area by using an abrasive paste (Nuprep, Weaver and Company, Aurora) (45). EMG was acquired in a bipolar derivation through a wireless amplifier (DuePro, OT Bioelettronica, Turin, Italy) with a sampling frequency of 2,048 Hz in the 10–500 Hz frequency band.

### Proprioceptive Perception Ability

To test the correlation between the neurophysiological and the behavioral measurements, the perceptual proprioceptive threshold was computed for each participant. Perceptual threshold of the evoked ankle joint rotation was defined for the right leg using the proprioceptive stimulator and an adaptive-test algorithm (38). The right ankle was passively dorsiflexed at a varying angular velocity from 0.3 to 1.5°/s (interstimulus interval: 4 ± 0.25 s). Participants were instructed to fixate a black cross on a gray background on the screen in front of them and to press a response button with their right thumb as soon as they perceived the movement of the platform. The analog output of the response button was sampled at 1 kHz through the I/O board and it was used as a marker of the rotation perception. The detection or missing of a stimulus was used to adapt the angular velocity (i.e., decrease or increase of 0.1°/s) of the subsequent stimulus allowing for the identification of the individual proprioceptive threshold. The proprioceptive-perception threshold was defined as the lowest angular velocity with >50% correctly perceived stimuli and it was automatically updated throughout the test after each stimulus. The experimenter manually stopped the test if two criteria were met: *1*) a minimum of five stimuli at the threshold velocity were provided to the participant and *2*) at least a total of 25 rotations were delivered during the test.

### Corticokinematic Coherence

To compare the degree of cortical proprioceptive processing during the *active* and *passive* conditions, CKC was computed. The right ankle joint was stimulated at 2 Hz with a continuous 4° ankle rotation in dorsi and plantarflexion direction (8° total range of motion) at 25°/s angular velocity 3 min per condition and trial (in total 6 min of data per condition). A screen was placed 1.5 m in front of the participants to provide visual feedback during the tested conditions. During the *passive* condition, participants were instructed to relax their lower limbs and to fixate on a black cross on the screen in front of them. During the *active* condition, participants were instructed to apply a constant plantarflexion torque of 5 Nm (±2.5 Nm) about the axis of the rotating platform, and they were provided with visual real-time feedback displaying the applied torque and the desired target (Fig. 1*B*). The experimental design was planned to prevent visual contamination of CKC at the movement frequency. To this end, the torque feedback displayed on the screen to the participants was computed by averaging the torque signal over a 600 ms moving epoch with 300 ms overlap. This approach prevented continuous oscillation of the displayed torque signal at the 2-Hz proprioceptive stimulation frequency that could have led to strong CKC in the occipital visual cortices and consequent bias in our SM1 cortex CKC strength. Finally, to prevent any vertical raise of the heel from the rotating platform, the sole of the right foot was secured to the platform using a strap around the knee and an elastic Velcro around the midfoot. EMG signals were inspected in real time by the experimenter to ascertain that the participant was relaxed during the *passive* condition. The experimental setup was the same in the two experimental conditions. The order of the *active* and *passive* conditions was randomized, with the starting condition balanced across participants. Each recording always started with 30-s rest period followed by 3 min stimulation.

### Signal Analysis

Signal processing was entirely performed offline in Matlab R2022b (MathWorks Inc, Natick, MA). Angular displacement and torque signals were resampled at 2,048 Hz to match with EEG and EMG signals. An offline synchronization was performed by aligning all the recorded signals according to the rising edge of a common external trigger sent at the beginning of each trial.

### EEG and EMG Signal Preprocessing

FieldTrip Matlab toolbox was used for the EEG analysis (46). EEG data were first visually inspected to identify and mark the noisy channels. Then, EEG signals were bandpass filtered through a fourth-order Butterworth filter at 0.1–95 Hz, and independent component analysis was used to extract 30 EEG independent components to identify those related to artifacts (e.g., due to eye movements or neck/temporalis muscular activity). Eye blinks or eye movements were identified based on the highest correlation with the EOG pattern and then they were removed. Only after the independent component analysis, noisy channels were interpolated by replacing them with the average of all the neighboring channels.

Finally, a common average reference was applied to all EEG channels (47).

EMG signals were offline bandpass filtered at 20–400 Hz with fourth-order Butterworth filter.

### Corticokinematic Coherence Analysis

The formulation of Halliday et al. (48) was used to compute the coherence between EEG and the angular-displacement signal (i.e., the foot kinematics). EEG signals were split into 2-s epochs with 1.6 s overlap, yielding a frequency resolution of 0.5 Hz (49). EEG epochs exceeding 200 mV were considered to be corrupted by artifacts and were rejected. Coherence computation yielded cross, power, and coherence spectra between the foot kinematics and each EEG signal separately. The magnitude squared coherence was chosen as a coupling measure as done in earlier CKC studies (19, 21, 28). CKC strength was defined as the coherence value at the 2-Hz movement frequency in the peak EEG channel among all the 30 EEG channels for each participant and condition. Then, the averaged CKC value of the two trials for *active* or *passive* condition was used as the final CKC strength estimate for each participant. For visualization purposes, CKC spectra from the two trials of the same condition were also averaged separately for each participant and topographic representations of CKC were further visualized at the group level.

### Statistical Analysis

All results are given as mean ± SD. Statistical tests were performed in Matlab R2022b on the averaged data across the trials for both *active* and *passive* conditions (MathWorks Inc, Natick, MA). We tested the normal distribution of the data through a Shapiro–Wilk test for each condition. All the variables were non-normally distributed ($P < 0.05$), thus we used nonparametric statistical tests for the statistical analysis.

### EMG Activity during CKC Testing

EMG root-mean-square amplitude was computed to quantify the degree of muscular activation between conditions. The rest period (30 s) collected at the beginning of CKC recordings was considered as a baseline representative of a relaxed condition (i.e., without volitional muscular activation) and it was compared to the corresponding *active* and *passive* conditions to evaluate the presence and degree of the muscular activity of soleus and tibialis anterior. To this end, we conducted a Wilcoxon signed-rank test (nonparametric statistical test) to search for statistically significant differences between the muscular activity during rest, *active*, and *passive* conditions. We considered merged trials for the abovementioned comparison.

### Statistical Significance of CKC

The hypothesis of linear independence of Fourier coefficients at each frequency between epochs was used to assess the statistical significance of individual coherence levels (21, 48). To correct for multiple comparisons, the significance $\alpha$-level was set to 0.05/Nc, with Nc number of EEG electrodes, i.e., 30. Because of the non-normal distribution of the data, a Wilcoxon signed-rank test (nonparametric test) was used to assess differences between the two trials, separately per each condition to investigate the possibility of pooling trials together to further inspect the effect of muscle activation on CKC.

### Effect of Volitional Muscle Activation on CKC

As a result of the non-normal distribution of the data, a nonparametric test (Wilcoxon signed-rank test) was used to examine whether CKC strength differed between the *active* and *passive* conditions.

### Correlation Analysis

To evaluate the associations between CKC and proprioceptive-perception ability, the correlation of CKC strength to the proprioceptive-perception threshold was computed using Spearman rank correlation coefficient.

## RESULTS

Figure 2 shows raw EEG, EMG, and kinematic signals during rest, *active*, and *passive* conditions. The overall signal quality was good, without any notable artifact rising from the ankle-movement actuator or the external environment. For both conditions, we considered the same, fixed number of independent components (i.e., 30) explaining the 99.28 ± 0.43% of the variation for *active* condition and the 99.46 ± 0.33% for *passive* condition. On average, 3 ± 2 independent components were rejected from EEG signals, while the average number of discarded epochs was 3 ± 3 across conditions and participants. Within the CKC analysis, the number of epochs was fixed at the minimum number of epochs across the four trials and participants, i.e., 468 epochs per trial.

### EMG Activity during Proprioceptive Stimulations

Figure 3 shows the muscular activation levels in terms of EMG root-mean-square values of *active*, *passive*, and rest conditions (merged trials). As expected, activation levels were

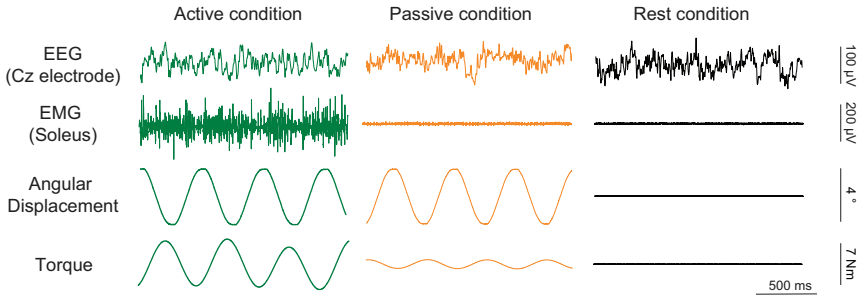


**Figure 2.** Example of preprocessed signals from a representative subject during 2 s from active, passive, and rest conditions. From *top* to *bottom*: bandpass filtered EEG (0.1–95 Hz) from Cz electrode, bandpass filtered EMG (20–400 Hz) from soleus muscle, angular displacement and torque signals applied on the pedal are represented. EEG, electroencephalographic; EMG, electromyographic signals.

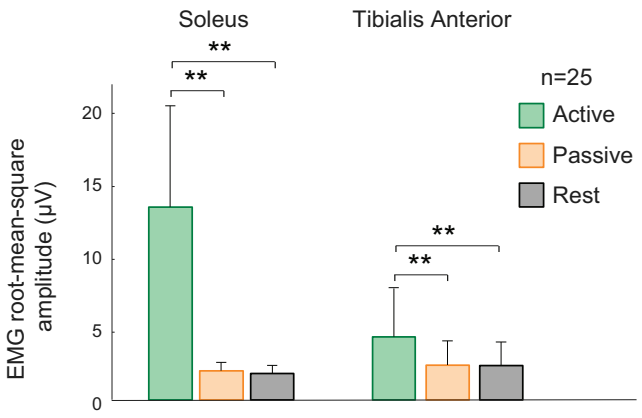


**Figure 3.** Bar diagrams showing the EMG root-mean-square amplitudes (μV) of soleus and tibialis anterior muscles during active, passive, and rest conditions averaged across participants ($n = 25$). Error bars indicate the standard deviation of the muscular activation levels across participants. Statistical analysis by Wilcoxon signed-rank test, $^{**}P < 0.01$.

significantly higher during the *active* condition than both rest and passive conditions ($P < 0.01$), both for soleus and tibialis anterior muscles without showing any statistically significant differences between *passive* and rest conditions. Although the task mainly required the activity of plantarflexor muscles (i.e., soleus), a slight co-contraction of the tibialis anterior muscle was also noticed.

### Corticokinematic Coherence

Figure 4 shows the CKC results. At the group level, CKC was stronger during the active than passive condition ($P < 0.01$). Figure 4*B* shows the individual CKC strengths at 2-Hz peak for the Cz electrode for both conditions. A striking increase in CKC was observed in 22 out of 25 participants from *passive* to *active* condition, while only 3 out of 25 participants showed an opposite tendency.

At the individual level, CKC was above the significance level in 21 out of 25 participants at the 2-Hz movement frequency for the *active* condition and in 11 out of 25 participants for the *passive* one. For all the participants, when above the statistical significance level, CKC was peaking at the level of Cz electrode (i.e., above the midline central scalp region as expected for ankle-joint stimulation) in both conditions. Figure 4*A* shows the coherence spectra for the *active* and *passive* conditions for the Cz electrode. The spectra show that the CKC strength was clearly stronger for the *active* than the *passive* condition at 2-Hz peak in the group level (*active* condition: 0.13 ± 0.14, *passive* condition: 0.03 ± 0.04) and peaked at the expected Cz electrode over the foot area of the SM1 cortex in both conditions. Although with weaker CKC values, results at the first harmonic (i.e., at 4 Hz) of the movement frequency confirmed what we found at the 2-Hz movement frequency in terms of spatial distribution and CKC strength trend between conditions (*active*: 0.04 ± 0.17, *passive*: 0.02 ± 0.05). Nevertheless, we found only 8/25 (*active* condition) and 4/25 (*passive* condition) participants with CKC above the significance level at the first harmonic.

### Correlation between CKC Strength and Proprioceptive-Perception Ability

Figure 5 shows the result of the proprioceptive perception ability test for a representative participant (threshold at 0.8°/s).

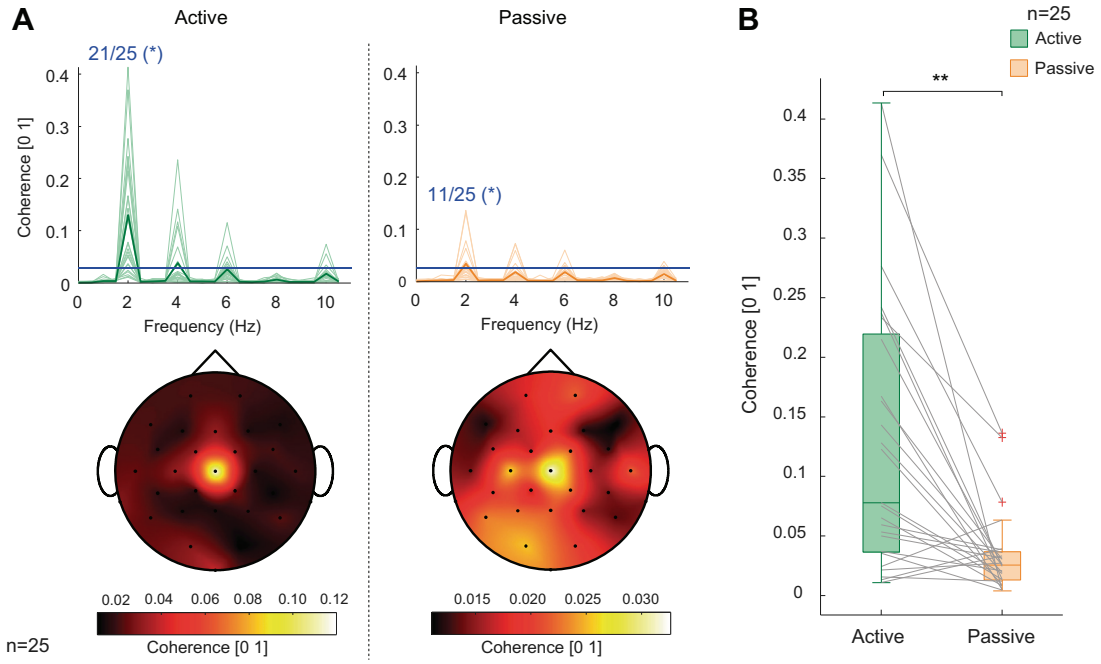


**Figure 4.** Corticokinematic coherence (CKC) results ($n = 25$ participants). *A*: CKC spectra of Cz electrode (*top*) and topographic representation of CKC strength at the movement frequency averaged across subjects (*bottom*) for active and passive conditions. The light-colored lines indicate the individual spectra, whereas the marked lines indicate the grand-average spectra. Horizontal blue line indicates the statistical significance level. Color bar scales of spatial topographies are different for the two conditions to highlight the spatial distribution of CKC strength over the scalp for both conditions. *B*: boxplot representations of Cz-electrode-CKC strengths at the movement frequency for both conditions. Statistical analysis by Wilcoxon signed-rank test, $^{*}P < 0.05$, $^{**}P < 0.01$.

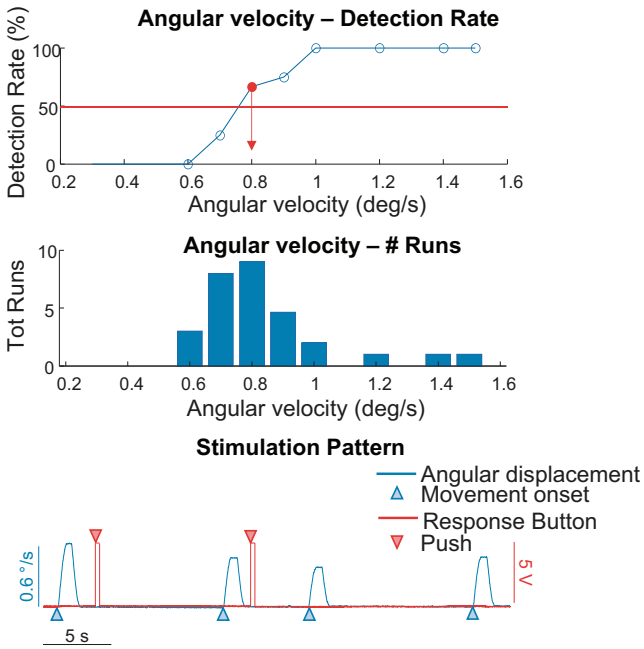


**Figure 5.** Evaluation of proprioceptive ability test performances of a representative subject. From top to bottom, representations of: angular velocity-detection rate, angular velocity-number of runs, and evaluation of response time.

The average proprioceptive threshold was 0.79 ± 0.19°/s across the participants.

However, no statistically significant correlation was found between CKC strength and proprioceptive threshold (*active* condition: $r = -0.07$, $P = 0.75$; *passive* condition: $r = -0.03$, $P = 0.87$; Fig. 6).

## DISCUSSION

Corticokinematic coherence was peaking at movement frequency and at the multiple harmonic frequencies as typically observed in EEG- or MEG-based studies (28, 30). However, as shown by Piitulainen et al. (34), CKC strength is slightly weaker in EEG than in MEG, also in harmonic frequencies. Therefore, because of the low number of participants with CKC above the significance level, we then performed the analysis focusing on the fundamental 2-Hz movement frequency only. The proprioceptive stimulation of the ankle joint evoked significant CKC in the EEG electrode above the foot region of the SM1 cortex. However, the CKC strength was weaker in the *passive* than in the *active* stimulation condition, supporting our hypothesis that volitional activation of the stimulated muscles would intensify the cortical proprioceptive processing because of *1*) the neuronal and mechanical sensitization of the ankle joint proprioceptors and/or *2*) the modulations of the neuronal proprioceptive processing in the spinal and cortical levels due to active motor control processes. This is a significant finding as it may extend the use of the CKC method to further examine the cortical neuronal mechanisms related to interplay or closed loop between motor efference and proprioceptive afference during active tasks and the related adaptations to exercise, rehabilitation, and disease.

### Effect of Muscle Activation on CKC

In line with our hypothesis, CKC was stronger during *active* than *passive* condition. From proprioceptors' point of view, the main difference between these conditions is the functional state of the muscle spindles and the mechanical condition of the ankle joint. The sensitivity of the muscle spindle to muscle-tendon length change is increased during active contractions (36, 37). This is because the motor efference activating the muscles is accompanied by simultaneous activation of the intrafusal fibers within the muscle spindle by gamma motoneurons improving the detection of muscle length change (50). It is also noteworthy that the muscle spindle is the predominant proprioceptor providing the proprioceptive afference to the CNS occurring at the mid-region of the range of motion, as was the case for both active and passive ankle rotations in the present study.

The mechanical state of the ankle joint also differed between the conditions. During the *active* condition, the constant 5-Nm torque increased the muscle-tendon unit tension and likely reduced muscle-tendon unit slack, which may increase not only the muscle spindle sensitivity, but also the firing rate of Golgi tendon organs that are responsible for detecting the change in force produced by the muscle or directed to the muscle-tendon unit (6). Therefore, we suggest that the combination of the increased firing rate of the

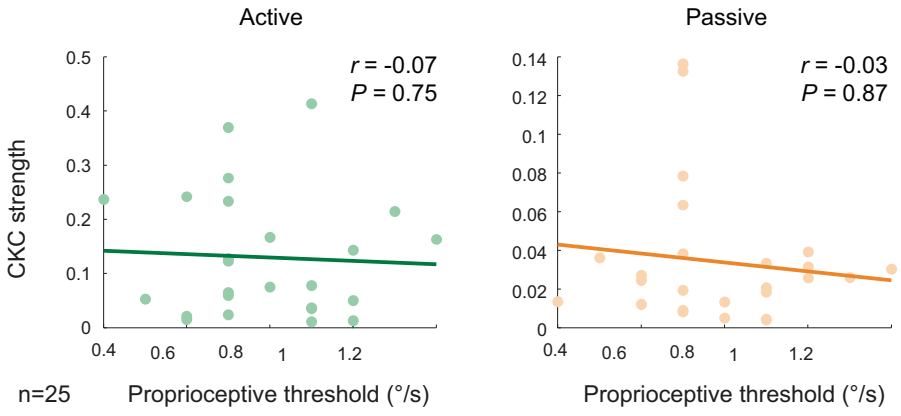


**Figure 6.** Correlation between corticokinematic coherence (CKC) strength at the movement frequency and proprioceptive threshold for active and passive conditions. Pearson correlation coefficients are superimposed ($n = 25$ participants).

abovementioned proprioceptors results in the intensification of the somatosensory afference to the SM1. This would in turn intensify the cortical processing of the proprioceptive afference and thus result in stronger CKC during the *active* than *passive* condition. In addition to the proprioceptors, the cutaneous tactile receptors may contribute to the enhancement of CKC during the *active* versus *passive* condition. The plantar pressure under the sole of the foot is stronger during the *active* condition as seen in the torque signal in Fig. 2. This might allow better activation of deep mechanoreceptors of the skin. To alleviate this difference, we used straps around the mid-foot to enhance the plantar pressure during the *passive* condition, and thus most of the plantar cutaneous receptors were likely activated in both conditions. The evoked movement inevitably also activates the tactile receptors in the skin around the ankle joint as the skin is being rhythmically stretched. However, the kinematics of the evoked movements were identical between *active* and *passive* conditions, thus a similar tactile afference is expected to occur. Finally, we do not consider this tactile activation strictly as a confounding factor, but as one of the plausible mechanisms for the stronger CKC during the *active* condition. The brain uses the tactile and proprioceptive afference in an integrated manner, and thus it is difficult or even unnecessary to separate them when examining naturalistic stimuli.

The brain can also modify its own somatosensory feedback both at spinal and cortical levels (51). Thus, the cortex may actively control its proprioceptive afference and spinal-level sensorimotor processing. This mechanism is especially evident during the active maintenance of the isometric contraction in the *active* condition. Therefore, it is likely that the spinal, medullary, and thalamic circuits influencing the afferent proprioceptive pathways to the SM1 cortex are modulated in a way that intensifies the associated cortical processing with respect to the *passive* condition. Such modulation can be also influenced by cortico-cortical connections. Thus, different cortical regions related to motor control and somatosensation can contribute to influencing the SM1 cortex processing of proprioceptive afference during the active motor task. This interpretation is in line with earlier observations in rodents. It has been shown that focal enhancement of rat motor cortex activity facilitated sensory-evoked responses of topographically aligned neurons in the primary somatosensory cortex (52).

The state of the SM1 cortex may also affect the CKC strength. It is well established that the SM1 cortex is activated just before (i.e., motor preparation) and during (i.e., due to both volitional motor output and somatosensory input) volitional muscle contraction. The state of SM1 cortex is altered also during the passive rotations of the ankle due to the consequent strong proprioceptive afference to the SM1 cortex. Nevertheless, the volitional motor processes are not effective in similar manner in *active* versus *passive* conditions. As an example, Piitulainen et al. (23) investigated CKC during active (i.e., self-performed) versus passive finger movements and they did not observe differences in CKC strength, spatial location, or coherence directionality between the conditions. Although this result might seem in contrast to ours (i.e., strengthened CKC during *active* vs. *passive* condition), the active task fundamentally differed between these studies, and thus the results are not directly comparable. Piitulainen et al. (23) used self-paced (i.e., active) dynamic finger movements. On the contrary, the current task was to maintain steady plantarflexion torque despite externally evoked perturbations (i.e., rotations) to the ankle joint. Thus, our active task did not include active movement, but active stabilization of the ankle joint. In addition, different limbs were investigated (hand vs. foot), thus we could not make any inferences between studies. In addition, also the sensorimotor processes are partly different between *active* and *passive* conditions. Indeed, CKC strength has been shown to be increased when attention is directed to the proprioceptive stimulation when compared with situation in which the attention was directed away from the stimulation to a visual task in passive conditions (29). In our active task, the attention was directed to the proprioceptive-motor task to stabilize the quasi-steady plantarflexion. The task was rather challenging as the ankle was being passively rotated simultaneously. Instead, during the *passive* condition, although attention was not expressively directed to the proprioceptive stimulation, participants followed the stimulations without being distracted by another visual or motor task. Consequently, these attentional differences may partly explain the enhanced CKC strength during *active* condition, but the attentional effects are expected only to minimally affect the dramatic difference in CKC strength between the conditions in the current study. Previous evidence demonstrated only a minor reduction in CKC strength (~9%) when attention was directed to the proprioceptive stimulation or away from it to a visual task (29). Indeed, given that there might have been more attention to the foot or the stimulus during the *active* condition, this should have led to a reduction in CKC, but we observed the opposite.

It is worth mentioning that less than 50% of our participants showed significant CKC at the movement frequency during the *passive* condition. This was somewhat surprising as strong CKC has been observed for ankle joint rotations in MEG (32). However, to the best of our knowledge, there are no EEG-based CKC studies involving passive stimulation for the lower limbs. Most of the CKC studies have focused on passive or self-performed upper limb movements in MEG (18, 21–23). For passive hand stimulation, CKC strength has been shown to be weaker for EEG than MEG (34). Furthermore, the use of spatial filters (i.e., bipolar, Laplacian filters) and 58-electrode EEG cap enhanced CKC strength when compared with common reference filter (34). However, we recently showed that the improvement associated with spatial filtering when using a 30-electrode EEG cap is not systematically observed with less dense EEG electrode caps (35). Therefore, we did not use spatial filters (bipolar or Laplacian) in the current study. Nevertheless, the use of a more dense EEG cap could be suggested for future CKC studies using passive proprioceptive stimulation of the ankle joint and EEG recordings for the abovementioned reasons. The more spatially selective EEG derivations could enhance the detection of CKC above the significance level in the lower limbs.

Furthermore, the weak CKC may be specific to the lower limbs compared with the upper limbs, which are more widely investigated using CKC (19, 21, 34) with respect to the few MEG lower limb studies (16, 32). First, the cortical representation of the hand region in the SM1 cortex is more

optimally located and oriented for EEG/MEG compared with the foot region that is located deeper and centrally in the posterior paracentral lobule, which is a U-shaped convolution that loops below the medial part of the central sulcus thus resulting in a deep localization of the source (53). The hand area is also wider with respect to the lower limb one. Consequently, noninvasive EEG recordings of cortical signals from the scalp surface will result in a weaker signal-to-noise ratio negatively influencing CKC strength.

### Correlation between CKC and Proprioceptive-Perception Ability

The proprioceptive-perception ability of the tested population was in line with the result of our previous studies on young healthy adults (39). We did not detect a significant correlation between behavioral and cortical (i.e., CKC strength) proprioception. Thus, our hypothesis that a lower proprioceptive-perception threshold (i.e., better behavioral performance) would be associated with weaker CKC was not supported. Nevertheless, it is worth mentioning that our sample consisted of a rather homogeneous population of highly performing healthy young adults without proprioceptive deficits. Therefore, the variation in behavioral proprioceptive performance was small. This potential association should be further examined in samples with more variable proprioceptive performance, such as cerebral palsy, developmental coordination disorder, or older adults (32, 38).

### Perspectives and Significance

The present study is the first to investigate the effect of volitional muscle activation on EEG-based CKC assessment of cortical proprioception of the ankle joint. We demonstrated that CKC was stronger when the muscles were active during proprioceptive ankle-joint stimulation when compared with *passive* stimulation condition. The intensified cortical proprioceptive processing may be related to neuronal and mechanical differences between *active* and *passive* conditions at muscle-tendon unit, receptor, spinal, medullar, thalamic, and cortical levels. The proposed methods and technologies could be further adopted in future research to deepen the understanding and adaptation of cortical proprioceptive processing during active motor tasks. As such, these measures will become potential tools to evaluate the effects of aging or neurological diseases such as stroke, Parkinson's, or developmental diseases on cortical proprioception.

## DATA AVAILABILITY

The data are not publicly available due to privacy or ethical restrictions. However, data are available upon request from the corresponding author.

## ACKNOWLEDGMENTS

We thank the chief technician Sakari Vekki from the University of Jyväskylä for technical support in building the experimental design.

## GRANTS

This study was supported by the Academy of Finland (grants #296240, #327288, and #326988 to H.P.), and "Brain changes across the life-span" profiling funding to University of Jyväskylä (grant #311877). A.G. is supported by a three-year PhD fellowship from Politecnico di Torino, Turin, Italy.

## DISCLOSURES

No conflicts of interest, financial or otherwise, are declared by the authors.

## AUTHOR CONTRIBUTIONS

H.P. conceived and designed research; A.G. performed experiments; A.G., G.L.C., A.B., and H.P. analyzed data; A.G. and H.P. interpreted results of experiments; A.G. prepared figures; A.G. and H.P. drafted manuscript; A.G., G.L.C., A.B., and H.P. edited and revised manuscript; A.G., G.L.C., A.B., and H.P. approved final version of manuscript.

## REFERENCES

1. **Moon KM**, **Kim J**, **Seong Y**, **Suh BC**, **Kang KJ**, **Choe HK**, **Kim K.** Proprioception, the regulator of motor function. *BMB Rep* 54: 393–402, 2021. doi:10.5483/BMBRep.2021.54.8.052.
2. **Grace Gaerlan M**, **Alpert PT**, **Cross C**, **Louis M**, **Kowalski S.** Postural balance in young adults: the role of visual, vestibular and somatosensory systems. *J Am Acad Nurse Pract* 24: 375–381, 2012. doi:10.1111/j.1745-7599.2012.00699.x.
3. **Means JH.** The integrative action of the endocrine system. *Ann Intern Med* . 34: 1311–1323, 1951. doi:10.7326/0003-4819-34-6-1311.
4. **Proske U**, **Gandevia SC.** The proprioceptive senses: their roles in signaling body shape, body position and movement, and muscle force. *Physiol Rev* 92: 1651–1697, 2012. doi:10.1152/physrev.00048.2011.
5. **Van Beers RJ**, **Baraduc P**, **Wolpert DM.** Role of uncertainty in sensorimotor control. *Philos Trans R Soc Lond B Biol Sci* 357: 1137–1145, 2002. doi:10.1098/rstb.2002.1101.
6. **Purves D**, **Augustine JG**, **Fitzpatrick D**, **Hall CW**, **LaMantia A-S**, **Mooney DR**, **Platt LM**, **White EL.** *Neuroscience* (6th ed.). New York: Oxford University Press Inc., 2018.
7. **Tuthill JC**, **Azim E.** Proprioception. *Curr Biol* 28: R194–R203, 2018. doi:10.1016/j.cub.2018.01.064.
8. **Khurana S.** Proprioception: an evidence based narrative review. *Res Inves Sports Med* 1: 13–17, 2017. doi:10.31031/rism.2017.01.000506.
9. **Gordon JC**, **Holt NC**, **Biewener A**, **Daley MA.** Tuning of feedforward control enables stable muscle force-length dynamics after loss of autogenic proprioceptive feedback. *eLife* 9: e53908, 2020. doi:10.7554/eLife.53908.
10. **Arnin J**, **Yamsa-Ard T**, **Triponyuwasin P**, **Wongsawat Y.** Development of practical functional electrical stimulation cycling systems based on an electromyography study of the Cybathlon 2016. *Eur J Transl Myol* 27: 7111–7301, 2017. doi:10.4081/ejtm.2017.7111.
11. **Wong JD**, **Kistemaker DA**, **Chin A**, **Gribble PL.** Can proprioceptive training improve motor learning? *J Neurophysiol* 108: 3313–3321, 2012. doi:10.1152/jn.00122.2012.
12. **Konczak J**, **Corcos DM**, **Horak F**, **Poizner H**, **Shapiro M**, **Tuite P**, **Volkmann J**, **Maschke M.** Proprioception and motor control in Parkinson's disease. *J Mot Behav* 41: 543–552, 2009. doi:10.3200/35-09-002.
13. **Lephart SM**, **Pincivero DM**, **Giraldo JL**, **Fu FH.** The role of proprioception in the management and rehabilitation of athletic injuries. *Am J Sports Med* 25: 130–137, 1997. doi:10.1177/036354659702500126.
14. **Toledo DR**, **Manzano GM**, **Barela JA**, **Kohn AF.** Cortical correlates of response time slowing in older adults: ERP and ERD/ERS analyses during passive ankle movement. *Clin Neurophysiol* 127: 655–663, 2016. doi:10.1016/j.clinph.2015.05.003.
15. **Han J**, **Anson J**, **Waddington G**, **Adams R**, **Liu Y.** The role of ankle proprioception for balance control in relation to sports performance and injury. *BioMed Res Int* 2015: 842804, 2015. doi:10.1155/2015/842804.
16. **Mujunen T**, **Seipäjärvi S**, **Nurminen M**, **Parviainen T**, **Piitulainen H.** Reproducibility of evoked and induced MEG responses to proprioceptive stimulation of the ankle joint. *Neuroimage: Reports* 2: 100110, 2022. doi:10.1016/j.ynirp.2022.100110.
17. **Seiss E**, **Hesse CW**, **Drane S**, **Oostenveld R**, **Wing AM**, **Praamstra P.** Proprioception-related evoked potentials: origin and sensitivity to

movement parameters. *Neuroimage* 17: 461–468, 2002. doi:10.1006/nimg.2002.1211.
18. **Nurmi T**, **Hakonen M**, **Bourguignon M**, **Piitulainen H.** Proprioceptive response strength in the primary sensorimotor cortex is invariant to the range of finger movement. *Neuroimage* 269: 119937, 2023. doi:10.1016/j.neuroimage.2023.119937.
19. **Smeds E**, **Vanhatalo S**, **Piitulainen H**, **Bourguignon M**, **Jousmäki V**, **Hari R.** Corticokinematic coherence as a new marker for somatosensory afference in newborns. *Clin Neurophysiol* 128: 647–655, 2017. doi:10.1016/j.clinph.2017.01.006.
20. **Jerbi K**, **Lachaux J-P**, **N'Diaye K**, **Pantazis D**, **Leahy RM**, **Garnero L**, **Baillet S.** Coherent neural representation of hand speed in humans revealed by MEG imaging. *Proc Natl Acad Sci USA* 104: 7676–7681, 2007. doi:10.1073/pnas.0609632104.
21. **Bourguignon M**, **De Tiège X**, **de Beeck MO**, **Pirotte B**, **Van Bogaert P**, **Goldman S**, **Hari R**, **Jousmäki V.** Functional motor-cortex mapping using corticokinematic coherence. *Neuroimage* 55: 1475–1479, 2011. doi:10.1016/j.neuroimage.2011.01.031.
22. **Bourguignon M**, **Piitulainen H**, **De Tiège X**, **Jousmäki V**, **Hari R.** Corticokinematic coherence mainly reflects movement-induced proprioceptive feedback. *Neuroimage* 106: 382–390, 2015. doi:10.1016/j.neuroimage.2014.11.026.
23. **Piitulainen H**, **Bourguignon M**, **De Tiège X**, **Hari R**, **Jousmäki V.** Corticokinematic coherence during active and passive finger movements. *Neuroscience* 238: 361–370, 2013. doi:10.1016/j.neuroscience.2013.02.002.
24. **Bourguignon M**, **Jousmäki V**, **Dalal SS**, **Jerbi K**, **De Tiège X.** Coupling between human brain activity and body movements: insights from non-invasive electromagnetic recordings. *Neuroimage* 203: 116177, 2019. doi:10.1016/j.neuroimage.2019.116177.
25. **Bourguignon M**, **Jousmäki V**, **Op de Beeck M**, **Van Bogaert P**, **Goldman S**, **De Tiège X.** Neuronal network coherent with hand kinematics during fast repetitive hand movements. *Neuroimage* 59: 1684–1691, 2012. doi:10.1016/j.neuroimage.2011.09.022.
26. **Piitulainen H**, **Bourguignon M**, **De Tiège X**, **Hari R**, **Jousmäki V.** Coherence between magnetoencephalography and hand-action-related acceleration, force, pressure, and electromyogram. *Neuroimage* 72: 83–90, 2013. doi:10.1016/j.neuroimage.2013.01.029.
27. **Piitulainen H**, **Bourguignon M**, **Hari R**, **Jousmäki V.** MEG-compatible pneumatic stimulator to elicit passive finger and toe movements. *Neuroimage* 112: 310–317, 2015. doi:10.1016/j.neuroimage.2015.03.006.
28. **Piitulainen H**, **Illman M**, **Laaksonen K**, **Jousmäki V**, **Forss N.** Reproducibility of corticokinematic coherence. *Neuroimage* 179: 596–603, 2018. doi:10.1016/j.neuroimage.2018.06.078.
29. **Piitulainen H**, **Nurmi T**, **Hakonen M.** Attention directed to proprioceptive stimulation alters its cortical processing in the primary sensorimotor cortex. *Eur J Neurosci* 54: 4269–4282, 2021. doi:10.1111/ejn.15251.
30. **Mujunen T**, **Nurmi T**, **Piitulainen H.** Corticokinematic coherence is stronger to regular than irregular proprioceptive stimulation of the hand. *J Neurophysiol* 126: 550–560, 2021. doi:10.1152/jn.00095.2021.
31. **Hakonen M**, **Nurmi T**, **Vallinoja J**, **Jaatela J**, **Piitulainen H.** More comprehensive proprioceptive stimulation of the hand amplifies its cortical processing. *J Neurophysiol* 128: 568–581, 2022. doi:10.1152/jn.00485.2021.
32. **Piitulainen H**, **Seipäjärvi S**, **Avela J**, **Parviainen T**, **Walker S.** Cortical proprioceptive processing is altered by aging. *Front Aging Neurosci* 10: 147, 2018. doi:10.3389/fnagi.2018.00147.
33. **Démas J**, **Bourguignon M**, **De Tiège X**, **Wens V**, **Coquelet N**, **Rovai A**, **Bouvier S**, **Bailly R**, **Brochard S**, **Dinomais M**, **Van Bogaert P.** Assessing spino-cortical proprioceptive processing in childhood unilateral cerebral palsy with corticokinematic coherence. *Neurophysiol Clin* 52: 33–43, 2022. doi:10.1016/j.neucli.2021.12.003.
34. **Piitulainen H**, **Illman M**, **Jousmäki V**, **Bourguignon M.** Feasibility and reproducibility of electroencephalography-based corticokinematic coherence. *J Neurophysiol* 124: 1959–1967, 2020. doi:10.1152/jn.00562.2020.
35. **Giangrande A**, **Cerone GL**, **Gazzoni M**, **Botter A**, **Piitulainen H.** Quantification of cortical proprioceptive processing through a wireless and miniaturized EEG amplifier. *Annu Int Conf IEEE Eng Med Biol Soc* 2022: 4797–4800, 2022. doi:10.1109/EMBC48229.2022.9871637.
36. **Edin BB**, **Vallbo AB.** Stretch sensitization of human muscle spindles. *J Physiol* 400: 101–111, 1988. doi:10.1113/jphysiol.1988.sp017113.
37. **Ribot-Ciscar E**, **Tardy-Gervet MF**, **Vedel JP**, **Roll JP.** Post-contraction changes in human muscle spindle resting discharge and stretch sensitivity. *Exp Brain Res* 86: 673–678, 1991. doi:10.1007/BF00230541.
38. **Piitulainen H**, **Nurmi T**, **Vuontela V**, **Mäenpää H**, **Lano A**, **Carlson S.** Perception of the ankle joint proprioception is impaired in extremely preterm-born adolescents and is associated with weaker fine-motor performance. *Gait Posture* 97: S159–S160, 2022. doi:10.1016/j.gaitpost.2022.07.105.
39. **Piitulainen H**, **Nurmi T**, **Vuontela V**, **Mäenpää H**, **Lano A**, **Carlson S.** Proprioceptive perception of the ankle joint is impaired in developmental coordination disorder. *Gait Posture* 90: 188–189, 2021. doi:10.1016/j.gaitpost.2021.09.098.
40. **Isman RE**, **Inman VT.** Anthropometric studies of the human foot and ankle. *Bull Prosthet Res* 11: 97–129, 1969.
41. **Cerone GL**, **Giangrande A**, **Ghislieri M**, **Gazzoni M**, **Piitulainen H**, **Botter A.** Design and validation of a wireless body sensor network for integrated EEG and HD-sEMG acquisitions. *IEEE Trans Neural Syst Rehabil Eng* 30: 61–71, 2022. doi:10.1109/TNSRE.2022.3140220.
42. **Cerone GL**, **Botter A**, **Gazzoni M.** A modular, smart, and wearable system for high density sEMG detection. *IEEE Trans Biomed Eng* 66: 3371–3380, 2019. doi:10.1109/TBME.2019.2904398.
43. **Cerone GL**, **Gazzoni M.** A wireless, minaturized multi-channel sEMG acquisition system for use in dynamic tasks. *2017 IEEE Biomedical Circuits and Systems Conference (BioCAS)*. Turin, Italy, 2017. doi:10.1109/BIOCAS.2017.8325129.
44. **Stegeman D**, **Hermens H.** Standards for surface electromyography: the European project "Surface EMG for non-invasive assessment of muscles (SENIAM). *Enschede: Roessingh Res Devel* 10: 8–12, 2007.
45. **Merletti R**, **Cerone GL.** Tutorial. Surface EMG detection, conditioning and pre-processing: Best practices. *J Electromyogr Kinesiol* 54: 102440, 2020. doi:10.1016/j.jelekin.2020.102440.
46. **Oostenveld R**, **Fries P**, **Maris E**, **Schoffelen J-M.** FieldTrip: open source software for advanced analysis of MEG. EEG, and invasive electrophysiological data. *Comput Intell Neurosci* 2011: 156869, 2011. doi:10.1155/2011/156869.
47. **McFarland DJ**, **McCane LM**, **David SV**, **Wolpaw JR.** Spatial filter selection for EEG-based communication. *Electroencephalogr Clin Neurophysiol* 103: 386–394, 1997. doi:10.1016/S0013-4694(97)00022-2.
48. **Halliday DM**, **Rosenberg JR**, **Amjad AM**, **Breeze P**, **Conway BA**, **Farmer SF.** A framework for the analysis of mixed time series/point process data—theory ad application to the study of physiological tremor, single motor unit discharges and electromyograms. *Prog Biophys Mol Biol* 64: 237–278, 1995. doi:10.1016/s0079-6107(96)00009-0.
49. **Bortel R**, **Sovka P.** Approximation of statistical distribution of magnitude squared coherence estimated with segment overlapping. *Signal Processing* 87: 1100–1117, 2007. doi:10.1016/j.sigpro.2006.10.003.
50. **Khan MN**, **Cherukuri P**, **Negro F**, **Rajput A**, **Fabrowski P**, **Bansal V**, **Lancelin C**, **Lee TI**, **Bian Y**, **Mayer WP**, **Akay T**, **Müller D**, **Bonn S**, **Farina D**, **Marquardt T.** ERR2 and ERR3 promote the development of gamma motor neuron functional properties required for proprioceptive movement control. *PLoS Biol* 20: e3001923, 2022. doi:10.1371/journal.pbio.3001923.
51. **McIlroy WE**, **Bishop DC**, **Staines WR**, **Nelson AJ**, **Maki BE**, **Brooke JD.** Modulation of afferent inflow during the control of balancing tasks using the lower limbs. *Brain Res* 961: 73–80, 2003. doi:10.1016/S0006-8993(02)03845-3.
52. **Lee S**, **Carvell GE**, **Simons DJ.** Motor modulation of afferent somatosensory circuits. *Nat Neurosci* 11: 1430–1438, 2008. doi:10.1038/nn.2227.
53. **Rao SM**, **Binder JR**, **Hammeke TA**, **Bandettini PA**, **Bobholz JA**, **Frost JA**, **Myklebust BM**, **Jacobson RD**, **Hyde JS.** Somatotopic mapping of the human primary motor cortex with functional magnetic resonance imaging. *Neurology* 45: 919–924, 1995. doi:10.1212/WNL.45.5.919.

# III

# MOTION ARTIFACTS IN DYNAMIC EEG RECORDINGS: EXPERIMENTAL OBSERVATIONS, ELECTRICAL MODELLING AND DESIGN CONSIDERATIONS

by

A. Giangrande, A. Botter, H. Piitulainen, G. L. Cerone

*Sensors*, 24: 6363, 2024.

https://doi.org/10.3390/s24196363

sensors

MDPI

*Article*

# Motion Artifacts in Dynamic EEG Recordings: Experimental Observations, Electrical Modelling, and Design Considerations

**Alessandra Giangrande [1,2], Alberto Botter [1], Harri Piitulainen [2] and Giacinto Luigi Cerone [1,*]**

[1] Laboratory of Neuromuscular System and Rehabilitation Engineering, Department of Electronics and Telecommunications, Politecnico di Torino, 10129 Turin, Italy; alessandra.giangrande@polito.it (A.G.); alberto.botter@polito.it (A.B.); giacintoluigi.cerone@polito.it (G.L.C).
[2] Faculty of Sport and Health Sciences, University of Jyväskylä, 40014 Jyväskylä, Finland; harri.t.piitulainen@jyu.fi (H.P.)
* Correspondence: giacintoluigi.cerone@polito.it

**Abstract:** Despite the progress in the development of innovative EEG acquisition systems, their use in dynamic applications is still limited by motion artifacts compromising the interpretation of the collected signals. Therefore, extensive research on the genesis of motion artifacts in EEG recordings is still needed to optimize existing technologies, shedding light on possible solutions to overcome the current limitations. We identified three potential sources of motion artifacts occurring at three different levels of a traditional biopotential acquisition chain: the skin-electrode interface, the connecting cables between the detection and the acquisition systems, and the electrode-amplifier system. The identified sources of motion artifacts were modelled starting from experimental observations carried out on EEG signals. Consequently, we designed customized EEG electrode systems aiming at experimentally disentangling the possible causes of motion artifacts. Both analytical and experimental observations indicated two main residual sites responsible for motion artifacts: the connecting cables between the electrodes and the amplifier and the sudden changes in electrode-skin impedance due to electrode movements. We concluded that further advancements in EEG technology should focus on the transduction stage of the biopotentials amplification chain, such as the electrode technology and its interfacing with the acquisition system.

**Keywords:** electroencephalography; biomedical instrumentation; motion artifacts; the brain; EEG electrodes; EEG cap design; electrode-amplifier system modelling

**Citation:** Giangrande, A.; Botter, A.; Piitulainen, H.; Cerone, G.L. Motion Artifacts in Dynamic EEG Recordings: Experimental Observations, Electrical Modelling, and Design Considerations. *Sensors* **2024**, *24*, x. https://doi.org/10.3390/xxxxx

Academic Editor(s): Name

Received: 23 August 2024
Revised: 19 September 2024
Accepted: 27 September 2024
Published: date



## 1. Introduction

Among the brain technologies, electroencephalography (EEG) is the most suitable for investigating the cortical sensorimotor integration processes during dynamic tasks thanks to its excellent spatiotemporal resolution, high portability, and relatively low costs [1]. Recent hardware developments allowed for the acquisition of biosignals through wireless, miniaturized, and portable devices, extending the range of signal acquisitions also outside lab environments [2–6]. The opportunities arising from the availability of these devices are, however, not fully exploited in practice due to the frequent presence of motion artifacts corrupting dynamic EEG signals. These artifacts are undesired signals with an amplitude of even two orders of magnitude greater than one of the signals of interest, thus strongly compromising the correct interpretation of cortical signals [7,8]. In the vast majority of the cases, motion artifacts are time-locked to the performed movements and greatly variable in terms of shape, repeatability, and spectral content, thus being hard or impossible to remove [9,10]. Indeed, motion artifacts can be observed both at low frequencies as baseline shifts and at high frequencies as spike-like variations [8]. Therefore, post-processing techniques are not always effective in removing these artifacts, considering the relatively low typical EEG frequency bandwidth (0.1 Hz–100 Hz) [11].

Whilst wavelet-based or blind source separation techniques are robust techniques excelling in removing physiological and repeatable EEG artifacts (e.g., eye blinks), their effectiveness in the context of motion artifact removal collapses. Indeed, it remains obscure to what extent they exclusively remove artifacts, entirely preserving the content of the physiological brain signals [9,12]. Over the past years, different solutions have been proposed to mitigate the recording of motion artifacts, including the use of active electrodes [13]. Although active electrodes were particularly effective in rejecting power line interference arising from the capacitive coupling between connecting cables and power line source, they have been proven comparable to passive electrodes in reducing motion artifacts during dynamic recordings [14]. Conversely, they contribute to increasing the encumbrance of the acquisition system, limiting its portability and usability in dynamic contexts. Other innovative solutions preventing the rising of motion artifacts concern the development of detection systems based on textiles, as they showed a reduced sensitivity to motion artifacts. However, their use is strictly limited to hairless cortical regions (i.e., frontal and temporal areas) and, therefore, not compatible with comprehensive studies on the role of the parietal sensorimotor cortices in movement control [15].

Despite these efforts, the genesis of motion artifacts in EEG recordings still remains a poorly understood topic. Therefore, given the increasing interest in dynamic EEG recordings in naturalistic, dynamic conditions [16–18], it is crucial to gain a deep understanding and to model the basic phenomena leading to the genesis of motion artifacts to optimize existing technologies and to develop new solutions for high-quality EEG detection.

Biopotential signal acquisition can be affected by the mutual interaction and superimposition of multiple factors occurring at different stages of the recordings (e.g., experimental setup preparation, detection, and acquisition technology) [19–21]. Although it is difficult to disentangle the sources of motion artifacts in the experimental practice, a model-based approach describing the basic phenomena underlying the generation of motion artifacts is hereby proposed. Specifically, in the following dissertation, we aim to provide further insights into the role of acquisition electronics, connecting cables, and electrode technology in EEG recordings, both from analytical and experimental perspectives. To achieve this, we (i) carried out observations on EEG signals during real experiments, (ii) identified and modelled the possible artifact sources, (iii) designed customized EEG electrode systems aimed at showing the influence of the detection system's features in EEG dynamic recordings, and (iv) performed a case study aimed at giving further grounds to the previously modelled phenomena behind the genesis of EEG motion artifacts.

## 2. Observations

Potential sources of motion artifacts can arise at each of the three main stages constituting a traditional biopotential acquisition chain [22,23]: (i) the skin-electrode interface (i.e., transduction stage), (ii) the electrode-amplifier connecting cables, and (iii) the electrode-amplifier system (i.e., acquisition stage). Other possible sources of artifacts affecting the EEG signals (e.g., eye movements and environment-related artifacts) were out of the scope of the current dissertation as they are either easily handled or can be treated as a particular case of the described ones. Following this approach, we were able to investigate the main factors that can influence the outcome of biopotential signal recordings. Firstly, the relative movement between the electrode and the skin creates a consequent alteration of the ion distribution at the electrode-skin interface that would be read as an additive artifact signal with respect to those of interest [19]. Secondly, due to triboelectric phenomena [24], the friction and deformation of the cable insulator caused by the movements of the cables generate an additive input voltage potential that will be amplified together with the signal of interest [25]. Thirdly, in case of poor electrode-skin contact (e.g., due to a brisk, partial detachment of the electrodes), movements might also trigger a modulation of the residual input-referred Power Line Interference (PLI). In the next sections, we

provide some examples taken from the abovementioned artifactual phenomena based on the observations of real recordings. These examples will then be used as starting points for the following electrical modelling.

### *2.1. Artifacts Arising from Phenomena at the Electrode-Skin Interface*

Figure 1 shows an example of motion artifacts corrupting individual channels (i.e., CP1 or, to a lesser extent, Pz of the parietal cortex) of a set of EEG signals recorded during overground walking. Such motion artifacts can be described as relatively slow changes in the baseline voltage potential highly correlated with the main frequency of the movement. In such cases, due to the slow and periodic changes of the voltage, we hypothesize that these artifacts are generated by relative shifts between the electrodes and the skin because of body movements related to the motor task. The artifact localization on a single channel is likely due to the movement of the individual exploring electrode (i.e., the electrode acquiring the monopolar EEG signal of interest with respect to the reference electrode). It is important to highlight that the example introduced in Figure 1 might be handled through post-processing techniques. However, if this type of artifact simultaneously affects multiple electrodes, including the reference one, the degree of signal corruption increases and the conventionally adopted techniques for artifact removal are critical to succeed due to the intricate superimposition of different effects.

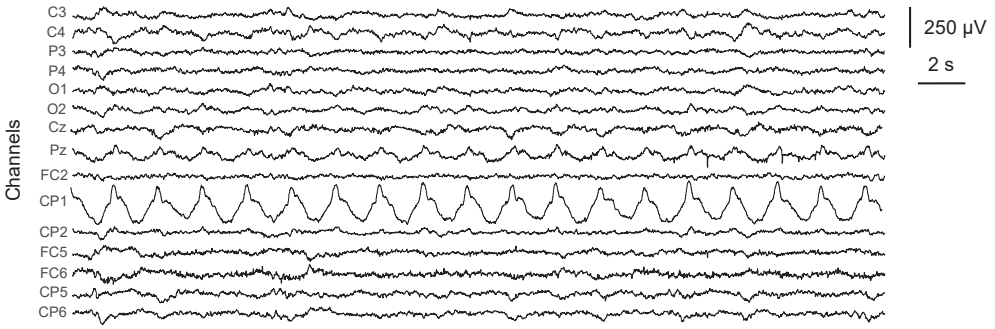


**Figure 1.** Examples of motion artifacts contamination on a set of EEG signals recorded during overground walking related to the movement of single exploring electrodes (CP1, Pz over the parietal cortex).

### *2.2. Artifacts Related to Connecting Cables Movements*

Figure 2 represents the result of an experimental test regarding the acquisition of EEG signals from a subject at rest while the experimenter was manually shaking the cables connecting the electrodes to the amplifier (i.e., a worst-case scenario). As evident from the spectral power distributions of Figure 2B, traditional signal processing techniques cannot be used to dampen the dramatic effect of motion artifacts on EEG signals. Indeed, motion artifacts related to the connecting cables typically occur not time-locked with the movements with a spike-like behavior and their spectral components are overlapped with the EEG bandwidth (0.1 Hz–100 Hz). Additionally, motion artifacts generated by the movement of the cables are hardly repeatable, especially in terms of shape. For these reasons, many filtering techniques are not found to be effective in removing non-brain activity from the EEG signals [12]. Similar considerations have been observed in the case of sEMG signals acquisitions [21].

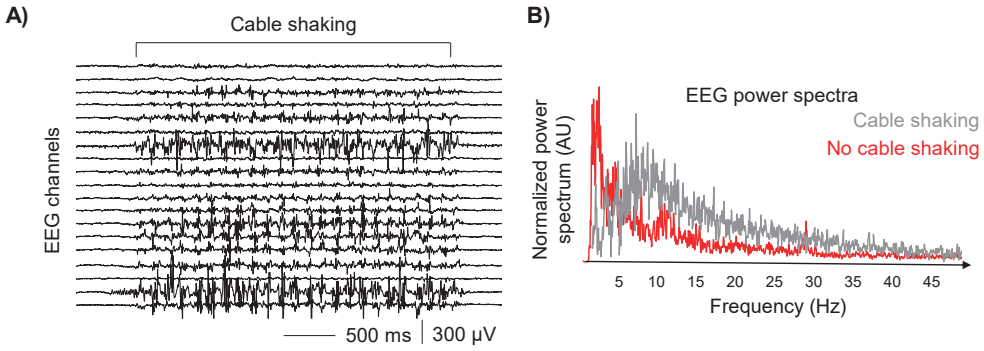


**Figure 2.** Motion artifacts caused by the movement of the connecting cables. (**A**) EEG signals recorded with the subject at rest while the experimenter is shaking the cables, wearing isolating insulating gloves. (**B**) Power spectra of a representative EEG signal with and without cable shaking.

### *2.3. Artifacts Related to the Electrode-Amplifier System Properties Leading to PLI Modulation*

Figure 3A shows experimental examples of artifacts due to PLI modulation on detected signals. In this case, we hypothesized that during movement, an unstable contact at the electrode-skin interface may induce a sudden variation of the electrode-skin imbalance between the exploring and reference electrodes, leading to a temporary increase of the input-referred PLI. Figure 3B represents a schematization of this phenomenon. The residual, input-referred PLI (red sinusoidal signal) is modulated by the movement (represented as the blue binary signal where the levels 0–1 are respectively referred to absence/presence of electrode-skin impedance variations due to a movement) providing in the output the corrupting signal (black color). Therefore, PLI signals (sinewave at 50 Hz/60 Hz) are modulated in time by the variations of electrode-skin imbalance, resulting in artifacts with different morphologies. As a result, the movement-related modulation is responsible for changing the spectral content of the whole recorded signal as it introduces spurious, unpredictable spectral components (different from PLI frequency) that may span throughout the entire EEG spectrum. These artifacts are, therefore, particularly challenging not only to be visually identified but also to be handled as they cannot be removed, e.g., through notch or adaptive filters [26].

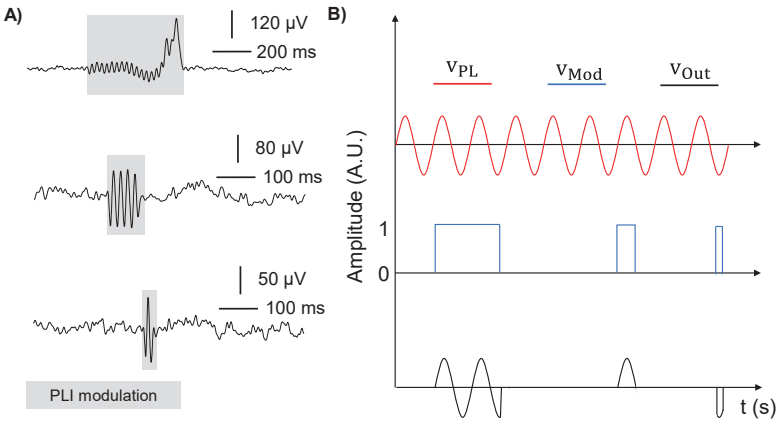


**Figure 3.** Examples of PLI modulation. (**A**) Three real examples of possible artifact morphology due to the brisk detachment of electrodes modulating power line noise. (**B**) Schematic representation of the hypothesized phenomenon. From top to bottom: power-line signal (red trace), modulating signal modelling the brisk electrode movement (blue trace), resulting detected signal (black trace) that will be superimposed to the physiological one.

## 3. Lumped Parameters Modelling

For each identified source of motion artifact (Observations 2.1, 2.2, and 2.3), an electrical lumped parameter model has been designed to describe and synthesize separately the experimentally observed phenomena.

### *3.1. Artifacts Arising from Phenomena at the Electrode-Skin Interface*

Figure 4 shows the electrical model of generation of motion artifacts arising from the movement of two exploring electrodes $e_1$ and $e_2$ (having electrode-skin impedances respectively of $Z_{e1}$ and $Z_{e2}$) in the case of monopolar configuration (monopolar reference electrode $e_r$, having impedance $Z_r$). This circuit has been synthesized to model common artifacts between adjacent electrodes due, as an example, to movement-related shifts between the electrodes and the skin. A purely resistive amplifier input impedance is considered for simplicity [27–29]. The voltage generator ($V_{AE}$) models a common-mode motion artifact source as the voltage change generated by the relative movements between two exploring electrodes. This is assumed as a realistic hypothesis when considering, for example, two neighbouring electrodes affected by the same mechanical excitation. It is worth noting that in this electrical model, we considered a single pair of electrodes, but the dissertation can be extended to the total number of exploring electrodes used during EEG measurements. In addition, similar models can be used to examine the effect of the movements at the reference electrode location or both reference and exploring electrodes. We focused on this case because it is the most critical one in light of the abovementioned observations. According to the electrical model of Figure 4, the voltage divider between the front-end amplifier input impedances and the electrode impedances will generate the following input-referred voltages at the input of the A1 and A2 biopotential amplifiers:

$$\begin{cases} V_{O1ir} = V_{AE}\dfrac{R_i}{R_i + Z_{e1}} \\ V_{O2ir} = V_{AE}\dfrac{R_i}{R_i + Z_{e2}} \end{cases} \quad (1)$$

To evaluate how the input common mode voltage artifact ($V_{AE}$) is translated into a differential-mode artifact at the amplifier output, we evaluated the difference between the two voltages $\Delta V = V_{O1ir} - V_{O2ir}$. Under the realistic hypothesis that the input amplifier impedance is greater than the electrode impedances (i.e., $R_i \gg Z_e$) [30], the voltage difference can be approximated as:

$$\Delta V \cong V_{AE}\frac{\Delta Z_e}{R_i} \quad (2)$$

This model is well known in the literature as the voltage divider effect, and it is often used to estimate the power line interference rejection capabilities of an electrode-amplifier system [21].

It is evident that, even when the source of the artifact ($V_{AE}$) is a common mode, the differential voltages computed at the output of the monopolar front-end may not be null, as they depend on the ratio between the electrode-skin imbalance and the amplifier input impedance. As a result, the difference between the impedance values $\Delta Z_e$ should be minimized as the greater the imbalance between the electrode impedances, the greater the voltage differences (i.e., artifact signal amplitude).

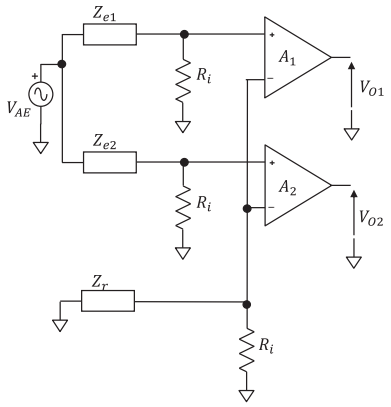


**Figure 4.** Electrical model of motion artifacts caused by movement-related shifts of two exploring electrodes ($e_1$ and $e_2$, with impedances $Z_{e_1}$ and $Z_{e_2}$). $R_i$ represents the amplifier input resistance. A differential signal acquisition in a monopolar configuration is represented.

### *3.2. Artifacts Related to Connecting Cables Movements*

One of the major sources of cable-related motion artifacts is the triboelectric effect, causing a net charge accumulation on the surface of the cables connecting the electrodes to the amplifier during their reciprocal movements [25]. The triboelectric effect describes the transfer of electric charge between two objects (i.e., the insulation layers of neighbouring cables) when they slide against each other or even only when they come into contact [24,31]. Phenomena like friction and deformation of the insulation layers of adjacent cables modify the electrostatic voltage according to the cable material properties, contact area, type of contact, and speed of the varying reciprocal distance [25]. With the aim of understanding the contribution of the cables' movement to motion artifacts in EEG recordings, we modeled two adjacent cables connecting two separated electrodes to the amplifier, as shown in Figure 5. $R_{c1}$, $R_{c2}$ are the electrical resistances of the cable conductors (typically copper, resistivity $\rho \cong 16.8\ \mathrm{m\Omega \cdot mm^2/m}$ ), $C_{i1}, C_{i2}$ model the parasitic capacitance due to the cable insulator layer (thickness $d_i$, dielectric constant $\varepsilon_r$) wrapping the inner conductive material, and $C_A$ represents the electrical capacitance due to the dielectric (i.e., air, dielectric constant $\varepsilon_A$) in between two conductive mediums (i.e., the charged insulator layers) separated by a distance $d_A$. Starting from this model, some simplifications can be conveniently introduced. First, the terms referring to the electrical resistances can be disregarded because of their small contribution to the impedance magnitude when considering standard cables with a transversal section of 0.5 mm$^2$ and a length of 1 cm (~tens of milli-ohm). Second, under the hypothesis of modelling the reactive components as capacitors, the equivalent capacitance of the model can be approximated to the sole contribution of $C_A$ as it dominates on the single $C_i$ because of the greater dielectric constant ($\varepsilon_r > \varepsilon_A$) and distance between the plates ($d_A > d_i$). In addition, the movement of the cable bundle is expected to affect $C_A$ more than $C_i$. Indeed, the parameter $d_A$ (distance among cables) is most likely to vary throughout the movements, which modulates $C_A$. This, in turn, alters the total capacitance of the model, affecting the electrical properties of the cables and generating motion artifacts. Indeed, the triboelectric-induced electrostatic voltage consequently polarizes the $C_A$ capacitor, generating a voltage drop $V_A$. The net charge $Q_A$ on the plates of the capacitor (planar faces approximation) is proportional to the potential difference $V_A$ across the two plates:

$$Q_A = C_A V_A \tag{3}$$

Under the reasonable assumption that the net charge, $Q_A$, accumulated through triboelectric effect remains constant during the cable movement, there will be a differential voltage change at the input of the biopotential amplifier $\Delta V_A = V_{A1} - V_{A2}$. Thus, the triboelectric-related voltage drop $\Delta V_A$ at the amplifier input can be modelled as an

additive, purely differential mode voltage, added to the biopotential signal of interest. It is worth noting that this additive signal will be amplified by the differential gain which possibly leads to a relevant contamination to the recorded EEG signals.

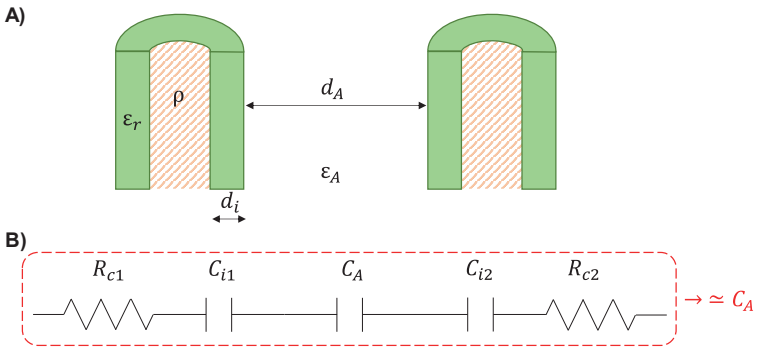


**Figure 5.** Model of two adjacent cables connecting EEG electrodes to the amplifier. (**A**) Schematic representation of the cross-section of two unipolar cables separated by a distance $d_A$ in a medium (air, dielectric constant $\boldsymbol{\varepsilon_A}$). Each cable is composed of a conductive wire (resistivity ϱ) embedded in an insulator sheath (thickness $d_i$, dielectric constant $\varepsilon_r$) (**B**) Equivalent electrical model of two adjacent cables, where $R_{c1,2}$ represent the electrical resistances of the conductive lead, $C_{i1,2}$ model the parasitic capacitances due to the cable insulator layer and $C_A$ depicts the electrical capacitance due to the dielectric $\varepsilon_A$. The red dashed rectangle indicates the simplified electrical model ($\simeq C_A$).

### *3.3. Artifacts Related to the Electrode-Amplifier System Properties Leading to PLI Modulation*

Figure 6 shows the electrical model representing the parasitic coupling between a subject, the power line, and the electrode-amplifier system. It is used to model the PLI modulation phenomena as a source of movement artifacts in case of a residual amount of PLI at the input of the biopotential acquisition chain. Ground-floating instrumentation and monopolar electrode configuration are represented together with a common mode excitation due to parasitic coupling between the subject and the power line [32–35]. It is well known that the degree of PLI affecting biopotentials depends on the common-mode voltage at the input of the electrode-amplifier system. This voltage is mainly due to the parasitic capacitive coupling between the subject, the power line source and the ground, and to the coupling between the front-end reference and the power line ground. With reference to Figure 6A: $C_1$ (typically ranging from 5 pF to 20 pF [21]) represents the parasitic capacitive coupling between the subject and the active phase of the power line [30]; $C_2$ (~50 pF to 10 nF [21]) models the parasitic capacitive coupling between the subject and the power line ground [21,36]; $C_p$ represents the parasitic coupling between the front-end amplifier reference and the power line ground and it ranges between ten pF and hundreds of pico-Farads [28,30,36]. The model of Figure 6 also includes $V_{PL}$ modelling the common mode excitation (i.e., power line source), $R_{e1}$ and $R_{e2}$ representing the resistive components of the impedance models of the exploring electrodes and the input resistances of the front-end amplifier ($R_i$) [28,37]. Given these assumptions, the common mode voltage at the input of the electrodes-amplifier system $V_C$ can be computed through the Thevenin equivalent circuit extracted from the electrical model of the power line-electrode-amplifier system (Figure 6B). Where:

$$\begin{cases} V_{eq} = V_{PL}\dfrac{C_1}{C_1 + C_2} \\ C_{eq} = \dfrac{(C_1 + C_2)C_p}{C_1 + C_2 + C_p} \\ R_{eq} = (R_{e2} + R_i) \oplus (R_{e2} + R_i) \end{cases} \quad (4)$$

Additional simplifications can be conveniently introduced. Indeed, the input impedance of the front-end amplifier circuit $R_i$ is in the order of Mega-Ohms, at least

three orders of magnitude greater than the electrode-skin impedance $R_e$ (tens of kΩ if 1cm2 Ag/AgCl are used) [21]. Therefore, since $R_i \gg R_e$, the equivalent resistance of the Thevenin electrical circuit is given by $R_{eq} \cong \frac{R_i}{2}$. Specifically, when considering a realistic EEG recording under a multichannel configuration (i.e., $R_{eN}$ with N ranging from 8 to 128 channels) and considering the common monopolar configuration having the inverting input shared between the channels, the total resistance at the monopolar reference input is obtained as the parallel of all the input resistances of each channel, i.e., $R_{eq} \cong \frac{R_i}{N}$. Furthermore, in practice, it is generally possible to reduce the common-mode input voltage $V_C$ by minimizing the value of the parasitic coupling $C_p$ between the amplifier's reference and the ground. This result may be obtained by designing battery powered, ground-floating, and miniaturized systems [22,38]. Therefore, the most common case within the present dissertation context leads to $C_{eq} \cong C_p$ since $C_p$ dominates over the combination of $C_1 + C_2$. Under these assumptions, the magnitude of the common mode voltage transfer function at the input of the electrodes-amplifier system $V_c$ results:

$$|V_C| = V_{eq} \frac{\omega \frac{R_i}{N} C_p}{\sqrt{1 + \left(\omega \frac{R_i}{N} C_p\right)^2}} \tag{5}$$

where N is the number of EEG channels. Given these considerations on the common mode input voltage $V_C$, it is well-known [21] that it is converted into a differential voltage $V_{IRN_{50}}$ according to (6):

$$V_{IRN_{50}} = V_C \left(\frac{R_{eN} - R_{e1}}{R_i} + \frac{1}{CMRR}\right) \tag{6}$$

where the term $(R_{eN} - R_{e1})$ is the interelectrode-skin impedances imbalance, Ri and CMRR are the amplifier's input resistance and the common mode rejection ratio (CMRR) respectively. Equation (6) enables practical considerations regarding the phenomenon of the movement-related modulation of $V_{IRN_{50}}$ described in Section 2.3. Indeed, $V_{IRN_{50}}$ depends on:

- The common mode input voltage ($V_C$), which depends on both the design of the amplifier (i.e., $R_i$ in cases in which a third zero-volt reference electrode is not used, CP, etc.) and on the experimental setup adopted during the recordings (i.e., electrodes preparation, coupling between the subject and the power line, etc.). Thus, it can vary according to the movements performed during the recordings. However, a varying common mode voltage is unlikely the cause of movement artifacts as its variation would have an effect, although potentially different, on all the channels and could consequently be removed e.g., through a common average offline referencing.
- The common mode rejection ratio (CMRR) of the amplifier and the input amplifier resistance ($R_i$), are, in turn, dependent on the design of the front-end amplifier. As a result, no movement-dependent changes on the CMRR nor on $R_i$ are expected to occur and therefore it cannot be the cause hindering the variation of the $V_{IRN_{50}}$ when a constant $V_C$ is applied.
- The electrodes-skin resistances imbalance ($\Delta R_e$). This parameter is the only one that can explain the observed modulation of power line interference on specific channels. Indeed, at a single channel level, the electrodes-skin resistance imbalance is obtained from the relative difference between the resistance of the exploring electrode and the one taken as a reference for the monopolar signal detection $\Delta R_e = R_{eN} - R_{e1}$. When performing a movement, the single values of electrode impedances may be affected by the changes caused by alteration of the skin-electrode contact due to e.g., reciprocal movements between the electrode and the skin, thus strongly contributing to the conversion of the common mode excitation to a differential one.

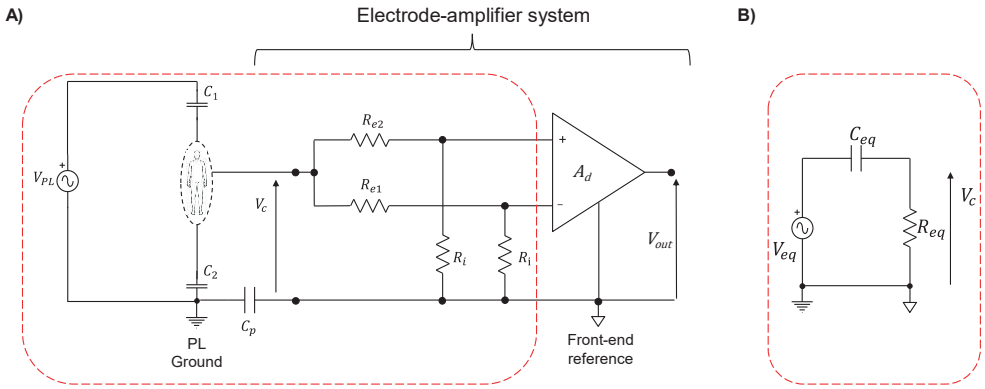


**Figure 6.** (**A**) Electrical model of the subject-electrode-amplifier system of a two-electrodes biopotential acquisition system. Ground-floating instrumentation and monopolar electrode configuration are represented together with a common mode excitation due to parasitic coupling between the subject and the power line ($C_1$ represents the parasitic capacitive coupling between the subject and the active phase of the power line, $C_2$ models the parasitic capacitive coupling between the subject and the power line ground). (**B**) Thevenin simplified the equivalent circuit of the power line-electrode-amplifier system when adopting battery-powered instrumentation.

## 4. Technological Developments

The previous sections on the sources of motion artifacts were aimed at analytically describing the main factors influencing the quality of EEG electrodes. We highlighted that two main aspects should be considered when dealing with the contamination of motion artifacts on EEG signals: the presence of connecting cables between the electrodes and the amplifier and the varying interelectrode impedances due to the electrode movements. The former aspect takes into account the artifacts generated by the movements of the cables (Section 2.2), while the latter includes those related to the phenomena occurring at the electrode level (i.e., Sections 2.1 and 2.3). In the following sections, we will describe the development and application of two EEG caps specifically designed to experimentally investigate the sources of motion artifacts identified in the previous paragraphs. Two customized EEG electrode systems have been designed to isolate the sources of motion artifacts and test the hypothesis on artifact genesis. The first EEG cap, hereafter referred to as ET Cap, is a textile-based system with electrical connections embedded into the fabric to minimize the effects of cable movement. The second EEG cap, named Lobster Cap, consists of a flexible PCB-based EEG electrode system aimed at reducing the effect of both connecting cables and electrode movement.

### *4.1. ET Cap: Textile-Based EEG Electrodes System*

Figure 7 shows the textile-based EEG electrode system (ET Cap). Figure 7A depicts the construction details of the textile traces. A commercially available EEG cap with thirty head-mounted electrodes (EasyCap GmbH, Gliching, Germany) was modified and adapted to our purposes. Specifically, the wires connecting the electrodes to the input amplifier have been replaced by conductive traces embedded in the fabric of the cap through a sewing machine. These traces are made of a conductive material coated with a thin insulating glaze (FIW diameter Ø = 0.1 mm, ELEKTRISOLA, Germany). The traces were incorporated into the textile substrate using a sinusoidal design to enhance the stretchability and reduce the mechanical stress on the wires during movements. Sinusoidal-shaped traces have been connected between a residual part of the electrode native cable (~5 mm), and the soldering pads of a flexible printed-circuits adaptor housing an FFC connector used to connect the cap with the MEACS EEG acquisition system [4,39] (ReC Bioengineering Laboratories and LISiN, Turin, Italy). To strengthen the welding points and to prevent their disruption, the electrode-textile traces connections were further reinforced through an epoxy adhesive glue (Pattex Power Epoxy), while the

soldering pads of the connector side were covered with a thin layer of silicone (RS PRO, Corbym, UK). The flexible PCB adapter was fixed onto the cap itself to minimize the cable lengths with the aim of placing the acquisition system on top of the head (see Figure 7B for details). Since the electrode technology was not changed with respect to the native one, the site preparation followed the practices in force for a standard EEG cap [21,30,40].

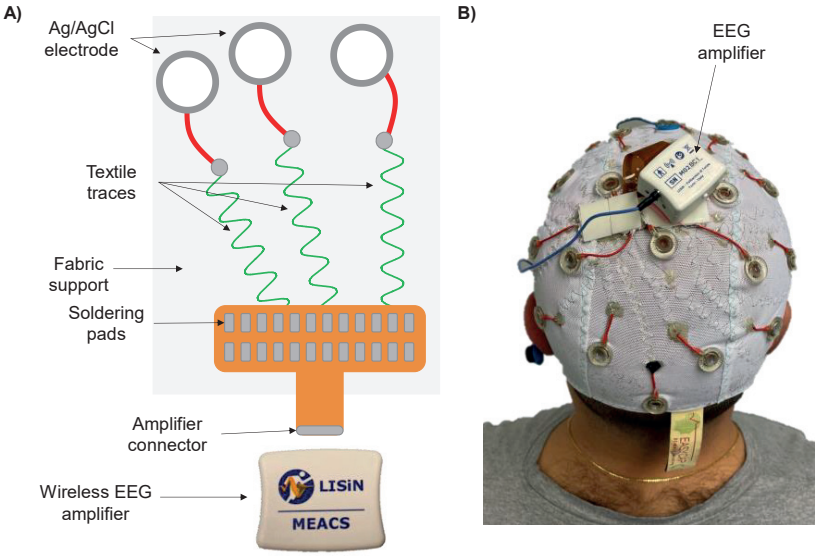


**Figure 7.** ET Cap. (**A**) Schematic representation of the textile traces sewed onto the EEG cap fabric and further connected to the exploring electrodes and the flexible connector constituting the input of the EEG amplifier. (**B**) Picture of a subject wearing the textile-based electrode system connected to the EEG amplifier.

### *4.2. Lobster Cap: Flexible PCB-Based EEG Electrodes System*

Figure 8 depicts the flexible PCB-based EEG electrode system (named Lobster Cap due to its shape, Figure 8A). It is a two-dimensional flexible system of electrodes with both electrodes and traces integrated into a flexible polyimide substrate (80 μm thick). The flexible printed circuit connects thirty silver ring-shaped electrodes (inner diameter Ø = 0.8 mm) to the input connector of the EEG acquisition system. Each electrode site is labelled according to the 10–20 system as they are intended to be placed on the subject's scalp according to the standardized positions identified and marked prior to the measurements. The Lobster Cap was designed to facilitate the adhesion of its branches to the subject's scalp to prevent electrode movements, thus limiting cables and electrode movements, identified as causes of movement artifacts (Sections 2 and 3). Figure 8B reports the detail of a single electrode showing three main layers allowing its adhesion to the scalp: a first double-sided adhesive tape (1 mm thick), an FR4 ring (~1 mm thick) needed to give mechanical support and to facilitate its bonding to the scalp through a final layer of biocompatible glue (Histoacryl, Braun Medical, Germany) used to further fix the electrodes in the correct position and avoid their relative movement with respect to the scalp. Finally, the electrode design included a ring shape allowing the user to inject the conductive gel after the electrode placement. Because of its design, the Lobster Cap is characterized by the total absence of free-to-move electrodes and connecting cables. It can also fit different head circumferences since the length of the different branches of the electrodes system are purposely designed to have a small slack allowing for a correct placement according to the subjects' scalp size. Figure 8C shows the final stage with the Lobster Cap applied to a subject. It is important to underline that the designed solution is not intended to be used in a wide range of standard EEG measures due to the fact that it can be used only on bald subjects and the electrode preparation is complex and time-consuming. Instead, it was specifically designed as a research tool to study the generation

of motion artifacts by mitigating two of their primary causes: movement of the cables and electrodes.

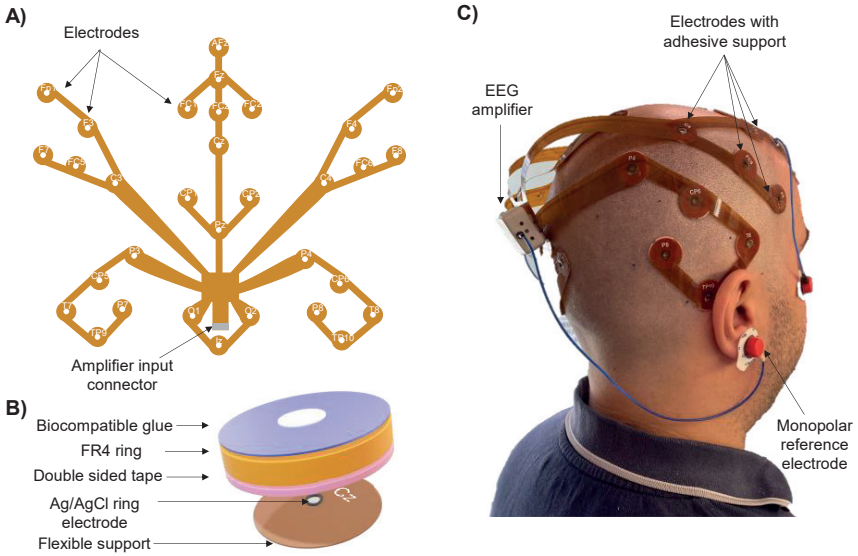


**Figure 8.** Lobster Cap. (**A**) Design of the entire system based on printed circuits on a flexible support. (**B**) Details of a single electrode preparation. An FR4 ring is attached on top of the electrode through a double-sided adhesive tape. Electrodes are then attached to the scalp by means of a biocompatible glue. (**C**) Picture of a subject wearing the Lobster Cap connected to the EEG amplifier.

## 5. Case Study

An experimental study was carried out to demonstrate the hypotheses on the genesis of motion artifacts in dynamic EEG. Since it is not possible to experimentally separate the abovementioned three possible sources of motion artifacts, a mixed effect is expected to occur as an effect of cable- and electrode-related artifacts on EEG signals during movements. To this end, we detected EEG signals during dynamic motor tasks with both standard (i.e., wet electrodes with connecting cables to the amplifier) and the customized caps described in the previous section (i.e., ET Cap and Lobster Cap prototypes). Time- and frequency-domain variables were extracted to investigate the influence of cables and electrode technologies to give further grounds and experimentally investigate the hypotheses modelled in the previous sections.

### *5.1. Experimental Design*

The study was conducted on a bald subject after having received approval from the University of Jyväskylä's Ethics Committee in accordance with the Declaration of Helsinki. Figure 9 shows the four EEG electrode systems used in the study: (A) a standard cap (*STN Cap)*, (B) the *ET Cap*, (C) the *Lobster-w Cap*, and (D) the *Lobster Cap*. The *STN* cap is a standard head-mounted electrode cap (EasyCap GmbH, Gliching, Germany) with 50 cm long cables between the electrode and the input connector of the acquisition system (Figure 9A); the *ET Cap* is the textile-based system (Figure 9B); the *Lobster-w Cap* is obtained from the Lobster Cap by adding a custom-made adapter constituted by 50 cm long connecting cables (Figure 9C); the *Lobster Cap* is the flexible PCB-based EEG electrodes system with no additional cables (Figure 9D). The four tested solutions were chosen to maximize the isolation of the identified sources of artifacts (i.e., cable movement and electrode shifts) in the experimental settings. Thirty EEG and two Electrooculograms (EOG) signals were recorded through a wireless EEG amplifier with a sampling frequency of 2048 Hz [2] (MEACS, ReC Bioengineering Laboratories and LISiN, Turin, Italy). The EEG channels involved in the recordings were the same for all four tested EEG electrode

systems following the layout of the standard EEG cap (EasyCap–BC-TMS-32). Electrodes were placed according to the 10-20 EEG system as reported in Figure 10—Schematic illustration of the electrode layout used for the study (30 EEG channels with the reference electrode placed on the right ear lobe). The table of coordinates can be found in Figure 10 [41]. The experimental setup also included a general-purpose acquisition unit collecting magneto-inertial signals (100 Hz sampling frequency) placed on the head to track its acceleration, while a second unit (DuePro, OT Bioelettronica, Turin, Italy) was used to collect an additional analog signal from a footswitch (force sensor-FlexiForce A201, Tekscan, Norwood, USA) placed under the right heel (2048 Hz sampling frequency). The synchronization unit introduced in [2] was adopted to synchronize all the abovementioned signals. The experimental protocol dealt with the repetition of three tasks: 60 s of (i) standing balance considered as a rest condition, (ii) treadmill walking at 4.6 km/h, and (iii) jogging at 6 km/h. Measurements were carried out on four different days (one EEG cap per day) to avoid any influence of consecutive scalp preparations on electrode-skin impedances. Subject preparation was performed following the recommended steps of electrode site abrasion and conductive gel injection [42]. At first, an abrasive paste (NuPrep, Weaver and Company, Aurora, CO, USA) was used to gently scrub the scalp by abrading the entire surface. Afterwards, the EEG electrode system was positioned and a conductive gel (NeurGel, SPES MEDICA, Genova, Italy) was inserted into the electrode cavities. Two additional electrodes (30 mm × 22 mm, Ambu s.r.l., Ballerup Denmark) placed in the upper-left and lower-right corners of the subject's eyes were used to record EOG signals. Finally, a further adhesive electrode (Ø = 24 mm, Kendall, Covidien-Medtronic, Minneapolis, MN, USA) was placed on the right ear lobe after a gentle skin abrasion and it served as the monopolar reference site for the EEG signals recordings. This reference electrode positioning was chosen both to standardize the reference electrode technology among the tested conditions and to minimize its movements. Indeed, being EEG signals recorded in a monopolar signal configuration, artifacts generated by the movements of the reference electrode could be confounding factors for the current artifact analysis.

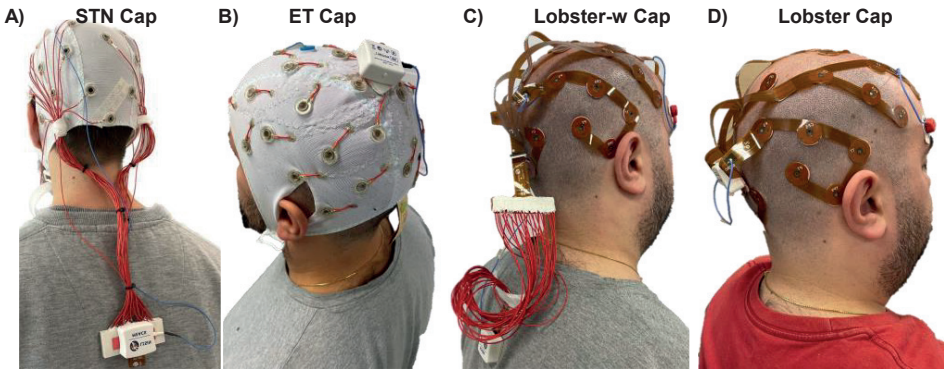


**Figure 9.** EEG electrodes systems used in the experimental case study: (**A**) STN—standard head-mounted electrodes with connecting cables, (**B**) ET Cap—textile-based system, (**C**) Lobster-w Cap flexible PCB-based system with connecting cables, (**D**) Lobster Cap flexible PCB-based system.

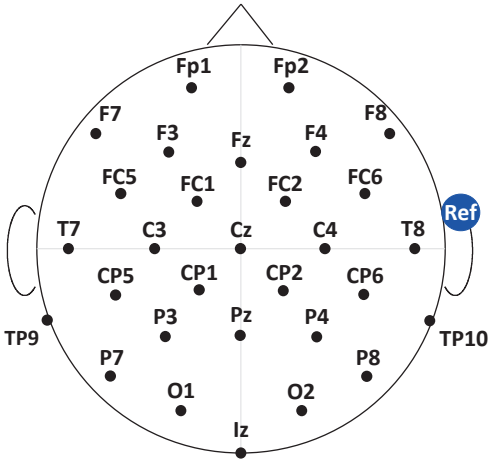


**Figure 10.** Schematic illustration of the electrode layout used for the study (30 EEG channels with the reference electrode placed on the right ear lobe). The table of coordinates can be found at [41]. Electrodes labels are reported according to the 10–20 system.

*5.2. Data Analysis*

EEG signals were initially evaluated through visual inspection to exclude possible interference caused by poor electrode-skin contact to avoid this confounding factor. However, no missing contacts were found in the current data, and thus there were no rejected channels. In addition, we did not apply standard artifact correction algorithms, such as independent component analysis, to keep intact both the artifacts and the brain signal. We used the Matlab Software R2022b (Mathwork Inc., Natick, MA, USA) to carry out the analyses both in time and frequency domains that are described in the following. Statistical analyses were performed using R Statistical Software (v4.1.2; R Core Team 2021). EEG signals were acquired with a bandwidth between 0.1 Hz and 500 Hz [2]. They were further pre-processed offline through a fourth-order Butterworth bandpass filter (0.1 Hz–100 Hz), and then a common average reference approach was used to subtract the average of all the channels from each individual EEG channel. For the offline re-referencing, we did not include the initial reference when computing the average signal to correct for the intrinsic rank deficiency of the monopolar referenced EEG data [43]. However, although it does not ensure a full rank of the data, it does not affect our evaluation in this study.

In light of what was discussed in the sections above, we expected signals corrupted by motion artifacts to be characterized by greater amplitudes. We therefore estimated the median Root-Mean-Square (RMS) value over 1-s epochs (50% overlap) for each signal. A one-way repeated measures ANOVA statistical test (Tukey's post-hoc correction) was applied to the RMS values to evaluate the effect of the EEG electrodes system on the recorded signal amplitudes. Afterwards, we identified two types of motion artifacts corrupting EEG signals and they are shown in Figure 11 as an example taken from the experimental observations. The former artifacts are characterized by spurious spike-like motion artifacts most likely generated by the movements of the cables, whereas the latter artifacts are displayed as strides-related low-frequency variations and they are likely due to the movements of the electrodes (Sections 2.1 and 2.2).

On one hand, to better investigate the influence of the cables, we compared the results of "cabled" electrode systems (STN and Lobster-w caps) to those of "non-cabled" caps (ET and Lobster). Therefore, the comparison was performed between the STN vs. ET caps and between the Lobster-w vs. Lobster Cap, having the same electrode technology. We hypothesized the presence of spurious spike-like artifacts to result in a heterogeneous distribution of amplitude values among EEG channels according to what was observed in Figure 2.

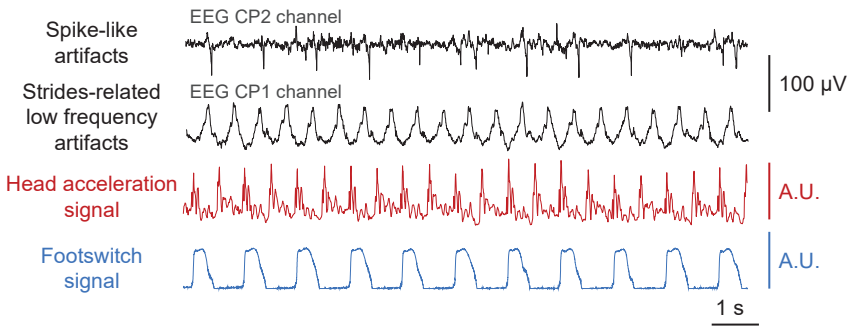


**Figure 11.** Examples of recorded EEG motion artifacts: spike-like and strides-related low-frequency artifacts recorded through a standard EEG electrode system. The head acceleration signal (Euclidean norm) and the force signal collected from the right heel are also reported timewise.

Thus, we first assessed the median kurtosis value of the amplitudes of the recorded EEG signals over 1 s long epochs (50% overlap). Then, the heterogeneity of the kurtosis values within the 30-EEG channels of the different electrode systems was quantified by calculating the variation coefficient for each kurtosis distribution. On the other hand, the effect of the electrode type was evaluated by comparing the results of the two custom-made solutions i.e., ET vs. Lobster caps. We expected repeatable artifacts time-locked to the heel strikes as shown in Figure 1 (i.e., strongly correlated with the gait frequency) when using standard electrodes (ET cap), with little to no strides-triggered artifacts when using electrodes attached to the scalp (Lobster cap). As a result, we used a two-step procedure to further assess the effect of the electrodes. At first, the wavelet coherence between cortical signals and the head acceleration signal was computed using the Matlab function coherence with default parameters (Morlet wavelet, 12 voices per octave, 15 octaves). The coherence spectra were averaged over time to identify the six EEG signals (i.e., 20% of the total amount of available channels) showing the highest coherence values. Afterwards, we extracted the average cortical response of the most coherent channels through a spike-triggered averaging technique with respect to the right heel strikes. Thus, the peak-to-peak amplitude values of the averaged response were finally compared to quantify the effect of electrode-related motion artifacts.

### *5.3. Results*

Figure 12 shows RMS amplitude values of the EEG signals recorded with the four electrode systems during rest, treadmill walking, and jogging. No statistically significant differences were found among RMS values of EEG signals recorded through the four electrode systems with the subject at rest or performing a treadmill walking task, except for the comparison between the cabled vs. non-cabled electrodes system (i.e., Lobster-w vs. Lobster). Results from the jogging task revealed, instead, statistically significant differences between RMS values obtained by cabled (STN and Lobster-w caps) versus non-cabled solutions (ET and Lobster caps). Additionally, further statistically significant differences were highlighted also between the STN versus the Lobster Cap.

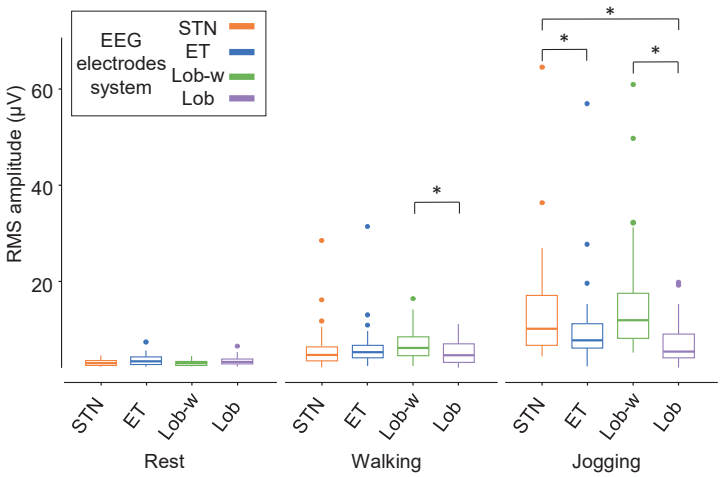


**Figure 12.** Boxplot of RMS amplitude values of 30 EEG signals recorded with the four electrode systems during rest, treadmill walking, and jogging. * $p < 0.05$ obtained with one-way ANOVA (Tukey post-hoc correction).

Figure 13 represents the kurtosis values distributions and their coefficients of variation calculated on the 30 EEG signals with the four electrode systems in all the performed tasks. According to our hypotheses, the greater the task dynamics and the resulting cable movements, the more heterogeneous the amplitude signal distribution because of a higher occurrence of spike-like artifacts. Therefore, the highest RMS values accompanied by the greatest variation coefficients of the kurtosis values were expected for signals recorded through cabled electrode systems during the jogging task. In line with these expectations, although it is not possible to robustly disentangle cable and electrode effects in the experimental practice as they both contribute to an overall increase of the recorded signal amplitudes, these observations suggest that the most discriminating factor influencing the EEG signals amplitude is the movement of the cables. Indeed, Figures 12 and 13 demonstrated that STN and Lobster-w caps (i.e., cabled) showed on average higher RMS amplitudes with a wider distribution according to the increase of task dynamics.

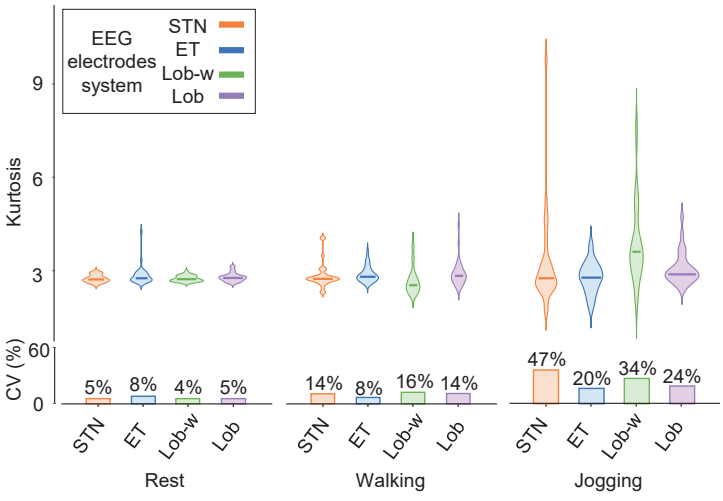


**Figure 13.** Top panel: violin plots displaying the median values of kurtosis computed over 1-s epochs for 30 EEG signals recorded through the four electrode systems in all the performed tasks. Bottom panel: bar diagrams of coefficients of variation (CV) of kurtosis values over the EEG electrodes in all the performed tasks.

Figure 14 shows the cortical responses averaged with respect to the right heel strikes across strides (n = 54 walking, n = 70 jogging) considering the most coherent channels with head acceleration during walking and jogging. Although different morphologies of cortical responses (e.g., even showing different polarities) might occur at the intra-electrode level, we found motion artifacts time-locked to the heel strikes, with high intra-electrode repeatability. In line with our expectations and discussions at the electrical modelling level, higher peak-to-peak amplitude values were obtained for the cortical responses recorded with the ET cap when compared to the Lobster cap (24.70 μV vs. 7.23 μV and 46.03 μV vs. 7.64 μV respectively during walking and jogging).

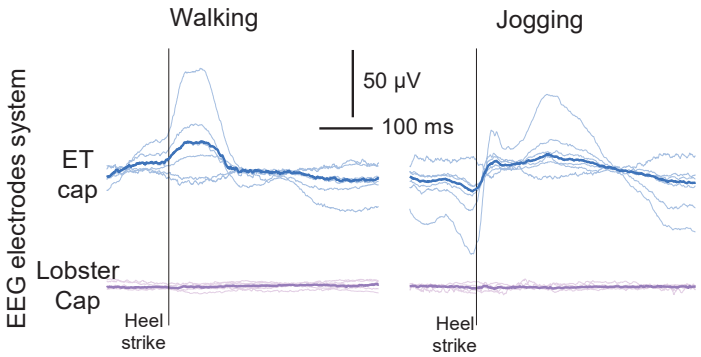


**Figure 14.** Averaged cortical responses with respect to the right heel strike onset were obtained from EEG signals recorded through the ET cap (blue traces) and the Lobster cap (violet traces) during walking and jogging motor tasks. Only the most 6 coherent EEG signals with the head acceleration are displayed.

## 6. Discussion and Conclusions

The present study delved into the investigation of the genesis of motion artifacts collected during dynamic EEG recordings. An in-depth analysis of the underlying phenomena through electrical models and experimental tests has been performed. Given the availability of miniaturized and wireless EEG acquisition systems, the analytical approach highlighted two residual sites responsible for motion artifacts contamination of EEG signals: (i) the connecting cables between the electrodes and the amplifier and (ii) the sudden changes of electrode-skin impedance due to the electrodes movements. It is worth noting that the conducted experimental setup was not intended to separately investigate the analytically described sources of motion artifacts. Indeed, it is unlikely to experimentally disentangle the main causes of motion artifacts as a combined effect of cables and electrodes is expected to occur. Nevertheless, the experimental results showed that minimizing the length of the EEG electrode systems connecting cables and ensuring stable electrode contacts mitigates the EEG signal motion artifacts. Therefore, this outcome contributed to endorsing the analytical study of the phenomena hindering the genesis of EEG motion artifacts.

The observed case study was performed only on a single subject. Although this may be considered a possible limitation of the experimental part of this work, it is important to underline that the aim of the study is not to study the collection of movement artifacts among a population, but rather to validate a possible electrical modelling framework allowing to better understand possible sources of motion artifacts during EEG signals collection. Therefore, the primary aim of the study was to collect a set of EEG signals, without consideration of the physiological response underlying the studied tasks that would require a population of subjects.

Two customized EEG electrode systems have been designed and proposed. Data analysis on EEG recorded during dynamic tasks (i.e., walking and jogging) experimentally demonstrated that when the movements of both cables and electrodes are

minimized, it is possible to record high-quality EEG signals even during dynamic movements. In light of what was obtained, practical considerations can be drawn up when dealing with EEG acquisition during movements:

- **Amplifier technology:** the state-of-art technology on miniaturized and wireless EEG acquisition systems seems to efficiently address the need for lightweight technology allowing for enough freedom of movement while recording brain signals [2,3,44]. In this regard, the use of active electrodes in the system electronics is intrinsically demonstrated not to provide an appreciable contribution in terms of mitigating motion artifact contamination on EEG signals. Indeed, their main contribution is to reduce the effect of capacitive coupling occurring downstream of the electrodes (e.g., parasitic capacitive coupling between connecting cables and power lines) [30]. On the contrary, their implementation becomes ineffectual towards electrode impedance imbalances occurring upstream the electrodes (i.e., $\Delta Z_e$ from (2)). This finding is in line with what was shown by Laszlo et al. [14] who experimentally showed that during rapid voltage fluctuations active electrodes are equally affected by movement artifacts related to changes at the electrode-skin interface with respect to passive electrodes. Conversely, the undesired result of using active electrodes in such contexts is the increase of the total system encumbrance and power consumption, thus contrasting with the need to develop miniaturized instrumentation.
- **Setup preparation:** Given that an ad-hoc preparation of the electrode sites is mandatory to ensure similar electrode-skin impedances magnitude among all the channels (i.e., to minimize $\Delta Z_e$ of (2) and (6)), it is also preferable to ensure a stable skin contact by avoiding temporary and brisk skin-electrodes detachments causing sudden electrodes impedance changes. This consideration applies also when dealing with the monopolar reference electrode as it affects all the recorded signals. Therefore, good practice recommendations regard the use of adhesive monopolar reference electrodes, preferably placed in body regions with limited movements (i.e., ear lobe). This is particularly important when recording electrophysiological signals under a monopolar signal configuration as perturbations additively interfering with the reference signal would affect all the channels. It could be hard to completely filter out these undesired perturbations e.g., by applying a common average filtering due to the superimposition of multiple confounding factors (i.e., additive noise, motion artifacts, etc.) simultaneously occurring at the level of exploring electrodes. In this regard, particular attention should be paid when applying re-referencing techniques, considering also possible processing-related needs [43].
- **Cap technology:** the choice of the EEG electrode system has a non-negligible influence on the quality of the collected signals in terms of motion artifact contamination. Indeed, as experimentally suggested by the proposed case study, the ideal case would be to keep the electrodes as fixed as possible such as in the case of the Lobster Cap. However, this type of solution, although optimal in terms of the quality of collected signals, holds intrinsic limitations from the applicability point of view: (i) it is usable only on either bald or short-haired subjects and (ii) it might require longer preparation times. However, considering the need for minimization of the connecting cable length and related reciprocal movements to mitigate the effects of triboelectric-related phenomena, embedding the connecting cables into the fabric of the cap of electrodes such as in the ET Cap could be a good compromise between usability and performance needs. Further technological advancements should therefore focus on the transduction stage of the biopotentials amplification chain such as the electrode technology and its interfacing to the acquisition system.

Although the present study focused on EEG signals during movements given their great clinical significance and relatively low signal-to-noise ratio, similar considerations may be applied to any biopotential acquired through surface electrodes.

In conclusion, the work presented herein constitutes a solid and widespread framework for modelling and understanding bio-electrical phenomena underlying the collection of motion artifacts during dynamic EEG. The insights, explanations and findings from this work could significantly contribute to driving technological developments and guide experimental setup practices in the field of dynamic EEG acquisitions.

## 7. Patent

An Italian patent application has been proposed by Politecnico di Torino for the ET Cap described in this study. All the authors have been recognized as inventors.

**Author Contributions:** A.G.: conceptualization; data collection; methodology; data analysis; data visualization and interpretation; writing-original draft. A.B.: conceptualization; methodology; data analysis; data visualization and interpretation; writing-original draft. H.P.: conceptualization; methodology; supervision. G.L.C.: conceptualization; data collection; resources; methodology; data visualization and interpretation supervision; writing-original draft, supervision. All authors have read and agreed to the published version of the manuscript.

**Funding:** The study was supported by the Academy of Finland grant (#296240) to H.P. and PhD scholarships promoted by Politecnico di Torino (090804, DET-Sensorimotor integration and corticomuscular coupling) and the Faculty of Sports and Health Sciences of the University of Jyväskylä to A.G (February-December 2024). G.L.C. holds a JYU fellowship grant from February 2023 to October 2023 (1643/13.00.05.00/2022) promoted by the JYU Visiting Fellow Programme Grant 2023.

**Institutional Review Board Statement:** The study was conducted in accordance with the Declaration of Helsinki, and approved by the Ethics Committee of the University of Jyväskylä (approval number: 369/13.00.04.00/2020).

**Informed Consent Statement:** Informed consent was obtained from the subject involved in the study.

**Data Availability Statement:** The data are not publicly available due to privacy or ethical restrictions. However, data are available upon request from the corresponding author.

**Conflicts of Interest:** A.B. and G.L.C. are involved in the activities of ReC Bioengineering Laboratories, a spin-off of the Laboratory for Engineering of the Neuromuscular System (Politecnico di Torino, Italy), which produces and commercializes devices for neuromuscular system assessment. The findings described in this paper are of general interest in the field of biomedical instrumentation and are not intended to promote or advertise any product or services of the company.

## References

1. Gwin, J.T.; Gramann, K.; Makeig, S.; Ferris, D.P. Removal of movement artifact from high-density EEG recorded during walking and running. *J. Neurophysiol.* **2010**, *103*, 3526–3534. https://doi.org/10.1152/jn.00105.2010.
2. Cerone, G.L.; Giangrande, A.; Ghislieri, M.; Gazzoni, M.; Piitulainen, H.; Botter, A. Design and Validation of a Wireless Body Sensor Network for Integrated EEG and HD-sEMG Acquisitions. *IEEE Trans. Neural Syst. Rehabil. Eng.* **2022**, *30*, 61–71. https://doi.org/10.1109/TNSRE.2022.3140220.
3. Niso, G.; Romero, E.; Moreau, J.T.; Araujo, A.; Krol, L.R. Wireless EEG: A survey of systems and studies. *Neuroimage* **2023**, *269*, 119774. https://doi.org/10.1016/j.neuroimage.2022.119774.
4. Cohen, J.W.; Vieira, T.; Ivanova, T.D.; Cerone, G.L.; Garland, S.J. Maintenance of standing posture during multi-directional leaning demands the recruitment of task-specific motor units in the ankle plantarflexors. *Exp. Brain Res.* **2021**, *239*, 2569–2581. https://doi.org/10.1007/s00221-021-06154-0.
5. dos Anjos, F.V.; Ghislieri, M.; Cerone, G.L.; Pinto, T.P.; Gazzoni, M. Changes in the distribution of muscle activity when using a passive trunk exoskeleton depend on the type of working task: A high-density surface EMG study. *J. Biomech.* **2022**, *130*, 110846. https://doi.org/10.1016/j.jbiomech.2021.110846.
6. Cerone, G.L.; Nicola, R.; Caruso, M.; Rossanigo, R.; Cereatti, A.; Vieira, T.M. Running speed changes the distribution of excitation within the biceps femoris muscle in 80 m sprints. *Scand. J. Med. Sci. Sport.* **2023**, *33*, 1104–1115. https://doi.org/10.1111/sms.14341.
7. Puce, A.; Hämäläinen, M.S. A review of issues related to data acquisition and analysis in EEG/MEG studies. *Brain Sci.* **2017**, *7*, 58. https://doi.org/10.3390/brainsci7060058.
8. Tandle, A.; Jog, N.; D'cunha, P.; Chheta, M. Classification of Artefacts in EEG Signal Recordings and Overview of Removing Techniques. *Int. J. Comput. Appl.* **2015**, *46*, 8887.

9. Kline, J.E.; Huang, H.J.; Snyder, K.L.; Ferris, D.P. Isolating gait-related movement artifacts in electroencephalography during human walking. *J. Neural Eng.* **2015**, *12*, 046022. https://doi.org/10.1088/1741-2560/12/4/046022.
10. Gwin, J.T.; Gramann, K.; Makeig, S.; Ferris, D.P. Electrocortical activity is coupled to gait cycle phase during treadmill walking. *Neuroimage* **2011**, *54*, 1289–1296. https://doi.org/10.1016/j.neuroimage.2010.08.066.
11. Neuper, C.; Pfurtscheller, G. Event-related dynamics of cortical rhythms: Frequency-specific features and functional correlates. *Int. J. Psychophysiol.* **2001**, *43*, 41–58. https://doi.org/10.1016/S0167-8760(01)00178-7.
12. Gorjan, D.; Gramann, K.; De Pauw, K.; Marusic, U. Removal of movement-induced EEG artifacts: Current state of the art and guidelines. *J. Neural Eng.* **2022**, *19*, 011004. https://doi.org/10.1088/1741-2552/ac542c.
13. MettingVanRijn, A.C.; Kuiper, A.P.; Dankers, T.E.; Grimbergen, C.A. Low-cost active electrode improves the resolution in biopotential recordings. In Proceedings of the 18th Annual International Conference of the IEEE Engineering in Medicine and Biology Society, Amsterdam, The Netherlands, 31 October 1996–3 November 1996; pp. 101–102. https://doi.org/10.1109/iembs.1996.656866.
14. Laszlo, S.; Ruiz-Blondet, M.; Khalifian, N.; Chu, F.; Jin, Z. A direct comparison of active and passive amplification electrodes in the same amplifier system. *J. Neurosci. Methods* **2014**, *235*, 298–307. https://doi.org/10.1016/j.jneumeth.2014.05.012.
15. Tseghai, G.B.; Malengier, B.; Fante, K.A.; Van Langenhove, L. The Status of Textile-Based Dry Eeg Electrodes. *Autex Res. J.* **2021**, *21*, 63–70. https://doi.org/10.2478/aut-2019-0071.
16. Delaux, A.; de Saint Aubert, J.B.; Ramanoël, S.; Bécu, M.; Gehrke, L.; Klug, M.; Arleo, A. Mobile brain or body imaging of landmark-based navigation with high-density EEG. *Eur. J. Neurosci.* **2021**, *54*, 8256–8282.
17. Kim, H.; Miyakoshi, M.; Iversen, J.R. Approaches for Hybrid Coregistration of Marker-Based and Markerless Coordinates Describing Complex Body/Object Interactions. *Sensors* **2023**, *23*, 6542. https://doi.org/10.3390/s23146542.
18. DRobles; Kuziek, J.W.P.; Wlasitz, N.A.; Bartlett, N.T.; Hurd, P.L.; Mathewson, K.E. EEG in motion: Using an oddball task to explore motor interference in active skateboarding. *Eur. J. Neurosci.* **2021**, *54*, 8196–8213. https://doi.org/10.1111/ejn.15163.
19. De Talhouet, H.; Webster, J.G. The origin of skin-stretch-caused motion artifacts under electrodes. *Physiol. Meas.* **1996**, *17*, 81. https://doi.org/10.1088/0967-3334/17/2/003.
20. Webster, J.G. Reducing Motion Artifacts and Interference in Biopotential Recording. *IEEE Trans. Biomed. Eng.* **1984**, *31*, 823–826. https://doi.org/10.1109/TBME.1984.325244.
21. Merletti, R.; Cerone, G.L. Tutorial. Surface EMG detection, conditioning and pre-processing: Best practices. *J. Electromyogr. Kinesiol.* **2020**, *54*, 102440. https://doi.org/10.1016/j.jelekin.2020.102440.
22. Cerone, G.L.; Botter, A.; Gazzoni, M. A modular, smart, and wearable system for high density sEMG detection. *IEEE Trans. Neural Syst. Rehabil. Eng.* **2019**, *66*, 3371–3380.
23. Yaziciouglu, F.R.; Van Hoof, C.; Puers, R. Introduction to Biopotential Acquisition. In *Biopotential Readout Circuits for Portable Acquisition Systems*; Springer: Dordrecht, The Netherlands, 2009; pp. 5–19.
24. Ratz, A.G. Triboelectric noise (Triboelectric noise in mechanically flexed low level signal cables for piezoelectric transducers with high gain amplifiers). *ISA Trans.* **1969**, *9*, 154–158.
25. Wartzek, T.; Lammersen, T.; Eilebrecht, B.; Walter, M.; Leonhardt, S. Triboelectricity in capacitive biopotential measurements. *IEEE Trans. Biomed. Eng.* **2011**, *58*, 1268–1277. https://doi.org/10.1109/TBME.2010.2100393.
26. Botter, A.; Vieira, T.M. Filtered virtual reference: A new method for the reduction of power line interference with minimal distortion of monopolar surface EMG. *IEEE Trans. Biomed. Eng.* **2015**, *62*, 2638–2647. https://doi.org/10.1109/TBME.2015.2438335.
27. Chi, Y.M.; Maier, C.; Cauwenberghs, G. Ultra-high input impedance, low noise integrated amplifier for noncontact biopotential sensing. *IEEE J. Emerg. Sel. Top. Circuits Syst.* **2011**, *1*, 526–535. https://doi.org/10.1109/JETCAS.2011.2179419.
28. van Rijn, A.C.M.; Peper, A.; Grimbergen, C.A. High-quality recording of bioelectric events. *Med. Biol. Eng. Comput.* **1990**, *28*, 389–397. https://doi.org/10.1007/bf02441961.
29. Spinelli, E.M.; Pallàs-Areny, R.; Mayosky, M.A. AC-coupled front-end for biopotential measurements. *IEEE Trans. Biomed. Eng.* **2003**, *50*, 391–395. https://doi.org/10.1109/TBME.2003.808826.
30. Spinelli, E.; Guerrero, F.N. *The Biological Amplifier*; World Scientific Publishing: Singapore, 2017; pp. 463–500. https://doi.org/10.1142/9789813147263_0012.
31. Klijn, J.A.J.; Kloprogge, M.J.G.M. Movement artefact suppressor during ECG monitoring. *Cardiovasc. Res.* **1974**, *8*, 149–152. https://doi.org/10.1093/cvrese/8.1.149.
32. Winter, B.B.; Winter, B.B. Driven-Right-Leg Circuit Design. *IEEE Trans. Biomed. Eng.* **1983**, *30*, 62–66. https://doi.org/10.1109/TBME.1983.325168.
33. Dobrev, D.; Neycheva, T.; Mudrov, N. Simple two-electrode biosignal amplifier. *Med. Biol. Eng. Comput.* **2005**, *43*, 725–730. https://doi.org/10.1007/BF02430949.
34. Dobrev, D. Two-electrode non-differential biopotential amplifier. *Med. Biol. Eng. Comput.* **2002**, *40*, 546–549. https://doi.org/10.1007/BF02345453.
35. Dobrev, D.P.; Neycheva, T.; Mudrov, N. Bootstrapped two-electrode biosignal amplifier. *Med. Biol. Eng. Comput.* **2008**, *46*, 613–619. https://doi.org/10.1007/s11517-008-0312-4.
36. Pallás-Areny, R.; Webster, J.G. Composite instrumentation amplifier for biopotentials. *Ann. Biomed. Eng.* **1990**, *18*, 251–262. https://doi.org/10.1007/BF02368441.
37. Burbank, D.P.; Webster, J.G. Reducing skin potential motion artefact by skin abrasion. *Med. Biol. Eng. Comput.* **1978**, *16*, 31–38. https://doi.org/10.1007/BF02442929.

38. Dellacorna. (12) Patent Application Publication (10). U.S. Patent US2006/0287608A1, 2006.
39. Cerone, G.L.; Giangrande, A.; Vieira, T.; Pisaturo, D.; Ionescu, M.; Gazzoni, M.; Botter, A. Design of a Programmable and Modular Neuromuscular Electrical Stimulator Integrated into a Wireless Body Sensor Network. *IEEE Access* **2021**, *9*, 163284–163296. https://doi.org/10.1109/ACCESS.2021.3133096.
40. Cattarello, P.; Merletti, R. Characterization of dry and wet Electrode-Skin interfaces on different skin treatments for HDsEMG. In Proceedings of the 2016 IEEE International Symposium on Medical Measurements and Applications (MeMeA), Benevento, Italy, 15–18 May 2016; pp. 1–6. https://doi.org/10.1109/MeMeA.2016.7533808.
41. EasyCap. EasyCap—BC-TMS-32-X6. Available online: https://cdn.shopify.com/s/files/1/0669/3729/1066/files/BC-TMS-32-X6.pdf?v=1697728138 (accessed on 9th August 2024).
42. Hari, R.; Puce, A. *MEG-EEG Primer*; Oxford University Press: Oxford, UK, 2017.
43. Kim, H.; Luo, J.; Chu, S.; Cannard, C.; Hoffmann, S.; Miyakoshi, M. ICA's bug: How ghost ICs emerge from effective rank deficiency caused by EEG electrode interpolation and incorrect re-referencing. *Front. Signal Process.* **2023**, *3*, 1–9. https://doi.org/10.3389/frsip.2023.1064138.
44. Shovon, S.K.F.A.; Islam, M.N.; Islam, M.R.; Rahaman, M.L.; Sadikuzzaman, M.; Chowdhury, M.I.B. Design of an Integrated Wireless Wearable Biosensor; pp. 2–5.

# IV

# MAINTAINED VOLITIONAL ACTIVATION OF THE MUSCLE ALTERS THE CORTICAL PROCESSING OF PROPRIOCEPTIVE AFFERENCE FROM THE ANKLE JOINT

by

A. Giangrande, T. Mujunen, G. L. Cerone, A. Botter, and H. Piitulainen

*Neuroscience*, 560: 314-325, 2024.

https://doi.org/10.1016/j.neuroscience.2024.09.049

Neuroscience 560 (2024) 314–325

Contents lists available at ScienceDirect

Neuroscience

journal homepage: www.elsevier.com/locate/nsc

# Maintained volitional activation of the muscle alters the cortical processing of proprioceptive afference from the ankle joint

Alessandra Giangrande [a,b,*], Toni Mujunen [a], Giacinto Luigi Cerone [b], Alberto Botter [b], Harri Piitulainen [a]

[a] Faculty of Sport and Health Sciences, University of Jyväskylä, Jyväskylä, Finland
[b] Laboratory of Neuromuscular System and Rehabilitation Engineering, Department of Electronics and Telecommunications, Politecnico di Torino, Turin, Italy

ARTICLE INFO

*Keywords:*
Electroencephalography
Proprioception
Beta modulations
Somatosensory processing

ABSTRACT

Cortical proprioceptive processing of intermittent, passive movements can be assessed by extracting evoked and induced electroencephalographic (EEG) responses to somatosensory stimuli. Although the existent prior research on somatosensory stimulations, it remains unknown to what extent ongoing volitional muscle activation modulates the proprioceptive cortical processing of passive ankle-joint rotations.

Twenty-five healthy volunteers (28.8 ± 7 yr, 14 males) underwent a total of 100 right ankle-joint passive rotations (4° dorsiflexions, 4 ± 0.25 s inter-stimulus interval, 30°/s peak angular velocity) evoked by a movement actuator during *passive* condition with relaxed ankle and *active* condition with a constant plantarflexion torque of 5 ± 2.5 Nm. Simultaneously, EEG, electromyographic (EMG) and kinematic signals were collected. Spatiotemporal features of evoked and induced EEG responses to the stimuli were extracted to estimate the modulation of the cortical proprioceptive processing between the *active* and *passive* conditions.

Proprioceptive stimuli during the *active* condition elicited robustly ~26 % larger evoked response and ~38 % larger beta suppression amplitudes, but ~42 % weaker beta rebound amplitude over the primary sensorimotor cortex than the *passive* condition, with no differences in terms of response latencies.

These findings indicate that the *active* volitional motor task during naturalistic proprioceptive stimulation of the ankle joint enhances related cortical activation and reduces related cortical inhibition with respect to the *passive* condition. Possible factors explaining these results include mechanisms occurring at several levels of the proprioceptive processing from the peripheral muscle (i.e. mechanical, muscle spindle status, etc.) to the different central (i.e. spinal, sub-cortical and cortical) levels.

## Introduction

The conscious sense of movement and posture of the body is referred to as proprioception (Proske and Gandevia, 2012). It is part of the somatosensory system that connects the periphery to the central nervous system through afferent pathways, mainly involving the dorsal column medial lemniscus pathway (Tuthill and Azim, 2018). Proprioceptors are mechanoreceptors located in the muscles and tendons (e.g. muscle spindles and Golgi tendon organs), joints (e.g. Golgi endings) and skin (e.g. Ruffini endings) (Taylor, 2009) sensitive to mechanical forces produced by the body or acting on it (Proske and Gandevia, 2012; Purves et al., 2018; Tuthill and Azim, 2018). Therefore, proprioceptors inform the brain about the state of the locomotor system. Changes in this state modulate the firing rate of the proprioceptors which is then transmitted to spinal cord, brainstem nuclei, cerebellum, thalamic nuclei and the cortex. The cortical target is wide spread, but most dense to the primary sensorimotor cortex (SM1), following specific topographic arrangements according to the modality and somatotopy (Purves et al., 2018). The role of proprioception is crucial in numerous every-day scenarios ranging from quiet standing (Gatev et al., 1999), locomotion (Farris and Sawicki, 2012) or efficient movement execution through an appropriate motor planning (Richardson et al., 2014). Therefore, impaired or improved proprioception has significant implications in training, ageing or motor diseases (Dietz, 2002; Ferlinc et al.,

*Abbreviations:* EEG, Electroencephalography; MEG, Magnetoencephalography; EMG, Electromyographic; ICA, Independent Component Analysis; EOG, Electrooculograms; RMS, Root Mean Square; TFR, Time-frequency representation; SM1, Primary somatosensory cortex.

* Corresponding author at: Faculty of Sport and Health Sciences, University of Jyväskylä, Jyväskylä, Finland.
*E-mail address:* alessandra.x.giangrande@jyu.fi (A. Giangrande).

https://doi.org/10.1016/j.neuroscience.2024.09.049
Received 7 May 2024; Accepted 28 September 2024
Available online 30 September 2024

2019; Han et al., 2016).

The quantification of the cortical processing of the proprioceptive input can provide tools to enhance the understanding in how the afferent information is integrated into movement control. To this purpose, neurophysiological recordings such as magnetoencephalography (MEG) and electroencephalography (EEG), have been used in combination with neuroimaging compatible movement actuators capable to produce accurate passive joint rotations (i.e. proprioceptive stimuli) (Piitulainen et al., 2018, 2020; Piitulainen et al., 2015a). The joint rotation stimulates the respective peripheral proprioceptors activating the cortical areas according to the stimulated limb (Nurmi et al., 2023; Piitulainen et al., 2015a). The study of the cortical response to these movements regarded the assessment of evoked (Alary et al., 1998; Piitulainen et al., 2015a; Smeds et al., 2017) and induced (Illman et al., 2023; Mujunen et al., 2022) responses to the proprioceptive afference. The former somatosensory evoked responses reflect the cortical excitation as a result of the sensory information travelling along the dorsal column pathway (Yamada, 2014). In contrast, the latter responses quantify the modulation of the SM1 cortex beta-band power (~14–32 Hz) to the proprioceptive stimulation and they have been proposed as measure of the degree of cortical inhibition-excitation. Specifically, the early reduction of the beta power over SM1 cortex (*suppression*, or event-related desynchronization) reflects cortical activation because of the somatosensory afference, and the delayed increase of the beta power (*rebound*, or event-related synchronization) likely represents intra- or intercortical inhibition phenomena (Barone and Rossiter, 2021; Engel and Fries, 2010; Salmelin and Hari, 1994; Tan et al., 2016).

It has been demonstrated that the SM1 proprioceptive processing is modulated as an effect of muscle activation in response to somatosensory stimulation during dynamic movement planning, execution, and visualization (Cebolla and Cheron, 2015; Cheron and Borenstein, 1987, 1992; Sugawara et al., 2016). The way in which cortical responses to somatosensory stimuli are modulated has been shown to be largely dependent on the experimental design including movement characteristics and context (Collins et al., 1998; Gantchev et al., 1994; Jiang et al., 1991; Mouchnino et al., 2015). Somatosensory evoked cortical responses are most often suppressed when the concurrent sensory input with motor processing is irrelevant to the motor task, and thus the disturbing information is inhibited to prioritize smooth or appropriate motor output (sensory gating phenomenon) (Morales-Muñoz et al., 2016; Morita et al., 1998; Rushton et al., 1981). On the contrary, the cortical response can be facilitated when the movement-related afferent information is relevant to the ongoing motor task (Misiaszek et al., 1997; Staines et al., 2000, 2002). Movement-related modulations of somatosensory inflow have been widely investigated in the upper limb during active, dynamic movements (Cheron and Borenstein, 1987; Huttunen and Lauronen, 2012; Kakigi et al., 1995) and only to a lesser extent in the lower limbs (Asanuma et al., 2003; Staines et al., 1998; Tinazzi et al., 1997). Furthermore, the previous studies exclusively relied on the use of electrical stimulation eliciting early cortical potentials, while little is known on the cortical responses to naturalistic proprioceptive stimulations during active conditions. Indeed, actuator-based joint rotation allows to stimulate peripheral proprioceptors in a more naturalistic way (i.e. triggering their firings similarly to a voluntary movement) and thus not necessarily initiating the same afferent mechanisms elicited by electrical stimulation (Abbruzzese et al., 1985; Mima et al., 1996; Piitulainen et al., 2013; Piitulainen et al., 2015a).

To the best of our knowledge, there is no prior study investigating the modulation of the cortical proprioceptive processing to naturalistic proprioceptive ankle-joint stimulation during active conditions. Therefore, the purpose of the present study was to quantify whether the steady volitional activation of the ankle plantar-flexor muscles affects the cortical processing of naturalistic proprioceptive afference arising from the respective muscles and joint. We aimed for close to real-world-naturalistic stimulation condition to obtain further insight into the role of the proprioception to motor control. We expected: (i) enhanced cortical activation (i.e. stronger evoked responses and beta power suppression) and (ii) reduced cortical inhibition to the proprioceptive stimuli during *active* than *passive* condition. We hypothesised that the *active* functional state affects the neuronal processing of the proprioceptive afference at all possible levels from the muscular (i.e. receptor level) to the spinal and brain (i.e. subcortical and cortical) levels, and the respective net effect would be detectable from the cortical responses. The results would guide the future studies investigating the role of cortical proprioception in motor performance and adaptation in, e.g., ageing, rehabilitation, training and neurological or developmental diseases.

## Materials and Methods

### *Participants*

We studied 25 young participants recruited through active advertisements by means of social media, university student and staff mailing lists and leafleting within the University of Jyväskylä campus (14 males, mean ± SD, age = 28.8 ± 7 years, height = 1.71 ± 0.8 m, mass = 71.6 ± 12.4 kg). Participants did not report any movement disorder or neuropsychiatric disease. Their Waterloo footedness inventory score was 42 ± 32 on a scale from −100 to 100 (van Melick et al., 2017) indicating a predominance of right-footed volunteers (23 out of 25 participants). All the participants received a thorough explanation of the study protocol before being asked to sign the informed consent. Prior to the measurements, the study received the approval from the University of Jyväskylä's Ethics Committee in accordance with the Declaration of Helsinki (approval number: 369/13.00.04.00/2020). The recruited group of volunteers underwent the data collection of the current study and the one described in our recent work (Giangrande et al., 2024) on the same day.

### *Experimental procedure and measurements*

The measurements were carried out at the Faculty of Sport and Health Sciences in the University of Jyväskylä, Jyväskylä, Finland. We stimulated participants' right ankle-joint by delivering intermittent rotations in the dorsiflexion direction through a custom-made movement actuator. Two conditions were tested: with volitional plantarflexion at a constant isomeric force (*active* condition) and while the ankle joint was relaxed (*passive* condition). Each condition was measured twice in two different 4-min trials, thus a total of four trials were performed by each participant.

**Experimental setup.** Fig. 1A shows the experimental setup adopted for the study. Participants sat in a chair equipped with a silent motorized ankle-movement actuator detailed in Fig. 1B. The actuator was constituted by two parts: a rotating platform for the foot and a control and automation section. Movements were generated by a servomotor controlled by a programmable logic controller. The rotating platform comes with the measurements of angular velocity and applied torque. Technical characteristics: maximum angular speed 200°/s, maximum torque 100 Nm. The same actuator was previously used in (Piitulainen et al., 2022). Participants placed the right foot on the rotating platform, maintaining the 90° position in both ankle and knee joint. The anatomical rotation axis of the talocrural ankle joint was identified according to Isman et al. (Isman and Inman, 1969), and it was aligned with the axis of the rotating platform. Participants wore shielded earplugs (ER-3C, 50 Ohm, Etymotic Research) to mask the low auditory noise produced by the ankle movement actuator. The vision of the moving foot was also blocked by using a brown cardboard in the line of sight. A screen was placed at 1.5 m in front of the participant to provide visual feedback in accordance with the experimental condition (Fig. 1C). The real-time data visualization as well as the stimulation pattern delivery was handled by a custom-made Graphical User Interface (Matlab R2022b, MathWorks Inc, Natick, MA, USA) properly configured for the

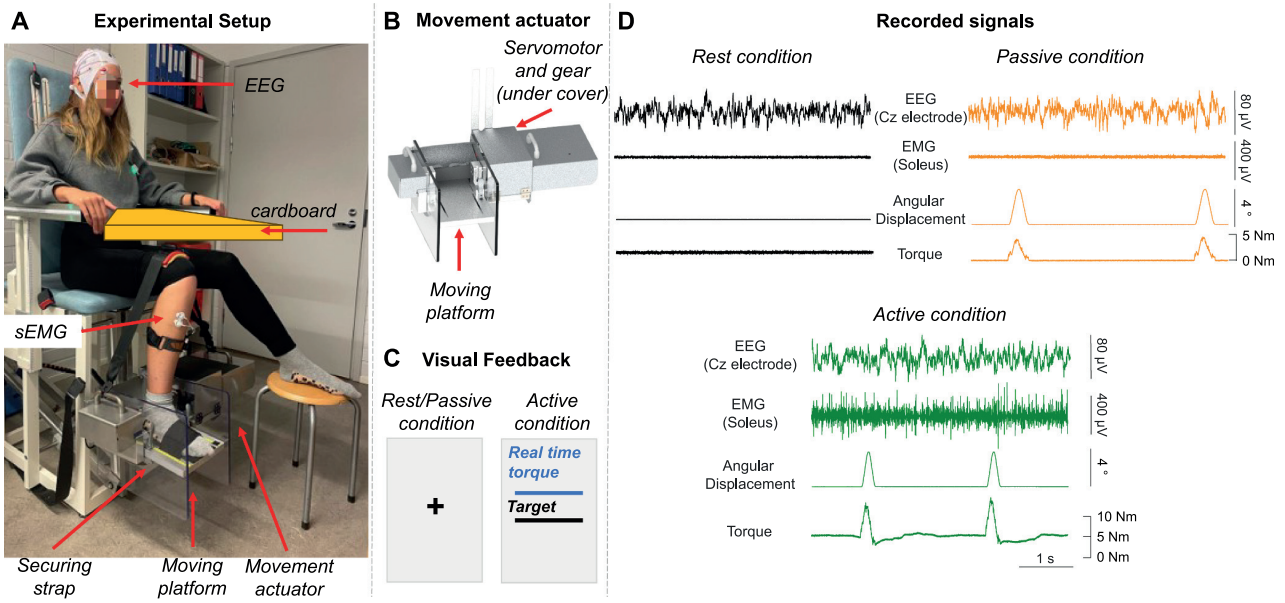


**Fig. 1.** Experimental Setup and measurements. A) Participant's right foot was placed on the rotating platform with knee and ankle joints at 90°. 30 EEG, 2 EOG channels and EMG from right soleus and tibialis anterior were recorded. B) Detail of the used movement actuator. C) Visual feedback varied between the conditions. A fixation cross was shown during the passive condition, and the real-time torque with 5 Nm target level during the active condition. D) Example of pre-processed signals (6 s) form a representative subject during active, passive and rest conditions. From top to bottom of each condition: EEG from Cz electrode, EMG from Soleus muscle, angular displacement and torque applied on the pedal are represented.

specific movement actuator through a data acquisition I/O board (USB-6216 CE-board, National Instrument Austin, 14 Texas, United States). During the experiment, EEG and electromyographic (EMG) signals as well as ankle-joint torque and foot angular displacement from the rotating platform were recorded.

**Measurements**. 30-EEG signals and two electro-oculograms (EOG) were recorded by means of a wireless EEG amplifier – MEACS, ReC Bioengineering Laboratories and LISiN, Turin, Italy (Cerone et al., 2019, 2022; Cerone and Gazzoni, 2018). We used a cap with 30 Ag/AgCl electrodes embedded into the fabric following the international 10–20 system (EasyCap GmbH, Gliching, Germany). To optimize the skin-electrode contact, each electrode site was carefully cleaned with an abrasive paste (NuPrep, Weaver and Company, Aurora, USA) and then filled with a conductive gel (NeurGel, SPES MEDICA, Genova, Italy). The EOGs were acquired using surface electrodes (Ø 24 mm Ambu s.r.l., Denmark) positioned in the up-left and down-right corners of the eye region to monitor eye movements and blinks. The raw EEG and EOG signals were collected using a monopolar derivation with the FCz electrode of the cap taken as a reference and were sampled at 2048 Hz with 0.1–500-Hz bandpass. EMG signals were recorded synchronously with EEG.

The EMG activity of two antagonist muscles of the leg (soleus and tibialis anterior) was measured. Prior to electrode positioning, the skin over the muscles of interest was treated with an abrasive paste (NuPrep, Weaver and Company, Aurora, USA). Afterwards, a pair of Ag/AgCl electrodes (Ø 24 mm Kendall, Covidien, Dublin, Ireland) was positioned on the right soleus medialis and tibialis anterior muscles 2-cm apart in accordance with the electrode placement guidelines of (Merletti and Cerone, 2020; Stegeman and Hermens, 2007). EMGs were recorded in bipolar derivation through a wireless amplifier (DuePro, OT Bioelettronica, Turin, Italy) with a sampling frequency of 2048 Hz in the frequency range of 10–500 Hz.

Ankle-joint torque and foot angular displacement from the rotating platform were recorded through the data acquisition unit with a sampling frequency of 1 kHz (output signal range: 0–5 V).

Data were then offline synchronized with EMG by means of a common external trigger introduced in (Cerone et al., 2022).

**Proprioceptive stimulation.** After EEG and EMG preparation, we recorded 30-s resting baseline data while participants sat in the armchair, and instructed to relax and gaze at a black fixation cross on a grey background displayed in the screen in front of them. Then, we delivered the proprioceptive stimuli every 4 ± 0.25 s (i.e. 4° ankle joint dorsiflexions) during the *active* and *passive* conditions. The peak angular velocity of the rotation was 30°/s starting with an ankle joint angle of 90° (Toledo et al., 2016). During the *passive* condition, participants were asked to relax their lower limbs and gaze at the fixation cross. During the *active* condition, participants were requested to apply a constant plantarflexion torque of 5 ± 2.5 Nm (i.e. opposite to the direction of the stimulation) throughout the duration of the stimulation. To this end, they were provided with visual feedback showing the target force level and the applied torque filtered with a 100-ms moving average (Fig. 1C). To avoid any visual contamination in the EEG responses caused by the brisk changes of the visual feedback due to the concurrent stimulation, the torque feedback line was kept constant for 800 ms after each stimulus onset. During this 800-ms window, the displayed torque was set to the average torque over 100-ms interval preceding the stimulus onset. A total of 100 stimulations were delivered separately for *active* and *passive* condition in four 50 repetition trials (two per condition) in pseudo-random order, balancing the starting condition among all participants.

### *Signal analysis*

Data were processed using MNE-Python software (Gramfort et al., 2013) and Matlab R2022b (MathWorks Inc, Natick, MA, USA). Foot angular displacement signals were resampled from 1000 Hz to a common sampling frequency of 2048 Hz and then synchronized to EEG and EMG data by offline aligning them according to a common external trigger sent at the beginning of each measurement trial.

**EEG preprocessing.** First, a visual inspection on EEG signals was carried out to identify the channels characterized by poor contact. Second, a bandpass 4th order Butterworth filter at 0.1–95 Hz was applied to EEG signals. Third, 30 EEG components were isolated through the Independent Component Analysis function to identify and discard the components associated with artifacts such as eye blinks, saccade

movements or neck, temporal, mastoids muscular activity contamination. Fourth, bad channels were interpolated by replacing them with the average of their neighbors. Finally, all EEG signals were offline referenced by applying a common average reference (McFarland et al., 1997).

**EMG preprocessing.** First, the EMG signals were bandpass filtered at 20–400 Hz with a 4th order Butterworth filter. To quantify the degree of muscular activation during *active* and *passive* conditions, root-mean square of EMG was computed for the whole stimulation duration separately for soleus and tibialis anterior. The root-mean square value of the initial 30-s period of resting without stimulation was used as a reference value.

**Evoked-EEG responses.** EEG signals were epoched from −200 to 1000 ms with respect to the stimulus onset occurring at 0 s. The epochs of the two trials of the same condition were concatenated together. Then, the epochs were averaged separately for each EEG channel and condition. The peak amplitude and latency of the most prominent negative (N1) and positive (P2) deflection, and their respective peak-to-peak amplitude were determined for each EEG channel separately. The EEG channel showing the strongest evoked response was identified and used in the final analysis to examine differences between the conditions. Finally, the grand average evoked responses were obtained by averaging the responses across all the participants to visualize topographic scalp distribution of the evoked responses in terms of quality and location.

**Induced-EEG responses.** Induced responses (i.e. ~ 20-Hz beta-band modulation) were quantified by means of the temporal spectral evolution method introduced by Salmelin and Hari (1994) (Salmelin and Hari, 1994). Preprocessed EEG signals were divided into epochs from −1 to 3 s with respect to the stimulus onset and evoked responses were subtracted from the data as suggested by David et al. (David et al., 2006). Average time–frequency representation (TFR) plots of the epochs were yielded on frequencies in the range 1–40 Hz (in 1-Hz steps) using Morlet wavelets (number of cycles = frequency/2) (Mujunen et al., 2022). TFR of the channel showing the highest peak to peak amplitude of the evoked responses was visually inspected to evaluate participants' individual beta bandwidth. Then, EEG data was filtered according to the specific beta bandwidth through a 4th order Butterworth filter (high-pass cut-off at 19 ± 5 Hz; low-pass cut-off at 28 ± 4 Hz). Next, EEG signals were rectified and averaged with respect to the stimulus onset and the signal envelope was extracted using the Hilbert function. A baseline correction (from –1000 to 0 ms) was applied to the averaged induced responses separately per condition. Participants who did not show beta modulations exceeding the noise level were excluded from the analysis, where the noise level was defined as three standard deviations of the EEG signal amplitude in the 1-s pre-stimulus baseline period. Similarly to evoked response analysis, we considered merged trials for those participants showing beta modulations and we averaged the epochs according to the EEG electrode site. The response at each EEG electrode site was characterized in terms of negative and positive (i.e. beta suppression and rebound respectively) peak amplitude and latency. Moreover, for both conditions we evaluated the area under the curve of the beta rebound (Akrawi et al., 1996) to estimate the differences between *active* and *passive* conditions in terms of beta recovery. Finally, the grand average induced response was obtained by averaging the individual responses across participants showing beta modulations above the noise level. Peak amplitudes of the grand average responses were used to obtain a topographic distribution of the response over the scalp and to determine the electrode site showing the largest and more robust positive and negative deflections to be used in the final analyses.

### *Statistical analysis*

All results are given as mean ± SE (standard errors). Statistical tests were performed in Matlab R2022b (Mathwork Inc, Natick, MA, USA). A Shapiro-Wilk test was used on the data to test the hypothesis of normality of its distribution which was rejected ($p < 0.05$). Additionally, we calculated the effect size in the Wilcoxon test based on the z value and interpreting the result according to Cohen et al. where the effect size r is considered to be small ($r \leq 0.1$), medium ($0.1 < r < 0.5$) or large ($r \geq 0.5$) (Cohen, 1988).

**Degree of muscle activation among conditions.** A non-parametric Wilcoxon signed rank test was adopted to identify statistically significant differences on the degree of muscular activity among rest, *active* and *passive* conditions. Bonferroni's method correction was further applied to adjust the significance level correcting for multiple comparisons.

**Effect of volitional muscle activation on EEG responses.** We tested the effect of volitional muscle activation on peak amplitude and latencies of the evoked and induced responses using Wilcoxon signed rank test (conditions: *active* vs. *passive*). For beta rebound, the area under curve parameter was also tested between the conditions.

## Results

Fig. 1 D shows a representative example of continuous pre-processed signals for rest, *passive* and *active* conditions. On average, 2 ± 3 independent components related to artifacts due to eye movements or muscular neck activity were rejected to reconstruct EEG signals. The signals were overall of good quality. Indeed, in the 68 % of cases no channels replacement was performed as all the channels were considered of good quality, whereas a single channel was replaced in the 20 % of the tested population and only the 12 % of cases reported 3 bad channels to be interpolated prior running the EEG data analysis. The most frequently replaced channels were Iz, Tp9 and Tp10 and it was not surprising because of their location particularly dependent on the individual subject scalp anatomy, likely resulting in a poor contact. The number of stimuli was fixed to 98 for both conditions, this was the minimum number of good quality EEG epochs across conditions and participants, i.e., 2 % of the stimuli were excluded.

**Degree of muscle activation among conditions.** Fig. 2 shows the soleus and tibialis anterior EMG-RMS amplitude during rest, *active* and *passive* conditions. As expected, the EMG-RMS was significantly higher ($p < 0.01$) for soleus (i.e. agonist) muscle during the *active* than both the rest and *passive* conditions (*active* 12.02 ± 1.41 μV, *passive* 1.98 ± 0.09 μV, rest 1.81 ± 0.11 μV). EMG-RMS amplitude during the *passive* condition did not differ from the rest condition. Similarly, the EMG amplitude of the tibialis anterior (i.e. antagonist) muscle during rest showed statistically significant differences ($p < 0.01$) only when compared to the *active* condition (*active* 4.46 ± 0.73 μV, *passive* 2.39 ± 0.34 μV, rest 2.37 ± 0.32 μV). The EMG-RMS values found during rest and the *passive* condition are within the range for typical EMG-RMS noise value when

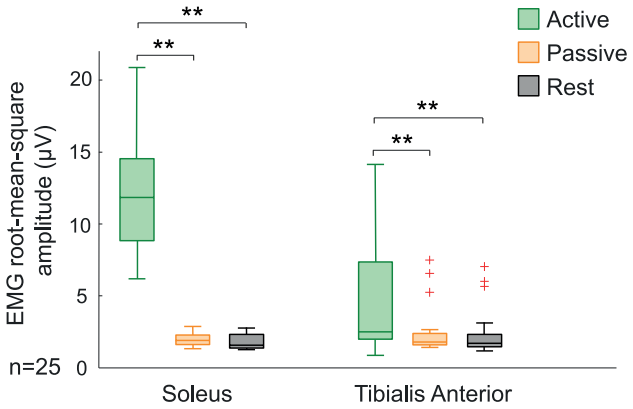


**Fig. 2.** Boxplots showing the muscular activation level (μV) of soleus and tibialis anterior muscles during trials for active, passive and 30-s rest conditions (n = 25 participants). Statistical analysis by Wilcoxon signed-rank test, **p < 0.01.

measured using Ag/AgCl electrode pairs (Piervirgili et al., 2014).

**Evoked-EEG responses.** Fig. 3 shows the evoked-EEG responses for both conditions. All participants showed a prominent evoked-EEG response peaking at the Cz electrode placed at the vertex (i.e., over the lower limb area of SM1 cortex). In accordance with the literature, we found N1 component at ~ 100 ms followed with a positive P2 component at ~ 200 ms with respect to the stimulus onset. Peak response characteristics for both conditions are shown in Table 1. Qualitatively, the evoked response shape in the peak response channel and spatial distribution across all EEG channels were similar for *active* and *passive* conditions for both N1 and P2. However, the peak-to-peak amplitude was 26 % larger for the *active* (14.51 ± 1.41 μV) than *passive* (11.3 ± 1.04 μV) condition ($p < 0.001$) with a large effect ($r = 0.68$). The latencies of N1 and P2 peaks did not show statistically significant differences between the conditions ($p > 0.05$).

**Induced-EEG responses.** Table 1 shows the beta suppression, rebound strength and respective latencies. 19 out of 25 participants showed significant beta modulations at the Cz electrode located over the foot area of SM1 cortex. Fig. 4 shows group level time–frequency representations and scalp topographies for suppression and rebound of the beta power for both conditions. The spatial distribution was similar with apparent difference in the peak suppression and rebound amplitudes. The time–frequency representations in Fig. 4 show typical evolution of beta power with early suppression followed with rebound. Fig. 5 shows the group level temporal- spectral evolution of beta power at ~ 25 Hz, and individual amplitudes for the beta suppression and rebound. Despite a noticeable inter-individual variation, the peak beta suppression was stronger ($p < 0.01$) and rebound weaker ($p < 0.05$) for *active* than *passive* condition, with a large effect ($r = 0.67$, $r = 0.57$ respectively for beta rebound and suppression amplitudes). Furthermore, the *passive* condition appeared to have a more prolonged rebound recovery than the *active* condition, and thus significantly larger area- We under-the-curve of the rebound ($p < 0.001$, Fig. 5 C) with a large effect ($r = 0.61$). No differences were found in the peak-response latencies between conditions ($p > 0.05$). Finally, the baseline beta power did not differ ($p > 0.05$) between *active* (2.0 ± 0.2 μV) and *passive* (2.1 ± 0.2 μV) conditions.

**Table 1**
Evoked and induced responses characteristics (peak amplitudes and latencies, mean ± SE) for passive and active conditions. Additionally, the P-value is shown to highlight the statistically significant differences between the two conditions (Statistical analysis by Wilcoxon signed-rank test, *p<0.05, ***p<0.001).

| | Active condition | Passive condition | p-value |
|---|---|---|---|
| **Evoked responses – N1** | | | |
| Peak amplitude (μV) | −7.20 ± 0.74 | −5.66 ± 0.59 | *0.001 (*)* |
| Latency (ms) | 119.5 ± 13.0 | 104.2 ± 2.6 | 0.129 |
| **Evoked responses – P2** | | | |
| Peak amplitude (μV) | 6.84 ± 0.38 | 5.47 ± 0.66 | *0.009 (**)* |
| Latency (ms) | 232.6 ± 7.2 | 285.5 ± 3.2 | 0.138 |
| **Evoked responses – Peak-to-peak** | | | |
| Amplitude (μV) | 14.04 ± 1.47 | 11.14 ± 1.12 | *0.0006 (***)* |
| **Induced responses – Suppression** | | | |
| Strength (μV) | −0.43 ± 0.91 | −0.31 ± 0.03 | *0.003 (*)* |
| Latency (ms) | 374.1 ± 6.2 | 262.3 ± 4.0 | 0.259 |
| **Induced responses – Rebound** | | | |
| Strength (μV) | 0.51 ± 0.07 | 0.88 ± 0.14 | *0.012 (*)* |
| Latency (ms) | 922.6 ± 3.48 | 1028.6 ± 4.9 | 0.055 |
| Area under curve (μV·s) | −0.0013 ± 0.0002 | −0.0020 ± 0.0003 | *0.0004 (***)* |

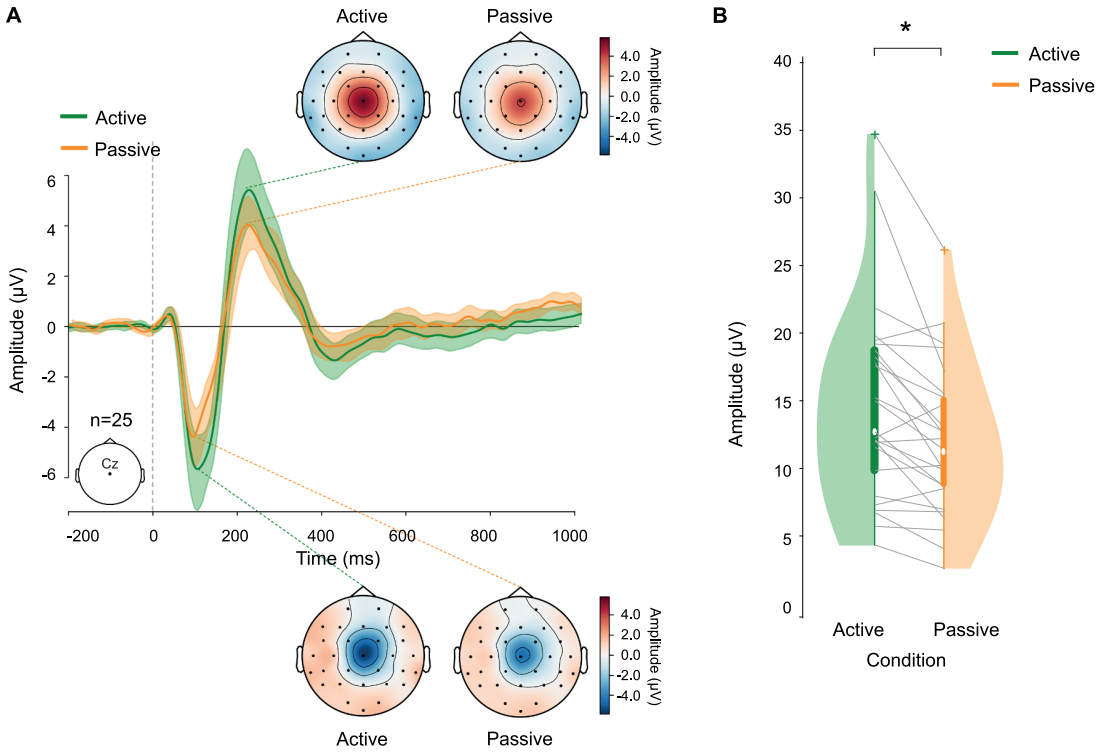


**Fig. 3.** Evoked response results. A) Grand average of evoked responses across participants for active (green) and passive (orange) conditions at Cz electrode level (n = 25 participants). Shaded areas correspond to the standard deviations across participants. Topographies at the most prominent peaks are represented for both conditions. B) Violin plots of peak-to-peak amplitude of evoked responses for both active (green) and passive (orange) conditions. Solid grey lines indicate individual values of peak-to-peak amplitude (Statistical analysis by Wilcoxon signed-rank test, *p < 0.05).

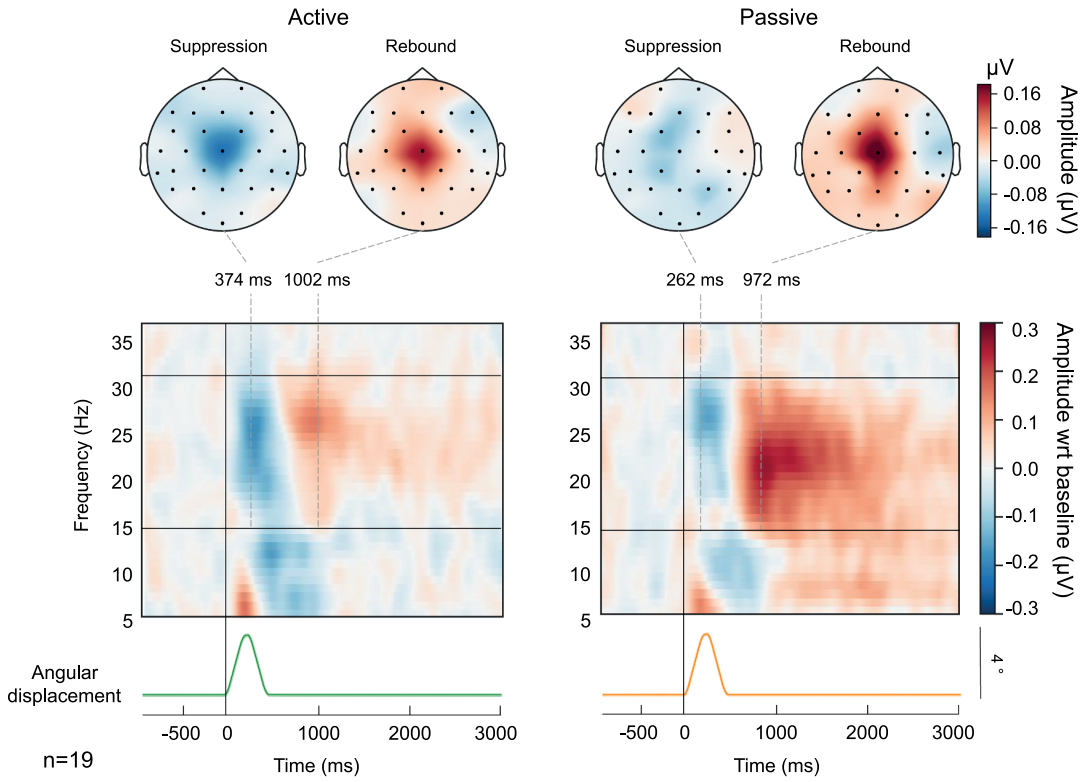


**Fig. 4.** Group average topography and time–frequency representations of active and passive conditions for those subjects showing induced responses (n = 19). Top panel shows topographies of time frequency representation within individual beta frequency band (n = 19) at peak suppression and rebound. Middle panel shows time frequency representations. Data is presented based on z-score transformations (baseline normalization: 1 s before the movement onset). Horizontal black lines indicate the lower and upper range of the individually chosen frequency bands. The vertical line at 0 s represents movement onset, whereas the dashed ones represent the group average latencies of peak suppression and rebound. Bottom panel shows the grand average of the angular displacement among participants.

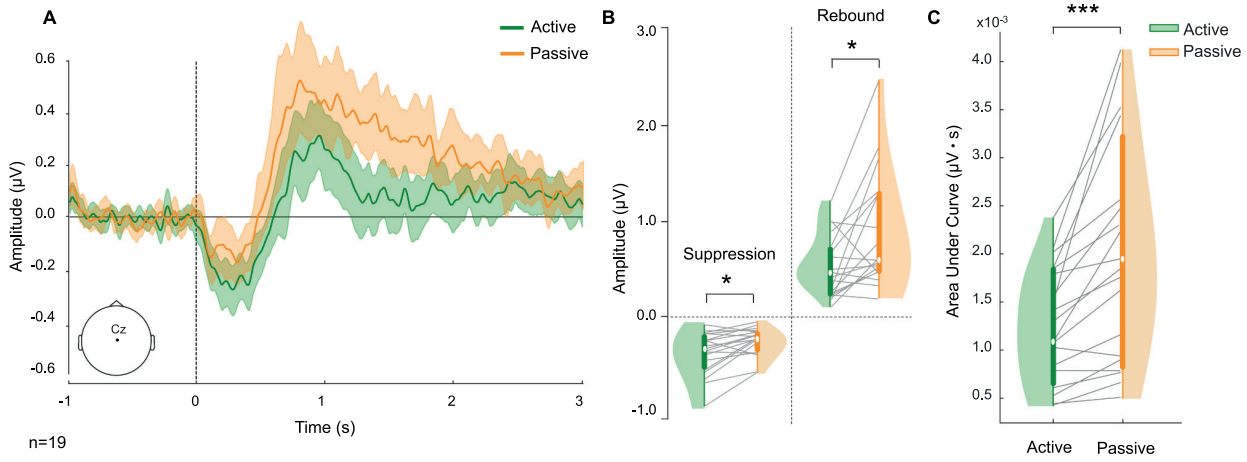


**Fig. 5.** Induced responses results (n = 19 participants). A) Grand average of induced responses at ~ 23 Hz across participants for active (green) and passive (orange) conditions at Cz electrode level. Shaded areas correspond to the standard deviations across participants. B) Violin plots of beta suppression and rebound peak amplitudes for both active (green) and passive (orange) conditions. C) Violin plots of the area under the rebound curve values for both active (green) and passive (orange) conditions. Solid grey lines indicate individual values (Statistical analysis by Wilcoxon signed-rank test, *p < 0.05, ***p < 0.001).

## Discussion

We examined the effect of volitional muscle activation on evoked and induced somatosensory EEG responses during proprioceptive stimulation of the ankle joint and we observed that the 'active' state of the sensorimotor system modulates the cortical processing of proprioceptive afference. In line with our hypothesis, we found that the cortex was more strongly activated by the stimulation during the *active* than *passive* condition. This result suggests intensified proprioceptive processing in the SM1 cortex during the *active* condition. We monitored EMG signals and the ankle-joint torque to ensure the *active* condition from the *passive* one, but our observations about the proprioceptive processing are limited to the cortical level only. Specifically, the *active* condition was accompanied with weaker beta-rebound amplitude than the *passive*

condition, suggesting weaker cortical inhibition when the motor cortex is in the 'active' state. There are several potential mechanisms for our observations. Firstly, volitional muscle activation is accompanied with efferent gamma motor neuron input to intrafusal fibers of the muscle spindles sensitizing them (Ellaway et al., 2015; Macefield and Knellwolf, 2018; Purves et al., 2018). This sensitization may lead to more synchronized afferent proprioceptive volleys to the SM1 cortex, enhancing the amplitude of the cortical responses. Secondly, the muscle–tendon units in the rotated joint naturally become mechanically more resistant to the rotational stimulus due to reduction in the muscle and tendon slack and increased muscle stiffness from a resting to the *active* condition. The increased stiffness will likely also enhance the activation and synchrony of the proprioceptors. Thirdly, the functional state of the SM1 cortex differs between *active* volitional and resting *passive* states and thus may influence the intra and intercortical processing of the proprioceptive stimulation. Moreover, subcortical and spinal modulations cannot be excluded as contributing to affect the overall sensorimotor processing (Fitzpatrick and McCloskey, 1994; McChesney and Woollacott, 2000; Nakamura et al., 2023; S.R. et al., 1994; Toledo and Barela, 2014). Finally, attentional and cognitive factors cannot be excluded as contributing mechanisms eliciting the observed differences in the cortical responses. These consistent results suggest that the currently used measures of cortical proprioception (i.e. evoked and induced EEG responses) show high potential as neurophysiological markers to investigate mechanisms and adaptations of cortical proprioceptive processing in other research and clinical contexts.

**Effect of volitional muscle activation on evoked-EEG responses.** The characteristics of evoked N1 and P2 components were in line with the descriptions of other colleagues investigating evoked responses of proprioceptive ankle-joint stimulations in young healthy adults (Toledo et al., 2016). The grand average responses revealed a stronger peak-to-peak amplitude of the evoked responses (N1 and P2) elicited during *active* than *passive* condition, while no clear differences appeared to be in the early P50 response, representing the earliest cortical processing of the proprioceptive afference. We did not investigate the early component at the individual level, since it was not robust enough to be quantified. Earlier components can be, indeed, quantified using electrical stimulation of the peripheral nerves, activating all afferents simultaneously (Allison et al., 1991; Halonen et al., 1988). However, in case of naturalistic ankle rotation stimulus, the proprioceptors are activated asynchronously (i.e. with varying timings of several milliseconds differences) at slightly different phases of the evoked movement. Therefore, the temporal spread of the afferents might result in a lower signal-to-noise ratio, thus "blurring" the earliest peak of the response (Piitulainen et al., 2015a).

The observed differences between the *active* and *passive* conditions might be influenced by attentional or cognitive factors. Indeed, the attention level of the participants could affect the amplitude of the cortical responses (Arnfred, 2005; Eimer and Driver, 2000; Eimer and Van Velzen, 2002; Gherri and Eimer, 2008; Hötting et al., 2003; Piitulainen et al., 2021; Quant et al., 2004). The attention was directed more to the foot during the *active* than the *passive* task, since participants had to actively maintain a constant torque through visual feedback. On the contrary, during the *passive* condition participants were instructed to be completely relaxed and to focus on the fixation cross on the feedback screen. Thus, it is reasonable to suggest that the cortical responses were amplified partly due to directed attention to the proprioceptive afference and the *active* task itself. Our group has previously shown that directed attention to the proprioceptive stimulation alone may enhance the SM1 cortex evoked-field amplitude to proprioceptive stimulation of the hand (Piitulainen et al., 2021).

Nevertheless, important mechanical and neuronal mechanisms at different levels of the proprioceptive processing pathway (i.e. from the muscle to the brain level) may explain the stronger cortical response during *active* than *passive* condition. Indeed, N1 has been shown to mainly reflect the somatosensory processing with proprioceptive emphasis (Toledo et al., 2016), whereas the P2 response in the SM1 cortex might be more affected by the wider top-down and other reciprocal processes of the sensorimotor integration in the brain. Anaesthetic studies have indicated that N1 response has been associated to the feedback from the muscle spindles (Abbruzzese et al., 1985; Starr and Cohen, 1985), with less contribution from the cutaneous tactile and joint mechanoreceptors. Thus, the mechanical and neuronal status of the peripheral proprioceptors between *active* and *passive* conditions might enhance especially the N1 response. In our case, the active muscle contraction increases the tension in the muscle–tendon unit, and thus increases the tissue stiffness and removes the muscle–tendon unit "slack" more evident in the *passive* condition. Therefore, the proprioceptors are more readily activated, and likely fire in better synchrony in occurrence of an external perturbation. The better synchrony of somatosensory afference would naturally be reflected as stronger cortical response, even in case of identical "amount" of the afference, as EEG is fundamentally a measure of synchrony among a large population of neurons. Thus, the better synchrony would in turn increase the EEG signal-to-noise ratio. On the other hand, it is hard to estimate how effective the ~ 5-Nm ankle-joint torque was to mechanically sensitize the proprioceptors. For example, the muscle spindles are extremely sensitive to tiny length changes (as low as 5 μm during vibration) of their parent muscle (Brown et al., 1967), and Pacinian corpuscles are capable to detect even 10 nm skin motions (Brisben et al., 1999). Possibly because of the high sensitivity of the proprioceptors, the evoked and induced SM1 cortex responses to proprioceptive stimuli are shown to be invariant to mechanical factors, such as the range of the movement stimulation (Nurmi et al., 2023).

The primary Ia-afferents of the muscle spindle are suggested to be the primary source for the somatosensory evoked EEG responses to joint stimulation (Drews et al., 1998; Mima et al., 1996). During the voluntary movement, the muscle spindles are further neuronally sensitized through a gamma motor-neuron input to their intrafusal muscle fibers occurring simultaneously with alpha motor-neuron input to the skeletal muscle fibers (Prochazka, 2015). The contraction of the intrafusal fibers of the muscle spindle will then contract the spindle together with the muscle, which may increase the overall Ia-afferent firing rate. When the motor task requires precision in the muscle force production, as was the case in the current *active* task, the baseline activity of the gamma motor neuron is further increased, increasing also the spindle responsiveness (Purves et al., 2018). Together, the mechanical and neuronal factors affecting the peripheral proprioceptors may intensify or alter the nature of the proprioceptive afference, that is then seen as stronger evoked-EEG response in the SM1 cortex.

In addition to the enhanced sensitivity of the proprioceptors, we cannot exclude that also the cutaneous tactile mechanoreceptors in the sole of the forefoot were sensitized during the *active* condition. However, the contribution of tactile afferents has shown to be weak. Indeed, there is prior evidence that even when the cutaneous and joint afferents of the hand and wrist were blocked using peripheral ischemic anaesthesia, while muscle afferents were left intact, the evoked early EEG potentials were not altered (Mima et al., 1996). Nevertheless, the effect of tactile afferents on the late cortical responses evoked by naturalistic stimuli to the lower limbs has not yet been explored in the literature. Thus, we did not rule out the contribution (albeit weak) of the cutaneous afference of the sole on the examined naturalistic phenomenon as the tactile input is an important part of proprioception and sensorimotor integration. However, it is worth mentioning that both the proprioceptors and tactile mechanoreceptors are very sensitive, and thus are likely partially activated even during the passive condition by the passive resistance of the tissues to the evoked movement.

Additionally, the neuronal mechanisms at the spinal and cortical very likely contributed to the differences in cortical activation to the proprioceptive stimulation between the *active* and *passive* conditions. The somatosensory afference from the peripheral receptors to the SM1 cortex is modulated along its pathway in spinal, medullary and thalamic

circuits, and actually, the brain can modify this feedback as well (McIlroy et al., 2003). For example, there is evidence from rodent models showing that the status of the cortex may facilitate or enhance the thalamic signalling towards the cortex through cortico-thalamic feedback loops (Alitto and Usrey, 2003; Briggs and Usrey, 2008; Soo-Hyun et al., 2008). Indeed, during voluntary muscle actions, the somatosensory receptor input to the spinal cord converges in the spinal circuits which are also under control by the efferent motor output from the brain (Seki et al., 2003). Thus, the cortical motor output may affect the proprioceptive afference at subcortical levels of the central nervous system before it reaches the cortex. This active multi-level peripheral mechanism may partly explain the currently observed differences in the cortical responses between the *active* and *passive* conditions.

The "state" of the sensorimotor cortices is fundamentally different between the *active* and *passive* condition. In both tasks, the cortical *status quo* is maintained, either by keeping the steady isometric plantarflexion or to remaining passive/relaxed. However, the *active* condition was associated with active motor output and directed attention towards the visuomotor force precision task. Thus, the active engagement of various cortices (motor, visual, etc.) and related sensorimotor integration, might have an effect also on the cortical sensorimotor processing with respect to the *passive* condition. We observed that the processing of the proprioceptive afference was intensified (i.e. stronger response) during the *active* task. Similar observation of facilitated cortical response has been observed before if the somatosensory afference has been relevant for the ongoing motor task (Gantchev et al., 1994; Staines et al., 2002). The ankle joint rotation was indeed very relevant, although distracting, for the current motor task. It is also possible that the stronger somatosensory potentials reflect a higher cortical activation which is more strongly pronounced during the active task due to active inhibition of the distracting joint rotation stimulus, disturbing the *status quo*. Active inhibition has been shown to be associated with emphasized SM1 cortex activation (i.e. beta-power suppression) to stabilize motor output against visual presentation of distracting dynamic hand actions when participants were attempting to maintain steady isometric pinch force (Hari et al., 2014). The authors suggested that the mechanism was likely related to activation of the mirror neuron system, but similar active inhibition, or "self-mirroring" could be present also for proprioceptive afference.

Our observations contrasted with some previous studies showing reduced somatosensory evoked responses to electrical peripheral nerve stimulation (Asanuma et al., 2003; Rushton et al., 1981; Takahara et al., 2020). Electrical stimulation activates the somatosensory afferents with high synchrony allowing, e.g., accurate detection of the earliest N20 peak for the upper limb (Huttunen and Lauronen, 2012; Kakigi et al., 1995), which is not possible to elicit for more time varying naturalistic proprioceptive stimuli of lower limb joints rotations. Indeed, "naturalistic" somatosensory stimulation such as ankle rotation, may activate the neuronal networks in a more purposeful manner and thus the previously observed inhibitory gating effect to peripheral electrical stimulation might be dampened. Furthermore, it might be that the cortical sensorimotor processing varies between upper (fine motor) and lower (gross-motor locomotion) limbs (Staines et al., 1998). There might be more direct cortico-motoneuronal connections from the motor cortex to the upper limb spinal lower motoneurons than to the lower limb ones (Lemon, 2021), suggesting that spinal level circuits could be more "independent" in the control of stereotyped gross-motor actions like gait.

Finally, the peak response latencies did not differ between the conditions. This finding was not surprising since we expect little to no changes in the conduction velocity and central processing times of the proprioceptive afference to fixed proprioceptive stimuli, and considering that we tested a population of young, healthy adults (Toledo et al., 2016).

**Effect of volitional muscle activation on induced EEG-responses.** The beta modulation was too weak to be quantified reliably in 27 % of the currently studied population, both for beta suppression and rebound. This result is typical, and it was in line with recent similar studies. Induced response amplitude is typically characterized by substantial inter-individual variation (Illman et al., 2022; Mujunen et al., 2022), and it is likely associated to differences in the individual functional anatomy. Thus, the source location and orientation may be more or less optimal, which can dramatically affect the beta power signal and thus its modulation amplitude. This issue is present even when using magnetoencephalographic (MEG) recordings, which has higher signal-to-noise ratio with respect to EEG, and thus allows more robust induced responses (Illman et al., 2022). Additionally, some other factors have been observed to affect the beta power modulation, such as variations in the circadian individual rhythm (Wilson et al., 2014). Nevertheless, the obtained induced responses agreed in spatiotemporal and spectral features with what has been previously shown by other colleagues investigating the cortical proprioceptive processing related to passive ankle joint stimulations (Toledo et al., 2016). For the first time, we showed clear differences in induced response amplitudes between *active* from *passive* conditions for somatosensory stimulus. The *active* condition elicited stronger beta suppression and weaker rebound compared to the *passive* condition. These findings are likely attributable to the stronger activation of the SM1 cortex and/or the active processes related to ongoing motor control that is much less emphasized in the *passive* condition. Induced responses reflect the dynamics of the brain oscillations driven by beta-burst activity in the SM1 cortex (Barone and Rossiter, 2021). Specifically, the beta suppression (i.e. reduction in the beta power) is thought to reflect the activation of the SM1 cortex and it has been found to occur, e.g., in response to active and passive movements, motor imagery, and action observation (Barone and Rossiter, 2021; Engel and Fries, 2010; Tan et al., 2016). Whereas the delayed beta rebound (i.e. increase in the beta power) has been attributed to the cortical inhibition or motor cortical deactivation and it has been thought to be an indicator of the movement outcome processing (Baker, 2007; Barone and Rossiter, 2021; Parkkonen et al., 2015; Pfurtscheller, 1992).

The EEG signal is primarily caused by the synchronous activity of large group of neurons, likely belonging to several different neuronal populations (Schutter and Hortensius, 2011). Therefore, a stronger cortical activation can be related to the increased synchrony of neuronal activity or to the larger number of neurons involved in the synchronous activity. In the current study, we indeed observed stronger beta suppression to the proprioceptive stimulation during *active* than *passive* condition. This observation thus suggests that the proprioceptive processing in the SM1 cortex was intensified due to the volitional muscle activation in line with what found by Heinrichs et al. (Heinrichs-Graham and Wilson, 2016) who demonstrated a significant positive correlation between the amplitude of beta suppression and spontaneous activity of the motor cortices (Heinrichs-Graham and Wilson, 2016). It is possible that the ongoing motor control in the SM1 cortex activated more strongly the cortical proprioceptive and/or sensorimotor integration neuronal network(s), thus intensifying the cortical proprioceptive processing. The stronger beta suppression of the *active* condition may also reflect the activation of early cortical inhibitory neuronal networks in favour of the continuous readjustments to maintain the *status quo* of the cortex throughout the task (Hari et al., 2014; Piitulainen et al., 2015b). This hypothesis is reinforced by TMS studies suggesting that the somatosensory afference to the SM1 cortex activates the cortical inhibitory neuronal networks as demonstrated by a reduction of the cortical motor output ~ 50 ms after the arrival of the somatosensory afference to the cortex (Bailey et al., 2016; Tokimura et al., 2000).

The cortical inhibition is partly controlled by sub cortical (e.g. thalamic and sub thalamic) structures, which are important in timing and pausing the motor output sequences. These structures regulate the activity of basal ganglia that further inhibit the thalamus to supress the thalamic facilitation of the motor cortices, and thus help to suppress the activation of competing motor programs in the motor cortex (Brittain et al. 2012). A marker of the reduced cortical excitability or inhibition of the thalamo-cortical circuitry is the enhancement of the post-movement

beta power (Pfurtscheller and Neuper, 1994). In the current study, the SM1 cortex after the stimulus was not at "rest" during the *active* condition, but more so during the *passive* one. Therefore, there was less room for post-movement beta modulation in the cortex, shown by weaker beta rebound amplitude (i.e. weaker cortical inhibition) during the *active* than *passive* condition, probably reflecting some higher-level mechanisms such as sensorimotor integration and directed attention to maintain the steady precision force output task. This suggestion is further reinforced by the faster rate of beta recovery (i.e. inhibition recovery) of the *active* condition with respect to the *passive* one, highlighted by the smaller area under the rebound curve. In fact, the beta rebound obtained during the *passive* condition not only showed a higher amplitude but it took longer to recover back to the baseline when compared to the one obtained from the *active* condition. These findings are in line with prior observations of Cassim et al. where a larger and longer beta rebound was found for brief movements with respect to sustained ones (Cassim et al., 2000).

Finally, also for induced responses motor imagery and attentional effects can potentially partly explain the obtained results. Specifically, motor imagery has been shown to induce beta power modulation, with initial beta suppression followed with a rebound in similar manner as observed after active volitional movements (Neuper and Pfurtscheller, 2001). In addition, our group has shown earlier that beta power is supressed when attention is directed, to the proprioceptive stimulation of the hand (Piitulainen et al., 2021). We designed the experimental protocol to minimize possible effects of the motor imagery by not instructing the participants to focus on the movement stimuli. However, we cannot completely rule out that the motor imagery or attentional effects on the induced response amplitudes.

### Study limitations and future perspectives

Although clear evoked and induced EEG responses were obtained in the present study for both *active* and *passive* conditions, caution must be taken when interpreting the results. Indeed, in addition to the mechanical and sensorimotor neuronal mechanisms, motor imagery and attentional effects cannot be excluded as possible contribution to the observed differences between *active* and *passive* condition. In this view, the contribution of attention and motor imagery should be quantified in the future studies to comprehensively understand the multi-mechanistic nature of the cortical processes related to proprioception during *active* and *passive* conditions. There are some further methodological enhancements that should be considered in future experiments to confirm the current observations, e.g.: (i) use of high-density EEG for better identification of the cortical proprioceptive sources, (ii) use of individual anatomical magnetic resonance images of the participants' head to confirm the results also in the source level, (iii) experimentally account for the influence of alpha-gamma coactivation by, e.g., repeating the experiment with a progressive increase of voluntary contraction (Watanabe and Hirayama, 1976), (iv) incorporate spinal (e.g. through H-reflex measures) and spindle (e.g. through microneurography) sensitivity measurements to quantify the differences at peripheral and spinal levels between conditions and further clarify the related proprioceptive mechanisms. Finally, the obtained results are not necessarily extendable to upper extremities or other muscular groups/activations. We cannot exclude that different mechanisms regarding the proprioceptive processing could take part when investigating other joints or limbs. Indeed, different cortical neuronal populations are involved when a different part of the body is stimulated with somatosensory stimuli, evidenced with distinct frequency bands for the beta rebound in the sensorimotor cortex (i.e. lower frequencies for the hand than for the foot stimulations) (Pfurtscheller and Neuper, 1994; Salmelin et al., 1995). Therefore, specific studies focusing on the upper extremities or performing movements in different directions should be separately performed to further investigate this aspect.

Owing to the importance of proprioception during development, aging, sport and motor disorders, understanding how the sensorimotor information is gathered within the cortical neuronal networks appears of paramount importance. Our findings showed that cortical responses are modulated by volitional muscular activation, thus contributing to the understanding of the neurophysiological mechanisms of proprioception, which are still poorly described. We proved that EEG-based variables can robustly track changes in the integration between the afferent-efferent pathways. However, although the use of EEG/MEG variables as biomarker of sensorimotor cortical function has already been demonstrated in recent studies on developmental diseases (Illman et al., 2023; Piitulainen et al., 2020), post-stroke patients (Keser et al., 2022; Parkkonen et al., 2015) and elderly (Walker et al., 2020), the effect of voluntary muscle contraction on cortical proprioceptive processing in motor disorders has not yet been assessed. Proprioceptive responses can be quantified in reproducible manner using EEG (Illman et al., 2022) and the proprioceptive stimuli can be repeated identically using a motorized-movement actuator. Therefore, longitudinal studies on patient groups are needed to track the effects of rehabilitation, ageing or neurological diseases on cortical proprioception.

### Conclusion

Our study was the first one evaluating the effect of volitional muscular activation on the processing of proprioceptive afference in the SM1 cortex for the ankle-joint rotation stimuli using EEG. We demonstrated a stronger cortical activation and weaker inhibition in response to naturalistic proprioceptive stimulation of the ankle joint during *active* steady volitional motor task when compared to *passive* condition. These changes in SM1 cortex processing and integration of proprioceptive afference may find an explanation at different levels of the proprioceptive processing occurring both at peripheral (i.e. proprioceptors) and central (i.e. cortical, sub-cortical and spinal) levels. When compared to the *passive* condition, the *active* task is accompanied with a mechanical and neuronal sensitization of the peripheral proprioceptors, and active alterations in the neuronal interactions occurring at spinal, subcortical and cortical levels. We demonstrated that evoked and induced EEG responses can robustly track the effects of the active motor control and are thus feasible markers to study human cortical sensorimotor integration, allowing the examination of the cortical proprioceptive processing during *active* and *passive* tasks in both healthy and likely also in pathological populations. This would enable a greater insight about the role of proprioception which holds a non-negligible relevance in numerous scenarios ranging from quiet standing, locomotion or efficient movement execution.

### Patient Consent Statement

Prior to measurements, all participants signed a written informed consent.

### Funding Statement

This study was supported by the Academy of Finland (grants #296240 and #327288) to HP, Jane and Aatos Erkko Foundation (602.274) to HP, and "Brain changes across the life-span" profiling funding to University of Jyväskylä (grant #311877). The study was supported also by a three-years PhD scholarship from Politecnico di Torino, Turin to AG and by a one-year PhD scholarship from the Faculty of Sports and Health Sciences of University of Jyväskylä (JYU) to AG.

### Ethical Approval

The study conformed to the Declaration of Helsinki and all the experiments were approved by the ethics committee of University of Jyväskylä.

## Credit authorship contribution statement

**Alessandra Giangrande:** Writing – review & editing, Writing – original draft, Validation, Methodology, Investigation, Formal analysis, Data curation. **Toni Mujunen:** Writing – original draft, Methodology. **Giacinto Luigi Cerone:** Software, Resources, Methodology. **Alberto Botter:** Writing – original draft, Supervision, Resources, Methodology, Formal analysis, Data curation. **Harri Piitulainen:** Writing – review & editing, Writing – original draft, Supervision, Project administration, Methodology, Formal analysis, Data curation, Conceptualization.

## Declaration of competing interest

The authors declare that they have no known competing financial interests or personal relationships that could have appeared to influence the work reported in this paper.

## Acknowledgments

The authors gratefully acknowledge Sakari Vekki, chief technician from the University of Jyväskylä, for his precious technical assistance in building the experimental design.

## References

Abbruzzese, G., Berardelli, A., Rothwell, J.C., Day, B.L., Marsden, C.D., 1985. Cerebral potentials and electromyographic responses evoked by stretch of wrist muscles in man. Exp. Brain Res. 58 (3), 544–551. https://doi.org/10.1007/BF00235870.

Akrawi, W.P., Drummond, J.C., Kalkman, C.J., Patel, P.M., 1996. A comparison of the electrophysiologic characteristics of EEG burst-suppression as produced by isoflurane, thiopental, etomidate, and propofol. J. Neurosurg. Anesthesiol. 8 (1), 40–46. https://doi.org/10.1097/00008506-199601000-00010.

Alary, F., Doyon, B., Loubinoux, I., Carel, C., Boulanouar, K., Ranjeva, J. P., Celsis, P., and Chollet, F. (1998). Passive movements in humans: Event related potentials, source analysis and comparison to fMRI. NeuroImage, 7(4 PART II), 377–390. Doi: 10.1016/s1053-8119(18)31249-7.

Alitto, H.J., Usrey, W.M., 2003. Corticothalamic feedback and sensory processing. Curr. Opin. Neurobiol. 13 (4), 440–445. https://doi.org/10.1016/S0959-4388(03)00096-5.

Allison, T., McCarthy, G., Wood, C.C., Jones, S.J., 1991. Potentials evoked in human and monkey cerebral cortex by stimulation of the median nerve. Brain 114 (6), 2465–2503. https://doi.org/10.1093/brain/114.6.2465.

Arnfred, S.M., 2005. Proprioceptive event related potentials: Gating and task effects. Clin. Neurophysiol. 116 (4), 849–860. https://doi.org/10.1016/j.clinph.2004.11.010.

Asanuma, K., Urushihara, R., Nakamura, K., Kitaoka, K., Sei, H., Morita, Y., Shibasaki, H., Kaji, R., 2003. Premovement gating of somatosensory evoked potentials after tibial nerve stimulation. Neuroreport 14 (3), 375–379. https://doi.org/10.1097/00001756-200303030-00016.

Bailey, A.Z., Asmussen, M.J., Nelson, A.J., 2016. Short-latency afferent inhibition determined by the sensory afferent volley. J. Neurophysiol. 116 (2), 637–644. https://doi.org/10.1152/jn.00276.2016.

Baker, S.N., 2007. Oscillatory interactions between sensorimotor cortex and the periphery. Curr. Opin. Neurobiol. 17 (6), 649–655. https://doi.org/10.1016/j.conb.2008.01.007.

Barone, J., Rossiter, H.E., 2021. Understanding the Role of Sensorimotor Beta Oscillations. Front. Syst. Neurosci. 15 (May), 1–7. https://doi.org/10.3389/fnsys.2021.655886.

Briggs, F., Usrey, W.M., 2008. Emerging views of corticothalamic function. Curr. Opin. Neurobiol. 18 (4), 403–407. https://doi.org/10.1016/j.conb.2008.09.002.

Brisben, A.J., Hsiao, S.S., Johnson, K.O., 1999. Detection of vibration transmitted through an object grasped in the hand. J. Neurophysiol. 81 (4), 1548–1558. https://doi.org/10.1152/jn.1999.81.4.1548.

Brown, B.M.C., Engberg, I., Matthews, P.B.C., 1967. Relative Sensitivity. 44, 773–800.

Cassim, F., Szurhaj, W., Sediri, H., Devos, D., Bourriez, J.L., Poirot, I., Derambure, P., Defebvre, L., Guieu, J.D., 2000. Brief and sustained movements: Differences in event-related (de)synchronization (ERD/ERS) patterns. Clin. Neurophysiol. 111 (11), 2032–2039. https://doi.org/10.1016/S1388-2457(00)00455-7.

Cebolla, A.M., Cheron, G., 2015. Sensorimotor and cognitive involvement of the beta-gamma oscillation in the frontal N30 component of somatosensory evoked potentials. Neuropsychologia 79, 215–222. https://doi.org/10.1016/j.neuropsychologia.2015.04.033.

Cerone, G.L., Botter, A., Gazzoni, M., 2019. A modular, smart, and wearable system for high density sEMG detection. IEEE Trans. Neural Syst. Rehabil. Eng. 66 (22), 3371–3380.

Cerone, G.L., Gazzoni, M., 2018. A wireless, minaturized multi-channel sEMG acquisition system for use in dynamic tasks. In: 2017 IEEE Biomedical Circuits and Systems Conference. https://doi.org/10.1109/BIOCAS.2017.8325129.

Cerone, G.L., Giangrande, A., Ghislieri, M., Gazzoni, M., Piitulainen, H., Botter, A., 2022. Design and Validation of a Wireless Body Sensor Network for Integrated EEG and HD-sEMG Acquisitions. IEEE Trans. Neural Syst. Rehabil. Eng. 30, 61–71. https://doi.org/10.1109/TNSRE.2022.3140220.

Cheron, G., Borenstein, S., 1987. Specific gating of the early somatosensory evoked potentials during active movement. Electroencephal. Clin. Neurophysiol. 67, 537–548. https://doi.org/10.1111/j.1748-1716.1962.tb02520.x.

Cheron, G., Borenstein, S., 1992. Mental movement simulation affects the N30 frontal component of the somatosensory evoked potential. Electroencephalogr. Clin. Neurophysiol./Evoked Potentials 84 (3), 288–292. https://doi.org/10.1016/0168-5597(92)90010-9.

Cohen, J., 1988. Statistical power for the behavioural sciences. Hilsdale. NY: Lawrence Erlbaum 58 (1), 7–19.

Collins, D.F., Cameron, T., Gillard, D.M., Prochazka, A., 1998. Muscular sense is attenuated when humans move. J. Physiol. 508 (2), 635–643. https://doi.org/10.1111/j.1469-7793.1998.00635.x.

David, O., Kilner, J.M., Friston, K.J., 2006. Mechanisms of evoked and induced responses in MEG/EEG. Neuroimage 31 (4), 1580–1591. https://doi.org/10.1016/j.neuroimage.2006.02.034.

Dietz, V., 2002. Proprioception and locomotor disorders. Nat. Rev. Neurosci. 3 (10), 781–790. https://doi.org/10.1038/nrn939.

Drews, H., Gerilovsky, L., Studer, L.M., Ruegg, D.G., 1998. Contribution of a Ia muscle afferent activation to the rise of H reflexes and somatosensory evoked potentials in man. Somatosens. Mot. Res. 15 (2), 109–117. https://doi.org/10.1080/08990229870835.

Eimer, M., Driver, J., 2000. An event-related brain potential study of cross-modal links in spatial attention between vision and touch. Psychophysiology 37 (5), 697–705. https://doi.org/10.1111/1469-8986.3750697.

Eimer, M., Van Velzen, J., 2002. Crossmodal links in spatial attention are mediated by supramodal control processes: Evidence from event-related potentials. Psychophysiology 39 (4), 437–449. https://doi.org/10.1017/S0048577201393162.

Ellaway, P.H., Taylor, A., Durbaba, R., 2015. Muscle spindle and fusimotor activity in locomotion. J. Anat. 227 (2), 157–166. https://doi.org/10.1111/joa.12299.

Engel, A.K., Fries, P., 2010. Beta-band oscillations-signalling the status quo? Curr. Opin. Neurobiol. 20 (2), 156–165. https://doi.org/10.1016/j.conb.2010.02.015.

Farris, D.J., Sawicki, G.S., 2012. The mechanics and energetics of human walking and running: A joint level perspective. J. R. Soc. Interface 9 (66), 110–118. https://doi.org/10.1098/rsif.2011.0182.

Ferlinc, A., Fabiani, E., Velnar, T., Gradisnik, L., 2019. The Importance and Role of Proprioception in the Elderly: a Short Review. Materia Socio-Medica 31 (3), 219–221. https://doi.org/10.5455/msm.2019.31.219-221.

Fitzpatrick, R., McCloskey, D.I., 1994. Proprioceptive, visual and vestibular thresholds for the perception of sway during standing in humans. J. Physiol. 478 (1), 173–186. https://doi.org/10.1113/jphysiol.1994.sp020240.

Gantchev, G., Gavrilenko, T., Concek, V., 1994. Somatosensory evoked potentials modification related to isometric voluntary contraction. Int. J. Psychophysiol. 17 (3), 191–196. https://doi.org/10.1016/0167-8760(94)90062-0.

Gatev, P., Thomas, S., Kepple, T., Hallett, M., 1999. Feedforward ankle strategy of balance during quiet stance in adults. J. Physiol. 514 (3), 915–928. https://doi.org/10.1111/j.1469-7793.1999.915ad.x.

Gherri, E., Eimer, M., 2008. Links between eye movement preparation and the attentional processing of tactile events: An event-related brain potential study. Clin. Neurophysiol. 119 (11), 2587–2597. https://doi.org/10.1016/j.clinph.2008.07.214.

Giangrande, A., Cerone, G.L., Botter, A., Piitulainen, H., 2024. Volitional muscle activation intensifies neuronal processing of proprioceptive afference in the primary sensorimotor cortex: an EEG study. J. Neurophysiol. 131 (1), 28–37. https://doi.org/10.1152/JN.00340.2023.

Gramfort, A., Luessi, M., Larson, E., Engemann, D. A., Strohmeier, D., Brodbeck, C., Goj, R., Jas, M., Brooks, T., Parkkonen, L., & Hämäläinen, M. (2013). MEG and EEG data analysis with MNE-Python. Front. Neurosci., 7(7 DEC), 1–13. Doi: 10.3389/fnins.2013.00267.

Halonen, J.P., Jones, S., Shawkat, F., 1988. Contribution of cutaneous and muscle afferent fibres to cortical SEPs following median and radial nerve stimulation in man. Electroencephalogr. Clin. Neurophysiol./ Evoked Potentials 71 (5), 331–335. https://doi.org/10.1016/0168-5597(88)90035-4.

Han, J., Waddington, G., Adams, R., Anson, J., Liu, Y., 2016. Assessing proprioception: A critical review of methods. J. Sport Health Sci. 5 (1), 80–90. https://doi.org/10.1016/j.jshs.2014.10.004.

Hari, R., Bourguignon, M., Piitulainen, H., Smeds, E., De Tiège, X., Jousmäki, V., 2014. Human primary motor cortex is both activated and stabilized during observation of other person's phasic motor actions. Philos. Trans. R. Soc., B 369 (1644), 26–30. https://doi.org/10.1098/rstb.2013.0171.

Heinrichs-Graham, E., Wilson, T.W., 2016. Is an absolute level of cortical beta suppression required for proper movement? Magnetoencephalographic evidence from healthy aging. Neuroimage 134, 514–521. https://doi.org/10.1016/j.neuroimage.2016.04.032.

Hötting, K., Rösler, F., Röder, B., 2003. Crossmodal and intermodal attention modulate event-related brain potentials to tactile and auditory stimuli. Exp. Brain Res. 148 (1), 26–37. https://doi.org/10.1007/s00221-002-1261-z.

Huttunen, J., Lauronen, L., 2012. Intracortical modulation of somatosensory evoked fields during movement: Evidence for selective suppression of postsynaptic inhibition. Brain Res. 1459, 43–51. https://doi.org/10.1016/j.brainres.2012.04.023.

Illman, M., Laaksonen, K., Jousmäki, V., Forss, N., Piitulainen, H., 2022. Reproducibility of Rolandic beta rhythm modulation in MEG and EEG. J. Neurophysiol. 127 (2), 559–570. https://doi.org/10.1152/jn.00267.2021.

Illman, M., Jaatela, J., Vallinoja, J., Nurmi, T., Mäenpää, H., Piitulainen, H., 2023. Altered excitation-inhibition balance in the primary sensorimotor cortex to proprioceptive hand stimulation in cerebral palsy. Clin. Neurophysiol. 157, 25–36. https://doi.org/10.1016/j.clinph.2023.10.016.

Isman, R.E., Inman, V.T., 1969. Anthropometric Studies of the Human Foot and Ankle. In. Foot Ankle 11, 97–129. http://www.rehab.research.va.gov/jour/69/6/1/97.pdf.

Jiang, W., Chapman, C.E., Lamarre, Y., 1991. Modulation of the cutaneous responsiveness of neurones in the primary somatosensory cortex during conditioned arm movements in the monkey W. Exp. Brain Res. 84, 342–354.

Kakigi, R., Koyama, S., Hoshiyama, M., Watanabe, S., Shimojo, M., Kitamura, Y., 1995. Gating of somatosensory evoked responses during active finger movements: magnetoencephalographic studies. J. Neurol. Sci. 128 (2), 195–204. https://doi.org/10.1016/0022-510X(94)00230-L.

Keser, Z., Buchl, S.C., Seven, N.A., Markota, M., Clark, H.M., Jones, D.T., Lanzino, G., Brown, R.D., Worrell, G.A., Lundstrom, B.N., 2022. Electroencephalogram (EEG) With or Without Transcranial Magnetic Stimulation (TMS) as Biomarkers for Post-stroke Recovery: A Narrative Review. Front. Neurol. 13 (February). https://doi.org/10.3389/fneur.2022.827866.

Lemon, R.N., 2021. The cortical "upper motoneuron" in health and disease. Brain Sci. 11 (5). https://doi.org/10.3390/brainsci11050619.

Lord, S.R., Ward, J.A., Williams, P., Anstey, K.J., 1994. Physiological factors associated with falls in older community-dwelling women. J. Am. Geriatr. Soc. 42 (10), 1110–1117. http://ovidsp.ovid.com/ovidweb.cgi?T=JS&PAGE=reference&D=emed3&NEWS=N&AN=1994310539.

Macefield, V.G., Knellwolf, T.P., 2018. Functional properties of human muscle spindles. J. Neurophysiol. 120 (2), 452–467. https://doi.org/10.1152/jn.00071.2018.

McChesney, J.W., Woollacott, M.H., 2000. The effect of age-related declines in proprioception and total knee replacement on postural control. J. Gerontol. - Series A Biol. Sci. Med. Sci. 55 (11), M658–M666. https://doi.org/10.1093/gerona/55.11.M658.

McFarland, D.J., McCane, L.M., David, S.V., Wolpaw, J.R., 1997. Spatial filter selection for EEG-based communication. Electroencephalogr. Clin. Neurophysiol. 103 (3), 386–394. https://doi.org/10.1016/S0013-4694(97)00022-2.

McIlroy, W.E., Bishop, D.C., Staines, W.R., Nelson, A.J., Maki, B.E., Brooke, J.D., 2003. Modulation of afferent inflow during the control of balancing tasks using the lower limbs. Brain Res. 961 (1), 73–80. https://doi.org/10.1016/S0006-8993(02)03845-3.

Merletti, R., Cerone, G.L., 2020. Tutorial. Surface EMG detection, conditioning and pre-processing: Best practices. J. Electromyogr. Kinesiol. 54, 102440. https://doi.org/10.1016/j.jelekin.2020.102440.

Mima, T., Terada, K., Maekawa, M., Nagamine, T., Ikeda, A., Shibasaki, H., 1996. Somatosensory evoked potentials following proprioceptive stimulation of finger in man. Exp. Brain Res. 111 (2), 233–245. https://doi.org/10.1007/BF00227300.

Misiaszek, J.E., Staines, W.R., Aging, C.S., Physiology, C.D., Alberta, U., Brooke, J.D., Cheng, J., Collins, D.F., McIlroy, W.E., 1997. Sensori-sensory afferent conditioning with leg movement: gain control in spinal reflex and ascending paths. Prog. Neurobiol. 51 (4), 393–421. http://www.ncbi.nlm.nih.gov/pubmed/9106899.

Morales-Muñoz, I., Jurado-Barba, R., Fernández-Guinea, S., Rodríguez-Jiménez, R., Jiménez-Arriero, M.Á., Criado, J.R., Rubio, G., 2016. Sensory gating deficits in first-episode psychosis. J. Nerv. Ment. Dis. 204 (12), 877–884. https://doi.org/10.1097/NMD.0000000000000572.

Morita, H., Petersen, N., Nielsen, J., 1998. Gating of somatosensory evoked potentials during voluntary movement of the lower limb in man. Exp. Brain Res. 120 (2), 143–152. https://doi.org/10.1007/s002210050388.

Mouchnino, L., Fontan, A., Tandonnet, C., Perrier, J., Saradjian, A., Blouin, J., Simoneau, M., 2015. Facilitation of cutaneous inputs during the planning phase of gait initiation. J. Neurophysiol. 114 (1), 301–308. https://doi.org/10.1152/jn.00668.2014.

Mujunen, T., Seipäjärvi, S., Nurminen, M., Parviainen, T., Piitulainen, H., 2022. Reproducibility of evoked and induced MEG responses to proprioceptive stimulation of the ankle joint. Neuroimage: Reports 2 (3), 100110. https://doi.org/10.1016/j.ynirp.2022.100110.

Nakamura, A., Miura, R., Suzuki, Y., Morasso, P., Nomura, T., 2023. Discrete cortical control during quiet stance revealed by desynchronization and rebound of beta oscillations. Neurosci. Lett. 814, 137443. https://doi.org/10.1016/j.neulet.2023.137443.

Neuper, C., Pfurtscheller, G., 2001. Event-related dynamics of cortical rhythms: Frequency-specific features and functional correlates. Int. J. Psychophysiol. 43 (1), 41–58. https://doi.org/10.1016/S0167-8760(01)00178-7.

Nurmi, T., Hakonen, M., Bourguignon, M., and Piitulainen, H. (2023). Proprioceptive response strength in the primary sensorimotor cortex is invariant to the range of finger movement. NeuroImage, 269(December 2022), 119937. Doi: 10.1016/j.neuroimage.2023.119937.

Parkkonen, E., Laaksonen, K., Piitulainen, H., Parkkonen, L., and Forss, N. (2015). Modulation of the~20-Hz motor-cortex rhythm to passivemovement and tactile stimulation. Doi: 10.1002/brb3.328.

Pfurtscheller, G., 1992. Event-related synchronization (ERS): an electrophysiological correlate of cortical areas at rest. Electroencephalogr. Clin. Neurophysiol. 83 (1), 62–69. https://doi.org/10.1016/0013-4694(92)90133-3.

Pfurtscheller, G., Neuper, C., 1994. Event-related synchronization of mu rhythm in the EEG over the cortical hand area in man. Neurosci. Lett. 174 (1), 93–96. https://doi.org/10.1016/0304-3940(94)90127-9.

Piervirgili, G., Petracca, F., Merletti, R., 2014. A new method to assess skin treatments for lowering the impedance and noise of individual gelled Ag-AgCl electrodes. Physiol. Meas. 35 (10), 2101–2118. https://doi.org/10.1088/0967-3334/35/10/2101.

Piitulainen, H., Bourguignon, M., De Tiège, X., Hari, R., Jousmäki, V., 2013. Corticokinematic coherence during active and passive finger movements. Neuroscience 238, 361–370. https://doi.org/10.1016/j.neuroscience.2013.02.002.

Piitulainen, H., Bourguignon, M., Hari, R., Jousmäki, V., 2015a. MEG-compatible pneumatic stimulator to elicit passive finger and toe movements. Neuroimage 112, 310–317. https://doi.org/10.1016/j.neuroimage.2015.03.006.

Piitulainen, H., Bourguignon, M., Smeds, E., de Tiège, X., Jousmäki, V., Hari, R., 2015b. Phasic stabilization of motor output after auditory and visual distractors. Hum. Brain Mapp. 36 (12), 5168–5182. https://doi.org/10.1002/hbm.23001.

Piitulainen, H., Seipäjärvi, S., Avela, J., Parviainen, T., Walker, S., 2018. Cortical proprioceptive processing is altered by aging. *Frontiers in Aging*. Neuroscience 10 (JUN), 1–13. https://doi.org/10.3389/fnagi.2018.00147.

Piitulainen, H., Illman, M., Jousmäki, V., Bourguignon, M., 2020. Feasibility and reproducibility of electroencephalography-based corticokinematic coherence. J. Neurophysiol. 124 (6), 1959–1967. https://doi.org/10.1152/jn.00562.2020.

Piitulainen, H., Nurmi, T., Hakonen, M., 2021. Attention directed to proprioceptive stimulation alters its cortical processing in the primary sensorimotor cortex. Eur. J. Neurosci. 54 (1), 4269–4282. https://doi.org/10.1111/ejn.15251.

Piitulainen, H., Nurmi, T., Vuontela, V., Mäenpää, H., Lano, A., Carlson, S., 2022. Perception of the ankle joint proprioception is impaired in extremely preterm-born adolescents and is associated with weaker fine-motor performance. Gait Posture 97, S159–S160. https://doi.org/10.1016/j.gaitpost.2022.07.105.

Prochazka, A., 2015. Sensory control of normal movement and of movement aided by neural prostheses. J. Anat. 227 (2), 167–177. https://doi.org/10.1111/joa.12311.

Proske, U., Gandevia, S.C., 2012. The proprioceptive senses: Their roles in signaling body shape, body position and movement, and muscle force. Physiol. Rev. 92 (4), 1651–1697. https://doi.org/10.1152/physrev.00048.2011.

Purves, D., Augustine, J. G., Fitzpatrick, D., Hall, C. W., LaMantia, A.-S., Mooney, D. R., Platt, L. M., & White, E. L. (2018). Neuroscience. In Oxford University Press Inc. (6th ed.). Oxford University Press Inc.

Quant, S., Adkin, A.L., Staines, W.R., Maki, B.E., McIlroy, W.E., 2004. The effect of a concurrent cognitive task on cortical potentials evoked by unpredictable balance perturbations. BMC Neurosci. 5, 1–12. https://doi.org/10.1186/1471-2202-5-18.

Richardson, J.K., Demott, T., Allet, L., Kim, H., Ashton-Miller, J.A., 2014. Hip strength: ankle proprioceptive threshold ratio predicts falls and injury in diabetic neuropathy. Muscle Nerve 50, 437–442. https://doi.org/10.1002/mus.24134.

Rushton, D.N., Roghwell, J.C., Craggs, M.D., 1981. Gating of somatosensory evoked potentials during different kinds of movement in man. Brain 104 (3), 465–491. https://doi.org/10.1093/brain/104.3.465.

Salmelin, R., Hämäläinen, M., Kajola, M., Hari, R., 1995. Functional segregation of movement-related rhythmic activity in the human brain. In NeuroImage 2 (4), 237–243. https://doi.org/10.1006/nimg.1995.1031.

Salmelin, R., Hari, R., 1994. Spatiotemporal characteristics of rhythmic neuromagnetic activity related to thumb movement. Neuroscience 60 (94), 537–550. http://www.sciencedirect.com/science/article/pii/0306452294902631.

Schutter, D.J.L.G., Hortensius, R., 2011. Brain oscillations and frequency-dependent modulation of cortical excitability. Brain Stimul. 4 (2), 97–103. https://doi.org/10.1016/j.brs.2010.07.002.

Seki, K., Perlmutter, S.I., Fetz, E.E., 2003. Sensory input to primate spinal cord is presynaptically inhibited during voluntary movement. Nat. Neurosci. 6 (12), 1309–1316. https://doi.org/10.1038/nn1154.

Smeds, E., Vanhatalo, S., Piitulainen, H., Bourguignon, M., Jousmäki, V., Hari, R., 2017. Corticokinematic coherence as a new marker for somatosensory afference in newborns. Clin. Neurophysiol. 128 (4), 647–655. https://doi.org/10.1016/j.clinph.2017.01.006.

SooHyun, L., George, E.C., Daniel, J.S., 2008. Motor modulation of afferent somatosensory circuits. Nat. Neurosci. 11 (12), 1430–1438. https://doi.org/10.1038/nn.2227.Motor.

Staines, W.R., Brooke, J.D., Angerilli, P.A., McIlroy, W.E., 1998. Generalisability of sensory gating during passive movement of the legs. Brain Res. 801 (1–2), 125–129. https://doi.org/10.1016/S0006-8993(98)00553-8.

Staines, W.R., Brooke, J.D., McIlroy, W.E., 2000. Task-relevant selective modulation of somatosensory afferent paths from the lower limb. Neuroreport 11 (8), 1713–1719. https://doi.org/10.1097/00001756-200006050-00024.

Staines, W.R., Graham, S.J., Black, S.E., McIlroy, W.E., 2002. Task-relevant modulation of contralateral and ipsilateral primary somatosensory cortex and the role of a prefrontal-cortical sensory gating system. Neuroimage 15 (1), 190–199. https://doi.org/10.1006/nimg.2001.0953.

Starr, A., Cohen, L.G., 1985. "Gating" of somatosensory evoked potentials begins before the onset of voluntary movement in man. Brain Res. 348 (1), 183–186. https://doi.org/10.1016/0006-8993(85)90377-4.

Stegeman, D., Hermens, H., 2007. Standards for surface electromyography: The European project Surface EMG for non-invasive assessment of muscles (SENIAM). Línea). Disponible En: Http://www. Med, 108–112. http://www.seniam.org/%5Cnhttp://www.med.uni-jena.de/motorik/pdf/stegeman.pdf.

Sugawara, K., Onishi, H., Yamashiro, K., Kotan, S., Kojima, S., Miyaguchi, S., Tsubaki, A., Kirimoto, H., Tamaki, H., Shirozu, H., Kameyama, S., 2016. Effect of muscle contraction strength on gating of somatosensory magnetic fields. Exp. Brain Res. 234 (11), 3389–3398. https://doi.org/10.1007/s00221-016-4736-z.

Takahara, T., Yamaguchi, H., Seki, K., Onodera, S., 2020. Sensory gating and suppression of subjective peripheral sensations during voluntary muscle contraction. BMC Neurosci. 21 (1), 1–6. https://doi.org/10.1186/s12868-020-00592-2.

Tan, H., Wade, C., Brown, P., 2016. Post-movement beta activity in sensorimotor cortex indexes confidence in the estimations from internal models. J. Neurosci. 36 (5), 1516–1528. https://doi.org/10.1523/JNEUROSCI.3204-15.2016.

Taylor, J.L., 2009. Proprioception. https://doi.org/10.1016/B978-008045046-9.01907-0.

Tinazzi, M., Zanette, G., La Porta, F., Polo, A., Volpato, D., Fiaschi, A., Mauguière, F., 1997. Selective gating of lower limb cortical somatosensory evoked potentials (SEPs) during passive and active foot movements. Electroencephalogr. Clin. Neurophysiol. – Evoked Potentials 104 (4), 312–321. https://doi.org/10.1016/S0168-5597(97)00023-3.

Tokimura, H., Di Lazzaro, V., Tokimura, Y., Oliviero, A., Profice, P., Insola, A., Mazzone, P., Tonali, P., Rothwell, J.C., 2000. Short latency inhibition of human hand motor cortex by somatosensory input from the hand. J. Physiol. 523 (2), 503–513. https://doi.org/10.1111/j.1469-7793.2000.t01-1-00503.x.

Toledo, D.R., Barela, J.A., 2014. Age-related differences in postural control: Effects of the complexity of visual manipulation and sensorimotor contribution to postural performance. Exp. Brain Res. 232 (2), 493–502. https://doi.org/10.1007/s00221-013-3756-1.

Toledo, D.R., Manzano, G.M., Barela, J.A., Kohn, A.F., 2016. Cortical correlates of response time slowing in older adults: ERP and ERD/ERS analyses during passive ankle movement. Clin. Neurophysiol. 127 (1), 655–663. https://doi.org/10.1016/j.clinph.2015.05.003.

Tuthill, J.C., Azim, E., 2018. Proprioception. Curr. Biol. 28 (5), R194–R203. https://doi.org/10.1016/j.cub.2018.01.064.

van Melick, N., Meddeler, B.M., Hoogeboom, T.J., Nijhuis-van der Sanden, M.W.G., van Cingel, R.E.H., 2017. How to determine leg dominance: The agreement between self-reported and observed performance in healthy adults. PLoS One 12 (12), 1–9. https://doi.org/10.1371/journal.pone.0189876.

Walker, S., Monto, S., Piirainen, J.M., Avela, J., Tarkka, I.M., Parviainen, T.M., Piitulainen, H., 2020. Older Age Increases the Amplitude of Muscle Stretch-Induced Cortical Beta-Band Suppression But Does not Affect Rebound Strength. Front. Aging Neurosci. 12. https://doi.org/10.3389/fnagi.2020.00117.

Watanabe, S., Hirayama, K., 1976. Alpha-Gamma Linkage in Man during Varied Contraction. Prog. Brain Res. 44 (C), 339–351. https://doi.org/10.1016/S0079-6123(08)60743-8.

Wilson, T.W., Heinrichs-Graham, E., Becker, K.M., 2014. Circadian modulation of motor-related beta oscillatory responses. Neuroimage 102 (P2), 531–539. https://doi.org/10.1016/j.neuroimage.2014.08.013.

Yamada, T., 2014. Somatosensory Evoked Potentials. Encyclopedia Neurol. Sci. 4, 230–238. https://doi.org/10.1016/B978-0-12-385157-4.00544-3.